Stony Brook University

Biophysical Insights into Amyloid Formation by Islet Amyloid Polypeptide

A Dissertation Presented

by

Peter James Marek

to

The Graduate School

in Partial Fulfillment of the

Requirements

for the Degree of

Doctor of Philosophy

in

Chemistry

Stony Brook University

May 2012

Stony Brook University

The Graduate School

Peter James Marek

We, the dissertation committee for the above candidate for the

Doctor of Philosophy degree, hereby recommend

acceptance of this dissertation.

Daniel P. Raleigh, Ph.D. – Dissertation Advisor
Professor, Department of Chemistry

Peter J. Tonge, Ph.D. – Chairperson of Defense
Professor, Department of Chemistry

Isaac S. Carrico, Ph.D. – Third Member
Professor, Department of Chemistry

Jean Baum, Ph.D. – Outside Member
Rutgers University, Professor, Department of Chemistry and Chemical Biology

This dissertation is accepted by the Graduate School

Charles Taber
Interim Dean of the Graduate School

Abstract of the Dissertation

Biophysical Insights into Amyloid Formation by Islet Amyloid Polypeptide

by

Peter James Marek

Doctor of Philosophy

in

Chemistry

Stony Brook University

2012

Amyloid deposition has been implicated to play a role in the pathology of over 40 human diseases including Alzheimer's, Parkinson's, type 2 diabetes and systemic amyloidosis, to name a few. All amyloid fibrils are characterized by a cross β-pleated sheet structure with interstrand hydrogen bonds running parallel to the long axis of the fibril. Islet amyloid polypeptide (IAPP) is a 37-residue peptide hormone that is the major proteinaceous component of pancreatic islet amyloid deposition that develops during type 2 diabetes. These deposits have been shown to play a role in the decrease of islet mass and β-cell apoptosis, which are typical pathologies developed during type 2 diabetes. The aggregation process of how IAPP goes from an unstructured monomer to an ordered peptide aggregate with significant β-sheet secondary structure is highly complex and involves a number of transient species that are highly dynamic and metastable. This research provides insights into the biophysical mechanisms and environmental components that can enhance amyloid assembly by IAPP using chemical, biophysical and kinetic methods.

My work included the development of a new method to synthesize IAPP via microwave solid-phase peptide synthesis; the examination of the role of aromatic amino acids in IAPP via a triple mutant in which the three aromatic amino acids were substituted with leucines; probing the nature lag phase species populated during amyloid formation via the unnatural fluorescent amino acid, *p*-cyanophenylalanine; and the study of the effects of ionic strength and ion composition on amyloid formation by IAPP. These studies aim to provide a better understanding of the intrinsic factors inherent to IAPP, as well as extrinsic environmental factors, that can decrease the stability of monomeric IAPP and induce amyloid formation.

Table of Contents

List of Figures

List of Tables

List of Abbreviations

2D-IR	Two-dimensional infrared spectroscopy
Aβ	The proteolytical fragment of the precursor protein that is responsible for amyloid formation in Alzheimer's disease
$A\beta_{1-40}$	The 40-residue isoform of Aβ
$A\beta_{1-42}$	The 42-residue isoform of Aβ
AFM	Atomic force microscopy
CPE	Carboxypeptidase E
CD	Circular dichroism
DMF	*N,N*-dimethylformamide
DMSO	Dimethyl sulfoxide
EDC	*N*-Ethyl-*N*′-(3-dimethylaminopropyl)carbodiimide
ER	Endoplasmic reticulum
F_0	Fluorescence in the absence of quencher
$F_{C\equiv N}$	*p*-Cyanophenylalanine
Fmoc	9-Fluorenylmethoxycarbonyl
FRET	Fluorescence resonance energy transfer
FTIR	Fourier transform infrared spectroscopy
GC-MS	Gas chromatography-mass spectrometry
HBTU	O-benzotriazole-N,N,N',N'-tetramethyluronium hexafluorophosphate
HFIP	Hexafluoroisopropanol
HPLC	High-performance liquid chromatography

HSPG	Heparan sulfate proteoglycan
$[IAPP]_{t=0}$	Concentration of IAPP at the start of a kinetic assay
IAPP	Islet amyloid polypeptide
IAPP-3XL	A peptide corresponding to full-length IAPP with Phe-15, Phe-23 and Tyr -37 all mutated to leucines
IL-1β	Interleukin-1β
K_{SV}	Stern-Volmer constant
LC-MS	Liquid chromatography-mass spectrometry
MALDI-TOF-MS	Matrix-assisted laser desorption ionization time-of-flight mass spectrometry
NMR	Nuclear magnetic resonance
PAL-PEG-PS	Pegylated polystyrene support resin, 5-(4'-Fmoc-aminomethyl-3', 5-dimethoxyphenol) valeric acid
PAM	Peptidylglycine alpha-amidating monooxygenase
PC1/3	Subtilisin-like prohormone convertase 1/3
PC2	Subtilisin-like prohormone convertase 2
preproIAPP	Precursor sequence of proIAPP and mature IAPP
proIAPP	Pro-islet amyloid polypeptide
R_0	Förster distance, the distance at which the energy transfer efficiency is 50% between in donor-acceptor pair in FRET
RP-HPLC	Reverse phase high-performance liquid chromatography
ssNMR	Solid-state NMR
SPPS	Solid-phase peptide synthesis

τ	Time constant of the transition at t_{50}
t_{50}	Time to 50% completion of fibril formation during a thioflavin-T kinetic assay
t_{lag}	Time required to reach 10% of the total fluorescence intensity during a thioflavin-T kinetic assay or $t_{50} - 2\tau$
TEM	Transmission electron microscopy
TFA	Trifluoroacetic acid
UV	Ultraviolet
v_{max}	Maximum velocity or the rate of fibril formation at t_{50}
v/v	Volume to volume

Acknowledgements

This work could not have been accomplished without the support, encouragement and guidance of my advisor Prof. Daniel P. Raleigh. I could not have asked for a better experience during my tenure in the lab and have learned much from him, both scientifically and about life in general.

Thank you to my committee members, Prof. Peter Tonge and Prof. Isaac Carrico, for useful advice and help throughout the years. It has been a pleasure interacting with such great scientists. Also, thank you to my outside member, Prof. Jean Baum from Rutgers University, for making the trip out to Stony Brook and participating in my defense.

Thank you to all of the wonderful members of the Raleigh lab, from the past: Dr. Andisheh Abedini, Trisha Barua, Dr. Ruchi Gupta, Dr. Fanling Meng, Dr. Bing Shan, Dr. Benben Song, Dr. Humeyra Taskent, Dr. Lauren Wickstrom; and the present: Rehana Akter, Ping Cao, Cynthia Li, Bowu Luan, Wenli Meng, Harris Noor, Vadim Patsalo, Ivan Peran, Matt Watson, Hui Wang and Shifeng Xiao. It has been a pleasure working, learning and interacting with such great scientists, many of whom who were not only colleagues, but also great friends.

Thank you to all of the scientists with whom I have collaborated with over the years from various laboratories: Prof. Martin Zanni from the University of Wisconsin-Madison and his group, especially Dr. Chris Middleton, Sudipta Mukherjee and Ann Marie Woys, for the collaboration on the FTIR and 2D-IR studies. Dr. Bruce Verchere from the University of British Columbia and his group, especially Dr. Kate Potter, for the collaboration with the porcine IAPP and islet viability studies. Dr. Steven Kahn and Dr. Sakeneh Zraika from the University of Washington for the collaboration with the neprilysin and MMP-9 studies.

Thank you to all of the office staff in the Chemistry Department, especially Kathryn Hughes and Heidi Ciolfi, the Department wouldn't be what it is if it were not for them; also, thank you to Mike Teta for help with broken equipment, leaky pipes and moving heavy equipment.

A big thank you to two sets of families. First, my Mother and Father for their love and support, both morally and financially; I could not have asked for more. I am grateful for their encouragement, and more importantly, patience, throughout my PhD. Also, thank you to my sister, Kate, and brother, Andrew, for being wonderful siblings. The second family, that of my girlfriend's: Michael, Debbie, Sarah and Molly, for their love, support, food, and for putting up with me.

Lastly, and most importantly, thank you to my wonderful girlfriend, Emma Mack, for loving, clothing, feeding, believing in me and basically keeping me alive and sane for the past 5 years. I would not have accomplished all that I have if it were not for her support.

Publications

1. **Marek, P.**; Abedini, A.; Song, B.; Kanungo, M.; Johnson, M.E.; Gupta, R.; Zaman, W.; Wong, S.S.; Raleigh, D.P. (2007) Aromatic interactions are not required for amyloid fibril formation by islet amyloid polypeptide but do influence the rate of fibril formation and fibril morphology. *Biochemistry*, 46, 3255-3261.

2. Meng, F.; **Marek, P.**; Potter, K.J.; Verchere, D.B.; Raleigh, D.P. (2008) Rifampicin does not prevent amyloid fibril formation by human islet amyloid polypeptide but does inhibit fibril thioflavin-T interactions: implications for mechanistic studies of beta-cell death. *Biochemistry*, 47, 6016-6024.

3. **Marek, P.**; Gupta, R.; Raleigh, D.P. (2008) The fluorescent amino acid *p*-cyanophenylalanine provides an intrinsic probe of amyloid formation. *Chembiochem*, 9, 1372-1374.

4. Potter, K.J.; Abedini, A.; **Marek, P.**; Klimek, A.; Butterworth, S.; Driscoll, M.; Baker, R.; Nilsson, M.; Bertera, S.; Trucco, M.; Fraser, P. E.; Raleigh, D. P.; Verchere, C. B. (2010) Islet amyloid deposition limits the viability of human islet grafts but not porcine islet grafts. *Proc. Natl. Acad. Sci.*, 107, 4305-4310.

5. Zraika, S.; Aston-Mourney, K.; **Marek, P.**; Hull, R.L.; Green, P.; Udayasankar, J.; Subramanian, S.L.; Raleigh, D.P.; Kahn, S.E. (2010) Neprilysin impedes islet amyloid formation by inhibition of fibril formation rather than peptide degradation. *J. Biol. Chem.*, 285, 18177-18183.

6. **Marek, P.**; Mukherjee, S.; Zanni, M.T.; Raleigh, D.P. (2010) Residue specific, real time characterization of lag phase species and fibril growth during amyloid formation: A combined fluorescence and IR study of *p*-cyanophenylalanine analogs of islet amyloid polypeptide. *J. Mol. Biol.*, 400, 878-888.

7. Taskent-Szegin, H.; **Marek, P.**; Thomas, R.; Goldberg, D.; Chung, J.; Carrico, I.; Raleigh, D.P. (2010) Modulation of *p*-cyanophenylalanine fluorescence by amino acid side-chains and rational design of fluorescence probes of α-helix formation. *Biochemistry*, 49, 6290-6295.

8. **Marek, P.**; Woys, A.M.; Sutton, K.; Zanni, M.T.; Raleigh, D.P. (2010) An efficient microwave assisted synthesis of human islet amyloid polypeptide designed to facilitate the specific incorporation of labeled amino acids. *Org. Lett.,* 12, 2848-2851.

9. Wang, L.; Middleton, C.T.; Singh, S.; Reddy, A.S.; Woys, A.M.; Strasfeld, D.B**.; Marek, P.**; Raleigh, D.P.; de Pablo, J.J.; Zanni, M.T.; Skinner, J.L. (2011) 2DIR spectroscopy of human amylin fibrils reflects stable β-sheet structure. *J. Am. Chem. Soc.,* 133, 16062-16071.

10. Middleton, C.T.; **Marek, P.**; Cao, P.; Chiu, C-C.; Singh, S.; Woys, A.M.; de Pablo, J.J.; Raleigh, D.P.; Zanni, M.T. (2012) Two-dimensional infrared spectroscopy reveals the complex behavior of an amyloid fibril inhibitor. *Nat. Chem.*, In Press, doi:10.1038/nchem.1293.

11. **Marek, P.**; Raleigh, D.P. (In Preparation) Ionic Strength Effects on Amyloid Formation, a Complicated Interplay Between Ion Selectivity, Hofmeister Effects and Screening.

Chapter 1. Introduction

Amyloid fibrils are insoluble fibrous protein aggregates that share a common secondary structural motif. Interest in these aggregates stems from their role in various humans diseases as and because they represent an alternative structural state for numerous proteins and peptides. Amyloid formation has been implicated in the pathology of over 40 human diseases including Alzheimer's, Parkinson's, Huntington's, type 2 diabetes and systemic amyloidosis, to name a few (1). It has also recently become clear that amyloid can play a beneficial structural or functional role in normal biology. A quantitative understanding of the biophysical and structural characteristics during the transition from soluble protein monomers to fibrils is needed to obtain insight into the kinetics of this process. This introduction summarizes the current understanding of the biological, biochemical and biophysical properties that trigger amyloid formation, primarily focusing on islet amyloid polypeptide (IAPP), a peptide responsible for islet amyloid deposition in the pancreas during type 2 diabetes.

1.1 General features of amyloid

1.1.1 Structure

Amyloid fibrils are unbranched, 5-15 nm in diameter, vary in length, are resistant to proteolysis and most can bind histological dyes such as Congo Red and thioflavin-T (2, 3). An abundance of evidence exists that links either the fibrils themselves, or more importantly, precursor protein oligomers with clinically relevant roles in the pathogenesis of numerous human diseases (4-10). A large number of proteins and peptides can form amyloid despite differences

in amino acid sequence and native secondary structure (Table 1.1) (1). Amyloid deposition can result from the aggregation of both natively unstructured or globularly folded proteins and peptides. Regardless of the vast differences in native state conformation, upon fibril formation all fibrils generate similar x-ray diffraction patterns, fourier transform infrared (FT-IR) spectra and circular dichroism (CD) spectra, and electron and atomic microscopy images, with very slight differences. All amyloid fibrils are characterized by a cross β-pleated sheet structure with interstrand hydrogen bonds running parallel to the long axis of the fibril (Figure 1.1) (2). These fibrils often consist of multiple thin fibrils, or protofibrils, that intertwine around one another in a helical fashion, giving a twisted ultrastructural appearance with regular periodicity (11, 12). Despite these global similarities amongst different amyloid-forming proteins, at the microscopic level fibrils can contain a number of detailed structural differences (13). These differences can be detected via seeding reactions, to be explained in the next section, and structural studies, although inhomogeneous structures formed by fibrils from the same amyloid-forming protein can complicate experiments (13-16).

Utilizing recent advances in high-resolution techniques such as x-ray crystallography, solid-state nuclear magnetic resonance (ssNMR), 2D-IR and cryoelectron microscopy, highly detailed perspectives of several amyloid structures at the microscopic level have been realized (13, 17-19). What has emerged is that all amyloid fibrils contain a β-sheet core that drives its stability, as originally hypothesized. However, the manner with which the sheets coalesce into a tertiary and quaternary fold can be quite different at the microscopic level (13). Two major structures have been found to form in amyloid fibrils: the β-sandwich and the β-solenoid (Figure 1.1) (13). In the β-sandwich, two β-sheets on the same molecule come face-to-face separated by an unstructured loop region. β-strands align and form a pleated β-sheet structure down the axis

of the fibril. In this scenario, a single polypeptide forms a single layer or rung of the fibril. Fibrils from the peptides that form amyloid in Alzheimer's disease, Aβ, and type 2 diabetes, IAPP, are both modeled to form these types of structures as derived from ssNMR data (20, 21). Fibrils that adopt a β-solenoid fold contain a polypeptide that can form multiple layers or rungs along the length of the fibril. Solenoids can form either a β-helix, where three β-strands from a single polypeptide forms a triangular layer and loops back to form an additional layer; or a β-roll, where two β-strands come together similar to a β-sandwich, but an individual polypeptide forms multiple layers of the β-sheet (Figure 1.1). These structures are formed by the HET-s prion protein and a number of other prion proteins (22, 23).

Within each of the supramolecular assemblies described above, the β-sheets can assemble into two distinct conformations: parallel or anti-parallel (Figure 1.1). Parallel β-sheets can further be categorized into either in-register or out-of-register sheets. In-register sheets contain individual strands that are aligned with one another such that identical residues on separate strands are in register with one another along the entire length of the sheet. A majority of amyloid fibrils consist of parallel, in-register β-sheets, allowing a templating mechanism for fibril self-polymerization (13, 24).

The ability of a given polypeptide to form amyloid is highly dependent on its amino acid sequence. Proteins rich in hydrophobic, non-charged amino acids with a high propensity for β-sheet formation tend to have a greater propensity to form amyloid (25, 26). Replacing amino acids in amyloidogenic proteins with proline residues often hinders or completely inhibits amyloid formation, as proline is known to be a β-sheet breaking residue (27, 28). Most, if not all proteins found in nature, contain stretches of hydrophobic, non-polar amino acids that form the hydrophobic core of a folded protein. There have been a large number of reports on the

formation of amyloid by non-disease related proteins, leading to the conclusion that the ability to form amyloid is a generic property of polypeptide chains (29-31).

1.1.2 Kinetics of fibril assembly

The exact mechanism of amyloid formation at the microscopic level is extremely complex, not entirely understood and garners much attention in the literature. Experimental evidence suggests that polypeptides form amyloid fibrils in a nucleation-dependent event. For intrinsically disordered peptides, the limiting step is the formation of a seed or nucleus that templates further aggregation (32-34). For natively folded globular proteins, a partial unfolding of the native state or the trapping of an unstable intermediate with lifetimes sufficient to allow for interprotein interactions to occur precedes nucleation of fibril formation (35, 36). This step requires a mutation to the amino acid sequence or a change or fluctuation in the pH, temperature, pressure, solvent or ionic strength in order for the protein to populate a non-native, aggregation-prone state.

As noted earlier, amyloid fibrils can bind histological dyes such as Congo red and thioflavin-T (37, 38). Thioflavin-T is widely used as an *in vitro* fluorescent probe of amyloid formation. Thioflavin-T is a benzothiazole salt and assays utilizing this molecule typically yield a sigmoidal curve (Figure 1.2). In solution, the twist between the benzothiazole and aniline segments of the molecule oscillates rapidly leading to non-radiative decay and a low fluorescence quantum yield (39, 40). Thus, during the lag phase in the presence of monomers or small un-ordered oligomers, thioflavin-T gives a very low fluorescence signal. However, upon fibril formation thioflavin-T binds to the growing fibrils, binding to grooves on the surface of the fibrils generated by aligned side chains, locking the benzothiazole and aniline segments of

thioflavin-T in place and generating a fluorescence signal (41, 42). A crystal structure of thioflavin-T bound to an Aβ amyloid protofibril is shown in Figure 1.2 (41). The thioflavin-T fluorescence eventually reaches a plateau at which fibrils and monomers are in equilibrium.

The molecular details of the events that occur during the lag phase prior to fibril formation are largely unknown, however, the species that populate the aggregation pathway during this period are most likely highly dynamic and metastable (Figure 1.3) (1). Once the critical amyloid seed or nucleation-event forms, fibril formation is essentially a downhill event along the free energy landscape. Intrinsically disordered peptides such as IAPP and Aβ sample α-helical conformations and form soluble oligomers with large conformational fluctuations en route to fibril formation (43-45). The oligomers are largely believed to be the cytotoxic entity, which will be described in the next section. The lag phase can be bypassed by adding seeds or pre-formed fibrils of the same protein (Figure 1.2). The seed acts as a template for addition at monomers. Seeding is usually, but not always, specific in the sense that fibrils are best at seeding amyloid formation by the same protein. Cross-seeding reactions, where fibrils formed by one protein are used to seed the reaction of a separate amyloidogenic protein, can be used to infer structural similarities among different fibrils as well as a protein's ability to form amyloid or different amyloid structures. For example, IAPP fibrils cannot cross-seed $A\beta_{1\text{-}40}$ fibrillization, however, $A\beta_{1\text{-}40}$ fibrils can seed IAPP fibrillization (14).

The primary nucleation event, involving the formation of a seed or nucleus that induces fibril growth, is followed by secondary nucleation events. Secondary nucleation generates new fibril ends that are produced mostly via fragmentation of the growing fibrils (32). Recent models of fibril formation and growth have implicated secondary nucleation as the major determinant of the kinetics of amyloid formation (32, 46, 47). The growth phase of fibril formation consists of

the addition of monomers to the fibril ends. Water is expelled upon binding of monomers creating a dry interface between the added monomer and fibril end (48, 49). Entropy gained from released water molecules and favorable interpeptide hydrogen bonds compensate for the loss of entropy of the newly bound monomer (49, 50).

1.1.3 Proposed mechanisms of toxicity, role in disease and inhibition

Cell toxicity via amyloid deposition was initially linked to the fibril form of the aggregated protein (51-53). For some amyloid diseases, such as systemic amyloidosis, this may be the case as the amyloid fibrils disrupt tissue structure and organ function (54, 55). For many amyloid diseases however, studies have emerged which suggest that transient, metastable low molecular weight, soluble oligomers are the defining feature of toxicity. It should also be noted that the presence of amyloid in the pathology of a disease does not necessarily denote causation. As discussed earlier, the kinetics of amyloid formation are highly complex, involving many species along the aggregation pathway. This makes it extremely difficult to determine at what step and which entity of the amyloid formation pathway is toxic. It is possible that the toxic entity differs from protein to protein and disease to disease. It has also been realized that not all amyloids are toxic. Amyloid fibrils perform a structural function in bacterial biofilms, are thought to play a role in the storage of peptide hormones, and aid in melanin formation (56-58). Controlled growth and the type of amyloid formed may account for the lack of toxicity displayed in these scenarios (59, 60).

It is apparent that the majority of effects observed in amyloid-related diseases result from a protein's gain-of-toxic-function (61). Various mechanisms have been proposed to explain a general toxic effect for the soluble toxic oligomers (62). These include membrane disruption via

formation of pores, impairment of lysosomal or proteasomal protein degradation, induction of endoplasmic reticulum (ER) stress and Golgi fragmentation (63-66). Amyloid toxicity can also result from a loss of function associated with protein aggregation, in which functionally important proteins, such as anti-apoptotic proteins, are sequestered and mislocalized into growing aggregates (67).

There is an abundance of pharmaceutical interest in amyloid formation owing to its association with a number of diseases. Many approaches have focused on the inhibition of fibril formation via small molecule and peptide inhibitors to inhibit cytotoxicity. Small molecules and peptides have been targeted to combat and decrease the rate of fibril growth, to degrade pre-formed fibrils and oligomers, drive aggregating proteins into non-amyloid amorphous aggregates or stabilize the soluble form of the protein (68, 69). A number of these approaches have decreased cytotoxicity in cell and animal models, but as of yet few have made it to clinical trial and been approved for use in humans (70-72). A recent interesting approach, based on the theory that fibrils are not the toxic entity, was to search for small molecules that induce amyloid formation by Aβ (73). This decreases the amount of time an aggregating protein spends as a toxic oligomer or bypasses this phase altogether. One such small molecule, a derivative of orcein, decreased the concentration of oligomers and suppressed inhibition of long-term potentiation by Aβ oligomers in hippocampal brain slices.

1.2 Islet Amyloid Polypeptide (IAPP)

1.2.1 Biosynthesis and function in vivo

The majority of IAPP biosynthesis in humans occurs in the islet β-cells of the pancreas. There is also evidence for production of IAPP in the dorsal root ganglia, the gastrointestinal tract

and the developing kidney (74-76). IAPP is a 37-residue polypeptide hormone co-localized, co-processed and secreted with insulin in the islet β-cells of the pancreas. IAPP is secreted at a ratio of approximately 1:100 (IAPP:insulin) with insulin from the secretory granules of the β-cells, where its storage concentration is in the millimolar range (77, 78). It is thought that the low pH and the crystalline storage form of insulin in the secretory granule are what prevent fibril formation at such high concentrations (79, 80). The concentration of IAPP circulating in the blood stream under fasting conditions is approximately 15 nM (77). IAPP belongs to the calcitonin peptide family based on sequence and structure homology (81). As a hormone, along with insulin, it is a part of the glucoregulatory cascade and is important for maintaining glucose homeostasis inhibiting the appearance of nutrient, especially glucose, in the plasma. IAPP slows the appearance of exogenous glucose via the reduction of gastric emptying and inhibition of digestive secretion (82, 83).

IAPP is first transcribed on the ribosome as an 89-residue prohormone precursor where it is transported to the lumen of the rough endoplasmic reticulum (84, 85). Here, a 22-residue N-terminal leader sequence is cleaved generating the 67-residue prohormone, proIAPP. proIAPP is packaged into a secretory granule with proinsulin where both proIAPP and proinsulin are processed by the same proprotein convertases PC2 and PC1/3 prior to sercretion (85). PC2 processes the N-terminal cleavage site between Arg-11 and Lys-12 and PC1/3 cleaves between Arg-51 and Asn-52 at the C-terminus (Figure 1.4). In the absence of PC1/3, it has been shown that PC2 can process the C-terminal cleavage site as well, albeit not as effectively (86). Improperly processed IAPP has been detected *in vivo* and results in an increase in the levels of amyloid fibrils (87-89). This has led to the hypothesis that improper processing could lead to fibril formation *in vivo*, which will be discussed in further detail in the next section (90). Lys-50

and Arg-51 are cleaved from the C-terminus of the peptide by carboxypeptidases E (CPE) (91). The C-terminal glycine that results from this cleavage is catalytically truncated between the α-carbon and amine via the enzyme peptidylglycine alpha-amidating monooxygenase (PAM), yielding an amidated C-terminus (92). IAPP also contains a disulfide bond between cysteine residues at positions 2 and 7. The sequences and cleavage schematic of prepro-, pro- and mature IAPP are outlined in Figure 1.4.

1.2.2 IAPP and type 2 diabetes

Amyloid deposits were first discovered in the islets of the pancreas at the beginning of the 20th century; however, it was not until 1987 that IAPP was discovered to be the principle proteinaceous component of the aggregates (93, 94). Amyloid deposits have not been found in all individuals suffering from diabetes, varying from as much as 100% of individuals in one study to as little as 40% in another (95-98). Furthermore, the deposits are also observed in nondiabetic individuals, but effect fewer islets and occurs to a lesser extent (99-101). IAPP has been conserved through evolution and has been characterized in mammals, birds and teleostean fish (Figure 1.5) (102-106). While islet amyloid deposition has been documented in a number of mammal species, including domesticated cats and primates, but it does not appear in animals most commonly used for diabetes research such as mice and rats, as well as a number of other species (107). While the majority of the IAPP sequence is conserved across species, there is some variation, most notably in the 20-29 region (Figure 1.5). Five out of the six differences between the human and rat peptide are found in this region, most notably three proline residues that are found in the rat peptide, but not human. Proline residues are notorious for preventing β-sheet formation and are the primary reason why rat IAPP cannot form amyloid. It was long

thought that the 20-29 region of IAPP, which forms amyloid on its own, is necessary for fibril formation and forms the amyloid core (108, 109). However, proline mutations outside of the 20-29 region also disrupt amyloid formation and other fragments of IAPP can form amyloid that do not include the 20-29 region (110, 111). There is one known mutation in the IAPP gene associated with an increased risk to develop in type 2 diabetes, IAPP S20G (112, 113). This mutation has only been found in Asian population, and *in vitro* the mutated peptide has an increased propensity to form amyloid in comparison to wild type IAPP (112).

While it is difficult to study the effect of islet amyloidosis on type 2 diabetes in humans, a number of studies have done so in domestic cats, primates and mice transgenic for human IAPP (114-118). As stated above, IAPP mice and rats do not form amyloid, and these species also do not develop type 2 diabetes. However, rats transgenic for human IAPP have developed type 2 diabetes when fed a diet high in fat (119-123). In addition, inhibition of proIAPP expression by small interfering RNA and treatment with an inhibitor of IAPP amyloid formation enhanced β-cell survival in cultured islets (124). These works have revealed the importance of islet amyloid on the diabetic state. While it has yet to be determined whether islet amyloid deposition is the cause or the consequence of the β-cell dysfunction and hyperglycemia observed in type 2 diabetes, it has been shown that islet amyloid plays a causative role in the reduction of islet volume via β-cell apoptosis and decline in β-cell mass (125-128). The reduction in β-cell mass is not a reliable explanation for the insufficient insulin response in type 2 diabetes, but some evidence indicates that remaining islets may no longer be functional due to amyloid or oligomer deposition (129).

The bulk of islet amyloid appears to occur extracellularly, however, intracellular deposits have also been noted in a number of studies with transgenic mice, diabetic baboons and human

islets transplanted into nude mice (Figure 1.6) (90, 130-132). Peripheral insulin resistance is a hallmark pathology of type 2 diabetes leading to an increased demand for insulin release. Increased insulin biosynthesis is paralleled by an increase in IAPP synthesis (87, 133, 134). In the early phases of type 2 diabetes, elevated levels of proinsulin and improperly processed intermediates have been detected, suggesting a malfunction of the proprotein convertases PC2 and PC1/3, which as noted earlier aid in the maturation of proIAPP (87). Using immune electron microscopy with antibodies specific for proIAPP, amyloid deposits consisting of proIAPP were detected intracellularly (90, 135). *In vitro*, proIAPP has been shown to be highly amyloidogenic, although not as much as mature IAPP (136, 137). Improperly processed IAPP containing the N-terminal pro-extension, $proIAPP_{1-48}$, has been shown to bind heparan sulfate proteoglycan (HSPG), a glycosaminoglycan present in the basement membrane of cells (138, 139). HSPG can nucleate fibril formation of $proIAPP_{1-48}$ by binding the peptide at the N-terminus and creating a high local concentration of peptide, thus acting like a seed (137). It has been hypothesized that improperly processed proIAPP forms amyloid intracellularly, inducing cell death, leading to an extracellular amyloid seed that can nucleate mature IAPP fibrils extracellularly (90).

IAPP is also reported to play a role in the failure of pancreatic islet transplants as a treatment for type 1 diabetes (140, 141). Transplantation of islets from nondiabetic donors into diabetic subjects has been a promising, yet complicated treatment to achieve complete glucose control and independence of extraneous insulin. Clinical trials involving islet transplantation carried out in the 1980's and 1990's were a failure in that only 10% of the diabetic subjects were able to maintain normoglycemia without insulin therapy over the course of two years (142, 143). While initially nearly all of the subjects achieved insulin-independence, it was concluded that there was a progressive loss of islet function over time and this correlated with appearance of

IAPP islet amyloid formation (141, 144). Transplanted murine islets transgenic for human IAPP also display a deposition of amyloid in the transplanted islets and fail to achieve normoglycemia (145). Xenotransplantation of islets using pigs or other animals has been an attractive alternative given the lack of islet donors. Porcine islets have been shown to maintain long-term function and restoration of normoglycemia following transplantation into nonhuman primates (146, 147). The porcine form of IAPP does not readily form amyloid and amyloid deposition limits the viability of human transplanted islet grafts, but not porcine grafts (148).

1.2.3 Toxicity

The cytotoxicity of IAPP to adult human and rat islet cells *in vitro* was first noted in 1994; however, it was thought that fibrils were the cytotoxic entity (51, 149). Follow-up studies, which added extraneous amyloid fibrils to islet cells in culture, showed that apoptosis was not induced and the cells were viable, yet they were decorated with amyloid (150). Freshly prepared, monomeric solutions of IAPP added to cell cultures can reproducibly induce apoptosis (150). It has since become generally accepted that small soluble, oligomeric IAPP aggregates are the toxic entity, although these oligomers have yet to be directly detected *in vivo (5, 151, 152)*. Oligomer-binding antibodies have been raised for IAPP and have been shown not to bind to IAPP-derived monomers or fibrils (153, 154). Recent reports of non-specific binding of the antibodies to anti-aggregation heat shock proteins and α-synuclein amyloid fibrils limit the interpretation of the original studies (155, 156).

The islets of Langerhans constitute only 1-2% of pancreatic tissue mass, yet many essential hormones for glucose homeostasis are secreted directly into the blood stream from cells located in the islets, including glucagon, insulin, IAPP, somatostatin, ghrelin and the pancreatic

polypeptide (157). Islets consist of α-, β-, ε-, δ- and PP-cells, with the insulin- and IAPP-producing β-cells constituting 65-80% of the islet cell mass, as measured from rat pancreas (158, 159). A number of theories have been postulated for the role of IAPP in β-cell death and the decrease in islet mass during type 2 diabetes including disruption of the cytoarchitecture of the islets, inducing endoplasmic reticulum stress via the unfolded protein response, cellular membrane disruption, mitochondrial membrane disruption, disturbance in the maturation of autophagolysosomes and activation of the inflammasome (119, 160-164).

A number of *in vitro* studies have suggested that prefibrillar, soluble oligomers form nonselective, ion channel-like pores and induce membrane disruption (4, 7, 165). Amyloid proteins have been shown to induce ionic conductance in both artificial and cell plasma membranes (166, 167). This mechanism has been proposed to be a universal property of most amyloidogenic proteins, and the size of the pore-forming oligomeric species differs from system to system (9). The interpretation of experiments performed with artificial membranes can be complicated as the charge and composition of the lipids used can highly influence the results (168). There are many reports of IAPP inducing leakage in artificial membranes; however, rat IAPP, which does not form amyloid, has been reported to induce leakage as well, albeit at higher concentrations (169-172). The complexity of the kinetics and the rate at which IAPP forms amyloid has made it difficult to determine an exact mechanism of membrane leakage and the size or structure of membrane-disruptng oligomers. It is generally accepted that IAPP-membrane interactions are mediated by α-helical conformations in the N-terminal 23 residues (Figure 1.7) (173). The literature disagrees on how IAPP perturbs lipid bilayers. One scenario suggests fibril growth occurs on the membrane, mediated by a high local concentration of exposed highly amyloidogenic C-termini, and this leads to invagination and perforation of the

lipid bilayer (Figure 1.7) (173). Other scenarios suggest the formation of toroidal pores or nonspecific membrane disruption due to excessive negative curvature strain (9, 165).

It has been documented that the addition of human IAPP to immortalized β-cells or rat islets induces multiple apoptotic pathways, including caspase-8, JNK, p38 kinase and Fas-associated signaling pathways (174-177). Recently it was also shown that human IAPP, but not nonamyloidogenic rat IAPP, induces production of interleukin-1β (IL-1β) and activation of the inflammasome, a multimeric protein complex responsible for activation of inflammatory processes (163). IL-1β, which has been well documented to play a role in type 1 diabetes and is a risk factor for type 2 diabetes, has a profound effect on the function of pancreatic beta cells and has been shown to play a major role in the induction of apoptosis (178-180).

1.2.4 Amyloid formation by IAPP

As mentioned earlier, IAPP contains a disulfide bond between Cys-2 and Cys-7, and an amidated C-terminus. IAPP is a natively unfolded polypeptide and adopts a fluctuating coil configuration with very low levels of secondary structure in aqueous buffer based on circular dichroism and NMR spectra. IAPP samples transient α-helical conformations involving residues in the 9-22 region, which is thought to play a role *in vivo* for the binding to receptor complexes (181). As noted earlier, the helical conformation also plays a role in membrane binding and is most likely an on-pathway intermediate for amyloid formation in solution. Rat IAPP also samples helical conformations in the N-terminal part of the peptide, but the transformation to amyloid is impeded by the presence of prolines in the C-terminal portion of the peptide (181). A number of mutations have been made throughout the IAPP gene as part of biophysical studies. Many point mutants have been realized that can render the peptide incapable of forming amyloid

formation and a few even enhance the amyloidogenic properties of IAPP. These studies combined have shown that the size, β-sheet propensity, hydrophobicity and charge of individual amino acid side chains are very important factors of amyloid formation by IAPP. Based on a number of studies on amyloidogenic peptides and their subsequent fragments, it was hypothesized that π-π interactions between aromatic interactions were absolutely critical for amyloid formation by serving as functional and structural elements that direct molecular recognition and self-assembly (182, 183). One of my research projects tested this hypothesis via the characterization of a triple leucine mutant of IAPP (IAPP-3XL), in which each aromatic amino acid was replaced by a leucine (184). This work and the results are described in more detail in Chapter 3.

The detection of lag phase species during amyloid formation by IAPP is very difficult. IAPP is one of the most amyloidogenic naturally occurring proteins and as such, high-resolution spectroscopic techniques such as solution-state NMR lack the time resolution necessary to obtain meaningful information prior to fibril formation. As proteins aggregate, the line-widths of NMR peaks begin to broaden and eventually are lost. Other biophysical methods, such as light scattering and analytical centrifugation, which can deduce the size of oligomers, are also hindered by time constraints. Methods using fluorescence, other than thioflavin-T assays, have given some clue as to interactions between individual residues and their environments during the fibril formation process. Evidence for a collapsed monomer state was shown via triplet quenching between a C-terminal tryptophan mutant and disulfide bond contacts (185). Anisotropic fluorescence measurements of the C-terminal tyrosine indicate that upon fibril formation the residue is packed in a well-defined environment in a frozen-like, rigid state (186). My research utilized the non-canonical fluorescent amino acid, *p*-cyanophenylalanine ($F_{C\equiv N}$), to

use as a site-specific probe of amyloid formation (187, 188). Each aromatic residue was separately replaced by $F_{C\equiv N}$ and I showed that the substitutions do not perturb amyloid formation relative to wild type IAPP. The fluorescence can be monitored in real-time and provides information about the nature of lag phase species and fibril structure. This work and the results are described in more detail in Chapter 4.

The kinetics of IAPP amyloid formation *in vitro* are dependent on a number of external forces including pH, temperature, pressure, ionic strength and co-solvents. The environment of the secretory granule in which IAPP is stored, is such that the peptide should readily form amyloid. The concentration of IAPP is high, in the millimolar range, and the granule contains high concentrations of Zn^{2+} (20 mM), which is primarily associated with insulin, Ca^{2+} (120 mM), Mg^{2+} (70 mM), HPO_4^{2-} (70 mM) and adenine nucleotides (10 mM) (189). It is thought that IAPP fibril formation is inhibited by the low pH of the granules (pH 5.5) and interaction with insulin, a known inhibitor of IAPP fibril formation (190). A number of changes occur to the pH and components of the secretory granules concomitantly with the development of type 2 diabetes and β-cell dysfunction (191, 192). Previous studies have determined that amyloid formation by IAPP is drastically reduced at low pH, demonstrating the importance on the total ionization state of IAPP on amyloid formation (86, 190). Specifically, His-18 and the N-terminus are the only titratable groups in IAPP over the pH range from 5.5 to 8.0, where there is a drastic change in the kinetics (193). Part of my research examined the effects of screening out these charges with anions at both low and high pH. The results indicate that the effects of anions on fibril formation are not only due to Debye-Hückel effects of electrostatic screening, but also involve electroselectivity and Hofmeister effects and their relative importance varies at different ionic strengths. This work and the results are described in more detail in Chapter 5.

As discussed earlier, data from CD, solid-state NMR, 2D-IR and x-ray diffraction confirm that amyloid fibrils consist of cross β-strands that run perpendicular to and forms hydrogen bonds along the axis of the fibrils. There have been a number of models derived for the fibril state of IAPP including a model that proposed IAPP folds into an "e" conformation, with a mixture of parallel and anti-parallel β-sheets; a model in which IAPP adopts an "s" shaped or β-serpentine fold; and a model in which the nearly the entire length of the peptide from residues 12-37 form parallel hydrogen bonded β-strands (84, 194, 195). The most popular and plausible model, based on subsequent structural studies, has been proposed from the laboratory of Rob Tycko based on data from solid-state NMR data (Figure 1.8) (20). In this model IAPP forms in-register, parallel β-sheets with two β-strands per molecule. Residues 8-17 form one β-strand and residues 28-37 form the other, separated by a chain-reversing bend comprising residues 18-27. The N-terminus remains unstructured due to constraints imposed by the disulfide bond.

1.3 Figures

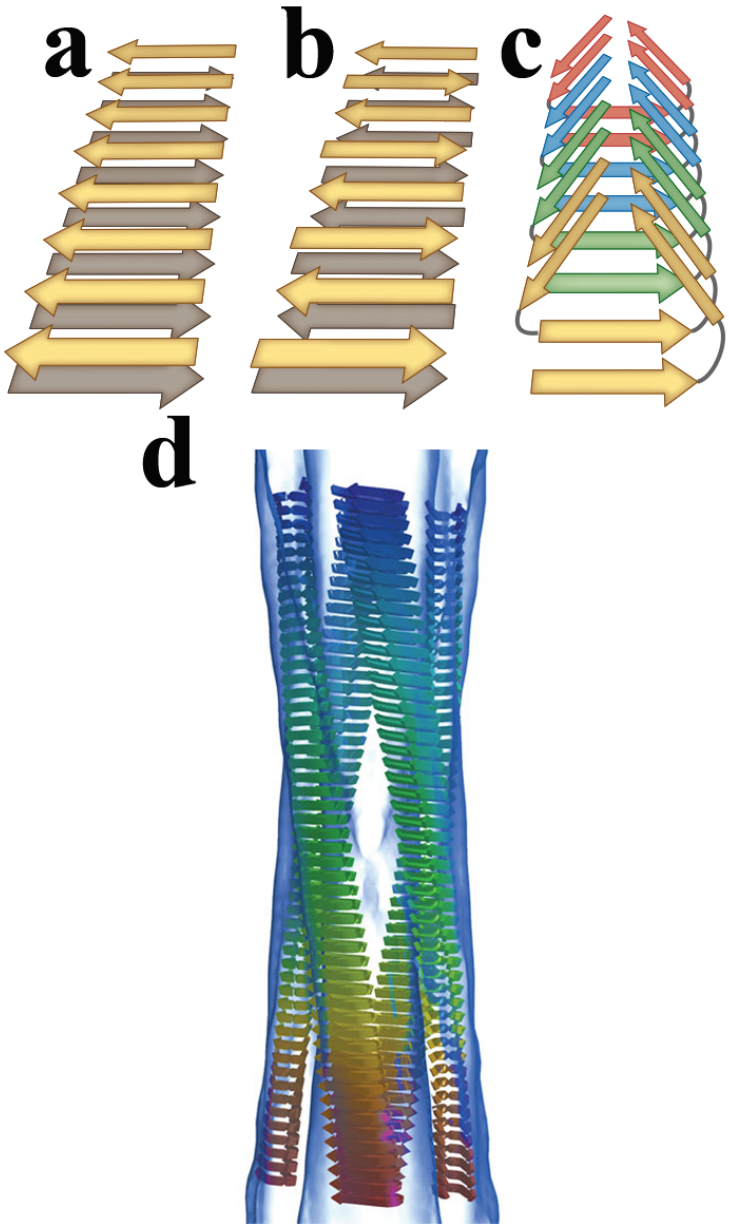

Figure 1.1: Ribbon diagrams of the cross-β structures formed by (a) parallel β-sheets, (b) anti-parallel β-sheets and (c) β-helices. These so-called protofibrillar structures coalesce and wrap around one another to form a mature fibril (d) with a periodic twisted pitch. Adapted from reference (13).

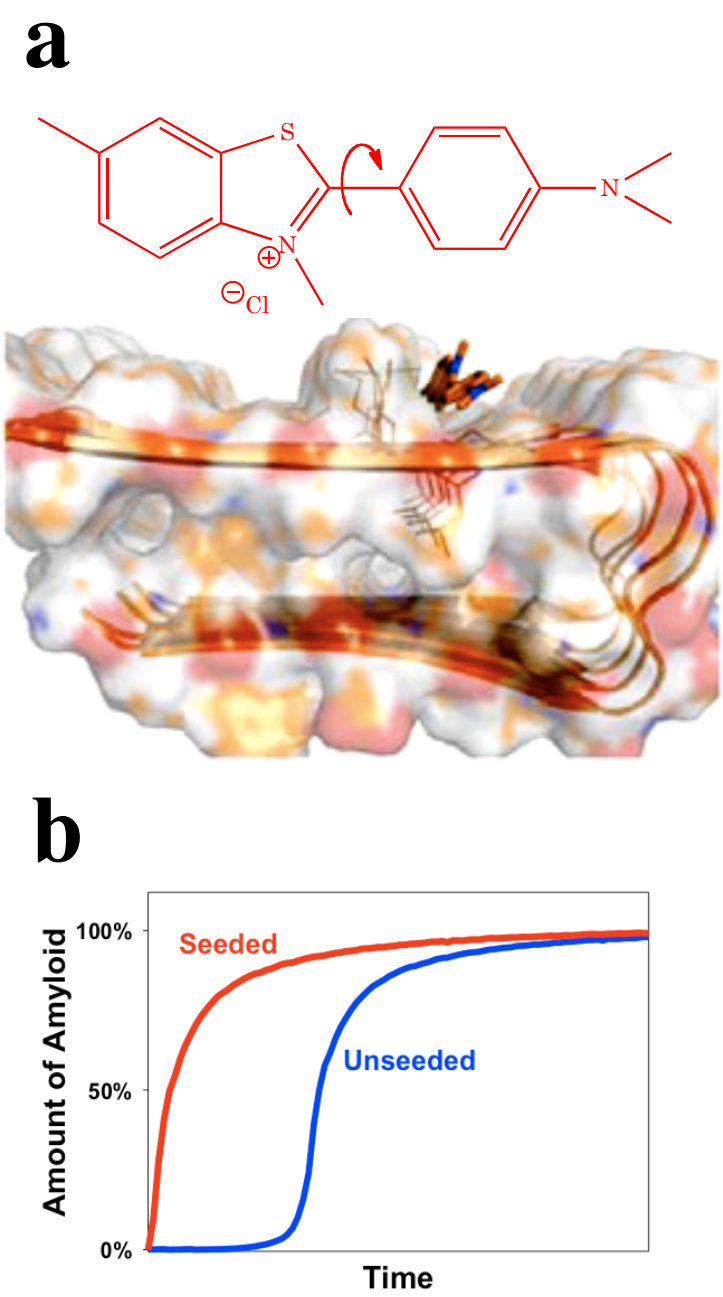

Figure 1.2: (a) Model of thioflavin-T binding to $A\beta_{1\text{-}42}$ amyloid fibrils, based on x-ray crystallography data and theoretical calculations. Thioflavin-T, structure at top, is a benzothiaole salt. Its fluorescence is dependent upon the amount of twist between the benzothiazole and aniline segments of the molecule. Thioflavin-T binds to grooves on the surface of growing fibrils generated by aligned side chains, locking the benzothiazole and aniline segments in place and generating a fluorescence signal. Figure adapted from reference (41). (b) Unseeded thioflavin-T amyloid assays (blue) yield a typical sigmoidal curve: a lag phase where monomers and oligomers are prevalent, a growth phase upon nucleation where monomeric protein is being added to the fibril ends and a plateau phase where fibrils and monomers are in equilibrium. Thioflavin-T assays may be seeded (red) by adding fibrils formed from previous assays to bypass the lag phase.

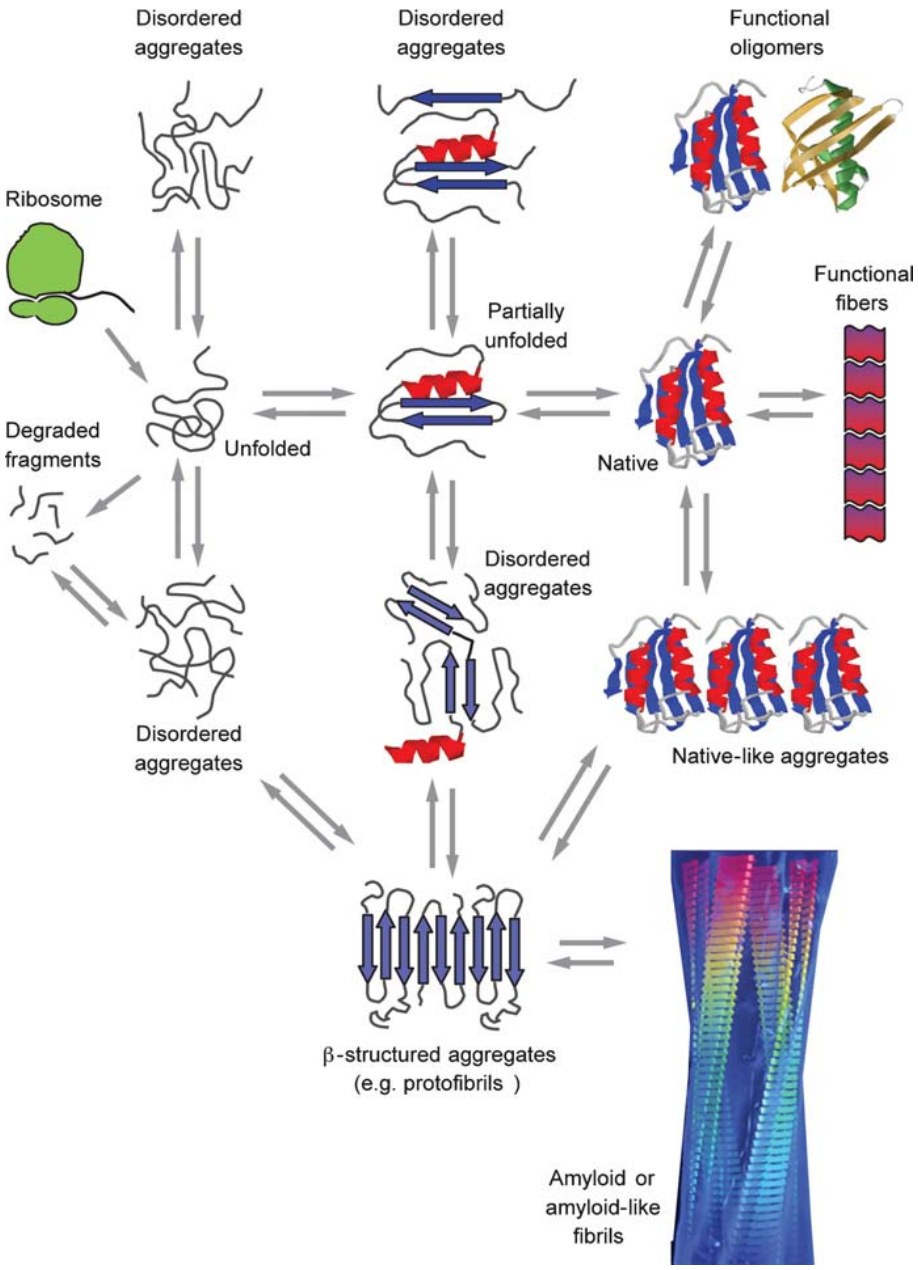

Figure 1.3: A schematic representation of all major conformational states a protein can undertake en route to aggregation and the development of amyloid fibrils. Once synthesized on the ribosome, proteins can adopt a multitude of conformations over a wide range of timescales. The process of protein folding is highly regulated by chaperones, enzymes, degradation pathways and quality control mechanisms. When these processes fail, proteins can freely misfold and aggregate leading to a number of metabolic disorders. Figure adapted from reference (1).

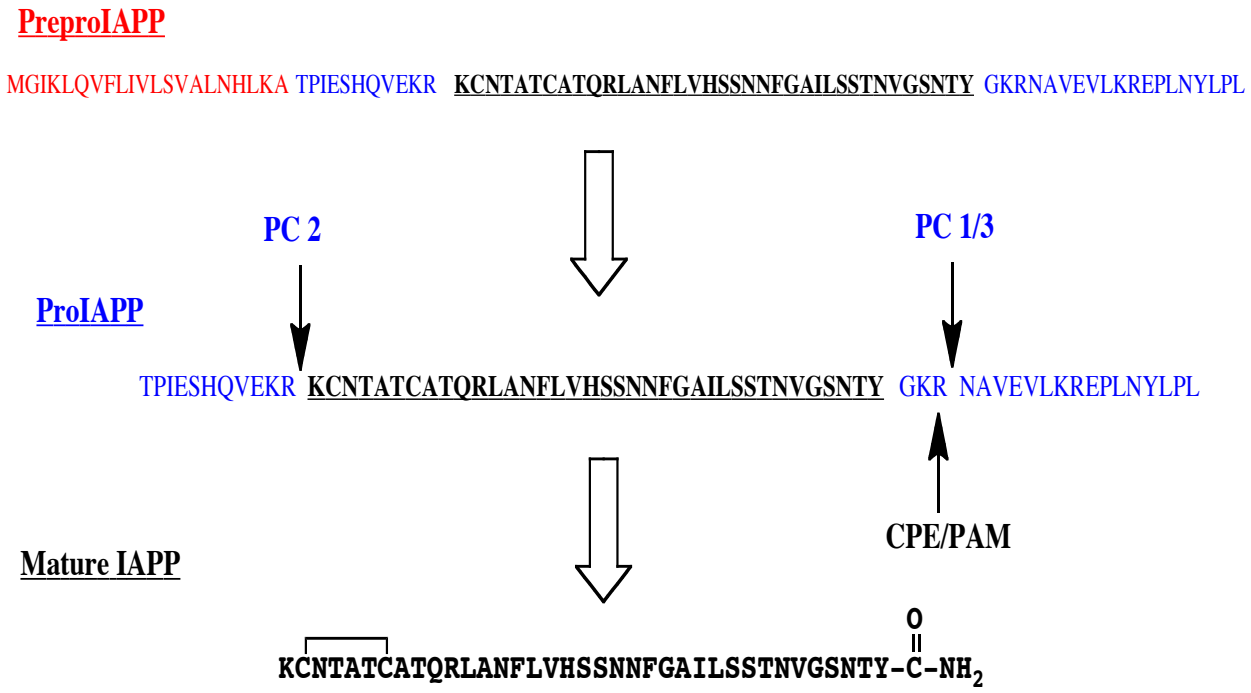

Figure 1.4: Processing of prepro-IAPP to mature IAPP within the β-cells of the pancreas. The 22-residue N-terminal leader sequence (red) of prepro-IAPP is cleaved after transport to the rough endoplasmic reticulum. ProIAPP (blue flanking regions) is packaged into secretory vesicles and is matured by PC2 at the N-terminus and PC1/3 at the C-terminus. CPE and PAM further process proIAPP into the mature form (black) with a resulting amidated C-terminus and disulfide bond between Cys-2 and Cys-7.

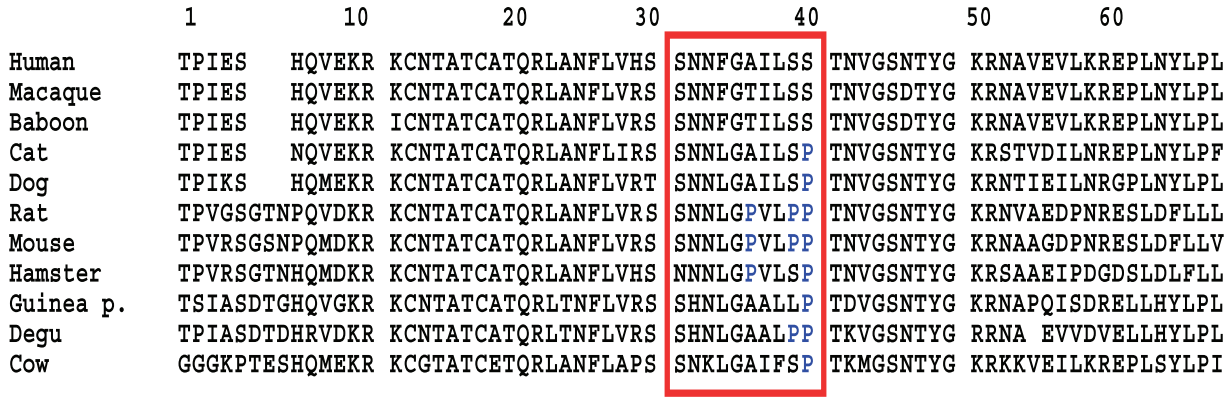

Figure 1.5: Amino acid sequences of human proIAPP and a number of mammalian species. The residues are numbered according to the human sequence. Highlighted in the red box, residues 31-40 of proIAPP correspond to the 20-29 region of the mature form. This region contains a significant number of mutations across all species compared to human IAPP, most notably by a number of proline residues that are known to inhibit amyloid formation. The first five species including human (human to dog) all form islet amyloid deposits *in vivo* and develop type 2 diabetes. The bottom six species (mouse to cow) have not been found to form islet amyloid and are not known to develop type 2 diabetes. Figure adapted from reference (196).

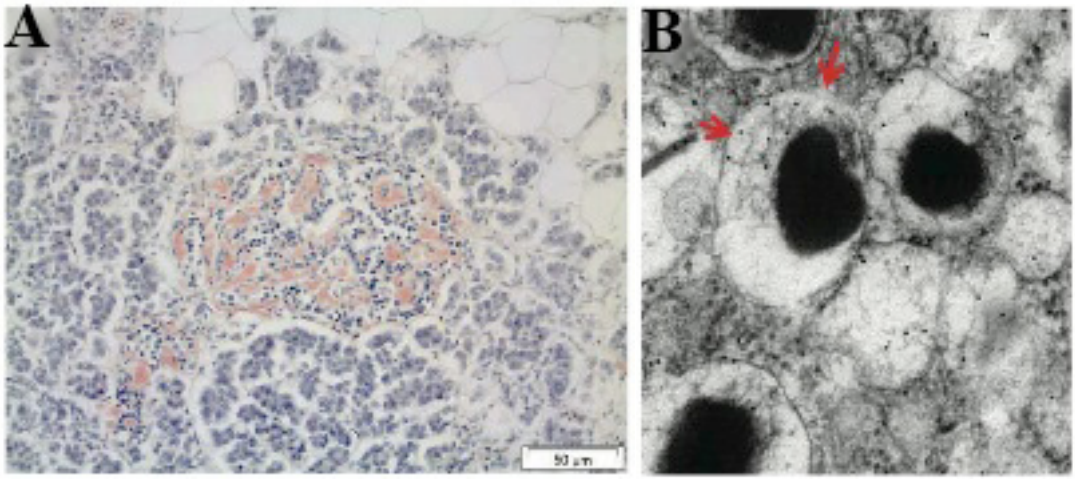

Figure 1.6: Human pancreatic islets and β-cells with IAPP amyloid deposition. (A) Pancreatic islet stained with Congo red displaying extracellular amyloid deposits. Scale bar is 50 μm. (B) Electron micrograph of a portion of a β-cell focusing on the granules. Small intragranular fibrils in the halo region are immunolabeled with proIAPP specific antibodies (red arrows). Adapted from reference (196).

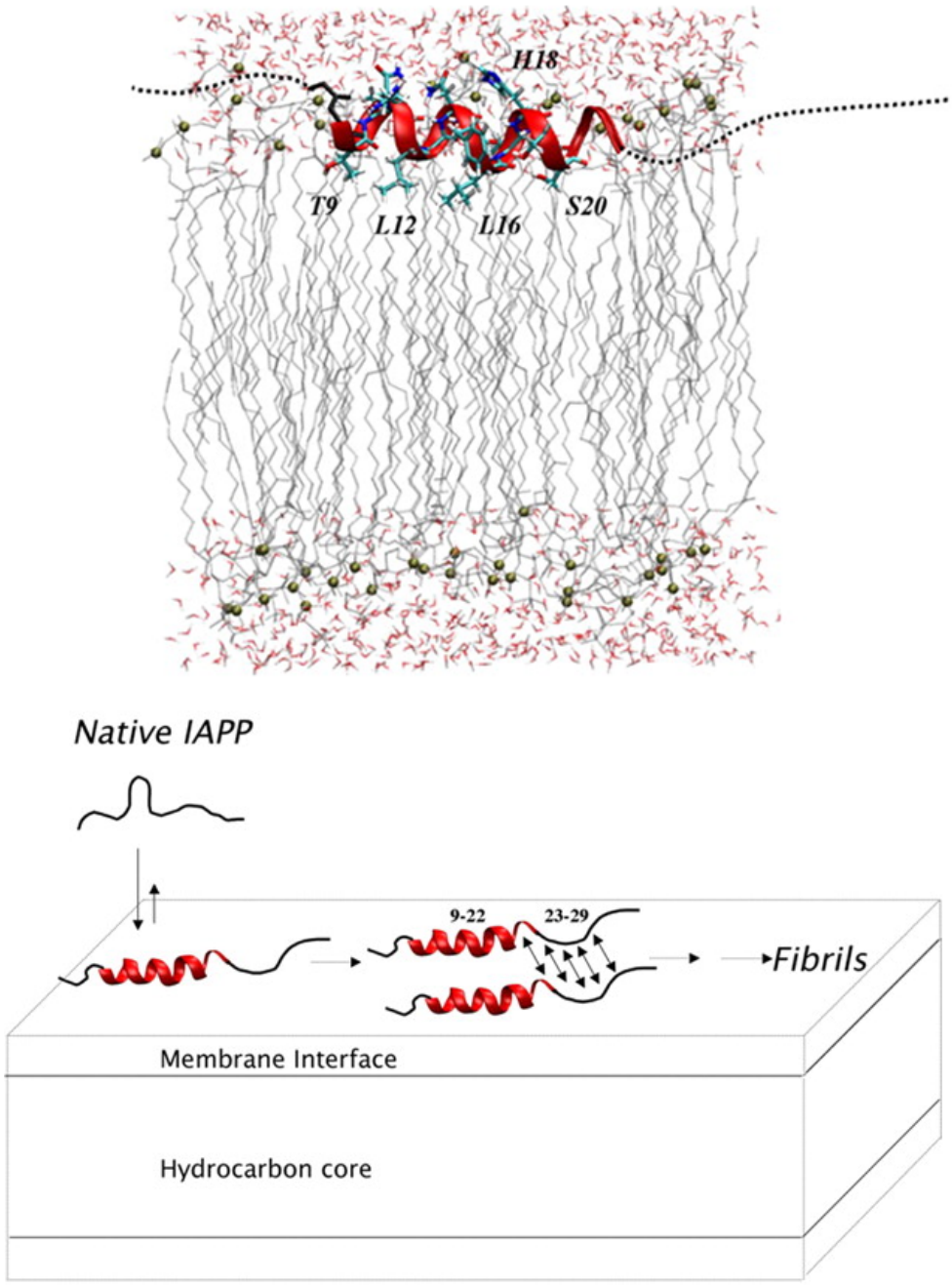

Figure 1.7: Structural and mechanistic models of IAPP-membrane interactions based on electron paramagnetic resonance spectroscopy. Top, residues 9-20 of IAPP are shown in an α-helical conformation interacting with the lipid bilayer. The dashed lines represent the N- and C-termini that were not detected to interact with the membrane. Phosphates are depicted as gold spheres. Bottom, model for membrane-bound amyloid formation by IAPP. Interaction of the helical portion of the protein drives the normally unstructured peptide to interact with the lipid bilayer. The C-terminal portion of the peptide that does not interact with the membrane is predicted to interact and initiate amyloid formation. Figure adapted from reference (173).

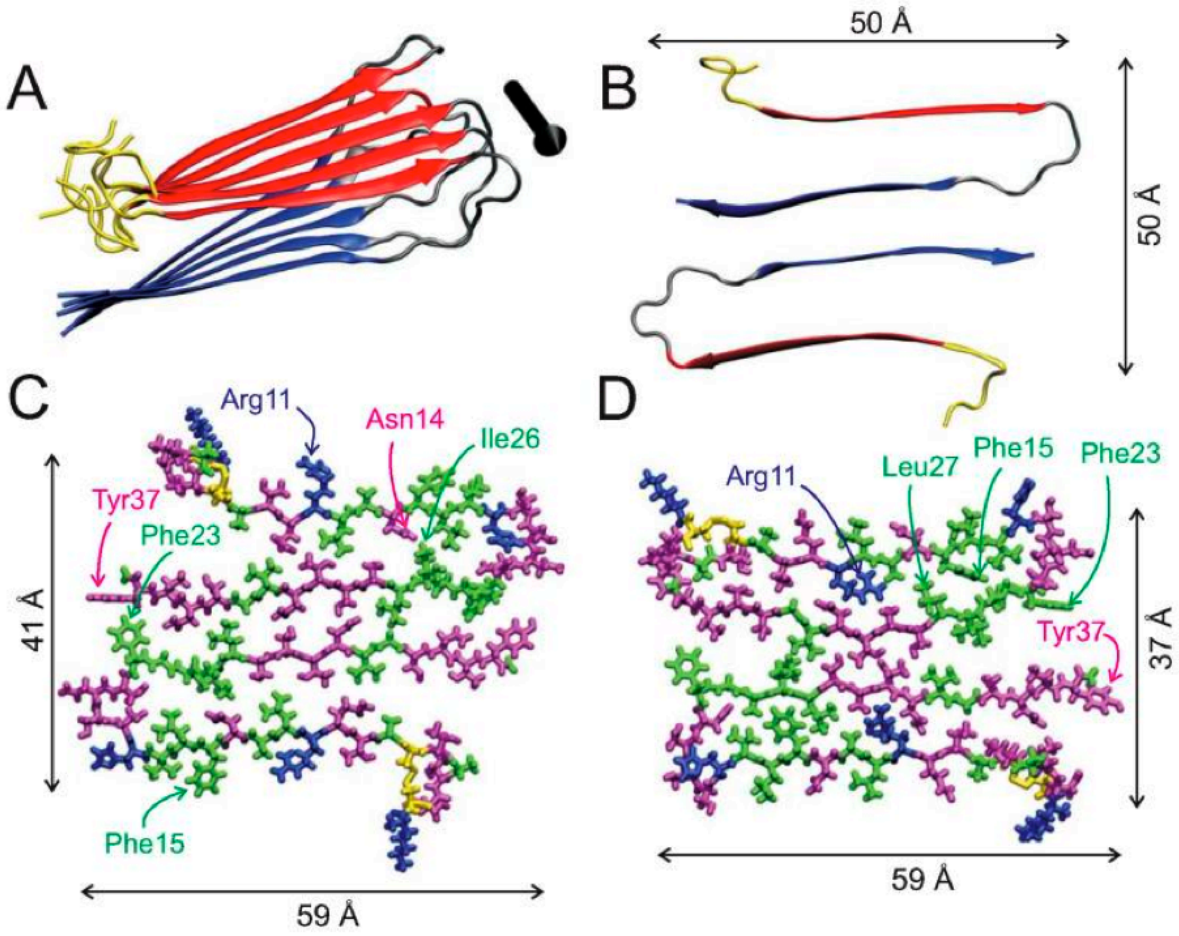

Figure 1.8: Structural models for IAPP protofibrils derived from solid-state NMR data. (A) A short segment of a cross β-sheet protofibril. The black arrow indicates the fibril axis. The unstructured N-terminal region comprising residues 1-7 is colored yellow. Residues 8-17 form the N-terminal β-strands (red) and residues 28-37 form the C-terminal β-strands (blue). (B) Ribbon representation of single peptide chains from two interacting protofibrils, as viewed down the axis of the fibril. (C) and (D) All-atom representations of two probable models depicting side chain contacts derived from (B). The differences between the two models are the different sets of side chain contacts between the β-sheet layers of the two protofibrils. Hydrophobic residues are shown in green, polar residues in magenta, positively charged residues in blue and the cysteine residues in yellow. Model D is less likely to form amyloid because it buries the charged Arg in a hydrophobic environment. Adapted from reference (20).

1.4 Tables

Disease	Aggregating protein or peptide	Number of residues[a]	Native structure of protein or peptide[b]
Neurodegenerative diseases			
Alzheimer's disease[c]	Amyloid β peptide	40 or 42[f]	Natively unfolded
Spongiform encephalopathies[c,e]	Prion protein or fragments thereof	253	Natively unfolded (residues 1–120) and α-helical (residues 121–230)
Parkinson's disease[c]	α-Synuclein	140	Natively unfolded
Dementia with Lewy bodies[c]	α-Synuclein	140	Natively unfolded
Frontotemporal dementia with Parkinsonism[c]	Tau	352–441[f]	Natively unfolded
Amyotrophic lateral sclerosis[c]	Superoxide dismutase 1	153	All-β, Ig like
Huntington's disease[d]	Huntingtin with polyQ expansion	3144[g]	Largely natively unfolded
Spinocerebellar ataxias[d]	Ataxins with polyQ expansion	816[g,h]	All-β, AXH domain (residues 562–694); the rest are unknown
Spinocerebellar ataxia 17[d]	TATA box-binding protein with polyQ expansion	339[g]	α+β, TBP like (residues 159–339); unknown (residues 1–158)
Spinal and bulbar muscular atrophy[d]	Androgen receptor with polyQ expansion	919[g]	All-α, nuclear receptor ligand-binding domain (residues 669–919); the rest are unknown
Hereditary dentatorubral-pallidoluysian atrophy[d]	Atrophin-1 with polyQ expansion	1185[g]	Unknown
Familial British dementia[d]	ABri	23	Natively unfolded
Familial Danish dementia[d]	ADan	23	Natively unfolded
Nonneuropathic systemic amyloidoses			
AL amyloidosis[c]	Immunoglobulin light chains or fragments	~90[f]	All-β, Ig like
AA amyloidosis[c]	Fragments of serum amyloid A protein	76–104[f]	All-α, unknown fold
Familial Mediterranean fever[c]	Fragments of serum amyloid A protein	76–104[f]	All-α, unknown fold
Senile systemic amyloidosis[c]	Wild-type transthyretin	127	All-β, prealbumin like
Familial amyloidotic polyneuropathy[d]	Mutants of transthyretin	127	All-β, prealbumin like
Hemodialysis-related amyloidosis[c]	β2-microglobulin	99	All-β, Ig like
ApoAI amyloidosis[d]	N-terminal fragments of apolipoprotein AI	80–93[f]	Natively unfolded
ApoAII amyloidosis[d]	N-terminal fragment of apolipoprotein AII	98[i]	Unknown
ApoAIV amyloidosis[c]	N-terminal fragment of apolipoprotein AIV	~70	Unknown
Finnish hereditary amyloidosis[d]	Fragments of gelsolin mutants	71	Natively unfolded
Lysozyme amyloidosis[d]	Mutants of lysozyme	130	α+β, lysozyme fold
Fibrinogen amyloidosis[d]	Variants of fibrinogen α-chain	27–81[f]	Unknown
Icelandic hereditary cerebral amyloid angiopathy[d]	Mutant of cystatin C	120	α+β, cystatin like
Nonneuropathic localized diseases			
Type II diabetes[c]	Amylin, also called islet amyloid polypeptide (IAPP)	37	Natively unfolded
Medullary carcinoma of the thyroid[c]	Calcitonin	32	Natively unfolded
Atrial amyloidosis[c]	Atrial natriuretic factor	28	Natively unfolded
Hereditary cerebral haemorrhage with amyloidosis[d]	Mutants of amyloid β peptide	40 or 42[f]	Natively unfolded
Pituitary prolactinoma	Prolactin	199	All-α, 4-helical cytokines
Injection-localized amyloidosis[c]	Insulin	21 + 30[j]	All-α, insulin like
Aortic medial amyloidosis[c]	Medin	50[k]	Unknown
Hereditary lattice corneal dystrophy[d]	Mainly C-terminal fragments of kerato-epithelin	50–200[f]	Unknown
Corneal amylodosis associated with trichiasis[c]	Lactoferrin	692	α+β, periplasmic-binding protein like II
Cataract[c]	γ-Crystallins	Variable	All-β, γ-crystallin like
Calcifying epithelial odontogenic tumors[c]	Unknown	~46	Unknown
Pulmonary alveolar proteinosis[d]	Lung surfactant protein C	35	Unknown
Inclusion-body myositis[c]	Amyloid β peptide	40 or 42[f]	Natively unfolded
Cutaneous lichen amyloidosis[c]	Keratins	Variable	Unknown

Table 1.1: List of amyloid-associated human diseases and their respective amyloidogenic proteins. Adapted from reference (1). The number of residues and native structure of each protein is also listed, which refer to the mature, fibril forming protein not precursors.

1.5 References

1. Chiti, F., Dobson, C.M. (2006) Protein misfolding, functional amyloid and human disease, *Annu. Rev. Biochem.* **75**, 333-366.

2. Sipe, J.D., Benson, M.D., Buxbaum, J.N., Ikeda, S.-I., Merlini, G., Saraiva, M.J.M., Westermark, P. (2010) Amyloid fibril protein nomenclature: 2010 recommendations from the nomenclature committee of the International Society of Amyloidosis, *Amyloid* **17**, 101-104.

3. Cohen, A.S., Calkins, E. (1959) Electron microscopic observation on a fibrous component in amyloid of diverse origins, *Nature* **183**, 1202-1203.

4. Anguiano, M., Nowak, R.J., Lansbury, P.T.J. (2002) Protofibrillar islet amyloid polypeptide permeabilizes synthetic vesicles by a pore-like mechanism that may be relevant to type II diabetes, *Biochemistry* **41**, 11338-11343.

5. Glabe, C.G. (2008) Structural classification of toxic amyloid oligomers, *J. Biol. Chem.* **283**, 29639-29643.

6. Lashuel, H.A., Hartley, D., Petre, B.M., Walz, T., Lansbury, P.T.J. (2002) Neurodegenerative disease: amyloid pores from pathogenic mutations, *Nature* **418**, 291.

7. Mirzabekov, T.A., Lin, M., Kagan, B.L. (1996) Pore formation by the cytotoxic islet amyloid peptide amylin, *J. Biol. Chem.* **271**, 1988-1992.

8. Porat, Y., Kolusheva, S., Jelinek, R., Gazit, E. (2003) The human islet amyloid polypeptide formstransient membrane-active prefibrillar assemblies, *Biochemistry* **42**, 10971-10977.

9. Quist, A., Doudevski, I., Lin, H., Azimova, R., Ng, D., Frangione, B., Kagan, B., Ghiso, J., Lal, R. (2005) Amyloid ion channels: a common structural link for protein-misfolding disease, *Proc. Natl. Acad. Soc. U.S.A.* **102**, 10427-10432.

10. Zraika, S., Hull, R.L., Verchere, C.B., Clark, A., Potter, K.J., Fraser, P.E., Raleigh, D.P., Kahn, S.E. (2010) Toxic oligomers and islet beta cell death: guilty by association or convicted by circumstantial evidence?, *Diabetologia* **53**, 1046-1056.

11. Bladen, H.A., Nylen, M.U., Glenner, G.G. (1966) The ultrastructure of human amyloid as revealed by the negative staining technique, *J. Ultra. Res.* **14**, 449-459.

12. Harper, J.D., Lieber, C.M., Lansbury, P.T. (1997) Atomic force microscopic imaging of seeded fibril formation and fibril branching by the Alzheimer's disease amyloid-β protein, *Chem. Biol.* **4**, 951-959.

13. Tycko, R. (2011) Solid state NMR studies of amyloid fibril structure, *Annu. Rev. Phys. Chem* **62**, 279-299.

14. O'Nuallain, B., Williams, A.D., Westermark, P., Wetzel, R. (2004) Seeding specificity in amyloid growth induced by heterologous fibrils, *J. Biol. Chem.* **279**, 17490-17499.

15. Qiang, W.Q.W., Yau, W.M., Tycko, R. (2011) Structural evolution of Iowa mutant beta-amyloid fibrils from polymorphic to homogeneous states under repeated seeded growth, *J. Am. Chem. Soc.* **133**, 4018-4029.

16. Colletier, J.-P., Laganowsky, A., Landau, M., Zhao, M., Soriaga, A.B., Goldschmidt, L., et. al (2011) Molecular basis for amyloid-β polymorphism, *Proc. Natl. Acad. Soc. U.S.A.* **108**, 16938-16943.

17. Sawaya, M.R., Sambashivan, S., Nelson, R., Ivanova, I.I., Sievers, S.A., Apostol, M.I., et. al (2007) Atomic structures of amyloid cross-β spines reveal varied steric zippers, *Nature* **447**, 453-457.

18. Nelson, R., Sawaya, M.R., Balbirnie, M., Madsen, A., Riekel, C., Grothe, R., Eisenberg, D. (2005) Structure of the cross-β spine of amyloid-like fibrils, *Nature* **435**, 773-778.

19. Strasfeld, D.B., Ling, Y.L., Gupta, R., Raleigh, D.P., Zanni, M.T. (2009) Strategies for extracting structural information from 2D IR spectroscopy of amyloid: application to islet amyloid polypeptide, *J. Phys. Chem. B* **113**, 15679-15691.

20. Luca, S., Yau, W.-M., Leapman, R., Tycko, R. (2007) Peptide conformation and supramolecular organization in amylin fibrils: constraints from solid-state NMR *Biochemistry* **46**, 13505-13522.

21. Balbach, J.J., Petkova, A.T., Oyler, N.A., Antzutkin, O.N., Gordon, D.J., Meredith, S.C., Tycko, R. (2002) Supramolecular structure in full-length Alzheimer's beta-amyloid fibrils: evidence for a parallel beta-sheet organization from solid-state nuclear magnetic resonance, *Biophys. J.* **83**, 1205-1216.

22. Wasmer, C., Lange, A., Melckebeke, H.V., Siemer, A.B., Riek, R., Meier, B.H. (2008) Amyloid fibrils of HET-s(218-289) prionform a β-solenoid with a triangular hydrophobic core, *Science* **319**, 1523-1526.

23. Kajava, A.V., Steven, A.C. (2006) Beta‐rolls, beta‐helices, and other beta‐solenoid proteins, *Adv. Prot. Chem.* **73**, 55-96.

24. Margittai, M., Langen, R. (2008) Fibrils with parallel in-register structure constitute a major class of amyloid fibrils: molecular insights fromelectronparamagnetic resonance spectroscopy, *Q. Rev. Biophys.* **41**, 265-297.

25. Nerelius, C., Fitzen, M., Johansson, J. (2010) Amino acid sequence determinants and molecular chaperones in amyloid fibril formation, *Biochem. Biophys. Res. Comm.* **396**, 2-6.

26. Maurer-Stroh, S., Debulpaep, M., Kuemmerer, N. Lopez, M., Martins, I., Reumers, J., et. al (2010) Exploring the sequence determinants of amyloid structure using position-specific scoring matrices, *Nat. Methods* **7**, 237-242.

27. Moriarty, D.F., Raleigh, D.P. (1999) Effects of sequential proline substitutions on amyloid formation by human amylin 20-29, *Biochemistry* **38**, 1811-1818.

28. Abedini, A., Raleigh, D.P. (2006) Destabilization of human IAPP amyloid fibrils by proline mutations outside of the putative amyloidogenic domain: is there a critical amyloidogenic domain in human IAPP?, *J. Mol. Biol.* **355**, 274-281.

29. Guijarro, J.L., Sunde, M., Jones, J.A., Campbell, I.D., Dobson, C.M. (1998) Amyloid fibril formation by an SH3 domain, *Proc. Natl. Acad. Soc. U.S.A.* **95**, 4224-4228.

30. Uversky, V.N., Fink, A.L. (2004) Conformational constraints for amyloid formation: The importance of being unfolded, *Biochim. Biophys. Acta.* **1698**, 131-153.

31. Dobson, C.M. (2003) Protein folding and misfolding, *Nature* **426**, 884-890.

32. Xue, W.-F., Homans, S.W., Radford, S.E. (2008) Systematic analysis of nucleation dependent polymerization reveals new insights into the mechanism of amyloid self-assembly, *Proc. Natl. Acad. Soc. U.S.A.* **105**, 8926-8931.

33. Harper, J.D., Lansbury, P.T. (1997) Models of amyloid seeding in Alzheimer's disease and scrapie: Mechanistic truths and physiological consequences of the time-dependent solubility of amyloid proteins, *Annu. Rev. Biochem.* **66**, 385-407.

34. Lansbury, P.T. (1997) Structural, neurology: are seeds at the root of neuronal degeneration?, *Neuron* **19**, 1151-1154.

35. Ventura, S., Zurdo, J., Narayanan, S., Parreno, M., Mangues, R., Reif, B., et. al (2004) Short amino acid stretches can mediate amyloid formation in globular proteins: the Src homology 3 (SH3) case, *Proc. Natl. Acad. Soc. U.S.A.* **101**, 7258-7263.

36. Lara, C., Adamcik, J., Jordens, S., Mezzenga, R. (2011) General self-assembly mechanism converting hydrolyzed globular proteins into giant multistranded amyloid ribbons, *Biomacromolecules* **12**, 1868-1875.

37. Puchtler, H., Sweat, F., Levine, M. (1962) On the binding of Congo red by amyloid, *J. Histochem. Cytochem.* **10**, 355-364.

38. Levine, H. (1995) Thioflavin-T interactions with amyloid β-sheet structures, *Amyloid* **2**, 1-6.

39. Sulatskaya, A.I., Maskevich, A.A., Kuznetsova, I.M., Uversky, V.N., Turoverov, K.K. (2010) Fluorescence quantum yield of thioflavin T in rigid isotropic solution and incorporated into the amyloid fibrils, *Plos One* **5**, e15385.

40. Stsiapura, V.I., Maskevich, A.A., Kuzmitsky, V.A., Uversky, V.N., Kuznetsova, U.M., Turoverov, K.K. (2008) Thioflavin-T as a molecular rotor: fluorescent properties of thioflavin T in solvents with different viscosities, *J. Phys. Chem. B* **112**, 15893-15902.

41. Rodríguez-Rodríguez, C., Rimola, A., Rodríguez-Santiago, L., Ugliengo, P., Álvarez-Larena, A., Gutiérrez-de-Terán, H., et al. (2010) Crystal structure of thioflavin-T and its binding to amyloid fibrils: insights at the molecular level, *Chem. Commun.* **46**, 1156-1158.

42. Khurana, R., Coleman, C., Ionescu-Zanetti, C., Carter, S.A., Krishna, V., Grover, R.K., Roy, R., Singh, S. (2005) Mechanism of thioflavin T binding to amyloid fibrils., *J. Struct. Biol.* **151**, 229-238.

43. Williamson, J.A., Miranker, A.D. (2007) Direct detection of transient alpha-helical states in islet amyloid polypeptide, *Prot. Sci.* **16**, 110-117.

44. Abedini, A., Raleigh, D.P. (2009) A role for helical intermediates in amyloid formation by natively unfolded polypeptides?, *Phys. Biol.* **6**, 015005.

45. Kirkitadve, M.D., Condron, M.M., Teplow, D.B. (2001) Identification and characterization of key kinetic intermediates in amyloid beta-protein fibrillogenesis, *J. Mol. Biol.* **312**, 1103-1119.

46. Knowles, T.P.J., White, D.A., Abate, A.R., Agresti, J.J., Cohen, S.I.A., Sperling, R.A., De Genst, E.J., et. al (2011) Observation of spatial propagation of amyloid assembly from single nuclei, *Proc. Natl. Acad. Soc. U.S.A.* **108**, 14746-17751.

47. Knowles, T.P.J., Waudby, C.A., Devlin, G.L., Cohen, S.I.A., Sperling, Aguzzi, A., Vendruscolo, M., et. al (2009) An analytical solution to the kinetics of breakable filament assembly, *Science* **326**, 1533-1537.

48. Reddy, G., Straub, J.E., Thirumalai, D. (2009) Dynamics of locking of peptides onto growing amyloid fibrils, *Proc. Natl. Acad. Soc. U.S.A.* **106**, 11948-11953.

49. Thirumalai, D., Reddy, G., Straub, J.E. (2012) Role of water in protein aggregation and amyloid polymorphism, *Acc. Chem. Res.* **45**, 83-92.

50. Tran, H., Mao, A., Pappu, R. (2008) Role of backbone-solvent interactions in determining conformational equilibria of intrinsically disordered polypeptides, *Proc. Natl. Acad. Soc. U.S.A.* **384**, 279-297.

51. Lorenzo, A., Razzaboni, B., Weir, G.C., Yankner, B.A. (1994) Pancreatic islet cell toxicity of amylin associated with type-2 diabetes mellitus, *Nature* **368**, 756-760.

52. Yankner, B.A., Dawes, L.R., Fisher, S., Villa-Komaroff, L., Oster-Granite, M.L., Neve, R.L. (1989) Neurotoxicity of a fragment of the amyloid precursor associated with Alzheimer's disease, *Science* **245**, 417-420.

53. Yankner, B.A., Duffy, L.K., Kirschner, D.A. (1990) Neurotrophic and neurotoxic effects of amyloid protein: reversal by tachykinin neuropeptides, *Science* **250**, 279-282.

54. Merlini, G., Westermark, P. (2004) The systemic amyloidosis: clearer understanding of the molecular mechanisms offer hope for more effective therapies, *J. Intern. Med.* **255**, 159-178.

55. Pepys, M.B. (2006) Amyloidosis, *Annu. Rev. Med.* **57**, 233-241.

56. Maji, S.K., Perrin, M.H., Sawaya, M.R., Jessberger, S., Vadodaria, K., Rissman, R.A., et. al (2009) Functional amyloids as natural storage of peptide hormones in pituitary secretory granules, *Science* **325**, 328-332.

57. Chapman, M.R., Robinson, L.S., Pinkner, J.S., Roth, R., Heuser, J., et al. (2002) Role of Escherichia coli curli operons in directing amyloid fiber formation, *Science* **295**, 851-855.

58. Berson, J.F., Theos, A.C., Harper, D.C., Tenza, D., Raposo, G., Marks, M.S. (2003) Proprotein convertase cleavage liberates a fibrillogenic fragment of a resident glycoprotein to initiate melanosome biogenesis, *J. Cell. Biol.* **16**, 521-533.

59. Greenwald, J., and Riek, R. (2010) Biology of amyloid: structure, function, and regulation, *Structure* **18**, 1244-1260.

60. Watt, B., Tenza, D., Lemmon, M.A., Kerje, S., Raposo, G., Andersson, L., Marks, M.S. (2011) Mutations in or near the transmembrane domain alter PMEL amyloid formation from functional to pathogenic, *Plos Genet.* **7**, e1002286.

61. Winklhofer, K.F., Tatzelt, J., Haass, C. (2008) The two faces of protein misfolding: gain- and loss-of-function in neurodegenerative diseases, *EMBO* **27**, 336-349.

62. Glabe, C.G. (2006) Common mechanisms of amyloid oligomer pathogenesis in degenerative disease, *J. Neurobiol. Aging* **27**, 570-575.

63. Friedman, R., Pellarin, R., Caflisch, A. (2009) Amyloid aggregation on lipid bilayers and its impact on membrane permeability, *J. Mol. Biol.* **387**, 407-415.

64. Costes, S., Huang, C.J., Gurlo, T., Daval, M., Matveyenko, A.V., Rizza, R.A., Butler, A.E., Butler, P.C. (2011) Beta-cell dysfunctional ERAD/ubiquitin/proteasome system in type 2 diabetes mediated by IAPP-induced UCH-L1 deficiency, *Diabetes* **60**, 227-238.

65. Salminen, A., Kauppinen, A., Suuronen, T., Kaarniranta, K., Ojala, J. (2009) ER stress in Alzheimer's disease: a novel neuronal trigger for inflammation and Alzheimer's pathology, *J. Neuroinflamm.* **6**, 41-54.

66. Huang, C.J., Lin, C.Y., Haataja, L., Gurlo, T., Butler, A.E., Butler, P.C. (2007) High expression rates of human islet amyloid polypeptide induce endoplasmic reticulum stress mediated beta-cell apoptosis, a characteristic of humans with type 2 but not type 1 diabetes, *Diabetes* **56**, 2016-2027.

67. Olzscha, H., Schermann, S.M., Woerner, A.C., Pinkert, S., Hecht, M.H., Tartaglia, G.G., et. al (2011) Amyloid-like aggregates sequester numerous metastable proteins with essential cellular functions, *Cell* **144**, 67-78.

68. Mishra, R., Bullic, B., Sellin, D., Jha, S., Waldman, H., Winter, R. (2008) Small-molecule inhibitors of islet amyloid polypeptide fibril formation, *Angew. Chem. Int. Ed.* **47**, 4679-4682.

69. Necula, M., Kayed, R., Milton, S., Glabe, C.G. (2007) Small molecule inhibitors of aggregation indicate that amyloid beta oligomerization and fibrillization pathways are independent and distinct, *J. Biol. Chem.* **282**, 10311-10324.

70. Blazer, L.L., Neubig, R.R. (2009) Small molecule protein–protein interaction inhibitors as CNS therapeutic agents: Current progress and future hurdles, *Neuropsychopharmacology* **34**, 126-141.

71. Whitty, A., Kumaravel, G. (2006) Between a rock and a hard place?, *Nat. Chem. Biol.* **2**, 112-118.

72. Garber, K. (2012) Amyloid disease drug approved, *Nat. Biotechnol.* **30**, 121.

73. Bieschke, J., Herbst, M., Wiglenda, T., Friedrich, R.P., Boeddrich, A., Schiele, F., et. al (2011) Small-molecule conversion of toxic oligomers to nontoxic β-sheet-rich amyloid fibrils, *Nat. Chem. Biol.* **8**, 93-101.

74. Mulder, H., Leckstrom, A., Uddman, R. Ekbald, E., Westermark, P., Sundler, F. (1995) Islet amyloid polypeptide (amylin) is expressed in sensory neurons, *Neurosci.* **15**, 7625-7632.

75. Mulder, H., Ekelund, M., Ekbald, E., Sundler, F. (1997) Islet amyloid polypeptide in the gut and pancrease: Localization, ontogeny and gut motility effects, *Peptides* **18**, 771-783.

76. Ferrier, G., Pierson, A., Jones, P., Bloom, S., Girgis, S., Legon, S. (1989) Expression of rat amylin (IAPP/DAP) gene, *J. Mol. Endocrinol.* **3**, R1-R4.

77. Butler, P.C., Chou, J., Carter, W.B., Wang, Y.N., Bu, B.H., Chang, D., et. al (1990) Effects of meal ingestion on plasma IAPP concentration in NIDDM and nondiabetic humans, *Diabetes* **39**, 752-756.

78. Sanke, T., Hanabusa, T., Nakano, Y., Oki, C., Okai, K., Fujimoto, W.Y., et. al (1991) Plasma islet amyloid polypeptide (IAPP) levels and their responses to oral glucose in type-2 (non-insulin-dependent) diabetic patients, *Diabetologia* **34**, 129-132.

79. Knight, J.D., Williamson, J.A., Miranker, A.D. (2008) Interaction of membrane-bound islet amyloid polypeptide with soluble and crystalline insulin, *Prot. Sci.* **17**, 1-7.

80. Jaikaran, E.T., Nilsson, M.R., Clark, A. (2003) Pancreatic β-cell granule peptides form heteromolecular complexes which inhibit islet amyloid polypeptide fibril formation, *Biochem. J.* **377**, 709-716.

81. Cooper, G.J.S. (1994) IAPP compared with calcitonin gene-related peptide: Structure, biology, and relevance to metabolic disease, *Endocrine Rev* **15**, 163-201.

82. Castillo, M.J., Scheen, A.J. LeFebvre, P.J. (1995) Amylin/islet amyloid polypeptide: Biochemistry, physiology and pathophysiology, *Diab. Metab.* **21**, 3-25.

83. Leighton, B., Cooper, G.J.S. (1988) Pancreatic IAPP and calcitonin gene-related peptide cause resistance to insulin in skeletal-muscle *in vitro*, *Nature* **335**, 632-635.

84. Makin, S.O., Serpell, L.C. (2004) Structural characterization of islet amyloid polypeptide fibrils, *J. Mol. Biol.* **335**, 1279-1288.

85. Sanke, T., Bell, G.I. Sample, C., Rubenstein, A.H., Steiner, D.F. (1988) An islet amyloid peptide is derived from an 89-amino acid precursor by proteolytic processing, *J. Biol. Chem.* **263**, 17243-17246.

86. Jaikaran, E.T., Higham, C.E., Serpell, L.C., Zurdo, J., Gross, M., Clark, A., Fraser, P.E. (2001) Identification of a novel human islet amyloid polypeptide β-sheet domain and factors influencing fibrillogenesis, *J. Mol. Biol.* **308**, 515-525.

87. Zheng, X., Ren, W., Zhang, S., Liu, J., Li, S., Li, J., et. al (2010) Serum levels of proamylin and amylin in normal subjects and patients with impaired glucose regulation and type 2 diabetes mellitus, *Acta. Diabetol.* **47**, 265-270.

88. Higham, C.E., Hull, R.L., Lawrie, L., Shennan, K.I., Morris, J.F., Birch, N.P., Docherty, K., Clark, A. (2000) Processing of synthetic pro-islet amyloid polypeptide (proIAPP) "amylin" by recombinant prohormone convertase enzymes, PC2 and PC 3, in vitro, *Eur. J. Biochem.* **267**, 4998-5004.

89. Hou, X., Ling, Z., Quartier, E., Foriers, A., Schuit, F., Pipeleers, D., Van Schravendijk, C. (1999) Prolonged exposure of pancreatic beta cells to raised glucose concentrations results in increased cellular content of islet amyloid polypeptide precursors, *Diabetologia* **42**, 188-194.

90. Paulsson, J.F., Andersson, A., Westermark, P., Westermark, G.T. (2006) Intracellular amyloid-like deposits contain unprocessed pro islet amyloid polypeptide (proIAPP) in beta-cells of transgenic mice overexpressing human IAPP and transplanted human islets, *Diabetologia* **49**, 1237-1246.

91. Marzban, L., Soukhatcheva, G., Verchere, C.B. (2005) Role of carboxypeptidase E in processing of pro-islet amyloid polypeptide in β-cells, *Endocrinology* **146**, 1808-1817.

92. Milgram, S., Kho, S., Martin, G., Mains, R., Eipper, B. (1997) Localization of integral membrane peptidylglycine alpha- amidating monooxygenase in neuroendocrine cells, *J. Cell. Sci.* **110**, 695-706.

93. Cooper, G.J., Willis, A.C., Clark, A., Turner, R.C., Sim, R.B., Reid, K.B.M. (1987) Purification and characterization of a peptide from amyloid-rich pancreases of type 2 diabetic patients, *Proc. Natl. Acad. Soc. U.S.A.* **84**, 8628-8632.

94. Westermark, P., Wernstedt, C., Wilander, E., Hayden, D.W., O'Brien, T.D., Johnson, K.H. (1987) Amyloid fibrils in human insulinoma and islets of Langerhans of the diabetic cat are derived from a neuropeptide-like protein also present in normal islet cells, *Proc. Natl. Acad. Soc. U.S.A.* **84**, 3881-3885.

95. Bell, E.T. (1952) Hyalinization of the islets of Langerhans in diabetes mellitus, *Diabetes* **1**, 341-344.

96. Maloy, A.L., Longnecker, D.S., Greenberg, E.R. (1981) The relation of islet amyloid to the clinical type of diabetes, *Hum. Pathol.* **12**, 917-922.

97. Westermark, P. (1995). *Islet amyloid polypeptide and amyloid in the islets of Langerhans*. Diabetes: Clinical Science in Practice (Leslie, R. D. G., Robbins, D., Ed.), Cambridge Univ. Press, Cambridge, UK.

98. Zhao, H.L., Lai, F.M., Tong, P.C., Zhong, D.R., Yang, D., Tomlinson, B., Chan, J.C. (2003) Prevalence and clinicopathological characteristics of islet amyloid in Chinese patients with type 2 diabetes, *Diabetes* **52**, 2759-2766.

99. Bell, E.T. (1959) Hyalinization of the islets of Langerhans in nondiabetic individuals, *Am. J. Pathol.* **35**, 801-805.

100. Ludwig, G., Heitner, H. (1967) Zur Häufigkeit der Inselamyloidose des Pankreas beim Diabetes mellitus, *Zschr Inn Med* **22**, 814-818.

101. Westermark, P. (1972) Quantitative studies of amyloid in the islets of Langerhans, *Upsala J. Med. Sci.* **77**, 91-94.

102. Johnson, K.H., Wernstedt, C., O'Brien, T.D., Westermark, P. (1991) Amyloid in the pancreatic islets of the cougar (Felis concolor) is derived from islet amyloid polypeptide (IAPP), *Comp. Biochem. Physiol. B* **98**, 115-119.

103. Martínez-Álvarez, R.M., Volkoff, H., Munoz Cueto, J.A., Delgado, M.J. (2008) Molecular characterization of calcitonin gene-related peptide (CGRP) related peptides (CGRP, amylin, adrenomedullin and adrenomedullin-2/intermedin) in goldfish (Carassius auratus):cloning and distribution, *Peptides* **29**, 1534-1543.

104. Miyazato, M., Nakazato, M., Shiomi, K., Aburaya, J., Kangawa, K., Matsuo, H., Matsukura, S. (1992) Molecular forms of islet amyloid polypeptide (IAPP/amylin) in four mammals, *Diab. Res. Clin. Pract.* **7**, 31-36.

105. Nishi, M., Chan, S.J., Nagamatsu, S., Bell, G.I., Steiner, D.F. (1989) Conservation of the sequence of islet amyloid polypeptide in five mammals is consistent with its putative role as an islet hormone, *Proc. Natl. Acad. Soc. U.S.A.* **86**, 5738-5742.

106. Westermark, G.T., Falkmer, S., Steiner, D.F., Chan, S.J., Engström, U., Westermark, P. (2002) Islet amyloid polypeptide is expressed in the pancreatic islet parenchyma of the teleostean fish, Myoxocephalus (Cottus) scorpius, *Comp. Biochem. Physiol. B* **133**, 119-125.

107. Westermark, P., Johnson, K.H., O'Brien, T.D., Betsholtz, C. (1992) Islet amyloid polypeptide: a novel controversy in diabetes research, *Diabetologia* **35**, 297-303.

108. Westermark, P., Engström, U., Johnson, K.H., Westermark, G.T., Betsholtz, C. (1990) Islet amyloid polypeptide: Pinpointing amino acid residues linked to amyloid fibril formation, *Proc. Natl. Acad. Soc. U.S.A.* **87**, 5036-5040.

109. Tenidis, K., Waldner, M., Bernhagen, J., Fischle, W., Bergmann, M., Weber, M., et. al (2000) Identification of a penta- and hexapeptide of islet amyloid polypeptide (IAPP) with amyloidogenic and cytotoxic properties, *J. Mol. Biol.* **295**, 1055-1071.

110. Tracz, S.M., Abedini, A., Driscoll, M., Raleigh, D.P. (2004) The role of aromatic interactions n amyloid formation by polypeptides: Analysis of peptides derived from human amylin, *Biochemistry* **43**, 15901-15908.

111. Cao, P., Tu, L.-H., Abedini, A., Levsh, O., Akter, R., Patsalo, V., Schmidt, A.M., Raleigh, D.P. (2012) Sensitivity of amyloid formation by human islet amyloid polypeptide to mutations at residue 20, *J. Mol. Biol.* **In Press**, DOI: 10.1016/j.jmb.2011.12.032.

112. Seino, S. (2001) S20G mutation of the amylin gene is associated with Type II diabetes in Japanese, *Diabetologia* **44**, 906-909.

113. Sakagashira, S., Sanke, T., Hanabusa, T., Shimomura, H., Ohagi, S., Kumagaye, K.Y., et. al (1996) Missense mutation of amylin gene (S20G) in Japanese NIDDM patients, *Diabetes* **45**, 1279-1281.

114. De Koning, E.J.P., Bodkin, N.L., Hansen, B.C., Clark, A. (1993) Diabetes mellitus in Macaca mulatta monkeys is characterized by islet amyloidosis and reduction in beta-cell population, *Diabetologia* **36**, 378-384.

115. Howard, C.F.J. (1978) Insular amyloidosis and diabetes mellitus in Macaca nigra, *Diabetes* **27**, 357-364.

116. Howard, C.F.J. (1986) Longitudinal studies on the development of diabetes in individual Macaca nigra, *Diabetologia* **29**, 301-306.

117. Johnson, K.H., Stevens, J.B. (1973) Light and electron microscopic studies of islet amyloid in diabetic cats, *Diabetes* **22**, 81-90.

118. Johnson, K.H., O'Brien, T.D., Betsholtz, C., Westermark, P. (1989) Islet amyloid, islet-amyloid polypeptide, and diabetes mellitus, *N. Engl. J. Med.* **321**, 513-518.

119. Butler, A.E., Jang, J., Gurlo, T., Carty, M.D., Soeller, W.C., Butler, P.C. (2004) Diabetes due to a progressive defect in beta-cell mass in rats transgenic for human islet amyloid polypeptide (HIP Rat): a new model for type 2 diabetes, *Diabetes* **53**, 1509-1516.

120. D'Alessio, D.A., Verchere, C.B., Kahn, S.E., Hoagland, V., Baskin, D.G., Palmiter, R.D., Ensinck, J.W. (1994) Pancreatic expression and secretion of human islet amyloid polypeptide in a transgenic mouse, *Diabetes* **43**, 1457-1461.

121. Fox, N., Schrementi, J., Nishi, M., Ohagi, S., Chan, S.J., Heisserman, J.A., et. al (1993) Human islet amyloid polypeptide transgenic mice as a model of non-insulin-dependent diabetes mellitus (NIDDM), *FEBS Lett.* **323**, 40-44.

122. Matveyenko, A.V., Butler, P.C. (2006) Islet amyloid polypeptide (IAPP) transgenic rodents as models for type 2 diabetes, *ILAR J.* **47**, 225-233.

123. Yagui, K., Kanatsuka, A., Makino, H. (1994) Construction of transgenic mouse system expressing human islet amyloid polypeptide, *Nippon. Rinsho.* **52**, 2746-2750.

124. Marzban, L., Tomas, A., Becker, T.C., Rosenberg, L., Oberholzer, J., Fraser, P.E., Halban, P.A., & Verchere, C.B. (2008) Small interfering RNA-mediated suppression of proislet amyloid polypeptide expression inhibits islet amyloid formation and enhances survival of human islets in culture, *Diabetes* **57**, 3047-3055.

125. Clark, A., Wells, C.A., Buley, I.D., Cruickshank, J.K., Vanhegan, R.I., Matthews, D.R., et. al (1988) Islet amyloid, increased A-cells, reduced B-cells and exocrine fibrosis: quantitative changes in the pancreas in type 2 diabetes, *Diab. Res.* **9**, 151-159.

126. Klöppel, G., Drenck, C.R. (1983) Immunzytochemische Morphometrie beim Typ-1- und Typ-2-Diabetes mellitus, *Deutsch. Med. Wschr.* **108**, 188-189.

127. Saito, K., Yaginuma, N., Takahashi, T. (1979) Differential volumetry of A, B and D cells in the pancreatic islets of diabetic and nondiabetic subjects, *Tohoku J. Exp. Med.* **129**, 273-283.

128. Kahn, S.E. (2000) The importance of the beta-cell in the pathogenesis of type 2 diabetes, *Am. J. Med.* **108**, 2s-8s.

129. Kawahara, M., Kuroda, Y., Arispe, N., Rojas, E. (2000) Alzheimer's beta-amyloid, human islet amylin, and prion protein fragment evoke intracellular free calcium elevations by a common mechanism in a hypothalamic GnRH neuronal cell line., *J. Biol. Chem.* **275**, 14077-14083.

130. Guardado-Mendoza, R., Davalli, A.M., Chavez, A.O., Hubbard, G.B., Dick, E.J., Majluf-Cruz, A., et. al (2009) Pancreatic islet amyloidosis, cell apoptosis, and cell proliferation are determinants of islet remodeling in type-2 diabetic baboons., *Proc. Natl. Acad. Soc. U.S.A.* **106**, 13992-12997.

131. Janson, J., Soeller, W.C., Roche, P.C., Nelson, R.T., Torchia, A.J., Kreutter, D.K., Butler, P.C. (1996) Spontaneous diabetes mellitus in transgenic mice expressing human islet amyloid polypeptide, *Proc. Natl. Acad. Soc. U.S.A.* **93**, 7283-7288.

132. O'Brien, T.D., Butler, A.E., Roche, P.C., Johnson, K.H., Butler, P.C. (1994) Islet amyloid polypeptide in human insulinomas. Evidence for intracellular amyloidogenesis, *Diabetes* **43**, 329-336.

133. Mulder, H., Ahren, B., Sundler, F. (1996) Islet amyloid polypeptide and insulin gene expression are regulated in parallel by glucose in vivo in rats, *Am. J. Physiol.* **271**, E1008-E1014.

134. Hanabusa, T., Kuba, K., Oki, C., Nakano, Y., Okai, K., Sanke, T., Nanjo, K. (1992) Islet amyloid polypeptide secretion from islet cells and its plasma concentration in patients with non-insulin-dependent diabetes mellitus, *Diabetes Res. Clin. Pratt.* **15**, 89-96.

135. Paulsson, J.F., Westermark, G.T. (2005) Aberrant processing of human proislet amyloid polypeptide results in increased amyloid production, *Diabetes* **54**, 2117-2125.

136. Krampert, M., Bernhagen, J., Schmucker, J., Horn, A., Schmauder, A., Brunner, H., et. al (2000) Amyloidogenicity of recombinant human pro-islet amyloid polypeptide (ProIAPP), *Chem. Biol.* **7**, 855-871.

137. Meng, F., Abedini, A., Song, B., Raleigh, D.P. (2007) Amyloid formation by pro-islet amyloid polypeptide processing intermediates: examination of the role of protein heparan sulfate interactions and implications for islet amyloid formation in type 2 diabetes, *Biochemistry* **46**, 12091-12099.

138. Park, K., and Verchere, C. B. (2001) Identification of a heparin binding domain in the N-terminal cleavage site of pro-islet amyloid polypeptide. Implications for islet amyloid formation, *J. Biol. Chem.* **276**, 16611-16616.

139. Abedini, A., Tracz, S. M., Cho, J. H., and Raleigh, D. P. (2006) Characterization of the heparin binding site In the N-Terminus of human pro-Islet amyloid polypeptide: Implications for amyloid formation, *Biochemistry* **45**, 9228-9237.

140. Shapiro, A.M.J., Lakey, J.R.T., Ryan, E.A., Korbutt, G.S., Toth, E.L., Warnock, G.L., et. al (2000) Islet transplantation in seven patients with type 1 diabetes mellitus using a glucocorticoid free immunosuppressive regiment, *N. Engl. J. Med.* **343**, 230-238.

141. Westermark, P., Andersson, A., Westermark, G.T. (2005) Is aggregated IAPP a cause of beta-cell failure in transplanted human pancreatic islets?, *Curr. Diab. Rep.* **5**, 184-188.

142. Swift, S.M., Clayton, H.A., London, N.J., James, R.F. (1998) The potential contribution of rejection to survival of transplanted human islets, *Cell Transplant* **7**, 599-606.

143. Ryan, E.A., Paty, B.W., Senior, P.A., Bigam, D., Alfadhli, E., Kneteman, N.M., et. al (2005) Five-year follow up after clinical islet transplantation, *Diabetes* **54**, 2060-2069.

144. Davalli, A.M., Maffi, P., Socci, C., Sanvito, F., Freschi, M., Bertuzzi, F., et. al (2000) Insights from a successful case of intrahepatic islet transplantation into a type 1 diabetic patient, *J. Clin. Endocrinol. Metab.* **85**, 3847-3852.

145. Westermark, G.T., Westermark, P., Eizirik, D., Hellerström, C., Fox, N., Steiner, D.F., Andersson, A. (1999) Differences in amyloid deposition in islets of transgenic mice expressing human islet amyloid polypeptide versus human islets implanted into nude mice, *Metabolism* **48**, 448-454.

146. Emamaullee, J.A., Merani, S., Toso, C., Kin, T., Al-Saif, F., Truong, W. (2009) Porcine marginal mass islet autografts resist metabolic failure over time and are enhanced by early treatment with liraglutide, *Endocrinology* **150**, 2145-2152.

147. Korsgren, O., Sandler, S., Landström, A.S., Jansson, L., Andersson, A. (1988) Large-scale production of fetal porcine pancreatic isletlike cell clusters. An experimental tool for studies of islet cell differentiation and xenotransplantation, *Transplantation* **45**, 509-514.

148. Potter, K.J., Abedini, A., Marek, P., Klimek, A.M., Butterworth, S., Driscoll, M., et. al (2010) Islet amyloid deposition limits the viability of human islet grafts but not porcine islet grafts, *Proc. Natl. Acad. Soc. U.S.A.* **107**, 4305-4310.

149. Lorenzo, A., Yankner, B.A. (1996) Amyloid fibril toxicity in Alzheimer's disease and diabetes, *Ann. NY Acad. Sci.* **777**, 89-95.

150. Janson, J., Ashley, R.H., Harrison, D., McIntyre, S., Butler, P.C. (1999) The mechanism of islet amyloid polypeptide toxicity is membrane disruption by intermediate-sized toxic amyloid particles, *Diabetes* **48**, 491-498.

151. Kayed, R., Pensalfini, A., Margol, L., Sokolov, Y., Sarsoza, F., Head, E., Hall, J.E., Glabe, C. (2009) Annular protofibrils are a structurally and functionally distinct type of amyloid oligomer, *J. Biol. Chem.* **284**, 4230-4237.

152. Mizushima, N., Yamamoto, A., Matsui, M., Yoshimori, T., Ohsumi, Y. (2004) In vivo analysis of autophagy in response to nutrient starvation using transgenic mice expressing a fluorescent autophagosome marker, *Mol. Biol. Cell* **15**, 1101-1111.

153. Kayed, R., Glabe, C.G. (2006) Conformation-dependent anti-amyloid oligomer antibodies, *Methods Enzymol.* **413**, 326-344.

154. Kayed, R., Head, E., Thompson, J.L., McIntire, T.M., Cotman, C.W., Glabe, C.G. (2003) Common structure of soluble amyloid oligomers implies common mechanism of pathogenesis, *Science* **300**, 486-489.

155. Yoshiike, Y., Minai, R., Matsuo, Y., Chen, Y.R., Kimura, T., Takashima, A. (2008) Amyloid oligomer conformation in a group of natively folded proteins, *PloS One* **3**, e3235.

156. Masuda, M., Hasegawa, M., Nonaka, T., Oikawa, T., Yonetani, M., Yamaguchi, Y., et. al (2009) Inhibition of alpha-synuclein fibril assembly by small molecules: analysis using epitope-specific antibodies, *FEBS Lett.* **583**, 787-791.

157. Hazelwood, R.L. (1989). *The Endocrine Pancreas*, Prentice Hall, Englewood Cliffs, NJ.

158. Elayat, A.A., el-Naggar, M.M., Tahir, M. (1995) An immunocytochemical and morphometric study of the rat pancreatic islets, *J. Anatomy* **186**, 629-637.

159. Göpel, S.O., Kanno, T., Barg, S., Eliasson, L., Galvanovskis, J., Renström, E., Rorsman, P. (1999) Activation of Ca-dependent K channels contributes to rhythmic firing of action potentials in mouse pancreatic beta cells, *J. Gen. Physiol* **114**, 759-770.

160. Eizirik, D.L., Cardozo, A.K., Cnop, M. (2008) The role of endoplasmic reticulum stress in diabetes mellitus, *Endocrine Rev* **29**, 42-61.

161. Fonseca, S.G., Burcin, M., Gromada, J., Urano, F. (2009) Endoplasmic reticulum stress in beta-cells and development of diabetes, *Curr. Opin. Pharmacol.* **9**, 763-770.

162. Laybutt, D.R., Preston, A.M., Akerfeldt, M.C., Kench, J.G., Busch, A.K., Biankin, A.V., Biden, T.J. (2007) Endoplasmic reticulum stress contributes to beta cell apoptosis in type 2 diabetes, *Diabetologia* **50**, 752-763.

163. Masters, S.L., Dunne, A., Subramanian, S.L., Hull, R.L., Tannahil,l G.M., Sharp, F.A., et. al (2010) Activation of the NLRP3 inflammasome by islet amyloid polypeptide provides a mechanism for enhanced IL-1 in type 2 diabetes, *Nat. Immunol.* **11**, 897-904.

164. Matveyenko, A.V., Butler, P.C. (2006) Beta-cell deficit due to increased apoptosis in the human islet amyloid polypeptide transgenic (HIP) rat recapitulates the metabolic defects present in type 2 diabetes, *Diabetes* **55**, 2106-2114.

165. Smith, P.E.S., Brender, J.R., Ramamoorthy, A. (2009) Smith PES, Brender JR, Ramamoorthy A. Induction of negative curvature as a mechanism of cell toxicity by amyloidogenic peptides: the case of islet amyloid polypeptide, *J. Am. Chem. Soc.* **131**, 4470-4478.

166. Lin, H., Bhatia, R., Lal, R. (2001) Amyloid ß protein forms ion channels: implications for Alzheimer's disease pathophysiology, *FASEB* **15**, 2433-2444.

167. Etcheberrigaray, R., Ito, E., Kim, C.S., Alkon, D.L. (1994) Soluble beta-amyloid induction of Alzheimer's phenotype for human fibroblast K+ channels, *Science* **264**, 276-279.

168. Khemtemourian, L., Killian, J.A., Hoppener, J.W., Engel, M.F. (2008) Recent insights in islet amyloid polypeptide-induced membrane disruption and its role in beta-cell death in type 2 diabetes mellitus, *Exp. Diabetes Res.* **2008**, 421287.

169. Last, N.B., Rhoades, E., Miranker, A.D. (2011) Islet amyloid polypeptide demonstrates a persistent capacity to disrupt membrane integrity, *Proc. Natl. Acad. Soc. U.S.A.* **108**, 9460-9465.

170. Knight J. D., H.J.A., Miranker A. D. (2006) Conserved and cooperative assembly of membrane-bound alpha-helical states of islet amyloid polypeptide, *Biochemistry* **45**, 9496-9508.

171. Brender J. R., H.K., Reid K. R., Kennedy R. T., Ramamoorthy A. (2008) A single mutation in the nonamyloidogenic region of islet amyloid polypeptide greatly reduces toxicity, *Biochemistry* **47**, 12680-12688.

172. Magzoub, M., Miranker, A.D. (2012) Concentration-dependent transitions govern the subcellular localization of islet amyloid polypeptide, *FASEB* **26**, 1228-1238.

173. Apostolidou, M., Jayasinghe, S.A., Langen R. (2008) Structure of alpha-helical membrane-bound human islet amyloid polypeptide and its implications for membrane-mediated misfolding, *J. Biol. Chem.* **283**, 17205-17210.

174. Zhang, S., Liu, H., Liu, J., Tse, C.A., Dragunow, M., Cooper, G.J. (2006) Activation of activating transcription factor 2 by p38 MAP kinase during apoptosis induced by human amylin in cultured pancreatic beta-cells, *FEBS J.* **273**, 3779-3791.

175. Zhang, S., Liu, J., MacGibbon, G., Dragunow, M., Cooper, G.J. (2002) Increased expression and activation of c-Jun contributes to human amylin-induced apoptosis in pancreatic islet beta-cells, *J. Mol. Biol.* **324**, 271-285.

176. Zhang, S., Liu, J., Dragunow, M., Cooper, G.J. (2003) Fibrillogenic amylin evokes islet beta-cell apoptosis through linked activation of a caspase cascade and JNK1, *J. Biol. Chem.* **278**, 52810-52819.

177. Zhang, S., Liu, H., Yu, H., Cooper, G.J. (2008) Fas-associated death receptor signaling evoked by human amylin in islet beta-cells, *Diabetes* **57**, 348-356.

178. Bendtzen, K., Mandrup-Poulson, T., Nerup, J., Nielsen, J.H., Dinarello, C.A., Svenson, M. (1986) Cytotoxicity of human pI 7 interleukin-1 for pancreatic islets of Langerhans, *Science* **232**, 1545-1547.

179. Spanger, J., Kroke, A., Mohlig, M., Hoffman, K., Bergmann, M.M., Ristow, M., et. al (2003) Inflammatory cytokines and the risk to develop type 2 diabetes: results of the prospective population-based European Prospective Investigation into Cancer and Nutrition (EPIC)-Potsdam Study, *Diabetes* **52**, 812-817.

180. Lasrson, C.M., Faulenbach, M., Vaag, A., Volund, A., Ehses, J.A., Seifert, B., et. al (2007) Interleukin-1-receptor antagonist in type 2 diabetes mellitus, *N. Engl. J. Med.* **356**, 1517-1526.

181. Nanga, R.P.R., Brender, J.R., Xu, J., Hartman, K., Subramanian, V., Ramamoorthy, A. (2009) Three-dimensional structure and orientation of rat islet amyloid polypeptide protein in a membrane environment by solution NMR spectroscopy, *J. Am. Chem. Soc.* **131**, 8252-8261.

182. Azriel, R., Gazit, E. (2001) Analysis of the minimal amyloid-forming fragment of the islet amyloid polypeptide: An experimental support for the key role of the phenylalanine residue in amyloid formation, *J. Biol. Chem.* **276**, 34156-34161.

183. Gazit, E. (2002) A possible role for pi-stacking in self-assembly of amyloid fibrils, *FASEB J.* **16**, 77-83.

184. Marek, P., Abedini, A., Song, B., Kanungo, M., Johnson, M.E. Gupta, R., et. al (2007) Aromatic interactions are not required for amyloid fibril formation by islet amyloid

polypeptide but do influence the rate of fibril formation and fibril morphology, *Biochemistry* **46**, 3255-3261.

185. Vaiana, S.M., Best, R.B., Yau, W.M., Eaton, W.A., Hofrichter, J. (2009) Evidence for a partially structured state of the amylin monomer, *Biophys. J.* **97**, 2948-2957.

186. Padrick, S.B., Miranker, A.D. (2001) Islet amyloid polypeptide: identification of long-range contacts and local order on the fibrillogenesis pathway, *J. Mol. Biol.* **308**, 783-794.

187. Marek, P., Gupta, R., Raleigh, D.P. (2008) The fluorescent amino acid *p*-cyanophenylalanine provides an intrinsic probe of amyloid formation, *ChemBioChem* **9**, 1372-1374.

188. Marek, P., Mukherjee, S., Zanni, M.T., Raleigh, D.P. (2010) Residue-specific, real-time characterization of lag-phase species and fibril growth during amyloid formation: a combined fluorescence and IR study of p-cyanophenylalanine analogs of islet amyloid polypeptide, *J. Mol. Biol.* **400**, 878-888.

189. Foster, M.C., Leapman, R.D., Li, M.X., Atwater, I. (1993) Elemental composition of secretory granules in pancreatic islets of Langerhans, *Biophys. J.* **64**, 525-532.

190. Charge, S.B.P., de Koning, E.J.P., Clark, A. (1995) Effect of pH and insulin on fibrillogenesis of islet amyloid polypeptide *in vitro*, *Biochemistry* **34**, 14588-14593.

191. Porte, D., Kahn, S.E. (1989) Hyperproinsulinemia and amyloid in NIDDM: Clues to etiology of islet β-cell dysfunction?, *Diabetes* **38**, 1333-1336.

192. Westermark, P., Li, Z.-C., Westermark, G.T., Leckstrom, A., Steiner, D.F. (1996) Effects of beta cell granule components on human islet amyloid polypeptide fibril formation, *FEBS Lett.* **379**, 203-206.

193. Abedini, A., Raleigh, D.P. (2005) The role of His-18 in amyloid formation by human islet amyloid polypeptide, *Biochemistry* **44**, 16284-16291.

194. Jayasinghe, S.A., Langen, R. (2004) Identifying structural features of fibrillar islet amyloid polypeptide using site-directed spin labeling, *J. Biol. Chem.* **279**, 48420-48425.

195. Kajava, A.V., Aebi, U., Steven, A.C. (2005) The parallel superpleated beta structure as a model for amyloid fibrils of human amylin, *J. Mol. Biol.* **348**, 247-252.

196. Westermark, P., Andersson, A., Westermark, G.T. (2011) Islet amyloid polypeptide, islet amyloid, and diabetes mellitus, *Physiol. Rev.* **91**, 795-826.

Chapter 2. An efficient microwave assisted synthesis of human islet amyloid polypeptide designed to facilitate the specific incorporation of labeled amino acids.

Abstract

IAPP has typically been synthesized via conventional solid-phase peptide synthesis, requiring the use of three pseudoprolines and the double coupling of β-branched amino acids, pseudoprolines and the amino acids directly following these residues. A cost-efficient, time-reducing solid-phase synthesis of the amyloidogenic, 37 residue islet amyloid polypeptide (IAPP) has been developed using two pseudoprolines in combination with microwave technology. A yield twice that obtained with conventional syntheses is realized. The utility of this protocol is demonstrated by the synthesis of a $^{13}C^{18}O$-labeled Ser-20 IAPP variant, a prohibitively expensive and chemically challenging site to label via other protocols. TEM analysis shows the peptide forms normal amyloid and thioflavin-T kinetics determine that IAPP synthesized via microwave synthesis forms amyloid on the same time scale as conventionally synthesized IAPP.

NOTE: The material presented in this chapter has been published (Peter Marek, Ann Marie Woys, Kelvin Sutton, Martin T. Zanni, Daniel P. Raleigh. (2010) An efficient microwave assisted synthesis of human islet amyloid polypeptide designed to facilitate the specific incorporation of labeled amino acids, *Org. Lett.* **12**, 4848-4851). This chapter contains direct excerpts from the manuscript, which was written by me with suggestions and revisions from

Professors Daniel P. Raleigh and Martin T. Zanni. Ann Marie Woys and Kelvin Sutton prepared the $^{13}C^{18}O$-labeled serine.

2.1 Introduction

Human islet amyloid polypeptide (IAPP or amylin) is a highly amyloidogenic 37-residue peptide that is stored with insulin and co-secreted from the β -cells of the pancreas (1-3). The bioactive form contains an amidated C- terminus and a disulfide bond between two cysteine residues located at positions 2 and 7. IAPP forms amyloid deposits in the islets of the pancreas during type 2 diabetes, a process that is thought to contribute to the decline in β-cell mass observed in type 2 diabetes (1, 2, 4-6). Islet amyloid formation has been implicated as a potentially complicating factor in islet cell transplantation (7-10). These considerations have lead to broad interest in the polypeptide. Biophysical and biochemical investigations of amyloid formation by IAPP are active areas of research, but the peptide is very difficult to synthesize and expresses poorly. Thus, there is interest in improving methods for the preparation of IAPP. Of particular importance are effective and economical protocols that are compatible with the incorporation of labeled amino acids and non-genetically coded amino acids for IR, fluorescence and fluorescence resonance energy transfer (FRET) studies. Such derivatives have proved very useful in a range of biophysical and biochemical studies, but the required amino acids can be

expensive or difficult to prepare and it is essential that effective solid phase peptide synthesis protocols be utilized for their incorporation. Exploiting recent advancements in microwave solid phase peptide synthesis and utilizing pseudoproline dipeptide derivatives, we demonstrate a cost effective, rapid synthesis of IAPP that doubles the yield obtained from conventional synthesis in under half the time and cost.

The hydrophobicity of IAPP, combined with a significant number of β -branched amino acids leads to difficulties in the solid-phase peptide synthesis (SPPS) of the peptide. IAPP has been successfully synthesized via Fmoc chemistry by the incorporation of three pseudoproline dipeptide derivatives, together with the double coupling of 20 amino acids (11). Pseudoprolines induce significant kinks within the backbone of the growing chain, much like proline, remove hydrogen bond donors and disrupt secondary structure, thus aiding in the prevention of aggregation. Standard trifluoroacetic acid (TFA) cleavage procedures regenerate the native structure of the peptide (12). The use of pseudoproline dipeptides and double coupling of the pseudoprolines, β-branched residues and the residues immediately following the pseudoprolines and β-branched residues lead to a synthesis scheme which we have found typically generates 40-50 mg of pure peptide from a 0.25 mmol scale synthesis using PAL-PEG-PS resin (11). Kelly and co-workers modified this procedure to significantly reduce the number of double couplings and obtained yields on the order of 20 mg of pure peptide from a 0.1 mmol scale synthesis (13). Both of these methods used pseudoprolines at positions 8-9, 19-20 and 27-28.

Advances in microwave technology coupled with solid phase peptide synthesis have led to reports of syntheses of difficult, hydrophobic peptides at greater yields than reported using conventional synthesis (14-16). Microwave energy allows for rapid heating at the molecular level, driving the coupling and deprotection reaction rates forward while reducing aggregation. A

solid phase microwave assisted synthesis of IAPP on the 0.1 mmol scale has recently been reported, which avoided the use of pseudoproline derivatives (17). However, the protocol involved double coupling residues 1 to 17 and 24 to 37 while triple coupling residues 18 through 23. In all 80 couplings were required. Furthermore, ten equivalents of amino acid were used at 14 positions including all of the residues that were triple coupled. Thus, while the approach avoids the use of pseudoprolines, it consumes large amounts of amino acids and solvents, is time consuming and can be prohibitively expensive to incorporate costly labeled or non-canonical amino acids.

Here we demonstrate a much more rapid and cost effective synthetic strategy by combining a modified pseudoproline approach with microwave heating. Only two pseudoprolines were required, together with thirteen double couplings (Figure 2.1). Only five equivalents of Fmoc amino acids were used for each step, leading to a considerable savings in time and cost. The utility of the method is demonstrated by preparing normal human IAPP and by the incorporation of $^{13}C^{18}O$-labeled Ser at position-20, a region of the chain that is prone to low coupling efficiencies. The ability to label this segment of the polypeptide chain is important because it has been proposed to be a critical initiation site for amyloid fibril growth (18). Incorporation of labeled residues into this region will provide the spectroscopic markers required to test this conjecture. Unfortunately, the introduction of labeled residues at this site is prohibitively expensive using existing protocols since it would either require the preparation and double coupling of a labeled pseudoproline, or the use of a triple coupling with ten equivalents of amino acid per coupling. The approach described here incorporates the label using a single coupling with five equivalents of amino acid.

2.2 Materials and Methods

2.2.1 Peptide synthesis and purification

IAPP was synthesized on a 0.25 mmol scale with a CEM Liberty Microwave Peptide Synthesizer utilizing 9-fluorenylmethoxycarbonyl (Fmoc) chemistry. All solvents used were ACS grade. The power levels, final temperature and reaction times are listed in Table 2.1. The final temperature is reached after 1 minute of heating and is maintained by a feedback sensor, which monitors the final temperature. The final temperature is monitored at 30-second intervals and the microwave source is gated to maintain constant temperature. Fmoc amino acids and pseudoproline dipeptide derivatives were purchased from Novabiochem. All other reagents were purchased from Sigma and Fisher Scientific. Use of a 5-(4'-Fmoc-aminomehtyl-3', 5-dimethoxyphenol) valeric acid (PAL-PEG) resin (Novabiochem) afforded an amidated C-terminus. Residues A8-T9 and L27-S28 were attached to the growing peptide chain as pseudoproline dipeptide derivatives and double coupled. The following residues were also double coupled: N3 through C7, R11, L16, V17, I26, T30 and V32. The peptide was cleaved from the resin through the use of standard trifluoroacetic acid (TFA) methods; ethanedithiol, thioanisole and anisole were used as scavengers. The disulfide bond was formed via incubation in DMSO. IAPP was purified via reverse-phase high performance liquid chromatography (RP-HPLC) using a Vydac C18 preparative column. A two buffer system was utilized in which buffer A consisted of 0.045% HCl in H_2O (v/v) and buffer B of 80% acetonitrile and 0.045% HCl in H_2O (v/v). TFA was avoided since small amounts of TFA can influence aggregation rates. The purity of the peptide was checked by HPLC using a Vydac C18 analytical column and the identity was confirmed by matrix-assisted laser desorption ionization time-of-flight mass spectrometry (MALDI-TOF MS); observed 3903.9 Da, expected 3903.4. Da.

2.2.2 Analysis of the racemization of His and Cys

Analysis of the levels of racemization was performed by C.A.T. GmbH & Co., Tübingen, Germany (Analysis number 9998026-1/10) in accordance with GMP guidelines.

2.2.3 Synthesis, purification and characterization of 1-$^{13}C^{18}O$ Fmoc-O-tert-butyl-L-Ser.

1-^{13}C Fmoc-*O-tert*-butyl-L-Ser was ^{18}O isotope labeled using the protocol originally described by Seyfried et al. for Glu, Trp and Cys Fmoc-protected amino acids (19). Isotope-labeled chemicals were obtained from Cambridge Isotope Laboratories, Inc. Acetonitrile was distilled from CaH_2 and used shortly thereafter. All other materials were used without further purification. Glassware and stir bars were dried either by flame or with an oven. The isotope labeling reaction was performed under argon atmosphere. ^{1}H and ^{13}C NMR data were collected with a Varian UNITY 500 spectrometer. ^{1}H NMR spectra were referenced to trimethylsilane and ^{13}C spectra to $CDCl_3$. The efficiency of ^{18}O isotope labeling was determined by liquid chromatography-mass spectrometry (LC-MS) with a Shimadzu LCMS-2010A, which used the stationary phase, a Supelco (Bellefonte, PA) 15 cm x 2.1 mm C-18 wide-pore reverse-phase column, and a mobile phase, 0.1% formic acid in water and 0.1% formic acid in acetonitrile. Elutents were analyzed by electrospray ionization with a single quadrupole analyzer. The stereochemistry was evaluated with supercritical fluid chromatography (SFC) using a Bergman Analytix outfitted with a Daicel Chiracel OD-H column for stationary phase and MeOH/CO_2 for the mobile phase. The modifier, MeOH, was varied 10-25% for Fmoc-*O-tert*-butyl-Ser samples and 5-20% for the Fmoc-ala samples. A Micromass LCT (electrospray ionization, time-of-flight analyzer) instrument measured the molar mass.

3,5-Dimethylpyridine hydrobromide was prepared by dripping 3,5-lutidine into 2 M hydrobromic acid in 1:1 molar ratio, and the solvent evaporated. The resulting solid was dried by three cycles of adding anhydrous acetonitrile, sonicating the suspension, and removing the solvent. 1-^{13}C Fmoc-*O*-*tert*-butyl-L-Ser and *N*-Ethyl-*N*′-(3-dimethylaminopropyl)carbodiimide (EDC) were dried using the same procedure. The labeling reaction was performed twice using a 250 mg scale. 3,5-Dimethylpyridine hydrobromide (2.46 g, 20 eq.) was dissolved into anhydrous *N,N*-dimethylformamide (DMF, 6 mL). EDC (1.25 g) was added followed by 750 µL water (^{18}O, 97%, Cambridge Isotopes). Fmoc-*O*-*tert*-butyl-L-Ser (250 mg) in DMF (8 mL) was added by syringe, which was washed with 2-3 mL DMF. The reaction was stirred for 18 hours at room temperature. Another addition of EDC (1.25 g) was followed by stirring for another 8 hours. A third portion of EDC (1.25 g) was added. After 15 hours, the reaction mixture was diluted in ethyl acetate (90 mL) and washed with 0.1 M citric acid (75 mL) three times and then once with 0.1 M citric acid in brine (75 mL). The aqueous layers were back-extracted with ethyl acetate (90 mL). The organic phase was dried over $MgSO_4$(s) and filtered. After evaporating the solvent, the product was further purified by HPLC. Reverse phase prep scale purification was performed on a Jasco HPLC (Quaternary Gradient Pump) with C18 Vydac column (218TP1022) stationary phase and 0.05% trifluoroacetic acid in water / 0.05% trifluoroacetic acid in acetonitrile gradient mobile phase. LC-MS data was collected before and after HPLC purification (Figure 2.2). The isotope peaks for the sodium adduct in the product elutents were used to determine the isotope label uptake. The isotope labeling efficiency is calculated for the coupled amino acid assuming 50/50 carboxylic oxygen preference for the singly ^{18}O-labeled amino acid during peptide bond formation. Isotope enrichment was 93%, and no back-exchange was observed after HPLC purification. NMR data for the 1-^{13}C^{18}O Fmoc-tBu-L-Ser product (1)

is given in Figure 2.3. The mass, 387.1782 *m/z*, was calculated, and 387.1791 *m/z* was measured. Chiral separation using SFC (Figure 2.4) was monitored at 210 nm and indicated >99% proper stereochemistry.

2.3 Results and Discussion

IAPP was synthesized with a CEM Liberty 12-Channel Automated Peptide Synthesizer using standard reaction cycles. The sequence of IAPP and the coupling scheme is shown in Figure 2.1. Use of a PAL-PEG-PS resin afforded an amidated C-terminus and HBTU was used as the coupling agent. Two pseudoproline dipeptides were chosen for the synthesis, Fmoc-Ala-Thr(**Ψ**Me,Me Pro)-OH replaced residues Ala-8 and Thr-9 and Fmoc-Leu- Ser(**Ψ**Me,Me Pro)-OH replaced residues Leu-27 and Ser-28. A preliminary synthesis involving single coupling of all residues and no pseudoprolines was attempted, but lead to a large mixture of deletion peptides. Double couplings were performed for the pseudoprolines, for the residues following each pseudoproline, for Arg-11 and for every β-branched residue except for Thr-36 (Figure 2.1). In total 11 residues in addition to the two pseudoprolines were double coupled and five equivalents of amino acid were used for all couplings. The microwave power settings and conditions for the deprotection and coupling steps are listed in Table 2.1. Cys and His residues are known to be susceptible to racemization if coupling reactions are conducted at elevated temperatures. A maximum temperature of 50 °C was set for the His and Cys couplings to reduce the possibility of racemization. The synthesis was complete in less than 24 hours.

The peptide was cleaved from the resin and deprotected using standard TFA procedures with 1,2-ethanedithiol, anisole and thioanisole as scavengers. The crude, reduced peptide was analyzed using analytical HPLC and MALDI-TOF mass spectroscopy (Figure 2.5). The

analytical HPLC trace revealed a major peak centered at approximately 45 minutes, corresponding to 75% purity as judged by the integrated area of the peaks detected at 220 nm. The mass spectrum revealed an intense peak at 3904.9 Da, which corresponds to the expected m/z for reduced IAPP (3905.3 Da). The mass spectrum also revealed 3 deletion peptides of masses 1481.7, 1743.0 and 2982.9 Da.

The disulfide bond between Cys-2 and Cys-7 was formed by dissolving the crude peptide in dimethyl sulfoxide (DMSO) at a concentration of 10 mg/ml and allowing it to oxidize as previously reported (20). We feel this is the safest method to use as on-resin cyclization or the use of powerful oxidants can generate unwanted byproducts, over-oxidation of the cysteine to sulfonic acid, modification of the C-terminal Tyr or, depending on the conditions, aggregation of the peptide. HCl was used as the counter ion instead of the more commonly employed TFA as TFA can interfere with infrared studies. TFA-based HPLC buffers usually provide higher resolution separations than buffers that use HCl as the counter ion. The effective purification achieved here with the HCl system reflects the high efficiency of the synthetic protocol, which leads to crude material that is already relatively pure. Pure, oxidized IAPP was generated at a nearly 15% yield (~95 mg) based on the weight of the crude material. The purity of the peptide was analyzed via HPLC on a C18 analytical column and MALDI (Figure 2.6). The yield calculated based on the mass of the resin used was approximately 10%. This yield is higher than reported for the alternative 0.1 mmol microwave protocol despite requiring no triple couplings, far fewer double couplings and avoiding the use of 10 equivalents of amino acid. The levels of racemization were 0.95% and 1.36% D-enantiomer for the His and Cys residues, respectively, measured via GC-MS (Materials and Methods). The value for Cys reflects the total amount detected per IAPP molecule. These levels are below those reported for other peptides synthesized

by microwave synthesis (14).

IAPP synthesized by this approach behaved similarly to IAPP synthesized with other protocols, forming amyloid on the same time scale and forming fibrils of identical morphology. Figure 2.7 displays a thioflavin-T fluorescence kinetic experiment conducted with the microwave synthesized peptide. The time course is identical to that observed previously and the transmission electron microscopy (TEM) images of the final reaction products reveal dense mats of fibrils with the standard morphology.

We also prepared a variant of IAPP labeled at Ser-20 with $^{13}C^{18}O$. This site has been implicated as part of a critical initiation site for fibril growth (18). The ability to label at or near this site is important for future spectroscopic studies, but would be prohibitively expensive using either our original method, which required a pseudoproline at positions 19-20 or using the previously reported microwave assisted protocol which requires triple coupling with ten equivalents per coupling. Fmoc and t-butyl protected 1-$^{13}C^{18}O$ backbone labeled Ser was prepared adopting the approach of Seyfried and co-workers (Materials and Methods) (19). $^{13}C^{18}O$-Ser IAPP was synthesized using the same protocol as employed for the unlabeled peptide, but using a 0.1 mmol scale. Approximately 50 mg of pure material was obtained, a 13% yield based on the amount of resin used.

In summary, a protocol for the synthesis of IAPP with a yield comparable to or better than other strategies, but at a considerably reduced time and cost has been developed, by combining microwave assisted methods with the incorporation of only two strategically placed pseudoproline dipeptide derivatives. The protocol allows the cost-effective incorporation of labeled residues into critical regions of the polypeptide chain. The use of this approach is applicable to other variants of IAPP and to other hydrophobic and aggregation-prone peptides.

2.4 Figures

Figure 2.1: Primary sequence of IAPP, illustrating the coupling scheme used for the microwave solid phase peptide synthesis. Residues that were double coupled are in bold and underlined. The pseudoproline residues are colored blue.

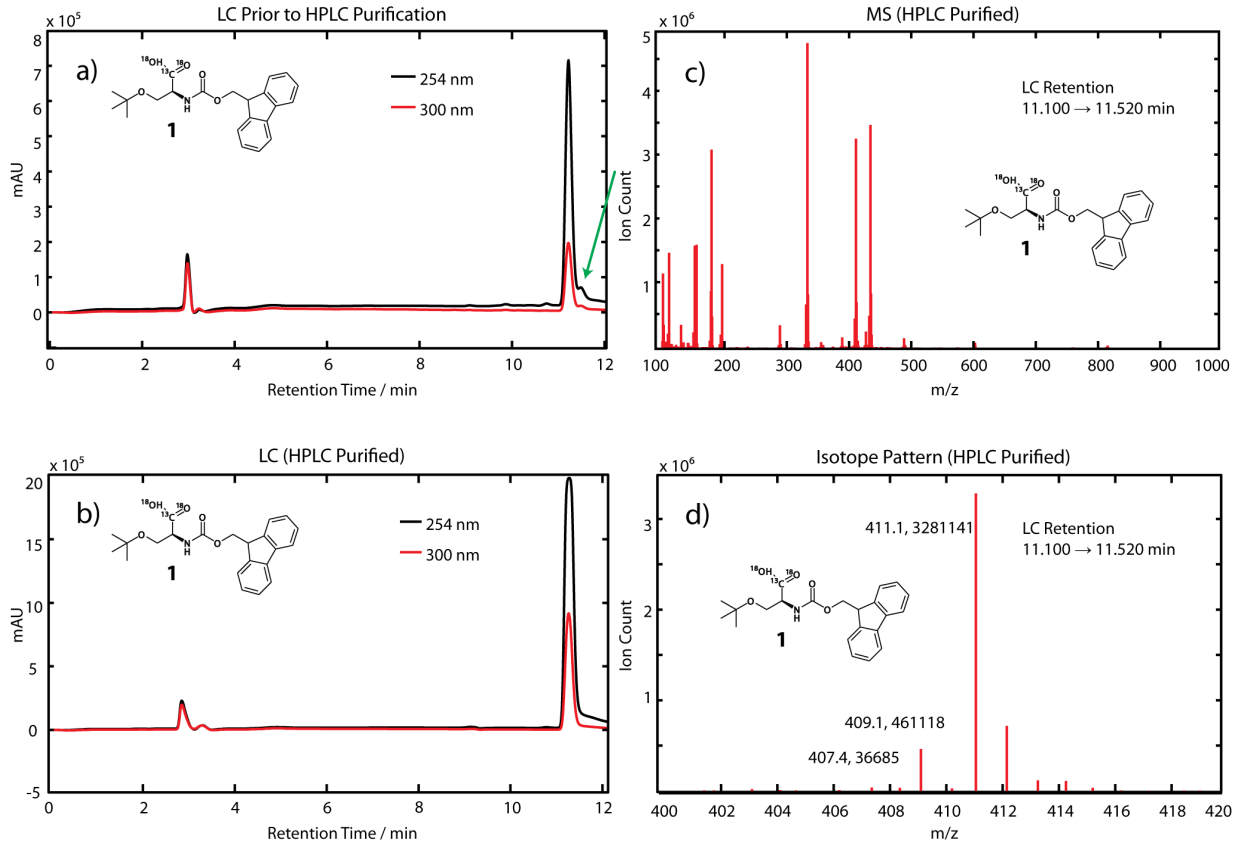

Figure 2.2: Crude (a) and HPLC purified (b-d) product from the ^{18}O labeling reaction of 1-$^{13}C^{18}O$ Fmoc-*O-tert*-butyl-L-Ser was analyzed by LC (gradient of 5:95 to 95:5 acetonitrile:water with 95:5 acetonitrile:water wash with 0.1% formic acid). a) LC-MS of crude $^{13}C^{18}O$ Fmoc-*O-tert*-butyl-L-Ser. The product peak is the major peak in the Total Ion Count (TIC) at 411.1 *m/z*. The shoulder (green arrow) is a by-product removed by HPLC purification. b) LC of pure 1-$^{13}C^{18}O$ Fmoc-*O-tert*-butyl-L-Ser after purification via HPLC. c) The integrated mass spectrum of purified 1-$^{13}C^{18}O$ Fmoc-*O-tert*-butyl-L-Ser. The product has the most intense mass at 411.1 *m/z* (product-sodium adduct). d) The isotope pattern for the 411.1 *m/z* was used to calculate isotope-labeling efficiency of 1-$^{13}C^{18}O$ Fmoc-*O-tert*-butyl-L-Ser.

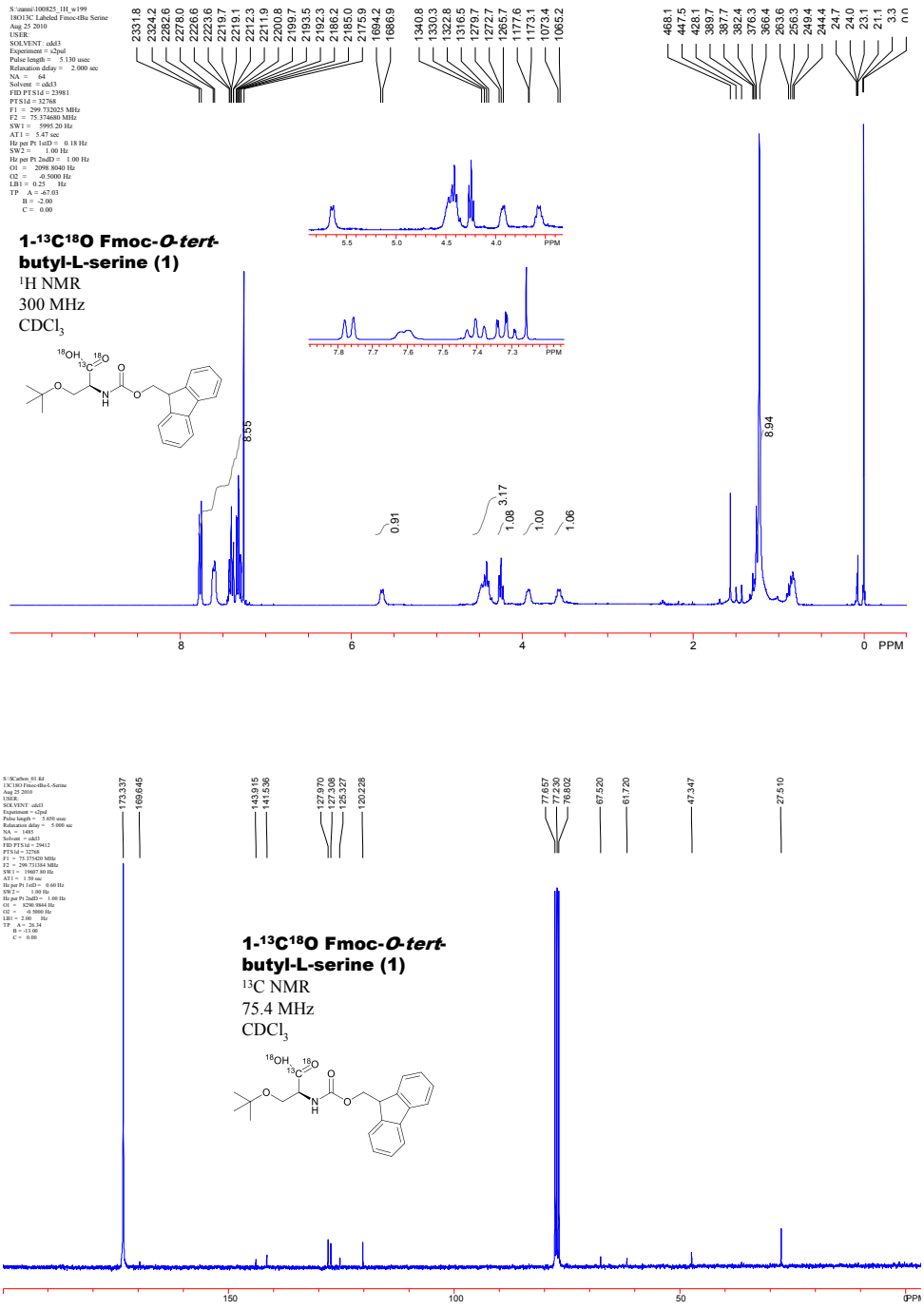

Figure 2.3: ^{1}H and ^{13}C NMR data for 1-^{13}C^{18}O Fmoc-*O-tert*-butyl-L-Ser (1): **^{1}H NMR:** (300 MHz, $CDCl_3$) δ 7.290-7.779 (m, 8 H, H_{arom}), 5.659 (d, 1 H, NH), 4.386-4.497 (m, 3 H, α-H, CH_{2Fmoc}), 4.248 (t, 1 H, CH_{Fmoc}), 3.920 (dd, 1 H, β'-H), 3.599 (dd, 1 H, β-H), 1.212 ppm (s, 9 H, $C(CH_3)_3$). **^{13}C NMR:** (75.4 MHz, $CDCl_3$) δ 173.3 ppm (s, 1 C, $^{13}C^{18}O^{18}OH$), 169.6 (s, 1 C, OCONH), 143.9, 141.5 (2 s, 4 C, C_{arom}), 128.0, 127.3, 125.3, 120.2 (4 s, CH_{arom}) , 67.5 (s, 1 C, CH_{2Fmoc}), 61.7 (s, 1 C, β-C), 47.3 (s, 1 C, CH_{Fmoc}), 27.5 (s, 1 C, $(CH_3)_3$).

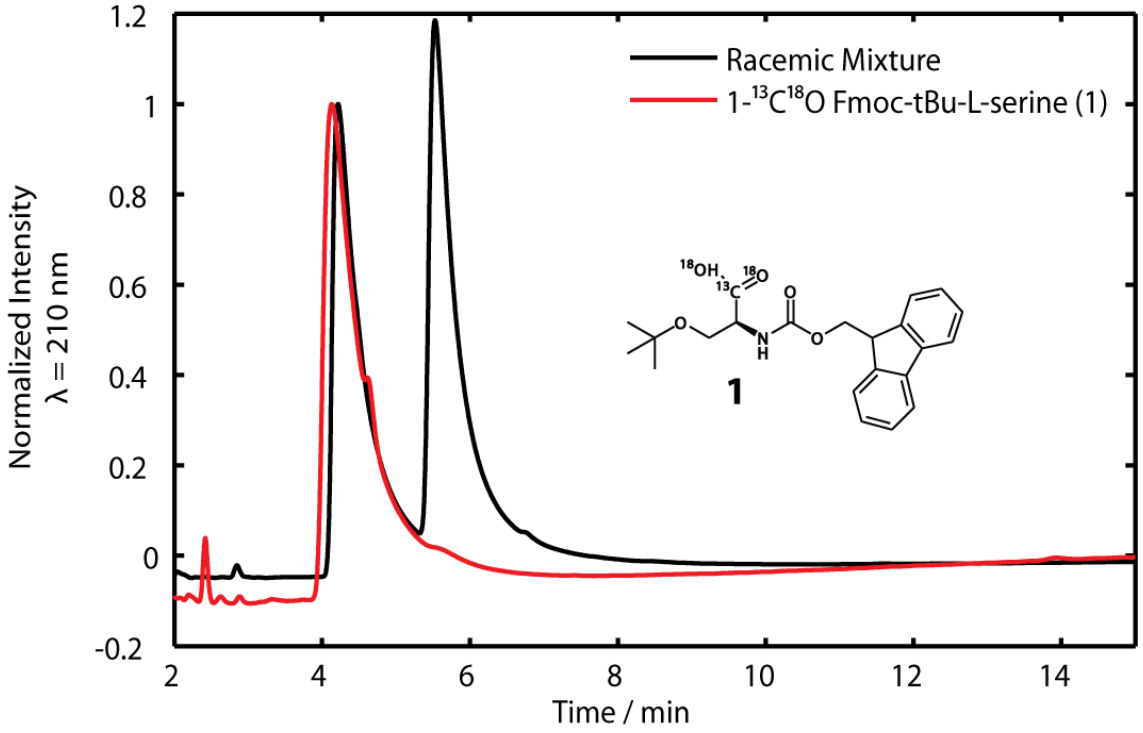

Figure 2.4: Supercritical fluid chromatography (SFC) spectrum monitored at 210 nm for a racemic mixture (i.e. standard) of unlabeled Fmoc-*O-tert*-butyl-Ser (black) and 1-^{13}C^{18}O Fmoc-*O-tert*-butyl-L-Ser product (red, 1).

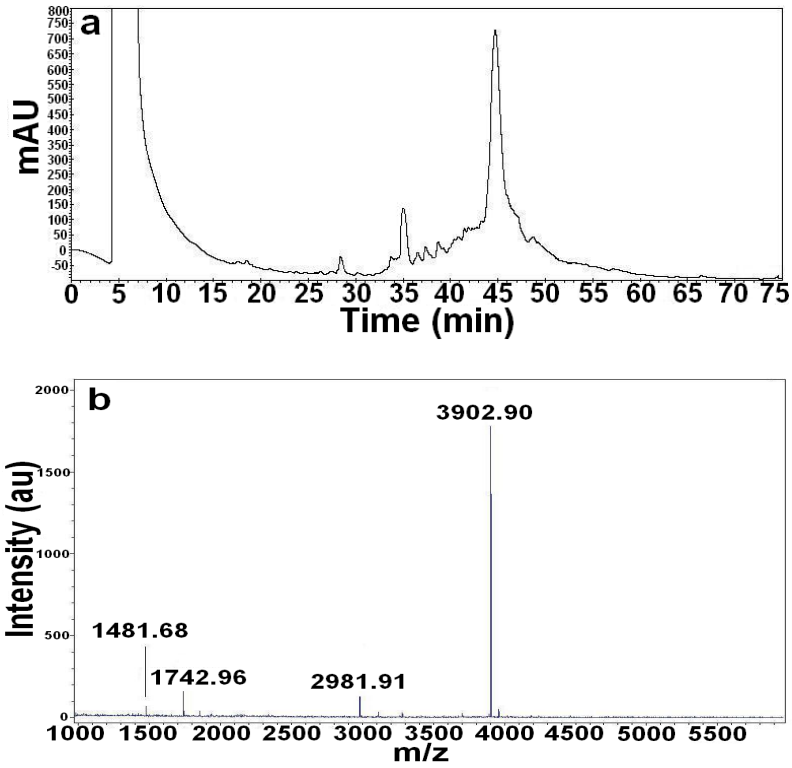

Figure 2.5: (a) Reversed-phase analytical HPLC trace and (b) MALDI spectrum of crude, reduced IAPP. The HPLC was run on a C18 Vydac analytical column at a flow rate of 1 ml/minute with a gradient of 0-90% buffer B (80% acetonitrile, 0.045% HCl) over 90 minutes.

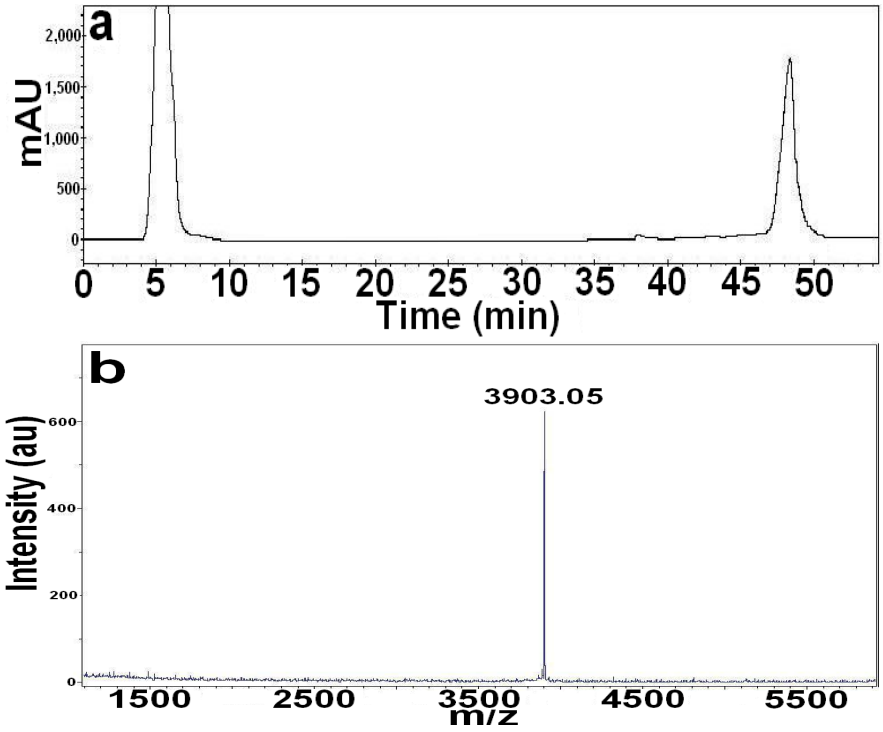

Figure 2.6: (a) Reversed-phase analytical HPLC trace and (b) MALDI mass spectrum of pure, oxidized IAPP. The HPLC was run on a C18 Vydac analytical column at a gradient of 0-90% buffer-B (80% acetonitrile, 0.045 % HCl) over 90 minutes. The pure peptide elutes at 48 minutes, corresponding to 48% buffer-B.

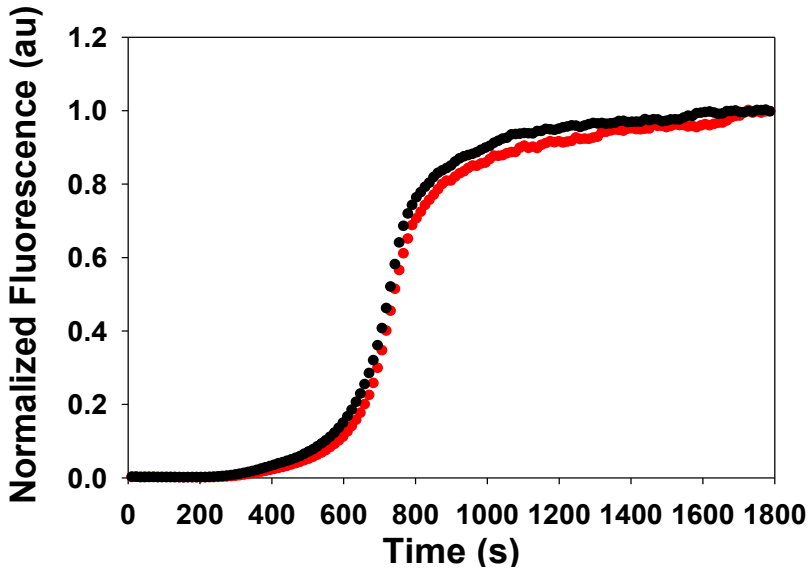

Figure 2.7: Thioflavin-T monitored kinetics of IAPP synthesized by microwave (red) and conventional (black) synthesis.

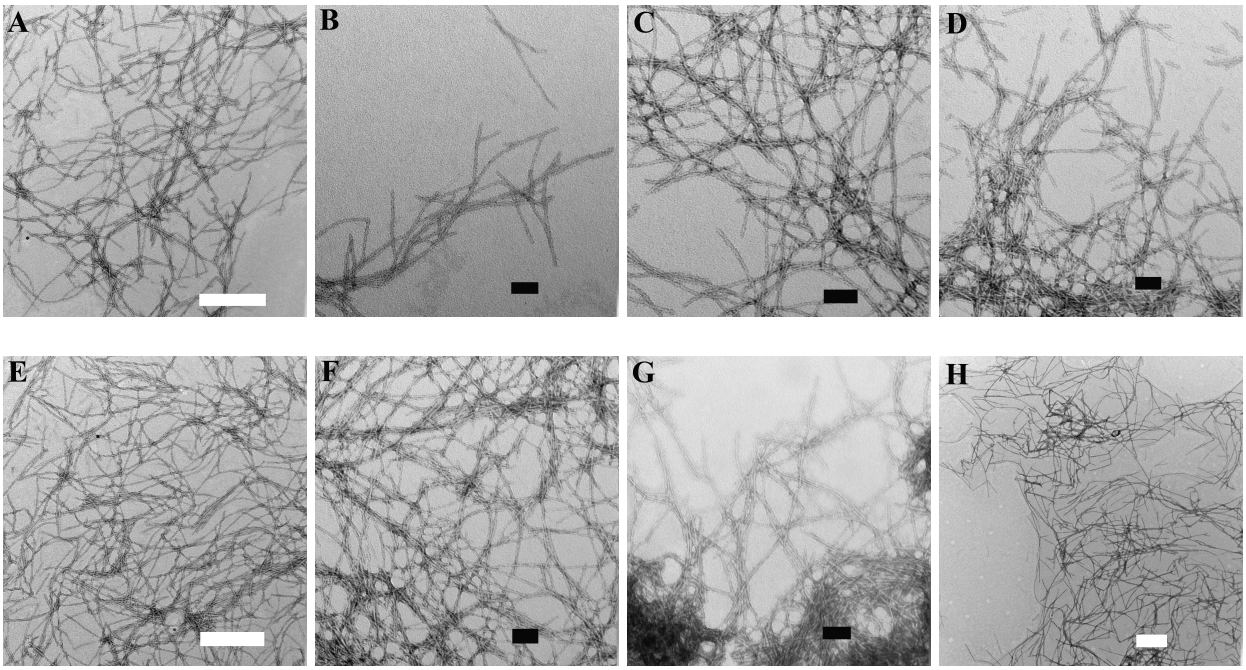

Figure 2.8: TEM images of fibrils formed by (A-D) microwave-synthesized and (E-H) conventionally-synthesized IAPP. White scale bar = 500 nm; black scale bar = 100 nm.

2.5 References

1.) Cooper, G.J.S., Willis, A.C., Clark, A., Turner, R.C., Sim, R.B., Reid, K.B.M. (1987) Purification and characterization of a peptide from amyloid rich pancreases of type II diabetic patients, *Proc. Natl. Acad. Sci. U.S.A.* **84**, 8628-8632.

2.) Westermark, P., Wernstedt, C., Wilander, E., Hayden D.W., O'Brien, T.D., Johnson, K.H. (1987) Amyloid fibrils in human insulinoma and islets of langerhans of the diabetic cat are derived from a neuropeptide-like protein also present in normal islet cells, *Proc. Natl. Acad. Sci. U.S.A.* **84**, 3881-3885.

3.) Kahn, S.E., D'Alessio, D.A., Schwartz, M.W., Fujimoto, W.Y., Ensinck, J.W., Taborsky, G.J.J., Porte, D.J. (1990) Evidence of cosecretion of islet amyloid polypeptide and insulin by β-cells, *Diabetes* **39**, 634-638.

4.) Kahn, S.E., Andrikopoulos, S., Verchere, C.B. (1999) Islet amyloid: A long-recognized but underappreciated pathological feature of type 2 diabetes, *Diabetes* **48**, 241-253.

5.) de Koning, E.J.P., Bodkin, N.L., Hansen, B.C., Clark, A. (1993) Diabetes mellitus in *Macaca mulatta* monkeys is characterised by islet amyloidosis and reduction in beta-cell population, *Diabetologia* **36**, 378-384.

6.) Butler, A.E., Janson, J., Bonner-Weir, S., Ritzel, R., Rizza, R.A., Butler, P.C. (2003) Beta-cell deficit and increased beta-cell apoptosis in humans with type 2 diabetes, *Diabetes*, **52**, 102-110.

7.) Udayasankar, J., Kodama, K., Hull, R.L., Zraika, S., Aston-Mourney, K., Subramanian, S.L., Tong, J., Faulenbach, M.V., Vidal, J., Kahn, S.E. (2009) Amyloid formation results in recurrence of hyperglycaemia following transplantation of human IAPP transgenic mouse islets, *Diabetologia*, **52**,145-53.

8.) Westermark, G. T., Westermark, P., Berne, C., Korsgren, O. (2008) Widespread amyloid deposition in transplanted human pancreatic islets, *N. Engl. J. Med.*, **359**, 977-979.

9.) Westermark, P., Eizirik, D. L., Pipeleers, D. G., Hellerström, C., Andersson, A. (1995) Rapid deposition of amyloid in human islets transplanted into nude mice, *Diabetologia* **38**, 543-549.

10.) Potter, K., Abedini, A., Marek, P., Butterworth, S., Driscoll, M., Baker, R., Nilsson, M., Bertera, S., Trucco, M., Fraser, P. E., Raleigh, D. P., Verchere, C. B. (2010) Islet amyloid deposition limits the viability of human islet grafts but not porcine islet grafts, *Proc. Natl. Acad. Sci. U.S.A.* **107**, 4305-4310.

11.) Abedini, A., Raleigh, D. P. (2005). Incorporation of pseudoproline derivatives allow the facile synthesis of human IAPP: A highly amyloidogenic and aggregation-prone polypeptide, *Org. Lett.* **7**, 693-696.

12.) Wöhr, T., Wahl, F., Nefzi, A., Rohwedder, B., Sato, T., Sun, X., Mutter, M. (1996) Pseudo-prolines as a solubilizing, structure-disrupting protection technique in peptide synthesis, *J. Am. Chem. Soc.* **118**, 9218-9227.

13.) Yonemoto, I.T., Kroon, G.J., Dyson, H.J., Balch, W.E., Kelly, J.W. (2008) Amylin proprotein processing generates progressively more amyloidogenic peptides that initially sample the helical state, *Biochemistry* **47**, 9900-9910.

14.) Palasek, S.A., Cox, Z.J., Collins, J.M. (2007) Limiting racemization and aspartimide formation in microwave-enhanced Fmoc solid phase peptide synthesis, *J. Pept. Sci.* **13**, 143-148.

15.) Basca, B., Horváti, K., Bõsze, S., Andreae, F., Kappe, C.O. (2008) Solid-phase synthesis of difficult peptide sequences at elevated temperatures: A critical comparison of microwave and conventional heating technologies, *J. Org. Chem.* **73**, 7532-7542.

16.) Basca, B., Bõsze, S., Kappe, C.O. (2010) Direct solid-phase synthesis of the beta-amyloid (1−42) peptide using controlled microwave heating, *J. Org. Chem.* **75**, 2103-2106.

17.) Muthusamy, K.; Alberico, F.; Arvidsson, P.T.; Govender, P.; Kruger, H.G.; Maguire, G.E.M.; Govender, T. J. (2010) Microwave assisted SPPS of amylin and its toxicity of the pure product to RIN-5F cells, *Pept. Sci.* **94**, 323-330.

18.) Shim, S.-H., Gupta, R., Ling, Y. L., Strasfeld, D. B., Raleigh, D. P., Zanni, M. T. (2009) Two-dimensional IR spectroscopy and isotope labeling defines the pathway of amyloid formation with residue-specific resolution, *Proc. Natl. Acad. Sci. U.S.A.* **106**, 6614-6619.

19.) Seyfried, M.S., Lauber, B.S., Luedtke, N.W. (2010) Multiple-turnover isotopic labeling of Fmoc- and Boc-protected amino acids with oxygen isotopes, *Org. Lett.* **12**, 104-106.

20.) Abedini, A., Singh, G., Raleigh, D. P. (2005) Recovery and purification of highly aggregation-prone disulfide-containing peptides: Application to islet amyloid polypeptide, *Anal. Biochem.* **351**, 181-186.

Chapter 3. Aromatic Interactions Are Not Required For Amyloid Fibril Formation by Islet Amyloid Polypeptide But Do Influence the Rate of Fibril Formation and Fibril Morphology

Abstract

Amyloid formation has been implicated in a wide range of human diseases and a diverse set of proteins is involved. There is considerable interest in elucidating the interactions which lead to amyloid formation and which contribute to amyloid fibril stability. Recent attention has been focused upon the potential role of aromatic-aromatic interactions and aromatic-hydrophobic interactions in amyloid formation by short to mid-sized polypeptides. Here we examine whether or not aromatic residues are necessary for amyloid formation by islet amyloid polypeptide (IAPP). IAPP is responsible for the formation of islet amyloid in type-II diabetes, which is thought to play a role in the pathology of the disease. IAPP is 37 residues in length and contains three aromatic residues, Phe-15, Phe-23 and Tyr-37. Structural models of IAPP amyloid fibrils postulate that Tyr-37 is near one of the phenylalanine residues and it is known that Tyr-37 interacts with one of the phenylalanines during fibrillization, but it is not known if aromatic-aromatic or aromatic-hydrophobic interactions are absolutely required for amyloid formation. A triple mutant F15L, F23L, Y37L (IAPP-3XL) was prepared and its ability to form amyloid was tested. CD, thioflavin-T binding assays, AFM and TEM measurements all show that the triple leucine mutant readily forms amyloid fibrils. The substitutions do however decrease the rate of fibril formation and alter the tendency of fibrils to aggregate. Thus, while aromatic residues are not an absolute requirement for amyloid formation by IAPP, they do play a role in the fibril assembly process.

NOTE: The material presented in this chapter has been published (Peter Marek, Andisheh Abedini, BenBen Song, Mandakini Kanungo, Megan E. Johnson, Ruchi Gupta, Warda Zaman, Stanislaus S. Wong, Daniel P. Raleigh (2007) Aromatic Interactions Are Not Required For Amyloid Fibril Formation by Islet Amyloid Polypeptide But Do Influence the Rate of Fibril Formation and Fibril Morphology. *Biochemistry*, **46**, 3255-3261). This chapter contains direct excerpts from the manuscript, which was written by me with suggestions and revisions from Professors Daniel P. Raleigh and Stanislaus S. Wong. Mandakini Kanungo, Megan E. Johnson and Warda Zaman performed the atomic force microscopy (AFM) experiments.

3.1 Introduction

Amyloid formation plays a role in a wide range of human diseases, including Alzheimer's disease and type-II diabetes, and a diverse set of proteins have been shown to form amyloid *in vivo* and i*n vitro*. There has been considerable interest in determining the factors and specific interactions, which lead to amyloid formation (1-10). Recent attention has been focused on the potential role of aromatic-aromatic and aromatic-hydrophobic interactions in amyloid formation (1-3, 5-6, 11-13). Aromatic-aromatic interactions are known to contribute to the stability of globular proteins and have been suggested to play a critical role in amyloid formation (11, 12). Initial experiments involving alanine scanning of peptides containing a single aromatic residue seemed to support this conjecture (12). In particular, substitution of aromatic residues in short peptides derived from islet amyloid polypeptide (IAPP, amylin) by alanine significantly

inhibited amyloid formation or abolished it. Alanine is, however, a non-conservative substitution for phenylalanine, particularly in regards to amyloid formation since it is smaller, less hydrophobic and has a smaller β-sheet propensity. Indeed, substitution of aromatic residues by leucine instead of alanine led to peptides, which still formed amyloid (13). These studies were performed on short fragments derived from IAPP or from other proteins. IAPP contains multiple aromatic residues and intrapeptide aromatic-aromatic interactions are formed during the fibrillization process, but it is not known if these intrapeptide aromatic-aromatic interactions are strictly required for amyloid formation by intact IAPP (14). The question is important because amyloid formation by IAPP is potentially of great medical significance and there have been suggestions that targeting aromatic-aromatic interactions is a viable strategy for the design of amyloid inhibitors, particularly for IAPP (15, 16).

IAPP is a hormone which is stored in the insulin secretory granule and is co-secreted with insulin (17, 18). In its normal soluble state it plays a role in regulating glucose metabolism, but in type-II diabetes IAPP forms amyloid deposits in the pancreas (17-23). Islet amyloid is believed to play a role in the pathology of type-II diabetes and more than 90% of patients with type-II diabetes exhibit islet amyloid upon autopsy (23). Furthermore, the extent of islet amyloid appears to correlate with the severity of the disease. The mature form of IAPP is 37 residues in length, has an amidated C-terminus and contains a disulfide bridge between residues two and seven (17, 18). The human form of the polypeptide contains three aromatic residues, Phe-15, Phe-23 and Tyr-37. FRET studies have shown that the C-terminal Tyr interacts with one or more of the Phe residues during the fibrillization process (14). FRET studies have also shown that Tyr-37 is relatively immobile in the final fibril structure, while structural models of the fibrils suggest that Tyr-37 could form aromatic-aromatic interactions with Phe-23 (14, 24).

These studies indicate that aromatic residues may be important in amyloid formation by the full-length peptide. Note that the studies with short peptides described above could not test the importance of these interactions because each peptide contained only one aromatic residue, thus intrapeptide aromatic-aromatic interactions were not possible.

A number of studies have suggested that targeting aromatic-aromatic interactions is a viable strategy for the design of amyloid inhibitors, particularly of IAPP (15, 16, 25). However, no studies have been reported which test if aromatic-aromatic or aromatic-hydrophobic interactions are absolutely necessary for islet amyloid formation. The question is important, both because of the increasing interest in inhibitors of IAPP aggregation and because of the general insight such a study might offer into amyloid formation in a broader context. Here we report the characterization of a triple mutant of IAPP in which all three aromatic residues are replaced by Leu. The peptide is denoted IAPP-3XL and, as described below, it readily forms amyloid. Thus, aromatic residues are not required for amyloid formation by IAPP, although amyloid formation is slower in their absence and the final morphology is subtly affected.

3.2 Material and Methods

3.2.1 Peptide synthesis and purification

IAPP-3XL was synthesized on a 0.25 mmol scale with an Applied Biosystems 433A Peptide Synthesizer utilizing 9-fluornylmethoxycarbonyl (Fmoc) chemistry. Solvents used were ACS-grade. Fmoc-protected pseudoproline (oxazolidine) dipeptide derivatives were used as previously described (26). They were purchased from Novabiochem. All other reagents were purchased from Advanced Chemtech, PE Biosystems, Sigma and Fisher Scientific. Use of a 5-(4'-Fmoc-aminomehtyl-3', 5-dimethoxyphenol) valeric acid (PAL-PEG) resin afforded an

amidated C terminus. Standard Fmoc reaction cycles were used. The first residue attached to the resin, all β-branched residues, the residue directly following a β-branched residue, all psuedoproline dipeptide derivatives and the residue directly following a pseudoproline dipeptide derivative were double-coupled. The peptide was cleaved from the resin through the use of standard trifluoroacetic acid (TFA) methods.

The crude peptide (100 mg) was dissolved in 10% acetic acid (v/v), frozen in liquid nitrogen and lyophilized to increase its solubility. The dry polypeptide was dissolved in 5 ml DMSO to promote the formation of the Cys-2 to Cys-7 disulfide bond (27). After 24 hours the solution was purified via reverse-phase high-performance liquid chromatography (RP-HPLC) using a Vydac C18 preparative column. A two-buffer system was utilized in which Buffer A consisted of H_2O and 0.045% HCl (v/v) and Buffer B consisted of 80% acetonitrile, 20% H_2O and 0.045% HCl (v/v). The identity of the pure polypeptide was confirmed by matrix-assisted laser desorption ionization time-of-flight mass spectrometry (MALDI-TOF MS) using a Bruker MALDI-TOS MS (for IAPP expected 3904.3 Da, observed 3904.6 Da; for IAPP-3XL expected 3786.2, observed 3786.6 Da). The purity of the polypeptide was checked by HPLC using a Vydac C18 analytical column.

3.2.2 Thioflavin-T fluorescence assays

A 0.53 mM peptide stock solution consisting of 1.9 mg purified IAPP-3XL in 1 mL 20 mM Tris-HCl buffer at pH 7.4 was prepared and allowed to incubate for two days at room temperature. A second 0.53 mM peptide stock solution was prepared on the second day and used to monitor events at time zero. Fluorescence was measured on a Jobin Yvon Horiba fluorescence spectrophotometer at 450 nm excitation and 485 nm emission wavelengths. The

emission and excitation slits were set to 5 nm and a 1.0 cm cuvette was used. The wavelength scan was measured from 462-650 nm. All thioflavin-T fluorescence experiments were performed by diluting 103 μL of the stock solution into a 20mM Tris-HCl buffer at pH 7.4 containing thioflavin-T. The final solution conditions were 32 μM peptide and 64 μM thioflavin-T at pH 7.4. All solutions were stirred during the wavelength scans to maintain solution homogeneity. As a control, a fluorescence spectrum was taken of a solution consisting of only buffer and thioflavin-T. This spectrum was flat in comparison to the spectrum of the solution containing the peptide, indicating that the fluorescence observed in the presence of the peptide is due to the peptide fibril-dye interactions. The background spectrum was subtracted from the spectra of the peptide samples. Wavelength scans were performed on both peptide stock solutions on the day of preparation and after 15 days of incubation. Studies were also conducted in which a 1.58 mM stock solution was prepared in 100% hexafluoroisopropanol (HFIP) as described (27). These conditions are used to ensure that IAPP is monomeric at the initiation of the kinetic assays. Kinetic studies were performed by diluting this stock solution by a factor of 50:1 in Tris-HCl buffer at pH 7.4 containing thioflavin-T and monitoring the thioflavin fluorescence as a function of time. Final solution conditions were 32 μM IAPP and 64 μM thioflavin-T at pH 7.4, 2 % HFIP (v/v). The kinetics of amyloid formation by IAPP are dependent on the size and shape of the cell used, the sample volume and whether or not samples are stirred as well as the solvent composition.

3.2.3 Circular dichroism (CD) experiments

Far-UV CD experiments were performed at 25 °C on an Aviv 62A DS CD spectrophotometer. For far-UV CD wavelength scans, an aliquot from the peptide stock was

diluted into 20 mM Tris-HCl buffer at pH 7.4, for a total volume of 250 μL. The final peptide concentration was 0.1 mg/mL in 20 mM Tris-HCl buffer. The spectrum is the average of three repeats in a 0.1 cm quartz cuvette and recorded over a range of 190-250 nm, at 1nm intervals with an averaging time of three seconds per scan. A background spectrum was subtracted from the collected data.

3.2.4 Transmission electron microscopy (TEM)

TEM was performed at the University Microscopy Imaging Center at the State University of New York at Stony Brook. A 4 μL sample from both the t=0 and t=2 days peptide stock solutions were placed on a carbon-coated 300-mesh copper grid and negatively stained with saturated uranyl acetate.

3.2.5 Atomic force microscopy (AFM)

The peptide samples were characterized using a Nanoscope IIIa Multimode atomic force microscope (Veeco, Inc. Santa Barbara, CA). Specifically, 1 μL of the peptide solution was diluted to 5 μL with deionized water in an Eppendorf tube and mixed gently for 10 seconds. A 2 μL aliquot of the diluted solution was spin coated onto a freshly cleaved mica surface at 3000 rpm for 30 seconds followed by air-drying for 30 minutes. The samples were subsequently imaged in ambient air using tapping mode mode scanning with conventional etched silicon Nanoprobes (k = 3-6 N/m). We used an E scanner for our imaging, with typical scan ranges of < 1μm to 5μm. The scan rate for imaging of the peptides was between 1-1.6 Hz; tapping frequency was between 60-90 kHz. The height, length, and periodicity data on the fibrils was obtained directly from flattened images using the as-provided Nanoscope data analysis software.

Height, length, and periodicity measurements were taken along a number of line profiles across randomly selected fibrillar features, with our measurements replicated over several images and taken above the mica background. Width measurements were not obtained due to non-trivial tip broadening effects that rendered the data less meaningful.

3.3 Results and Discussion

A triple mutant of human IAPP was synthesized in which each of the aromatic residues were replaced by Leu; F15L, F23L and Y37L. The polypeptide is denoted IAPP-3XL (Figure 3.1). Leucine substitutions were used to eliminate the aromatic interactions instead of Ala since Leu is more conservative in terms of its size, hydrophobicity and β-sheet and α-helical propensity (13). The ability of IAPP-3XL to form amyloid was first tested using thioflavin-T binding studies. Thioflavin-T is negligibly fluorescent in solution, but experiences a significant increase in quantum yield upon binding to amyloid fibrils. The results indicate that thioflavin-T fluorescence is considerably enhanced in the presence of aggregated IAPP-3XL, exhibiting the characteristic emission maximum near 480 nm associated with the amyloid-bound dye (Figure 3.2). These studies were conducted using samples prepared in aqueous buffer at initially relatively high concentrations (stock solution was 0.5 mM prior to dilution) as described in the materials and methods section. We also tested solutions that were first solubilized in 100% HFIP to remove any preformed seeds. Samples prepared by diluting HFIP stock solutions into aqueous buffer also show the characteristic thioflavin-T fluorescence associated with amyloid formation after a short lag phase. This experiment confirms that the positive thioflavin assay is not an artifact of the method of sample preparation. These results were confirmed by far-UV CD studies. Far-UV CD spectra of the triple leucine mutant show the classic conformational

transition for amyloid formation by wild type (WT) IAPP, shifting from a random coil structure at time zero to a β-sheet structure (Figure 3.3).

The morphology of the IAPP-3XL deposits was investigated using TEM. These experiments demonstrate that the material, which binds thioflavin-T, has the morphology commonly associated with amyloid fibrils. This is an important additional observation because there has been some speculation that thioflavin-T binding can yield false positives. Dense mats of long, un-branched fibrils were observed in the TEM images of samples of IAPP-3XL, which had been incubated for only 1 hour at pH 7.4 (Figure 3.4). Interestingly, the fibrils observed in samples that had been incubated for 48 hours appeared longer and slightly less prevalent, although they were still abundant.

We also used atomic force microscopy (AFM) to examine the topology of the fibrils formed by the 3XL mutant. Tapping mode AFM has been used to probe the morphology of amyloid fibrils formed by a wide range of proteins and polypeptides and is a complementary technique to TEM, since samples do not have to be either heavy metal stained or visualized under high vacuum conditions. Our ambient AFM data are consistent with the TEM studies and support the conclusion that the triple leucine mutant forms amyloid fibrils. Figure 3.5 compares AFM images of WT IAPP and IAPP 3X-L, both of which formed left-handed helical, slightly curved fibrils. The images are broadly similar and reveal features typically observed for AFM images of amyloid fibrils, including the same sense of the helical twist. There are differences in the details of the images however. For example, the twisted ribbon morphology was noticeably more pronounced for the WT fibrils. A distinct periodicity is observed for both peptides as is typical of amyloid. For the WT IAPP fibril the period is 47.2 ± 9.0 nm, whereas for the IAPP-3XL mutant the period is 62.1 ± 8.5 nm, indicative of observable macroscopic changes in the

fibril structure which result from differences in the two peptide sequences. A similar argument has been previously advanced to explain polymorphic fibrillar morphologies (28, 29). The distribution of fibril lengths is similar for the two peptides in the sense of ranging from 100 nm to several microns. However, there are differences in the distribution of heights worth discussing (Figure 3.6).

The mean height for the WT peptide is 5.16 ± 1.46 nm and the median is 4.71 nm. The measured fibril height is within the range expected and is in agreement with previous AFM data as well as electron microscopy results on human IAPP (30-33). Nonetheless, as is evident from Figure 3.5, the WT fibrils tend to occur mainly as pairs of fibrils and sometimes as triplets and multiplets of adjoining fibrillar structures. This result is consistent with a picture of WT fibrils as being composed of laterally intertwined component fibrillar building blocks forming higher-order structures and moreover, argues for the reasonable hypothesis that the aromatic residues help to mediate interfibril interactions. Our observation is also in agreement with previous reports on IAPP assemblies, where fibril structures were observed (34). In other words, it is plausible that the aromatic residues, through favorable π-stacking interactions or aromatic hydrophobic interactions, may encourage formation of a hierarchical fibrillar architecture. By contrast, the mean height for fibrils formed by the 3XL mutant, 3.39 ± 1.3 nm, is clearly lower than that of WT, as is the median height, 3.1 nm. This may result from an unfavorable tendency for component fibrils to aggregate in this system as compared with the WT.

The results of these experiments are all internally consistent and demonstrate that interactions involving aromatic residues are not required for amyloid formation by IAPP. However, these studies do not address whether or not aromatic-aromatic or aromatic-hydrophobic interactions influence the rate of assembly of IAPP fibrils. Consequently, we

conducted kinetic assays to compare the rate of amyloid formation by WT IAPP and the 3xL mutant. Figure 3.7 compares the time course of fibril formation as monitored by thioflavin-T binding. Both the WT and 3XL peptides exhibit a lag phase with little or no change in fluorescence followed by a rapid growth phase leading to the final plateau. The lag phase is noticeably longer for the 3XL mutant, increasing by approximately a factor of five. Interestingly, the affect on the growth phase is less pronounced.

3.4 Conclusions

Spectroscopy measurements, TEM and AFM studies of IAPP-3XL clearly demonstrate that it readily aggregates into fibrils that bind thioflavin-T, have considerable β-sheet structure and have the morphology expected for amyloid deposits. These studies unequivocally show that IAPP 3XL forms amyloid despite the complete absence of aromatic residues. We believe that our observations with full length IAPP are important because previous studies of the role of aromatic residues in fibril formation by IAPP involved studies of short peptides, which contained only a single aromatic amino acid. In contrast, mature IAPP contains three aromatic residues and aromatic contacts are known to be formed during the fibrillization process (14). Thus, the present study extends our earlier observations by showing that intrapeptide aromatic-aromatic interactions are not required for fibril formation. The present study together with recent studies of the role of aromatic interactions in amyloid formation by muscle acylphospatase and prior investigations of short peptides clearly demonstrate that that aromatic-aromatic or aromatic-hydrophobic interactions are not a requirement for amyloid formation in all systems (2, 13). Our kinetic studies, however, do show that interactions involving aromatic residues of IAPP are

important during the lag phase and our AFM measurements show that they influence the morphology of the deposits.

It is interesting to speculate about the molecular basis for the elongation of the lag phase caused by the aromatic to leucine substitutions. In principle, the substitutions could modulate conformational tendencies and fluctuations within the monomeric ensemble or they might destabilize specific intramolecular contacts or modulate important peptide-peptide interactions. Of course the substitutions could exert their net effect by some combination of these processes, although it is very difficult to quantify or differentiate these potential multiple effects. There is literature data, however, which suggests that at least part of the effects could be due to modulation of intramolecular aromatic-aromatic interactions. In particular, FRET based measurements showed that aromatic residues in wild-type IAPP form interactions during the lag phase of amyloid formation and demonstrated that the C-terminal tyrosine makes contacts with one or more of the phenylalanines (14). Our study compliments this investigation by showing that these interactions are likely to be kinetically important. These observations are important for mechanistic interpretation of amyloid fibril assembly of IAPP, and may be relevant for the design of inhibitors of aggregation (15, 16, 25).

Might aromatic-aromatic interactions be important in *in vivo* amyloid formation by IAPP? It can be very difficult to extrapolate effects observed in *in vitro* biophysical studies to *in vivo* amyloid formation in the complicated extracellular environment. *In vivo* amyloid formation is a dynamic process involving amyloid deposition, potential disruption of amyloid deposits and interactions with cellular quality control machinery. If the five-fold increase in the lag phase were translated into the *in vivo* environment, then the effects might indeed be significant and replace of the aromatic residue in IAPP might decrease amyloid formation. Conversely, the

aromatic residues in IAPP might actually inhibit amyloid formation by modulating interactions between IAPP and other molecules and their removal could then be deleterious. In particular, aromatic residues in IAPP have been implicated in IAPP-insulin interactions (35). This is potentially of great importance because insulin is a potent inhibitor of amyloid formation by IAPP *in vitro* and there has been speculation that this could be relevant *in vivo* (36-38). The concentration of IAPP in the secretory granule is well above concentrations that lead to rapid aggregation *in vitro*, leading to the question of why amyloid formation is inhibited in the granule. Insulin-IAPP interactions have been proposed to be the key. Thus, disruption of the insulin-IAPP interaction by replacement of the aromatic residues might promote amyloid formation.

In summary, our studies demonstrate that intramolecular or intermolecular aromatic-aromatic or aromatic-hydrophobic interactions are not required for amyloid formation by IAPP. However, the data presented here clearly supports a role for aromatic residues in the kinetics of amyloid assembly and shows that they influence the morphology of the deposits.

3.5 Figures

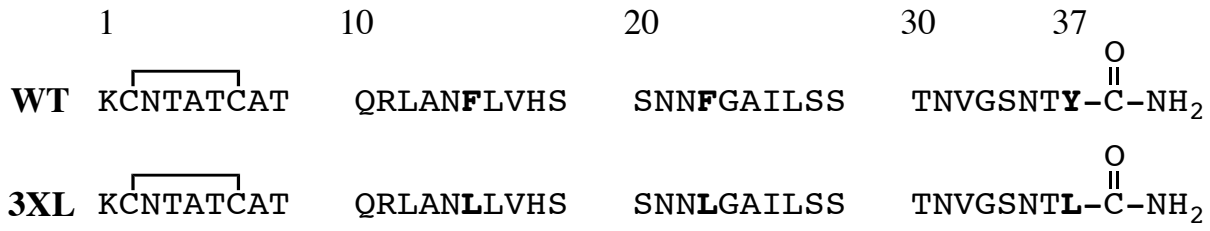

Figure 3.1: The primary sequence of WT human IAPP and F15L, F23L, Y37L (3XL) triple mutant. The peptides have an amidated C-terminus, a free N-terminus and a disulfide bridge between Cys-2 and Cys-7. Positions 15, 23 and 37 are highlighted in bold.

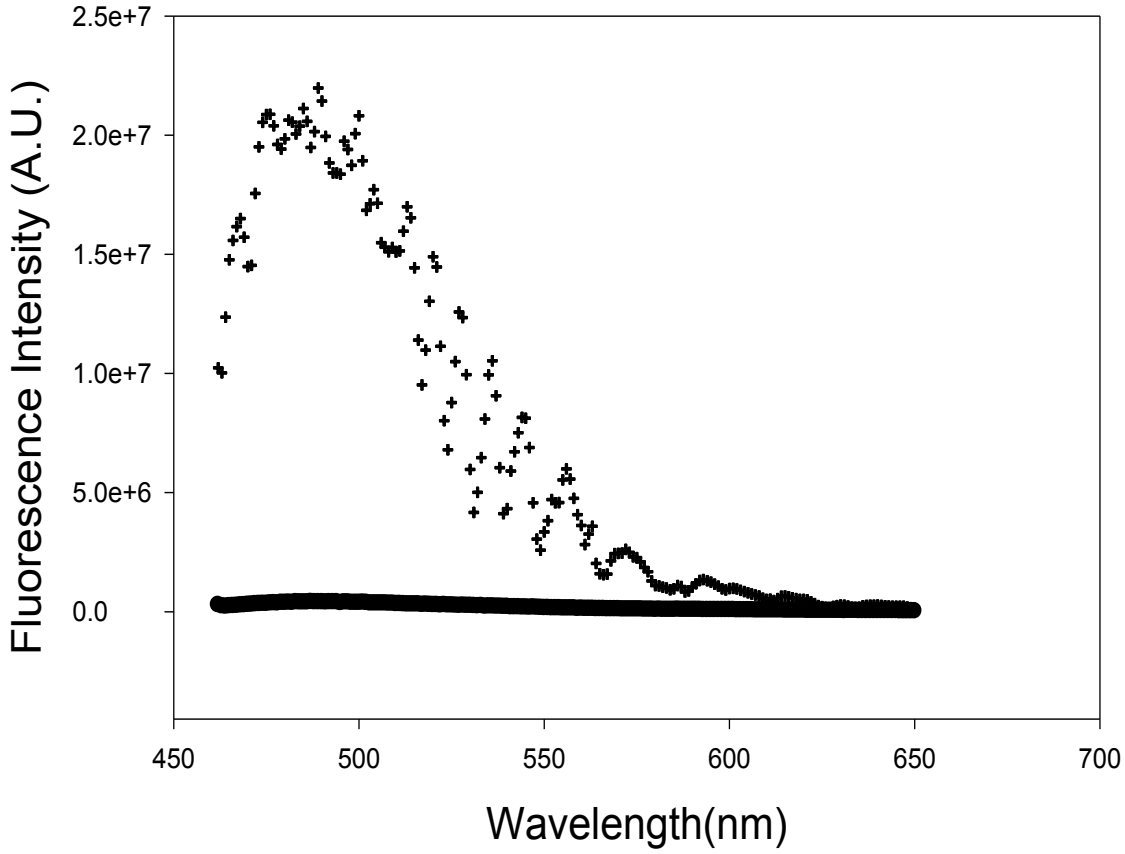

Figure 3.2: Thioflavin-T binds to IAPP-3XL. The solid curve is the thioflavin-T emission spectrum recorded in the presence of 0.50 mM IAPP-3XL, which had been incubated for two days. The dashed line represents thioflavin-T in buffer in the absence of peptide. Spectra were recorded at 25 °C in 20 mM Tris-HCl at pH 7.4.

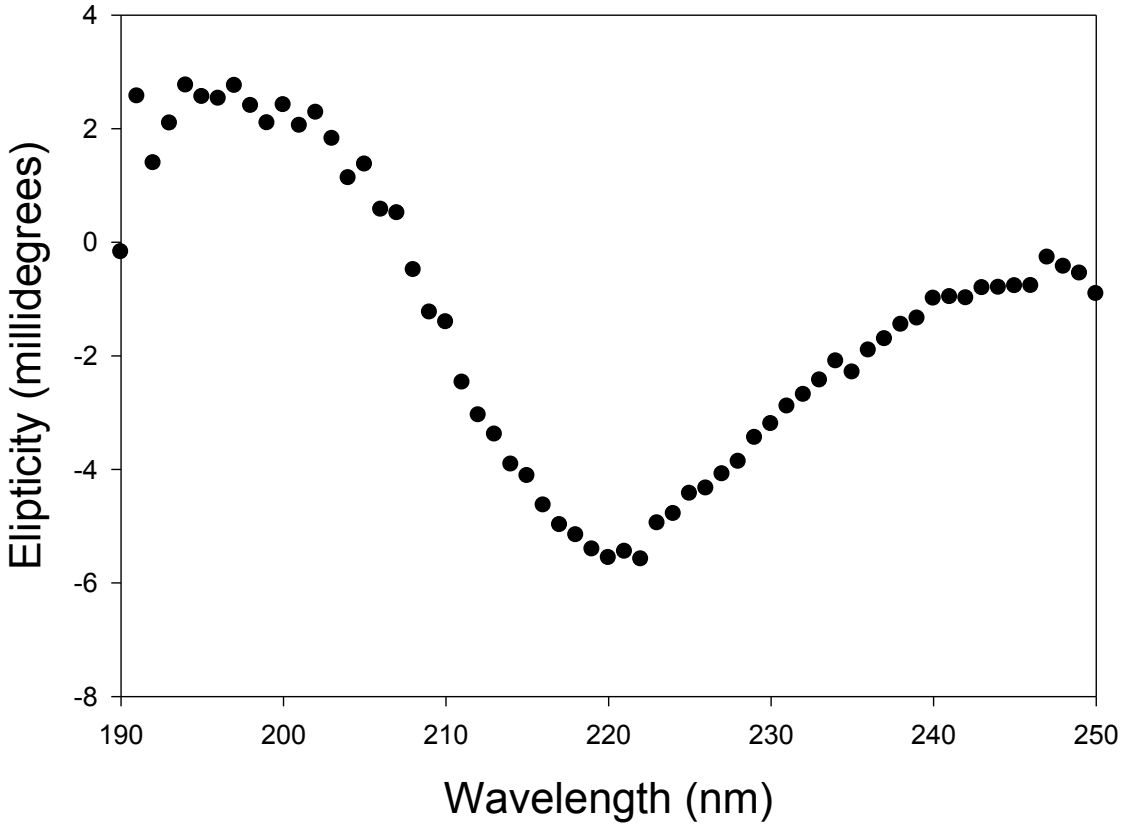

Figure 3.3: IAPP-3XL deposits are rich in β-sheet structure. Far UV-CD spectrum of a 32 μM sample of IAPP-3XL in 20 mM Tris-HCl at pH 7.4.

(A) (B)

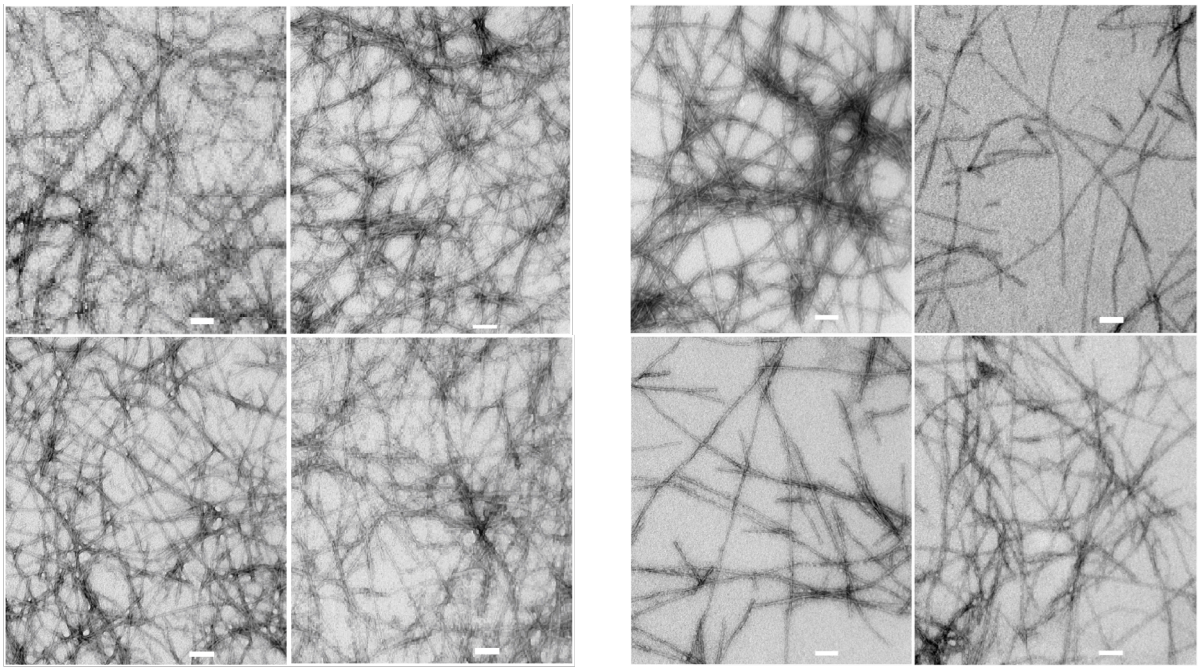

Figure 3.4: IAPP-3XL forms amyloid deposits. (A) TEM images recorded of a sample which had been incubated for 1 hour at 25 °C in 20 mM Tris-HCl at pH 7.4. (B) TEM images of samples incubated for two days under otherwise identical conditions. The scale bar represents 100 nm.

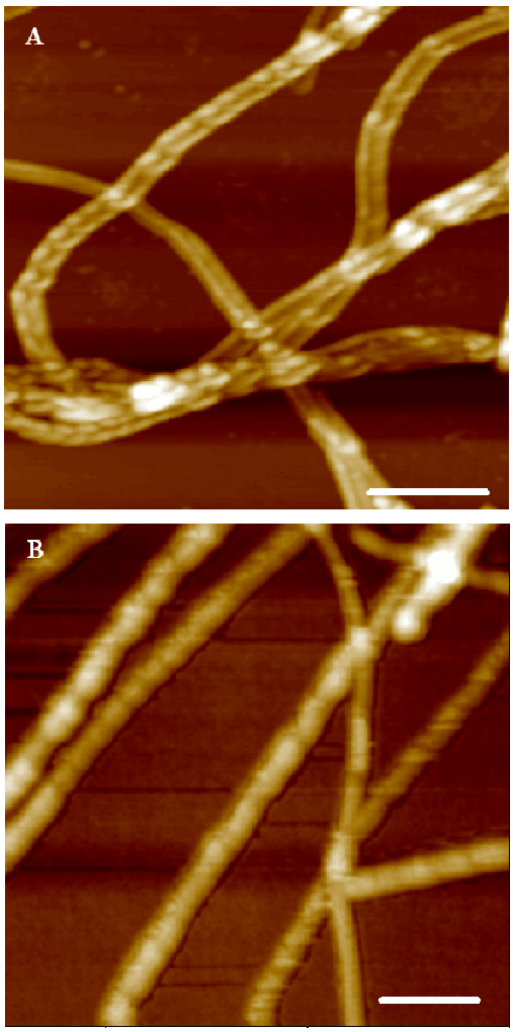

Figure 3.5: IAPP-3XL forms amyloid deposits. Tapping mode AFM images of (A) wild type human IAPP and (B) IAPP-3XL mutant. The horizontal scale bar represents 250 nm for (A) and 200 nm for (B). Vertical Z-scale is 60 nm for (A) and 20 nm for (B). Fibrils were prepared at pH 7.4, 25°C 20 mM Tris-HCl, 2% HFIP (V/V), yielding 0.14 mg/ml peptide.

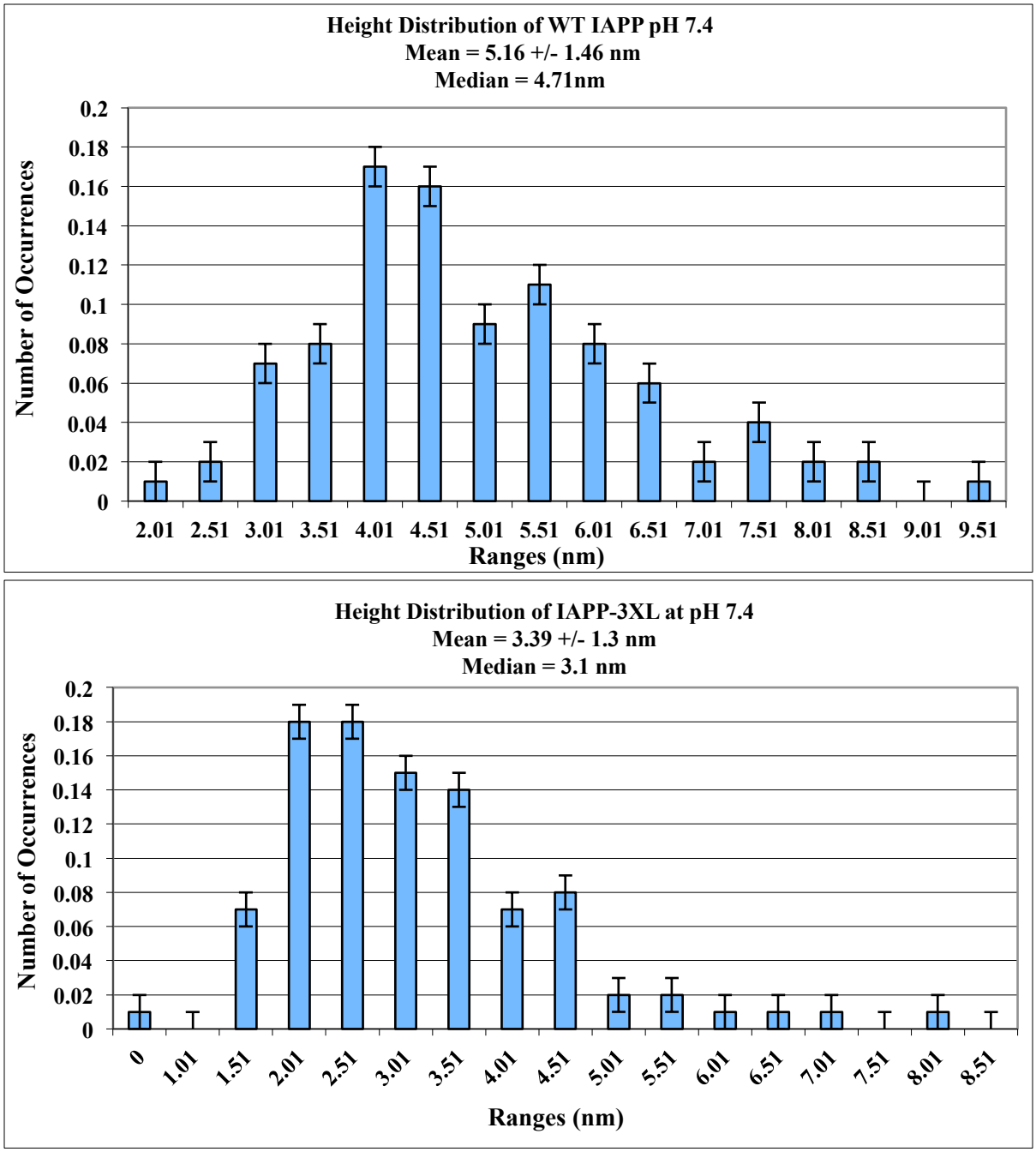

Figure 3.6: Two plots showing histograms of the height distributions of the wild-type amyloid fibrils (top) and of amyloid fibrils formed by the 3XL mutant (bottom), as determined by AFM. Fibrils were prepared at pH 7.4, 25°C 20 mM Tris-HCl, 2% HFIP (V/V), yielding 0.14 mg/ml peptide.

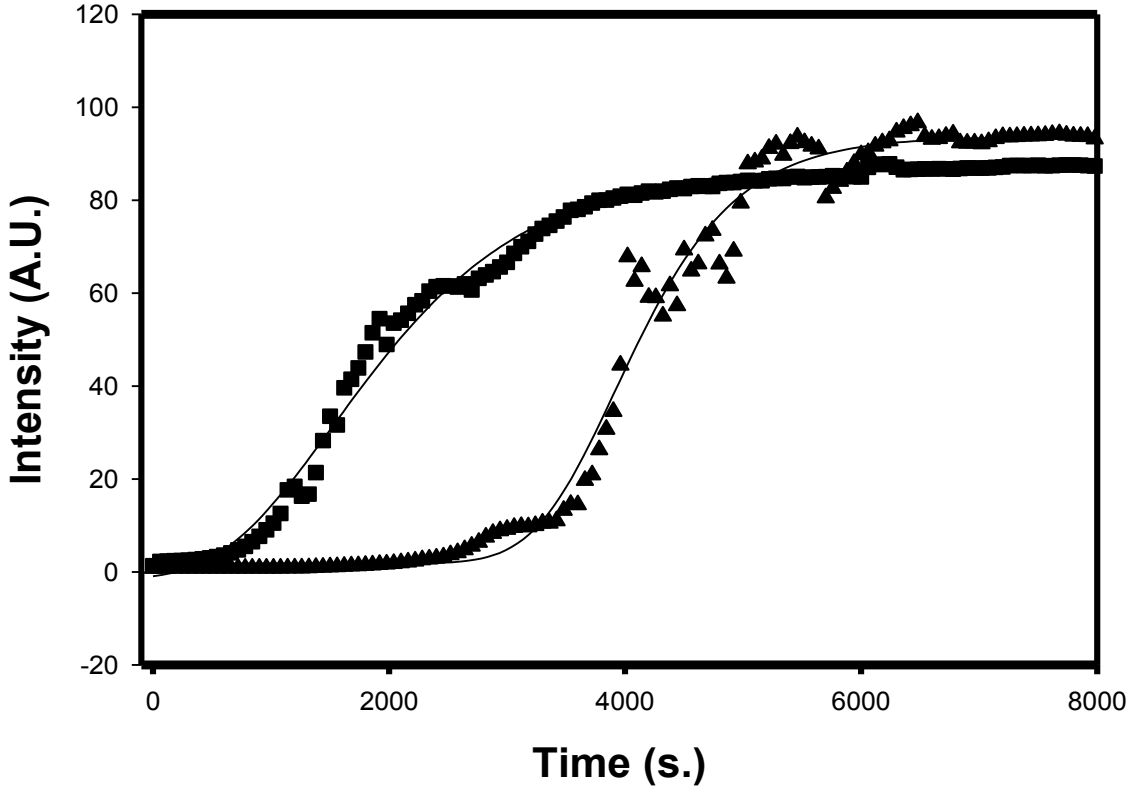

Figure 3.7: The 3XL mutant forms amyloid significantly more slowly than wild-type IAPP. Thioflavin fluorescence monitored kinetic assays of fibril formation by wild-type IAPP and IAPP-3XL. Reactions were initiated by diluting HFIP stock solutions into aqueous buffer. Final conditions were 64 μM thioflavin-T, 17 mM Tris-HCl at pH 7.4 and 0.14 mg/ml peptide. Experiments were performed with continuous stirring at 25 ºC. The solid line represents the best fit to a sigmodial curve.

3.6 References

1. Gazit, E. (2002) A possible role for π-stacking in the self-assembly of amyloid fibrils, *FASEB J.* **16**, 77-83.

2. Bemporad, F., Taddei, N., Stefani, M., Chiti, F. (2006) Assessing the role of aromatic residues in the amyloid aggregation of human muscle acylphosphatase, *Protein Sci.* **15**, 852-870.

3. Jack, E., Newsome, M., Stockley, P., Radford, S., Middleton, D. (2006) The organization of aromatic side groups in an amyloid fibril probed by solid-state 2H and 19F NMR spectroscopy, *J. Am. Chem. Soc.* **128**, 8098-8099.

4. Kapurniotu, A. (2001) Amyloidogenicity and cytotoxicity of islet amyloid polypeptide, *Peptide Sci.* **60**, 438-459.

5. Zanuy, D., Porat, Y., Gazit, E., Nussinov, R. (2004) Peptide sequence and amyloid formation: Molecular simulations and experimental study of a human islet amyloid polypeptide fragment and its analogs*, Structure* **12**, 439-455.

6. Tartaglia, G. G., Cavalli, A., Pellarin, R., Caflisch, A. (2004) The role of aromaticity, exposed surface and dipole moment in determing protein aggregation rates, *Protein Sci.* **13**, 1939-1941.

7. Yoon, S., Welsh, W. J. (2004) Detecting hidden sequence propensity for amyloid fibril formation, *Protein Sci.* **13**, 2149-2160.

8. Bemporad, F., Calloni, G., Campioni, S. Plakoutsi, G., Taddel, N., Chiti, F. (2006) Sequence and structural determinations of amyloid fibril formation, *Acc. Chem. Res.* **39**, 620-627.

9. Chiti, F., Stefani, M., Taddei, N., Ramponi, G., Dobson, C. M. (2003) Rationalization of the effects of mutations on peptide and protein aggregation, *Nature* **424**, 805-809.

10. Ferandez-Escamilla, A. M., Rousseau, F., Schymkowitz, J., Serrano, L. (2004) Predication of sequence-dependent and mutational effects on the aggregation of peptide and proteins, *Nature Biotechnol.* **22**, 1302-1306.

11. Burley, S.K., Petsko, G.A. (1988) Weakly polar interactions in proteins, *Adv. Protein Chem.* **39**, 125-189.

12. Azriel, R., Gazit, E. (2001) Analysis of the minimal amyloid-forming fragment of the islet amyloid polypeptide, *J. Biol. Chem.* **276**, 34156-34161.

13. Tracz, S., Abedini, A., Driscoll, M., Raleigh, D. (2004) Role of aromatic interactions in amyloid formation by peptides derived from human amylin, *Biochemistry* **43**, 15901-15908.

14. Padrick, S., Miranker, A. (2001) Islet amylyoid polypeptide: Identification of long-range contacts and local order on the fibrillogenesis pathway, *J. Mol. Biol.* **308**, 783-794.

15. Porat, Y., Mazor, Y., Efrat, S., Gazit, E. (2004) Inhibition of islet amyloid polypeptide fibril formation: A potential role for heteroaromatic interactions, *Biochemistry* **43**, 14454-14462.

16. Porat, Y., Abramowitz, A., Gazit, E. (2006) Inhibition of amyloid fibril formation by polyphenols: Structural similarity and aromatic interactions as a common inhibition mechanism, *Chem. Biol. Drug Des.* **67**, 27-37.

17. Cooper, G.J.S., Willis, A.C., Clark, A., Turner, R.C., Sim, R.B., Reid, K.B.M. (1987) Purification and characterization of a peptide from amyloid rich pancreases of type II diabetic patients, *Proc. Natl. Acad. Sci. U.S.A.* **84**, 8628-8632.

18. Westermark, P., Wernstedt, C., Wilander, E., Hayden D.W., O'Brien, T.D., Johnson, K.H. (1987) Amyloid fibrils in human insulinoma and islets of langerhans of the diabetic cat are derived from a neuropeptide-like protein also present in normal islet cells, *Proc. Natl. Acad. Sci. U.S.A.* **84**, 3881-3885.

19. Clark, A., Wells, C.A., Buley, I.D., Cruickshank. J.K., Vanhegan, R.I., Matthews, D.R., Cooper, G.J., Holman, R.R., Turner, R.C. (1988) Islet amyloid, increased A-cells, reduced B-cells. And exocrine fibrosis: Quantitative changes in the pancreas in type 2 diabetes, *Diabetes Res. Clin. Pract.* **9**, 151-159.

20. Kahn, S.E., D'Alessio, D.A., Schwartz, M.W., Fujimoto, W.Y., Ensinck, J.W., Taborsky, G.J.J., Porte, D.J. (1990) Evidence of cosecretion of islet amyloid polypeptide and insulin by β-cells, *Diabetes* **39**, 634-638.

21. Kahn, S.E., Andrikopoulos, S., Verchere, C.B. (1999) Islet amyloid: A long-recognized but underappreciated pathological feature of type 2 diabetes, *Diabetes* **48**, 241-253.

22. Jaikaran, E., Clark, A. (2001) Islet amyloid and type 2 diabetes: From molecular misfolding to islet pathophysiology, *Biochim. Biophys. Acta* **1537**, 179-203.

23. Clark, A., Lewis, C. E., Willis, A. C., Cooper, G. J. S., Morris, J. F., Reid, K. B. M., Turner, R. C. (1987) Islet amyloid formed from diabetes-associated peptide may be pathogenic in type-2 diabetes. *Lancet* **2**, 231-234.

24. Kajava, A.V., Aebi, U., Steven, A.C. (2005) The parallel superpleated β-structure as a model for amyloid fibrils of human amylin, *J. Mol. Biol.* **348**, 247-252.

25. Gazit, E. (2002) Mechanistic studies of the process of amyloid fibrils formation by the use of peptide fragments and analogues: Implications for the design of fibrillization inhibitors, *Curr. Med. Chem.* **9**, 1725-1735.

26. Abedini, A., Raleigh, D. P. (2005) Incorporation of pseudoproline derivatives allow the facile synthesis of human IAPP; A highly amyloidogenic and aggregation-prone polypeptide. *Org. Lett.* **7**, 693-696

27. Abedini, A., Raleigh, D. (2005) The role of His-18 in amyloid formation by human islet amyloid polypeptide, *Biochemistry* **44**, 16284-16291.

28. Lashuel, H.A., LaBrenz, S.R., Woo, L., Serpell, L.C., Kelly, J.W. (2000) Protofilaments, filaments, ribbons, and fibrils from peptidomimetic self-assembly: Implications for amyloid fibril formation and materials science, *J. Am. Chem. Soc.* **122**, 5262-5277.

29. Tenidis, K., Waldner, M., Bernhagen, J., Fischle, W., Bergmann, M., Weber, M., Merkle, M.-L., Voelter, W., Brunner, H., Kapurniotu, A. (2000) Identification of a penta- and hexapeptide of islet amyloid polypeptide (IAPP) with amyloidogenic and cytotoxic properties, *J. Mol. Biol.* **295**, 1055-1071.

30. Green, J. D., Goldsbury, C., Kistler, J., Cooper, G.J.S., Aebi, U. (2004) Human amylin oligomer growth and fibril elongation define two distinct phases in amyloid formation, *J. Biol. Chem.* **279**, 12206-12212.

31. Goldsbury, C., Kistler, J., Aebi, U., Arvinte, T., Cooper, G.J.S. (1999) Watching amyloid fibrils grow by time-lapse atomic force microscopy, *J. Mol. Biol.* **285**, 33-39.

32. Kayed, R., Bernhagen, J., Greenfield, N., Sweimeh, K., Brunner, H., Voelter, W., Kapurniotu, A. (1999) Conformational transitions of islet amyloid polypeptide (IAPP) in amyloid formation in vitro, *J. Mol. Biol.* **287**, 781-796.

33. Goldsbury, C.S., Cooper, G.J.S., Goldie, K.N., Muller, S.A., Saafi, E.L., Gruijters, W.T.M., Misur, M.P., Engel, A., Aebi, U., Kistler, J. (1997) Polymorphic fibrillar assembly of human amylin, *J. Struct. Biol.* **119**, 17-27.

34. Sedman, V.L., Allen, S., Chan, W.C., Davies, M.C., Roberts, C.J., Tendler, S.J.B. (2005) Atomic force microscopy of human amylin (20-29) fibrils, *Prot. Pept. Lett.* **12**, 79-83.

35. Gilead, S., Wolfenson, H., Gazit, E. (2006) Molecular mapping of the recognition interface between the islet amyloid polypeptide and insulin, *Angew. Chem. Int. Ed.* **45**, 6476-6480.

36. Westermark, P., Li, Z.C., Westermark, G.T., Leckstrom, A., Steiner, D.F. (1996) Effects of beta cell granule components on human islet amyloid polypeptide fibril formation, *FEBS Lett.* **379**, 203-206.

37. Kudva, Y.C., Mueske, C., Butler, P.C., Eberhardt, N.L. (1998) A novel assay in vitro of human islet amyloid polypeptide amyloidogenesis and effects of insulin secretory vesicle peptides on amyloid formation, *Biochem. J.* **331**, 809-813.

38. Larson, J.L., Miranker, A.D. (2004) The mechanism of insulin action on islet amyloid polypeptide fiber formation, *J. Mol. Biol.* **335**, 221-231.

39. Jaikaran, N.T., Nilsson, M.R., Clark, A. (2004) Pancreatic beta-cell granule peptides form heteromolecular complexes which inhibit islet amyloid polypeptide fibril formation, *Biochem. J.* **377**, 709-716.

4. Residue Specific, Real Time Characterization of Lag Phase Species and Fibril Growth During Amyloid Formation: A Combined Fluorescence and IR Study of *p*-Cyanophenylalanine Analogs of Islet Amyloid Polypeptide

Abstract

Amyloid formation normally exhibits a lag phase followed by a growth phase, which leads to amyloid fibrils. Characterization of the species populated during the lag phase is experimentally challenging, but is critical since the most toxic entities may be pre-fibrillar species. *p*-Cyanophenylalanine fluorescence is used to probe the nature of lag phase species populated during the formation of amyloid by human islet amyloid polypeptide. The polypeptide contains two phenylalanines at positions 15 and 23 and a single tyrosine located at the C-terminus. Each aromatic residue was separately replaced by *p*-cyanophenyalanine. The substitutions do not perturb amyloid formation relative to wild type IAPP as detected using thioflavin-T fluorescence and electron microscopy. *p*-Cyanophenylalanine fluorescence is high when the cyano group is hydrogen bonded and low when it is not. It can also be quenched via FRET to tyrosine. Fluorescence intensity was monitored in real time and revealed that all three positions remained exposed to solvent during the lag phase, but less exposed than unstructured model peptides. The time course of amyloid formation, as monitored by thioflavin-T fluorescence and *p*-cyanophenylalanine fluorescence, is virtually identical. Fluorescence quenching experiments confirmed that each residue remains exposed during the lag phase. These results place significant constraints on the nature of intermediates that are populated during the lag phase and indicate that significant sequestering of the aromatic side chains does not occur

until β-structure sufficient to bind thioflavin-T has developed. Seeding studies and analysis of maximum rates confirm that sequestering of the cyano groups occurs concomitantly with the development of thioflavin-T binding capability. Overall, the process of amyloid formation and growth appears to be remarkably homogenous in terms of side chain ordering. *p*-Cyanophenylalanine also provides information about fibril structure. Fluorescence emission measurements, infrared measurements and quenching studies indicate that the aromatic residues are differentially exposed in the fibril state with Phe-15 being the most exposed. *p*-Cyanophenylalanine is readily accommodated into proteins, thus the approach should be broadly applicable.

NOTE: The material presented in this chapter has been published (Peter Marek, Sudipta Mukherjee, Martin T. Zanni, Daniel P. Raleigh (2010) Residue Specific, Real Time Characterization of Lag Phase Species and Fibril Growth During Amyloid Formation: A Combined Fluorescence and IR Study of *p*-Cyanophenylalanine Analogs of Islet Amyloid Polypeptide. *J. Mol. Biol.*, **400**, 878-888). This chapter contains direct excerpts from the manuscript, which was written by me with suggestions and revisions from Professors Daniel P. Raleigh and Martin T. Zanni. Sudipta Mukherjee performed the FT-IR experiments.

4.1 Introduction

The process of amyloid formation has been implicated in a wide range of human diseases including Parkinson's disease, Alzheimer's disease and type-2 diabetes (1-5). The kinetics of amyloid formation are complex and normally exhibit a lag phase during which no amyloid fibrils are formed followed by a rapid growth phase leading to the final equilibrium between fibrils and soluble protein. The current view in the field is that intermediates in the assembly of amyloid may be the most toxic species and this has focused considerable attention on their properties (6-8).

Unfortunately, there are few methods available that provide precise structural information on amyloid assembly in real time. An important tool used to probe transition state structure in protein folding is the so-called ϕ-value or protein engineering method. However, this methodology is much less likely to be useful for studies of amyloid formation because the pathway of amyloid formation can be perturbed by mutations, amyloid fibrils can be polymorphic and fibril morphology can be altered by seemingly modest changes in primary sequence or in solution conditions (9-12). CD spectroscopy probes secondary structure formation, but is not residue-specific. Solution state NMR is generally not applicable because of the difficulty in obtaining high resolution spectra of rapidly aggregating systems and the time resolution of solid-state NMR is not sufficient for studying kinetics. 2D-IR, in conjunction with specific isotope labeling, holds considerable promise, but has not yet been applied to probe side chains, which may be the key to understanding the mechanism of amyloid formation (13).

The intrinsic fluorescence of Trp can be used to follow amyloid formation, but many biologically important amyloidogenic polypeptides lack Trp. These include the Aβ peptide from Alzheimer's disease, islet amyloid polypeptide (IAPP or amylin) which forms amyloid in type 2

diabetes, α-synuclein which is associated with Parkinson's disease and calcitonin. Trp can obviously be introduced into the polypeptide of interest, however, it is not always a conservative substitution and may perturb the kinetics and/or mechanism of amyloid formation, or alter fibril morphology. A more subtle point is that Trp fluorescence is sensitive to a variety of factors and can be difficult to develop an atomic level understanding of the features that control Trp fluorescence during amyloid formation. Intrinsic Tyr fluorescence is weaker than Trp fluorescence and suffers from the same drawbacks, including the fact that substitution of Tyr for Phe or for a hydrophobic amino acid is not completely conservative, particularly if the site is buried.

The most common method for studying the kinetics of amyloid formation *in vitro* is to use fluorescence-detected thioflavin-T binding assays. The fluorescence of thioflavin-T is negligible in the absence of amyloid, but is significantly enhanced upon binding to fibrils (14). However, it is not known what peptidic structure is necessary to bind thioflavin-T and the exact relationship between binding and the enhancement in quantum yield is not fully understood (12, 15-19). Thioflavin-T assays, while useful, provide no information about the lag phase species or about the role of specific side chains in the amyloid assembly process. In addition, thioflavin-T is not a completely amyloid specific dye and there have been reports of it binding to non-amyloidogenic structures (12, 16, 17). These issues led us to explore the use of fluorescent non-coded amino acids to follow the kinetics of amyloid formation, specifically *p*-cyanophenylalanine ($F_{C\equiv N}$ or cyanoPhe) (20).

$F_{C\equiv N}$ is a non-coded amino acid that can readily be incorporated into proteins by recombinant methods and by solid phase peptide synthesis (20-22). It has very desirable physiochemical and spectroscopic properties. The fluorescence of $F_{C\equiv N}$ is sensitive to hydrogen

bonding interactions involving the cyano group. The fluorescence quantum yield is high in water and low when the group is sequestered into a non-hydrogen bonding environment, such as the hydrophobic core of a protein, the interior of an amyloid fibril or in a protein-protein complex (20, 23, 24). $F_{C\equiv N}$ fluorescence can be selectively excited in the presence of a Tyr or a Trp and there are fewer problems associated with the water Raman peak than are observed with Tyr. The polarity of the cyano group is intermediate between that of an amide and a methylene, allowing it to be readily accommodated to the hydrophobic interior of a folded protein, and its size makes it a suitable substitution for Tyr or Phe (23). $F_{C\equiv N}$ also forms a useful FRET pair with Trp or Tyr in which $F_{C\equiv N}$ acts as the donor (23, 25-27). The R_0 for the $F_{C\equiv N}$-Trp pair is 16 Å and approximately 13 Å for a $F_{C\equiv N}$-Tyr pair. These are useful distances for studies of chain compaction during folding and aggregation (28, 29). The C≡N stretching frequency can also be useful as an infrared reporter of the local environment, providing information about solvation and internal electric fields (30-33). The C≡N stretch is found in an otherwise transparent region of protein IR spectra and shifts by ~10-12 cm^{-1} depending upon the degree of solvation (30).

We use $F_{C\equiv N}$ substitutions to follow amyloid formation by islet amyloid polypeptide (IAPP or amylin). IAPP is a 37 residue, highly amyloidogenic peptide that is stored and co-secreted with insulin from the β-cells of the pancreas (34, 35). Amyloid formation by IAPP is believed to contribute to the pathology of type 2 diabetes and amyloid deposits have been found in up to 90% of autopsied individuals who suffered from type 2 diabetes (36-40). Islet amyloid formation is thought to induce apoptosis of the β-cells and to contribute to the decline in the mass of β-cells during type 2 diabetes (34, 35, 41). There is also increasing evidence suggesting that IAPP amyloid formation may contribute to graft failure in islet transplantation (42-45). We have shown that $F_{C\equiv N}$ is a conservative substitution for the C-terminal Tyr of IAPP and that its

fluorescence can be used to detect fibril formation (20). In the present study we characterize three analogs of IAPP in which each aromatic residue is separately substituted with $F_{C\equiv N}$. We show that these substitutions provide non-perturbing probes of IAPP amyloid formation and use time-resolved studies of $F_{C\equiv N}$ fluorescence to follow the structural transitions that occur during amyloid formation. Chloride ion is an efficient quencher of $F_{C\equiv N}$ fluorescence and we exploit this effect to monitor the exposure of the three sites in real time. Seeding studies are used to follow the addition of soluble IAPP to pre-formed fibrils and provide site-specific information about the burial of each of the aromatic residues during fibril growth. Finally, the fluorescence studies are complimented by conducting IR measurements of the final fibril structure. The results reported here illustrate the utility of $F_{C\equiv N}$ fluorescence probes, as well as the advantages of combining fluorescence and IR studies. Virtually nothing is known about the nature of species populated during the lag phase and the present work provides new information about the process of IAPP amyloid assembly (46-48).

4.2 Materials and Methods

4.2.1 Peptide synthesis and purification

The $F_{C\equiv N}$ IAPP variants, wild type IAPP and a short control peptide ($GGF_{C\equiv N}AA$) were synthesized on a 0.25 mmol scale with an Applied Biosystems 433A Peptide Synthesizer, utilizing 9-fluornylmethoxycarbonyl (Fmoc) chemistry. Solvents used were ACS-grade. Fmoc-protected pseudoproline (oxazolidine) dipeptide derivatives were used as previously described (56). Fmoc amino acids and pseudoproline dipeptide derivatives were purchased from Novabiochem. Fmoc-L-4-cyanophenylalanine was purchased from Peptech Corporation. All other reagents were purchased from Advanced Chemtech, PE Biosystems, Sigma and Fisher

Scientific. Use of a 5-(4'-Fmoc-aminomehtyl-3', 5- dimethoxyphenol) valeric acid (PAL-PEG) resin afforded an amidated C-terminus. The N-termini of all peptides were free. Standard Fmoc reaction cycles were used. The first residue attached to the resin, all β-branched residues, the residue directly following a β-branched residue, all psuedoproline dipeptide derivatives and the residue directly following a pseudoproline dipeptide derivative were double-coupled. Peptides were cleaved from the resin through the use of standard trifluoroacetic acid (TFA) methods. The disulfide bond was formed via DMSO induced oxidation (57). The peptides were purified via reverse-phase high-performance liquid chromatography using a Vydac C18 preparative column. A two-buffer system was utilized in which Buffer A consisted of H_2O and 0.045% HCl (v/v) and Buffer B consisted of 80% acetonitrile, 20% H_2O and 0.045% HCl (v/v). HCl was used as the ion pairing agent since TFA causes problems with IR of polypeptides and residual TFA can influence the aggregation properties of amyloidogenic peptides (58). The identity of the pure polypeptide was confirmed by matrix-assisted laser desorption ionization time-of-flight mass spectrometry (MALDI-TOF MS). The expected mass for both IAPP $15F_{C\equiv N}$ and $23F_{C\equiv N}$ was 3929.3 Da and masses of 3928.6 Da and 3929.8 Da were observed, respectively. The expected mass of $37F_{C\equiv N}$ was 3912.3 Da and the observed mass was 3911.8 Da. The purity of the polypeptides was checked by HPLC using a Vydac C18 analytical column.

4.2.2 Fluorescence assays

All fluorescence assays were performed on a Photon Technology International fluorescence spectrophotometer. Thioflavin-T fluorescence was excited at 450 nm and monitored at 485 nm. $F_{C\equiv N}$ fluorescence was excited at 240 nm and the emission monitored at 296 nm. The emission and excitation slits were set to 5 nm and a 1.0 cm cuvette was used for all experiments.

The fluorescence of thioflavin-T and $F_{C\equiv N}$ was measured simultaneously for the same sample in dual dye mode during kinetic runs, which allows kinetic traces to be collected in an interleaved fashion. The kinetic experiments were performed by diluting a stock solution of peptide, 1.58 mM in HFIP, into 20 mM Tris-HCl buffer at pH 7.4 containing thioflavin-T. This is a standard protocol for biophysical studies of IAPP amyloid formation (20, 46, 51). The final solution conditions were 2% HFIP, 32 μM peptide and 32 μM thioflavin-T at pH 7.4 and 25ºC for all experiments. The HFIP stock solutions were filtered with a 0.45 μm GHP Acrodisc filter prior to dilution into buffer. All solutions were stirred during the experiments to maintain solution homogeneity. Stirring significantly accelerates the rate of amyloid formation. The fluorescence spectra of the final fibril state shown in Figure-3 were corrected for contributions from trace amounts of soluble IAPP. Fluorescence emission spectra were collected and the samples were then filtered through a 10,000 Da molecular weight ultrafiltration device by sedimentation at 22,000 g for 45 minutes. The supernatant contained only soluble IAPP as judged by the fact that the intensity of the thioflavin-T fluorescence was the same as observed at the start of the kinetic assay (data not shown). The $F_{C\equiv N}$ fluorescence spectra of these solutions were collected and subtracted from that of the unfiltered sample. The difference spectra represent the contribution from the fibril.

The apparent maximum rate, the rate at $t=t_{50}$, was calculated by numerically differentiating the $F_{C\equiv N}$ and thioflavin-T fluorescence vs. time curves. The maximum velocity, v_{max}, was calculated using the procedure described in reference 57. Briefly, the data were fit to the expression $r(t) = (m_1 + t + r_1)\alpha + (m_2 + t + r_2)(1-\alpha)$, where $\alpha = (1 + e^{((t_{50}-t)/\tau)})^{-1}$, which describes a sigmoidal curve. The time constant of the transition, τ, is converted to v_{max} by the

equation $v_{\max} = \frac{[IAPP]_{t=0}}{4\tau}$, where $[IAPP]_{t=0}$ is the total concentration of IAPP at the start of the reaction.

For the seeding assays, preformed wild type hIAPP fibrils were produced by diluting a 1.58 mM stock solution of peptide in HFIP into 20 mM Tris-HCl buffer containing thioflavin-T at pH 7.4 for a final concentration of 32 μM wild type hIAPP in 2% HFIP. The solution was incubated for 60 minutes and thioflavin-T fluorescence was monitored to ensure fibril formation had occurred. Fibrils from this reaction were diluted into buffer. The IAPP $F_{C\equiv N}$ variants, 1.58 mM stock solutions in HFIP, were then diluted into the seeded buffer for final conditions of 32 μM peptide, 32 μM thioflavin-T, 3.2 μM seed (in monomer units) and 2.2% HFIP at pH 7.4. Data was recorded with constant stirring at 25ºC.

The Stern-Volmer analyses were performed by following the time course of fibril formation via $F_{C\equiv N}$ fluorescence in buffers that contained increasing chloride concentrations ranging from 20-120 mM Cl^- at 20 mM intervals. Fluoride was used to keep the ionic strength constant at a total ionic strength (NaCl, NaF and Tris HCl) of 120 mM in each assay. Fluoride has no affect on $F_{C\equiv N}$ fluorescence. Final conditions were 32 μM peptide, 32 μM thioflavin-T, 100 mM salt, 20mM Tris HCl at pH 7.4 and 25ºC with constant stirring. F_0 is defined as the fluorescence in 20 mM Tris-HCl and 100 mM NaF. Stern-Volmer plots were generated for each peptide at the 60 s. time point which is during the lag phase, at 200 s. which is near the end of the lag phase and at 1000 s., which corresponds to fibril formation as judged by $F_{C\equiv N}$ and thioflavin-T fluorescence.

4.2.3 Transmission electron microscopy (TEM)

TEM was performed at the University Microscopy Imaging Center at the State University of New York at Stony Brook. 15 μL samples from the end of the kinetic experiments were placed on a carbon-coated 300-mesh copper grid and negatively stained with saturated uranyl acetate.

4.2.4 FTIR measurements

FTIR spectra were measured on a Thermo Scientific Nicolet IS 10 FTIR spectrometer with a resolution of 1 cm^{-1}. All measurements were done using a CaF_2 sample cell with a path length of 75 μm. The spectra were averaged for 500 scans for both the sample and the background. Final conditions were 2.5 mM peptide as determined by weight in 20 mM Tris-HCl at pH 7.4 and 2% HFIP.

4.3 Results

4.3.1 $F_{C\equiv N}$ substitutions do not perturb the kinetics of amyloid formation.

IAPP contains an amidated C-terminus, a disulfide bridge between residues 2 and 7 and three aromatic residues: two phenylalanines at positions 15 and 23 and a tyrosine at position 37. None of the aromatic residues are absolutely required for amyloid formation, although a triple mutant in which each aromatic residue is replaced by Leu forms amyloid approximately 5-fold more slowly than wild type (49). The sequence of wild type IAPP and the three $F_{C\equiv N}$ substituted peptides are shown in Figure 4.1 along with a molecular representation of $F_{C\equiv N}$.

The kinetics of amyloid formation for each of the three variants was followed by thioflavin-T fluorescence and compared to wild type (Figure 4.2). Amyloid formation by IAPP

follows the typical pattern observed for the time course of fibril assembly, namely, a lag phase during which no significant fibril formation occurs followed by a rapid growth phase which leads to the final state in which amyloid fibrils are in equilibrium with soluble peptide. Each of the three variants exhibit a thioflavin-T binding time course typical of those observed for IAPP. The substitution has no noticeable effect at positions 23 and 37 and the measured t_{50} values, defined as the time to 50% completion, are identical to wild type (Table 4.1). An $F_{C\equiv N}$ substitution at position 15 ($F15F_{C\equiv N}$) has a small but reproducible effect on the t_{50} value. The t_{50} is reduced from 960±60 seconds (the uncertainty is the apparent standard deviation determined from multiple measurements) for wild type IAPP under these conditions to 876±10 seconds, less than a 10% change. This is a modest effect and is less than has been observed for a number of other substitutions (48-50). The lag times, t_{lag} (defined as the time required to reach 10% of the total fluorescence intensity), are also very similar to wild type. The lag times of each of the variants differ from the wild type value by at most 8%. The maximum reaction velocities are also very close to the value observed for wild type. Overall, the data indicates that $F_{C\equiv N}$ substitutions have very modest effects on the time course of amyloid formation (Table 4.1). TEM images of each $F_{C\equiv N}$ peptide were recorded at the end of the reaction to check if the substitution perturbed fibril morphology. Dense mats of fibrils were observed for all three $F_{C\equiv N}$ variants and there were no detectable differences relative to wild type IAPP (Figure 4.2).

4.3.2 The side chains of residues 15, 23 and 37 remain exposed during the lag phase.

Having established that the substitutions do not significantly perturb the overall kinetic profile or the morphology of the fibrils, we next turned to use $F_{C\equiv N}$ fluorescence to probe fibril formation. We plotted the data as normalized fluorescence to facilitate a comparison of the three

variants and to normalize for any local sequence effects that might modulate $F_{C\equiv N}$ fluorescence intensity in the absence of any defined structure. For example, proximity in primary sequence to potential side chain quenchers. The non-normalized intensity of the t=0 spectra are very similar for each $F_{C\equiv N}$ variant and differ by less than 10% suggesting that each site samples similar environments at t=0 in terms of the relative exposure of the cyano group to solvent and/or quenching groups. Stern-Volmer analysis of quenching data described in subsequent sections indicates, however, that the cyano groups are less exposed to solvent early in the lag phase than found in a $GGF_{C\equiv N}AA$ control peptide.

A significant change in $F_{C\equiv N}$ fluorescence is observed for all three peptides upon amyloid formation (Figure 4.3 and Table 4.2), with the fluorescence intensity of the fibril state being significantly lower. There are differences in the final relative fluorescence intensity between the three $F_{C\equiv N}$ peptides that reflect differences in the local environment of the aromatic side chains. The final $F_{C\equiv N}$ fluorescence intensity decreases to 40±1%, 26±1%, and 18±1% of their initial values for the $15F_{C\equiv N}$, $23F_{C\equiv N}$ and $37F_{C\equiv N}$ IAPP variants, respectively. The fluorescence intensity of the fibril state was corrected for trace amounts of soluble IAPP present, as described in the methods. The correction is very small and does not alter the conclusions since the ratios are only changed by 3-4% (Figure 4.4). The decrease indicates that the cyano groups are less solvated in the fibrils and/or are in closer proximity to a side chain, which quenches their fluorescence. These effects are considered in more detail below in conjunction with the analysis of the FTIR data.

The fact that each labeled site experiences a significant fluorescence change upon fibril formation means that the $F_{C\equiv N}$ groups can be used as site-specific reporters. The time courses of thioflavin-T fluorescence and $F_{C\equiv N}$ fluorescence are displayed in Figure 4.5 for each variant.

The curves are normalized so that the total signal change varies from 0 to 1 in order to allow a direct comparison. There are two striking observations: The first is that the $F_{C\equiv N}$ and thioflavin-T fluorescence curves track each other extremely closely for each sample. The measured t_{50} and t_{lag} values determined by each method agree to within experimental uncertainty. The second is that the t_{50} and t_{lag} values are very similar for the different sites (Table 4.1 and Table 4.2). Note that the $F_{C\equiv N}$ fluorescence remains high and constant during the lag phase for all peptides and only begins to decline when thioflavin-T fluorescence starts to increase. This is an important observation since it shows that the cyano groups do not become desolvated until final fibril formation commences and also indicates that there are no significant changes in the distribution of $F_{C\equiv N}$-Tyr distances during the lag phase, or at least no changes that alter $F_{C\equiv N}$-Tyr FRET beyond those which occur during the 3 second dead time of the measurements. The constant $F_{C\equiv N}$ fluorescence signal during the lag phase is not a consequence of the normalization since the data was simply scaled on the y-axis by setting the maximum intensity to 1.0 and the minimum intensity to 0. The non-normalized curves are shown in the Figure 4.6. The results are also not an artifact caused by having thioflavin-T present during the $F_{C\equiv N}$ fluorescence measurements since similar $F_{C\equiv N}$ time courses were observed in the presence and absence of thioflavin-T. The measured t_{50} and t_{lag} values determined by thioflavin-T and $F_{C\equiv N}$ fluorescence are listed in Table 4.1 and Table 4.2, respectively.

4.3.3 The side chains of residues 15, 23 and 37 are buried at the same rate during fibril growth.

The apparent maximum rate during the growth phase, which is equal to the rate at $t=t_{50}$, can be easily calculated by numerically differentiating the kinetic progress curves to obtain $\left|\frac{dF(t)}{dt}\right|_{t=t_{50}}$, where F(t) is the fluorescence signal as a function of time. The rate reflects the

addition of soluble peptide to growing fibrils, either by binding to fibril ends or via secondary nucleation. The values for the three $F_{C\equiv N}$ curves are similar, varying by less than a factor of two (Table 4.2) and the values determined from the thioflavin-T curves (Table 4.1) are in good agreement with the values deduced from the $F_{C\equiv N}$ data. The absolute velocity at $t = t_{50}$, v_{max}, can be calculated using a simple analytical relationship and the known concentration of IAPP (Materials and Methods). The values calculated for the three $F_{C\equiv N}$ curves are similar and vary by approximately 40%. The values determined from the thioflavin-T data (Table 4.1) are also in good agreement with each other and with the absolute velocities calculated from the $F_{C\equiv N}$ data (Table 4.2).

Seeding studies using wild type IAPP were performed to investigate the burial of the $F_{C\equiv N}$ group as fibril formation occurs. Seeding reactions involve taking a small amount of preformed fibrils and adding them to the start of a fresh kinetic reaction. The preformed fibrils act as a "seed" and nucleate fibril formation, bypassing the lag phase typically seen during amyloid formation. The times to reach 50% completion of the seeded reaction, denoted here as t^s_{50}, were found to be 76, 90 and 96 s. for the $15F_{C\equiv N}$, $23F_{C\equiv N}$ and $37F_{C\equiv N}$ IAPP variants, respectively (Figure 4.7), based on the $F_{C\equiv N}$ fluorescence. These are modest differences and are even less when normalized by the respective t_{50} for the non-seeded reaction. As noted previously, the $F15F_{C\equiv N}$ substitution leads to a small, but reproducible, decrease in the t_{50} for a non-seeded reaction. The modest perturbation induced by the $F_{C\equiv N}$ replacement at position 15 can be accounted for by normalizing each value of the seeded t_{50} by the respective non-seeded t_{50}, $\frac{t^s_{50}}{t_{50}}$. The ratios (Table 4.1) vary by less than 10%, reinforcing the conclusions derived from the calculation of the rates at t_{50}.

4.3.4 Fluorescence quenching studies confirm that the side chains of residues 15, 23 and 37 remain exposed during the lag phase.

Chloride is an efficient quencher of $F_{C\equiv N}$ fluorescence and was used to probe the exposure of the $F_{C\equiv N}$ group throughout the time course of fibril formation by conducting kinetic experiments in the presence of increasing concentrations of Cl^-, 20-120 mM (23). Stern-Volmer plots were constructed to quantitatively measure exposure of the $F_{C\equiv N}$ groups in IAPP relative to a control peptide. As a control, a five residue peptide ($GGF_{C\equiv N}AA$) was used to determine the Stern-Volmer constant (K_{SV}) for a fully exposed (solvated) $F_{C\equiv N}$ residue. Significant changes in the ratio of the fluorescence measured in the absence (F_0) and presence (F) of quencher were detected over the range of 20 to 120 mM Cl^-. The value of K_{SV} for the pentapeptide was found to be 9.3 M^{-1} (Figure 4.8).

The rate of amyloid formation by IAPP is strongly dependent upon ionic strength and the t_{50} value was found to decrease from 960 s. for wild type at 20 mM ionic strength (20 mM Tris-HCl) to 406 s. for 120 mM ionic strength (20 mM Tris-HCl, 100 mM NaCl). The t_{50} value continues to decrease at higher ionic strengths. IAPP is a cationic peptide and the salt effect is likely due to the screening of unfavorable charge-charge interactions (51). Thus, the Cl^- quenching experiments were conducted using NaF to maintain constant ionic strength at 120 mM. Fluoride has no impact on $F_{C\equiv N}$ fluorescence. We tested for ion specific effects and found no differences in the kinetics of fibril formation caused by the substitution of F^- for Cl^-. Thus, NaF is a good salt for maintaining constant ionic strength. K_{SV} values of 4.1±0.6, 3.9±0.5 and 3.9±0.1 M^{-1} were measured for the $15F_{C\equiv N}$, $23F_{C\equiv N}$ and $37F_{C\equiv N}$ IAPP peptides, respectively, early in the lag phase (60 s.) (Figure 4.9 and Table 4.3). These values are less than 50% of the value observed for the control peptide suggesting that partial sequestration of the $F_{C\equiv N}$ groups from the

quencher occurs within the dead time of the experiment, or that the polypeptide samples conformations in its monomeric state which leads to partial protection or that neighboring residues provide more protection of the cyano group from quenchers in IAPP than in the control peptide.

The K_{SV} values remain constant throughout the lag phase (Figure 4.9 and Table 4.3). Near the end of the lag phase (200 s.) the K_{SV} values are 4.0±0.4 M^{-1} for the $F15F_{C\equiv N}$ variant and 3.7±0.3 M^{-1} for both the $F23F_{C\equiv N}$ and the $Y37F_{C\equiv N}$ variants. These values are within experimental uncertainty of each other and are within experimental uncertainty of the values at 60 s. Statistically significant differences were observed, however, when fibril formation was complete. K_{SV} values of 2.0±0.2, 1.3±0.2 and 1.5±0.03 M^{-1} were measured for the $15F_{C\equiv N}$, $23F_{C\equiv N}$ and $37F_{C\equiv N}$ IAPP peptides respectively at 1,000 s. (Figure 4.9 and Table 4.3). The experiments show that all three sites are equally exposed, within the precision of the quenching studies, during the initial stages of fibril assembly, but differences are observed in the final state, with residue 15 exhibiting a larger K_{SV} as compared to positions 23 or 37. This is in good agreement with the fluorescence intensities. Linear Stern-Volmer plots are observed for all three variants at all three times, consistent with the $F_{C\equiv N}$ residues sampling relatively homogenous environments, in terms of their exposure to quencher.

4.3.5 IR measurements probe the environment of the cyano groups in the fibril state.

As noted previously, the cyano group is an environmentally sensitive IR probe and this provides an independent means to test the conclusions derived from the fluorescence measurements (29). The expected frequency of an $F_{C\equiv N}$ group in water is 2237 cm^{-1} while in a non-polar solvent it is red shifted to 2228 cm^{-1} (30). The IR frequency of all three IAPP $F_{C\equiv N}$

variants in the fibril state differ from the $GGF_{C\equiv N}AA$ control peptide and all are red shifted, indicating that the $F_{C\equiv N}$ groups are less exposed to water. Interestingly, clear differences are observed for the three peptides (Figure 4.10 and Table 4.3). The IR frequency of the cyano labels at position 23 and 37 are within 1 cm^{-1} of each other (2229 cm^{-1} and 2230 cm^{-1}, respectively), while the band for $15F_{C\equiv N}$ is the least red shifted (2233 cm^{-1}) and closer to the control peptide (2236 cm^{-1}). This is consistent with a higher solvent exposure and in excellent agreement with the observed $F_{C\equiv N}$ fluorescence intensities and with the quenching studies.

4.4 Discussion and Conclusions

We have shown that the $F_{C\equiv N}$ IAPP derivatives are non-perturbing probes of amyloid formation by IAPP and have demonstrated that they allow amyloid formation to be followed by fluorescence emission, fluorescence quenching and IR. The data is remarkably self-consistent with the final fluorescence intensity, the Stern-Volmer analyses and the IR measurements, indicating that the $F_{C\equiv N}$ group at position 15 is more exposed in the fibril. Tycko and coworkers have used solid state NMR to develop two models of the amyloid fibril. F15 is the only aromatic residue of the three aromatic groups that resides in the β-sheet core, while F23 is located in a bend and Y37 appears partially exposed at the C-terminus (52). Interestingly, one of the models developed from the solid-state NMR constraints places F15 in a relatively solvent exposed position while the second model has it buried. Our data is consistent with the model that places F15 in the more exposed position. An alternative possibility is that the cyano group at position 15 is forming hydrogen bonds with another residue, since this will lead to increased fluorescence. Both of the solid-state models place the side chains of residues F23 and F37 in relatively exposed positions that, at first glance, may appear to be inconsistent with the

fluorescence and IR data. However, it is very important to remember that the details of fibril structure are sensitive to conditions and the material for the solid-state NMR studies was prepared using a lengthy procedure to produce a single polymorph. These conditions were necessary to achieve a homogenous sample, but are not compatible with real time kinetic experiments and differ from the ones required here. Thus, it should not be surprising that slight differences are observed between the present study and the NMR structures. Irrespective of any apparent minor ambiguities in fibril structure, we believe that the most interesting results are derived from the time-resolved studies.

To the best of our knowledge, this work represents the first study that monitors the side chain exposure of specific residues during amyloid formation by IAPP in real time. Our time-resolved fluorescence intensity measurements and Stern-Volmer analyses indicate that the $F_{C\equiv N}$ groups are exposed throughout the entire lag phase, but are less exposed than expected for a fully solvated $F_{C\equiv N}$ group. These results indicate that significant sequestering of the aromatic side chains does not occur until β-structure sufficient to bind thioflavin-T has developed. The seeding studies and analysis of the maximum rates further confirm that sequestering of the $F_{C\equiv N}$ groups occurs concomitantly with the development of thioflavin-T binding capability. Overall, the ordering of the side chains during amyloid formation and growth appears to be remarkably homogenous for the conditions used here (2% HFIP, pH 7.4 and constant stirring). Any models of lag phase intermediates need to take this into account.

Helical intermediates have been proposed to play a role in the early stages of amyloid formation by IAPP and Eisenberg and co-workers have proposed a model involving a partially helical dimer in which inter-helical contacts occur in the region near F15 (11, 48, 53). Our data

indicates that whatever the nature of the intermediate, it does not involve tight specific contacts which bury the aromatic side chain and remove them completely from water.

Weak FRET can be detected between Phe and Tyr and this effect was exploited in early studies of IAPP fibril formation (46). A 48% FRET efficiency was observed during the lag phase and was interpreted to indicate compaction of the chain during the lag phase, although the results are difficult to interpret in terms of specific pairwise distances since FRET could occur from either or both of the two Phe residues (46). Recent NMR-based diffusion measurements, as well as independent triplet quenching studies of a Y37W mutant, albeit performed under different conditions, also provide evidence that human IAPP samples compact conformations prior to amyloid formation (54, 55). As noted above, $F_{C\equiv N}$ fluorescence is quenched by FRET to Tyr and this provides an independent means of assessing compaction. The Förster distance (R_0) for a $F_{C\equiv N}$-Tyr pair is on the order of 12-13 Å. F15-Y37 distances ranged from 22 to 26 Å in the solid-state NMR model in which F15 is solvent exposed and 23 to 24 Å in the model in which F15 is buried. The F23-Y37 distances were measured to be from 6 to 13 Å in the model in which F15 is solvent exposed and 7 to 12 Å in the model in which F15 is buried. Thus, one would expect a significant increase in FRET involving $F_{C\equiv N}$ at position 23 and a corresponding decrease in fluorescence intensity if the polypeptide went from an extended conformation to a compact conformation, which approximated the fibril structure during the lag phase. The present data clearly indicates that this does not occur under the conditions of our experiments or if it does, it does so very rapidly in the initial stages of the lag phase that correspond to the dead time of our studies, since we detect no significant changes in $F_{C\equiv N}$ intensity during the lag phase. These observations place significant constraints on the conformation of lag phase intermediates.

The use of $F_{C\equiv N}$ is not limited to IAPP and can be applied to other systems. For example, both Aβ and α-synuclein contain multiple Phe and Tyr residues, 4 in Aβ and 6 in α-synuclein, but lack Trp. $F_{C\equiv N}$ analogs should also be useful for probing the interaction of amyloidogenic proteins with inhibitors and with membranes. Lifetime measurements also offer the possibility of obtaining more detailed information about local dynamics.

4.5 Figures

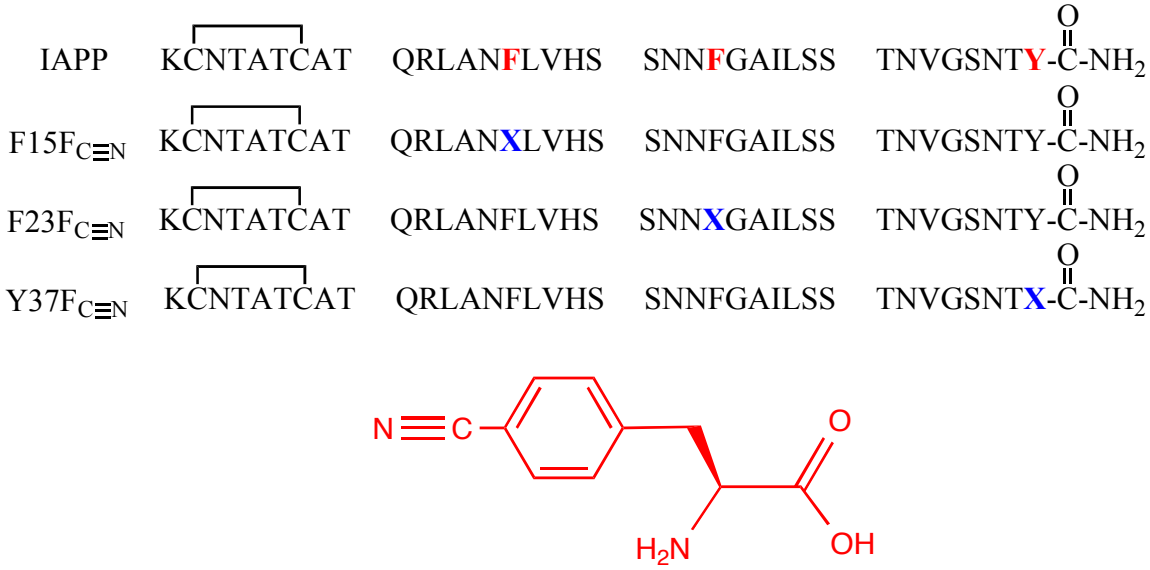

Figure 4.1: Primary sequence of human IAPP, with positions 15, 23 and 37 highlighted in red, and the three $F_{C\equiv N}$ variants. IAPP contains a disulfide between residues 2 and 7 and the C-terminus is amidated. X denotes the location of the $F_{C\equiv N}$ substitutions. Below, in red, shows the structure of *p*-cyanophenylalanine.

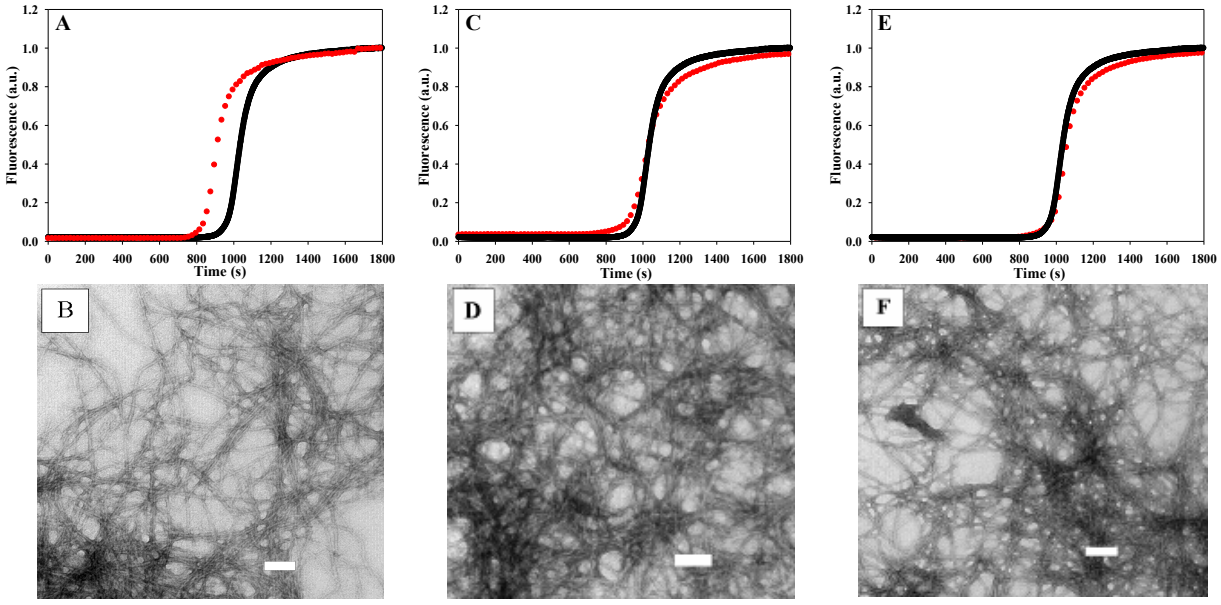

Figure 4.2: Thioflavin-T monitored kinetics of the $F_{C\equiv N}$ variants of IAPP compared to wild type, together with TEM images of the $F_{C\equiv N}$ variants collected at the end of the reaction. Red curves are $F_{C\equiv N}$ variants and the black curve is wild type IAPP. A and B, IAPP F15$F_{C\equiv N}$; C and D, IAPP F23$F_{C\equiv N}$; E and F, IAPP Y37$F_{C\equiv N}$. The scale bar in the TEM images represents 100 nm. Final conditions were 32 μM peptide, 2% HFIP, 20 mM Tris-HCl at pH 7.4 and 25 ºC.

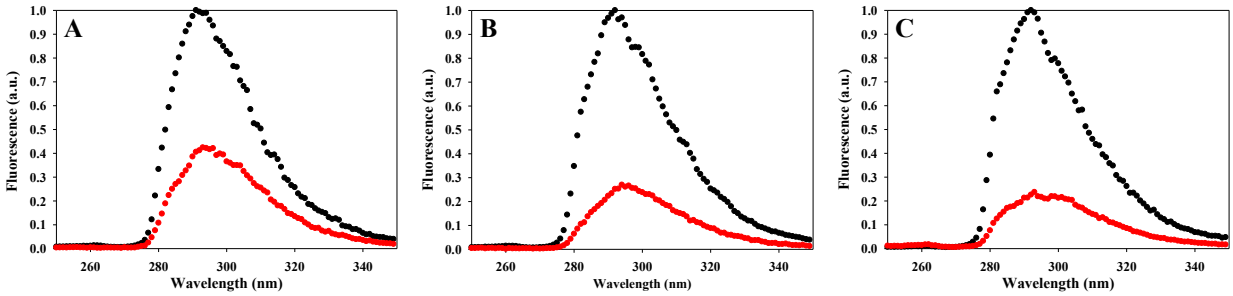

Figure 4.3: Fluorescence emission spectra of the $F_{C\equiv N}$ variants of IAPP collected at the start of the fibrillization reaction (black) and after amyloid formation is complete with any contributions from monomers subtracted out (see Material and Methods) (red). A, $15F_{C\equiv N}$; B, $23F_{C\equiv N}$; C, $37F_{C\equiv N}$. Fluorescence was excited at 240 nm. Final conditions were 32 μM peptide, 2% HFIP, 20 mM Tris-HCl at pH 7.4 and 25 ºC.

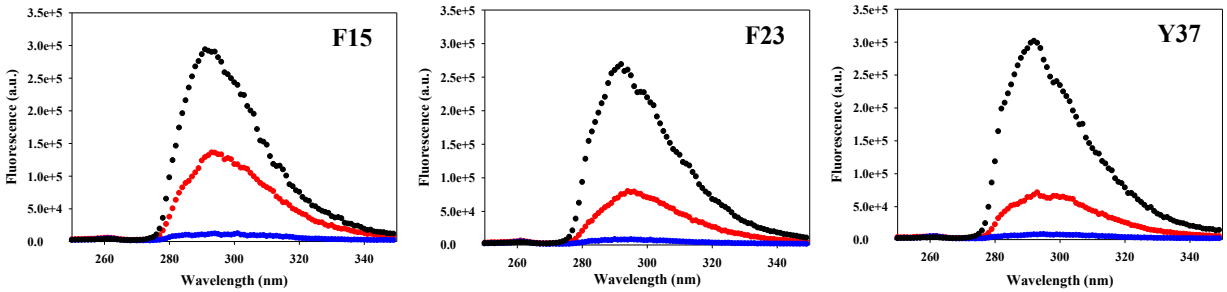

Figure 4.4: Comparison of the fluorescence emission spectra recorded at the start of a kinetic run (black curves) and the uncorrected spectra recorded at the end of the run, i.e. the fibril state (red curves). Also shown are the spectra of fibril solutions after filtration through a 10,000 Da molecular weight ultrafiltration device by sedimentation (blue curves). The curves represent the contributions from soluble IAPP present at the end of the kinetic run (see Methods). The contribution is very small and leads to a trivial change in the ratio of initial fluorescence to final fluorescence. The ratio for $F15F_{C\equiv N}$ is 0.40 for the corrected spectra, 0.44 for the uncorrected spectra; for $F23F_{C\equiv N}$ it is 0.26 corrected and 0.30 uncorrected; for $Y37F_{C\equiv N}$ it is 0.18 corrected and 0.21 uncorrected.

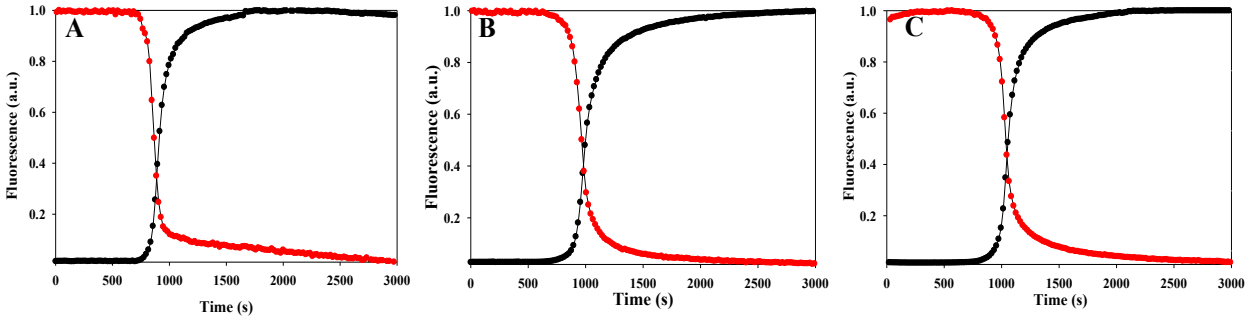

Figure 4.5: The kinetics of amyloid formation of the $F_{C\equiv N}$ variants of IAPP as monitored by $F_{C\equiv N}$ fluorescence (red) and thioflavin-T fluorescence (black). A, $15F_{C\equiv N}$; B, $23F_{C\equiv N}$; C, $37F_{C\equiv N}$. $F_{C\equiv N}$ fluorescence was excited at 240 nm and thioflavin-T fluorescence was excited at 450 nm. Final conditions were 32 μM peptide, 2% HFIP, 20 mM Tris-HCl at pH 7.4 and 25 ºC.

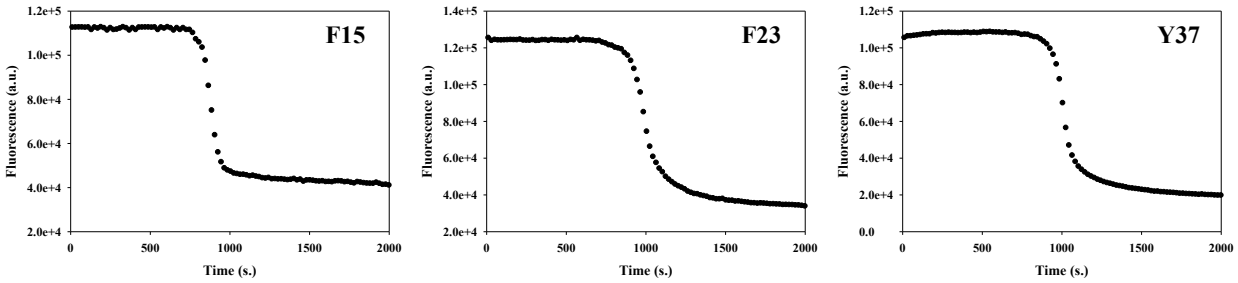

Figure 4.6: Non-normalized $F_{C\equiv N}$ monitored kinetics for the $15F_{C\equiv N}$, $23F_{C\equiv N}$ and $37F_{C\equiv N}$ IAPP variants with final conditions of 32 μM peptide, 2% HFIP and 20 mM Tris-HCl at pH 7.4 and 25 ºC.

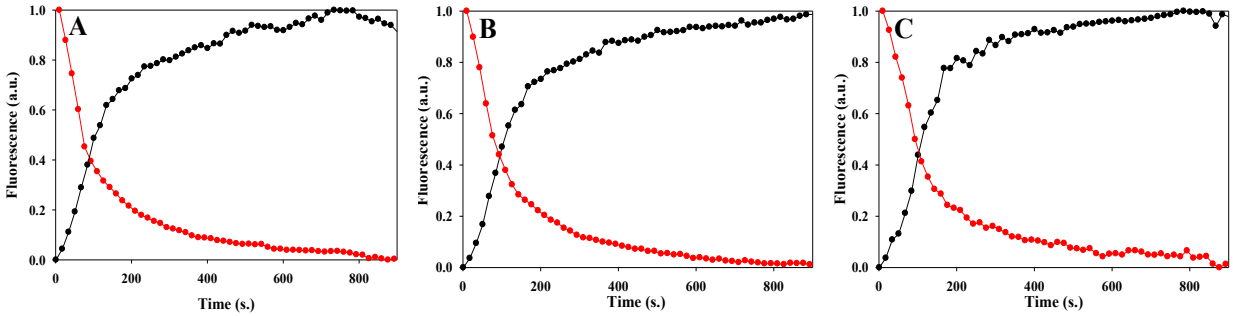

Figure 4.7: Seeding of $F_{C\equiv N}$ variants of IAPP by wild type IAPP. Black curves, thioflavin-T fluorescence. Red curves, $F_{C\equiv N}$ fluorescence. A, $15F_{C\equiv N}$; B, $23F_{C\equiv N}$; C, $37F_{C\equiv N}$. Experiments were performed by adding the various $F_{C\equiv N}$ variants of IAPP to preformed seeds of wild type human IAPP. Final conditions were 32 μM peptide, 3.2 μM seed (in monomer units), 2.2% HFIP, 20 mM Tris-HCl at pH 7.4 and 25 ºC.

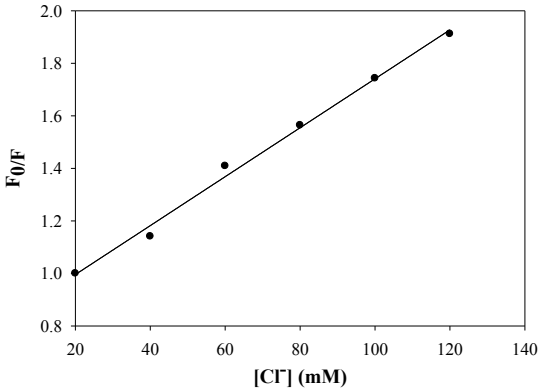

Figure 4.8: Stern-Volmer plot for Cl^- quenching of the $GGF_{C\equiv N}AA$ control peptide with final conditions of 32 μM peptide, 2% HFIP, 20 mM Tris-HCl, 100 mM salt (NaCl and NaF) at pH 7.4 and 25 ºC.

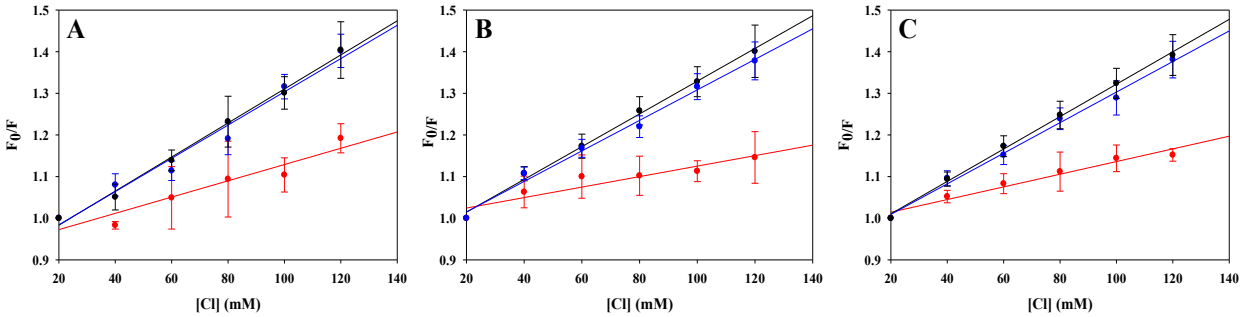

Figure 4.9: Stern-Volmer analysis of chloride induced quenching of $F_{C\equiv N}$ fluorescence. Data collected early in the lag phase (60 s.) is plotted in black, data collected near the end of the lag phase (200 s.) is plotted in blue and data collected after completion of fibril formation (1,000 s.) is plotted in red. A, $15F_{C\equiv N}$; B, $23F_{C\equiv N}$; C, $37F_{C\equiv N}$. Samples contained various concentrations of Cl^- and constant ionic strength was maintained by addition of F^-. Final conditions were 32 μM peptide, 2% HFIP, 20 mM Tris-HCl, 100 mM salt (NaCl and NaF) at pH 7.4 and 25 ºC. All samples contained at least 20 mM Cl^- and the fluorescence in 100 mM NaF, 20 mM Tris-HCl is defined as F_0.

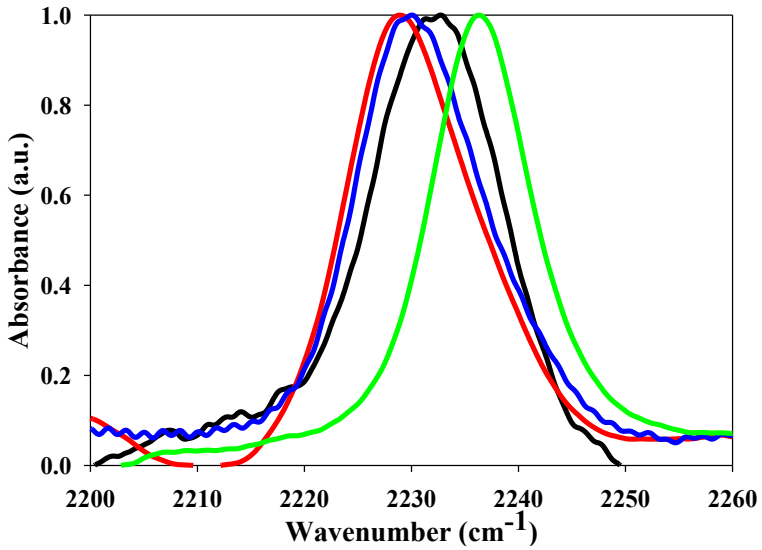

Figure 4.10: FTIR spectra of the $F_{C\equiv N}$ variants of IAPP. Black, $15F_{C\equiv N}$; Red, $23F_{C\equiv N}$; Blue, $37F_{C\equiv N}$; Green, $GGF_{C\equiv N}AA$ control peptide. Final conditions were 2.5 mM peptide, 2% HFIP in 20 mM Tris-HCl at pH 7.4.

4.6 Tables

	t_{50} (s)	t_{lag} (s)	$\left\|\frac{dF(t)}{dt}\right\|_{t=t_{50}}$ (s^{-1})	v_{max} (nM/s)	t^{s}_{50}/t_{50}
$15F_{C\equiv N}$	899±10	841±16	4.48±0.71 x10^{-3}	158±3	0.087
$23F_{C\equiv N}$	967±41	875±40	3.12±0.08 x10^{-3}	155±15	0.094
$37F_{C\equiv N}$	1013±100	935±75	4.15±0.11 x10^{-3}	142±8	0.096
WT	960±60	870±66	4.86±0.21x10^{-3}	168±13	-

Table 4.1: Time course of amyloid formation for wild type IAPP and the $F_{C\equiv N}$ variants as determined from the thioflavin-T detected kinetic experiments. Experiments were performed at 25 C, pH 7.4 and 2% HFIP with constant stirring. The quoted uncertainties represent the standard deviation calculated from three independent runs.

	Ratio of Final to Initial Fluorescence	t_{50} (s)	t_{lag} (s)	$\left\lvert \frac{dF(t)}{dt} \right\rvert_{t=t_{50}}$ (s^{-1})	v_{max} (nM/s)
$15F_{C\equiv N}$	0.44 ± 0.01	876±10	811±20	6.73±1.0 x10^{-3}	258±17
$23F_{C\equiv N}$	0.30 ± 0.01	957±41	842±44	3.82±0.41 x10^{-3}	168±12
$37F_{C\equiv N}$	0.21 ± 0.02	997±100	909±85	3.5±0.19 x10^{-3}	151±15

Table 4.2: Ratio of final to initial $F_{C\equiv N}$ fluorescence and the time course and kinetic parameters of amyloid formation of the $F_{C\equiv N}$ variants as determined from the $F_{C\equiv N}$ fluorescence assays. The quoted uncertainties represent the standard deviation calculated from three independent runs.

	Stern-Volmer Constants (K_{SV})			IR Peak Position	Bandwidth
	t = 60 s.	t = 200 s.	t = 1,000 s.		
$15F_{C\equiv N}$	4.1±0.6 M^{-1}	3.9±0.5 M^{-1}	2.0±0.2 M^{-1}	2233 cm^{-1}	14 cm^{-1}
$23F_{C\equiv N}$	3.9±0.5 M^{-1}	3.7±0.5 M^{-1}	1.3±0.2 M^{-1}	2229 cm^{-1}	14 cm^{-1}
$37F_{C\equiv N}$	3.9±0.1 M^{-1}	3.7±0.3 M^{-1}	1.5±0.03 M^{-1}	2230 cm^{-1}	14 cm^{-1}
$GGF_{C\equiv N}AA$[(a)]	9.3 M^{-1}	-	-	2236 cm^{-1}	11 cm^{-1}

Table 4.3: Stern-Volmer constants, IR peak positions and bandwidths for the $F_{C\equiv N}$ variants of IAPP and the $GGF_{C\equiv N}AA$ control peptide. (a) The control peptide does not aggregate and its K_{SV} value is independent of time.

4.7 References

1. Glenner, G. G. (1980) Amyloid deposits and amyloidosis; the β-fibrilloses, *N. Engl. J. Med.* **302**, 1283-1292.

2. Sipe, J. D., Cohen, A. S. (1994) Amyloidosis, *Crit. Rev. Clin. Lab Sci.* **31**, 325-354.

3. Selkoe, D. J. (2004) Cell biology of protein misfolding: The examples of Alzheimer's and Parkinson's diseases, *Nat. Cell Biol.* **6**, 1054-1061.

4. Chiti, F., Dobson, C. M. (2006) Protein misfolding, functional amyloid and human disease, *Annu. Rev. Biochem.* **75**, 333-366.

5. Dobson, C. M. (1999) Protein misfolding, evolution and disease, *Trends Biochem. Sci.* **24**, 329-332.

6. Nilsberth, C., Westlind-Danielsson, A., Eckman, C. B., Condron, M. M., Axelman, K., Forsell, C., Stenh, C., Luthman, J., Teplow, D. B., Younkin, S. G., Naslund, J., Lannefelt, L. (2001) The 'Arctic' APP mutation (E693G) causes Alzheimer's disease by enhanced A-beta protofibril formation, *Nat. Neurosci.* **4**, 887-893.

7. Marina, K. D., Bitan, G., Teplow, D. B. (2002) Paradigm shifts in Alzheimer's disease and other neurodegenerative disorders: The emerging role of oligomeric assemblies, *Neurosci. Res.* **69**, 567-577.

8. Caughey, C., Lansbury, P. T. (2003) Protofibrils, pores, fibrils, and neurodegeneration: Separating the responsible protein aggregates from the innocent bystanders, *Annu. Rev. Neurosci.* **26**, 267-298.

9. Petkova, A. T., Leapman, R. D., Guo, Z., Yau, W.-M., Mattson, M. P., Tycko, R. (2005) Self-propagating, molecular-level polymorphism in Alzheimer's beta-amyloid fibrils, *Science* **307**, 262-265.

10. Nilsson, M. R., Driscoll, M. D., Raleigh, D. P. (2002) Low levels of asparagine deamidation have a dramatic effect on aggregation: Implications for the study of amyloid formation, *Protein Sci.* **11**, 342-349.

11. Abedini, A., Raleigh, D. (2009) A critical assessment of the role of helical intermediates in amyloid formation by natively unfolded proteins and polypeptides, *Protein Eng. Des. Sel.* **22**, 453-459.

12. Chang, E. S.-H., Liao, T.-Y., Lim, T.-S., Fann, W., Chen, R. P.-Y. (2009) A new amyloid-like β-aggregate with amyloid characteristics, except fibril morphology, *J. Mol. Biol.* **385**, 1257-1265.

13. Shim, S.-H., Gupta, R., Ling, Y. L., Strasfeld, D. B., Raleigh, D. P., Zanni, M. T. (2009) Two-dimensional IR spectroscopy and isotope labeling defines the pathway of amyloid formation with residue-specific resolution, *Proc. Natl. Acad. Sci. U.S.A.* **106**, 6614-6619.

14. Krebs, M. R. H., Bromley, E. H. C., Donald, A. M. (2005) The binding of thioflavin-T to amyloid fibrils: localisation and implications, *J. Struct. Biol.* **149**, 30-37.

15. Levine, H. (1999) Quantification of beta-sheet amyloid fibril structures with thioflavin T, *Methods Enzymol.* **309**, 274-284.

16. Biancalana, M., Makabe, K., Koide, A., Koide, S. (2009) Molecular mechanism of thioflavin-T binding to the surface of β-rich -peptide self-assemblies, *J. Mol. Biol.* **385**, 1052-1063.

17. Groenning, M., Olsen, L., van de Weert, M., Flink, J. M., Frokjaer, S., Jørgensen, F. S. (2007) Study on the binding of thioflavin-T to β-sheet-rich and non-β-sheet cavities, *J. Struct. Biol.* **158**, 358-369.

18. Meng, F., Marek, P., Potter, K., Verchere, B., Raleigh, D. P. (2008) Rifampicin does not prevent amyloid fibril formation by human islet amyloid polypeptide but does inhibit fibril thioflavin-T interactions: implications for mechanistic studies of β-cell death, *Biochemistry* **47**, 6016-6024.

19. Tomiyama, T., Kaneko, H., Kataoka, K.-I., Asano, S., Endo, N. (1997) Rifampicin inhibits the toxicity of pre-aggregated amyloid peptides by binding to peptide fibrils and preventing amyloid-cell interaction, *Biochem. J.* **322**, 859-865.

20. Marek, P., Gupta, R., Raleigh, D. (2008) The fluorescent amino acid *p*-cyanophenylalanine provides an intrinsic probe of amyloid formation, *ChemBioChem* **9**, 1372-1374.

21. Aprilakis, K. N., Taskent, H., Raleigh, D. P. (2007) Use of the novel fluorescent amino acid *p*-cyanophenylalanine offers a direct probe of hydrophobic core formation during the folding of the N-terminal domain of the ribosomal protein L9 and provides evidence for two-state folding, *Biochemistry* **46**, 12308-12313.

22. Schultz, K. C., Supekova, L., Ryu, Y., Xie, J., Perera, R., Schultz, P. G. (2006) A genetically encoded infrared probe, *J. Am. Chem. Soc.* **128**, 13984-13985.

23. Tucker, M. J., Oyola, R., Gai, F. (2006) A novel fluorescent probe for protein binding and folding studies: *p*-cyanophenylalanine, *Bioploymers* **83**, 571-576.

24. Serrano, A. L., Troxler, T., Tucker, M. J., Gai, F. (2010) Photophysics of a fluorescent non-natural amino acid: *p*-Cyanophenylalanine, *Chem. Phys. Lett.* **487**, 303-306.

25. Tang, J., Signarvic, R. S., DeGrado, W. F., Gai, F. (2007) Role of helix nucleation in the kinetics of binding of Mastoparan X to phospholipid bilayer, *Biochemistry* **46**, 13856-13863.

26. Tucker, M. J., Tang, J., Gai, F. (2006) Probing the kinetics of membrane-mediated helix folding, *J. Phys. Chem. B* **110**, 8105-8109.

27. Rogers, J. M., Lippert, L. G., Gai, F. (2010) Non-natural amino acid fluorophores for one- and two-step fluorescence resonance energy transfer applications, *Anal. Biochem.* **399**, 182-189.

28. Tucker, M. J., Oyola, R., Gai, F. (2005) Conformational distribution of a 14-residue peptide in solution: A fluorescence resonance energy transfer study, *J. Phys. Chem. B* **109**, 4788-4795.

29. Taskent-Sezgin, H., Chung, J., Patsalo, V., Miyake-Stoner, S. J., Miller, A. M., Brewer, S. H., Mehl, R. A., Green, D. F., Raleigh, D. P., Carrico, I. (2009) Interpretation of *p*-cyanophenylalanine fluorescence in proteins in terms of solvent exposure and contribution of side-chain quenchers: A combined fluorescence, IR and molecular dynamics study, *Biochemistry* **48**, 9040-9046.

30. Getahun, Z., Huang, C. Y., Wang, T., Leon, B. D., DeGrado, W. F., Gai, F. (2003) Using nitrile-derivatized amino acids as infrared probes of local environment, *J. Am. Chem. Soc.* **125**, 405-411.

31. Tucker, M. J., Getahun, Z., Nanda, V., DeGrado, W. F., Gai, F. (2004) A new method for determining the local environment and orientation of individual side chains of membrane-binding peptides, *J. Am. Chem. Soc.* **126**, 5078-5079.

32. Suydam, I. T., Boxer, S. G. (2003) Vibrational stark effects calibrate the sensitivity of vibrational probes for electric fields in proteins, *Biochemistry* **42**, 12050-12055.

33. Dalosto, S. D., Vanderkooi, J. M., Sharp, K. A. (2004) Vibrational stark effects on carbonyl, nitrile, and nitrosyl compounds including heme ligands, CO, CN, and NO, studied with density functional theory, *J. Phys. Chem. B* **108**, 6450-6457.

34. Cooper, G., Willis, A. C., Clark, A., Turner, R. C., Sim, R. B., Reid, K. B. M. (1987) Purification and characterization of a peptide from amyloid-rich pancreases of type 2 diabetic patients, *Proc. Natl. Acad. Sci. U.S.A.* **84**, 8628-8632.

35. Westermark, P., Wernstedt, C., Wilander, E., Hayden, D. W., O'Brien, T. D., Johnson, K. H. (1987) Amyloid fibrils in human insulinoma and islets of Langerhans of the diabetic cat are derived from a neuropeptide-like protein also present in normal islet cells, *Proc. Natl. Acad. Sci. U.S.A.* **84**, 3881-3885.

36. Kahn, S. E., D'Alessio, D. A., Schwartz, M. W., Fujimoto, W. Y., Ensinck, J. W., Taborsky, G. J., Porte, D. (1990) Evidence of cosecretion of islet amyloid polypeptide and insulin by beta-cells, *Diabetes* **39**, 634-638.

37. Kahn, S. E., Andrikopoulos, S., Verchere, C. B. (1999) Islet amyloid: a long-recognized but underappreciated pathological feature of type 2 diabetes, *Diabetes* **48**, 241-253.

38. de Koning, E. J. P., Bodkin, N. L., Hansen, B. C., Clark, A. (1993) Diabetes mellitus in Macaca mulatta monkeys is characterised by islet amyloidosis and reduction in beta-cell population, *Diabetologia* **36**, 378-384.

39. Butler, A. E., Janson, J., Bonner-Weir, S., Ritzel, R., Rizza, R. A., Butler, P. C. (2003) Beta-cell deficit and increased beta-cell apoptosis in humans with type 2 diabetes, *Diabetes* **52**, 102-110.

40. Konarkowska, B., Aitken, J. F., Kistler, J., Zhang, S., Cooper, G.J. (2006) The aggregation potential of human amylin determines its cytotoxicity towards islet beta-cells, *FEBS J.* **273**, 3614-3624.

41. Guardado-Mendoza, R., Davalli, A. M., Chavez, A. O., Hubbard, G. B., Dick, E. J., Majluf-Cruz, A., Tene-Perez, C. E., Goldschmidt, L., Hart, J., Perego, C., Commuzzie, A. G., Tejero, M. E., et al. (2009) Pancreatic islet amyloidosis, beta-cell apoptosis, and alpha-cell proliferation are determinants of islet remodeling in type-2 diabetic baboons, *Proc. Natl. Acad. Sci. U.S.A.* **106**, 13992-13997.

42. Udayasankar, J., Kodama, K., Hull, R. L., Zraika, S., Aston-Mourney, K., Subramanian, S. L., Tong, J., Faulenbach, M. V., Vidal, J., Kahn, S. E. (2009) Amyloid formation results in recurrence of hyperglycaemia following transplantation of human IAPP transgenic mouse islets, *Diabetologia* **52**, 143-153.

43. Westermark, G. T., Westermark, P., Berne, C., Korsgren, O. (2008) Widespread amyloid deposition in transplanted human pancreatic islets, *N. Engl. J. Med.* **359**, 977-979.

44. Westermark, P., Eizirik, D. L., Pipeleers, D. G., Hellerström, C., Andersson, A. (1995) Rapid deposition of amyloid in human islets transplanted into nude mice, *Diabetologia* **38**, 543-549.

45. Potter, K., Abedini, A., Marek, P., Butterworth, S., Driscoll, M., Baker, R., Nilsson, M., Bertera, S., Trucco, M., Fraser, P. E., Raleigh, D. P., Verchere, C. B. (2010) Islet amyloid deposition limits the viability of human islet grafts but not porcine islet grafts, *Proc. Natl. Acad. Sci. U.S.A.* **107**, 4305-4310.

46. Padrick, S. B., Miranker, A. D. (2001) Islet amyloid polypeptide: Identification of long-range contacts and local order on the fibrillogenesis pathway, *J. Mol. Biol.* **308**, 783-794.

47. Goldsbury, C., Goldie, K., Pellaud, J., Seelig, J., Frey, P., Muller, S. A., Kistler, J., Cooper, G. J. S., Aebi, U. (2000) Amyloid fibril formation from full-length and fragments of amylin, *J. Struct. Biol.* **130**, 352-362.

48. Wiltzius, J. J. W., Sievers, S. A., Sawaya, M. R., Eisenberg, D. (2009) Atomic structures of IAPP (amylin) fusions suggest a mechanism for fibrillation and the role of insulin in the process, *Protein Sci.* **18**, 1521-1530.

49. Marek, P., Abedini, A., Song, B., Kanungo, M., Johnson, M. E., Gupta, R., Zaman, W., Wong, S. S., Raleigh, D. P. (2007) Aromatic interactions are not required for amyloid fibril formation by islet amyloid polypeptide but do influence the rate of fibril formation and fibril morphology, *Biochemistry* **46**, 3255-3261.

50. Koo, B. W., Hebda, J. A., Miranker, A. D. (2008) Amide inequivalence in the fibrillar assembly of islet amyloid polypeptide, *Protein Eng. Des. Sel.* **21**, 147-154.

51. Abedini, A., Raleigh, D. (2005) The role of His-18 in amyloid formation by human islet amyloid polypeptide, *Biochemistry* **44**, 16284-16291.

52. Luca, S., Yau, W. M., Leapman, R., Tycko, R. (2007) Peptide conformation and supramolecular organization in amylin fibrils: constraints from solid-state NMR, *Biochemistry* **48**, 13505-13522.

53. Williamson, J. A., Loria, J. P., Miranker, A. D. (2009) Helix stabilization precedes aqueous and bilayer-catalyzed fiber formation in islet amyloid polypeptide, *J. Mol. Biol.* **393**, 386-396.

54. Soong, R., Brender, J. R., Macdonald, P. M., Ramamoorthy, A. (2009) Association of highly compact type II diabetes related islet amyloid polypeptide intermediate species at physiological temperature revealed by diffusion NMR spectroscopy, *J. Am. Chem. Soc.* **131**, 7079-7085.

55. Vaiana, S. M., Best, R. B., Yau, W.-M., Eaton, W. A., Hofrichter, J. (2009) Evidence for a partially structured state of the amylin monomer, *Biophys. J.* **97**, 2948-2957.

56. Abedini, A., Raleigh, D. P. (2005) Incorporation of pseudoproline derivatives allow the facile synthesis of human IAPP: A highly amyloidogenic and aggregation-prone polypeptide, *Org. Lett.* **7**, 693-696.

57. Abedini, A., Singh, G., Raleigh, D. P. (2005) Recovery and purification of highly aggregation-prone disulfide-containing peptides: Application to islet amyloid polypeptide, *Anal. Biochem.* **351**, 181-186.

58. Nilsson, M., Raleigh, D. P. (1999) Analysis of amylin cleavage products provides new insights into the amyloidogenic region of human amylin, *J. Mol. Biol.* **294**, 1375-1385.

Chapter 5. Ionic Strength Effects on Amyloid Formation, a Complicated Interplay Between Debye Screening, Ion Selectivity, and Hofmeister Effects

Abstract

Amyloid formation has been implicated in a wide range of human diseases. The rate and extent of amyloid formation depends on solution conditions including pH and ionic strength. Amyloid fibrils often adopt structures with parallel, in-register β-sheets, which generate quasi-infinite arrays of aligned side chains. This can lead to significant electrostatic interactions between adjacent polypeptide chains. The effect of ionic strength and ion composition on the kinetics of amyloid formation by islet amyloid polypeptide (IAPP) is examined. IAPP is responsible for islet amyloid formation in type-2 diabetes and is a basic 37-residue polypeptide. The kinetics of IAPP amyloid formation are strongly dependent on ionic strength, varying by more than a factor of 10 over the range of 20 to 600 mM NaCl at pH 8.0, but the effect is not entirely due to Debye screening. At low ionic strengths the rate depends strongly on the identity of the anion, varying by a factor of nearly four, with the fastest rate observed for sulfate and the slowest with fluoride. The kinetics scale with the electroselectivity series, implicating anion binding. At high ionic strengths the variation in rate is much smaller, varying by only 8% and scales with the Hofmeister series. At intermediate ionic strengths no clear trend is detected, likely because of competition between different effects. The effects of salts on the growth phase and lag phase of amyloid formation are strongly correlated. The rate also depends strongly on ionic strength at pH 5.5 where the net charge on IAPP is larger, however, the effect of different anions scales with the electroselectivity series at all salt concentrations.

NOTE: The material presented in this chapter has been written for submission and publication to *Biochemistry* (Peter Marek, Daniel P. Raleigh. "Ionic Strength Effects on Amyloid Formation, a Complicated Interplay Between Debye Screening, Ion Selectivity, and Hofmeister Effects."). This chapter contains direct excerpts from the manuscript, which was written by me with suggestions and revisions from Professor Daniel P. Raleigh.

5.1 Introduction

Amyloid fibrils are highly stable, fibrous, protein aggregates, containing significant cross-beta structure and have been implicated in the pathology of a number of human diseases including Alzheimer's, Parkinson's and type 2 diabetes. Proteins that form amyloid can be divided into two broad structural classes; those which adopt a compact well-defined structure in their non-aggregated state and those that are highly flexible and do not fold into a globular structure in their monomeric states, i.e. are natively unfolded. Important examples of the latter class include the Aβ peptide of Alzheimer's disease and islet amyloid polypeptide (IAPP, amylin), the major component of the islet amyloid associated with type 2 diabetes.

The ability of a polypeptide to form amyloid is dependent on a range of factors; sequences that are rich in hydrophobic amino acids with a high β-sheet propensity, lack prolines and have a low net charge have high amyloidogenic propensity (1-6). Changes in the local environment of a normally soluble polypeptide can trigger and influence the rate of amyloid formation. These factors can include changes in pH, temperature, pressure, alterations in the solvent or co-solvent composition, interactions with membranes or components of the

extracellular matrix and changes in ionic strength (7-12). The structured regions in amyloid fibrils often adopt parallel, in-register β-strands. This leads to quasi-infinite stacks of identical residues and the in-register structure means that there is the potential for significant electrostatic interactions in amyloids (6, 13-15). Ionic strength dependent studies of amyloid formation have revealed that ions can greatly influence the kinetics and thermodynamics of the aggregation process (15-18). The effects differ from protein to protein, the underlying causes of which can be difficult to understand or interpret, in part because as many studies have been restricted to the use of one or only a few salts. Here, we analyze the ability of a wide range of salts to influence amyloid formation by islet amyloid polypeptide (IAPP, amylin) at pH 5.5 and 8.0. IAPP is one of the most amyloidogenic naturally occurring polypeptides and the process of islet amyloid formation is believed to contribute to type 2 diabetes and to the failure of islet cell transplants (19-21). The 37-residue polypeptide has no negatively charged groups, the C-terminus is amidated, and contains four potential positively charged groups. They are the N-terminus, Lys-1, Arg-11 and His-18 (Figure-1).

As a monomer, IAPP populates a fluctuating ensemble of conformations with modest local propensity to sample α-helical ϕ, ψ angles in the N-terminal half to two-thirds of the molecule, but is rich in β-sheet in the amyloid state (22, 23). IAPP carries a +2 to +4 charge at physiological pH depending on the protonation state of His-18 and the N-terminus. The kinetics of amyloid formation by IAPP is highly dependent on the pH, and is influenced significantly by the protonation state of His-18 and the N-terminus (15, 24). At low pH where the His is protonated, the time for amyloid formation is much longer than at pH's where it is deprotonated (15). The early stages of IAPP amyloid formation will involve oligomerization of the cationic peptide and the unfavorable electrostatic repulsion needs to be overcome by other interactions.

Growth of the amyloid fibrils will involve binding of soluble IAPP to fibril ends and will also involve unfavorable electrostatic effects.

IAPP is processed in parallel with insulin and stored in the insulin secretory granule (25, 26). The intragranular environment is significantly different from extracellular conditions. Immature granules have a depressed pH, ~5.5, relative to the extracellular environment. Insulin is packaged in a semi-crystalline form in the core of the granule, while IAPP is localized in the so-called halo region (27-31). The granule contains high concentrations of Zn^{2+} (20 mM), which is primarily associated with insulin, Ca^{2+} (120 mM), Mg^{2+} (70 mM), HPO_4^{2-} (70 mM) and adenine nucleotides (10 mM) (29, 32).

Much of our knowledge of ion-protein interactions is gleaned from studies with soluble globular proteins (33). Quantitative studies of the effects of salts on proteins date back to Hofmeister's observations in the late 1800's that different ions salted-out proteins from egg white with varying effectiveness (34). Salts can influence protein stability by specific binding, by altering the properties of the protein-solvent system (Hofmeister effects) and by screening of electrostatic interactions (Debye-Hückel effects). At high ionic strengths ions are thought to exert their influence through non-specific clustering around charged protein groups, causing stabilizing charge-charge electrostatic interactions to decrease in strength, referred to as Debye-Hückel screening. In a similar manner, repulsive interactions are screened as well, allowing the forces that govern intermolecular association to predominate. Given that many amyloid fibrils, including those formed by IAPP, contain arrays of like-charges, screening effects are likely to stabilize amyloids. So-called Hofmeister effects can also contribute at high ionic strength and arises from the effects of ions on the properties of water (33, 35). The Hofmeister series ranks ions on their ability to precipitate proteins. The effect of different ions can be quantified in a

variety of ways; one useful method involves the Jones-Dole viscosity equation, specifically the B-coefficient, which is a measure of the strength of ion-water interactions normalized to the strength of water-water interactions in bulk solution. Ions with a positive B-coefficient, termed kosmotropes, are strongly hydrated, small ions of high charge density and promote the stability and folding of globular proteins, and decrease protein solubility. Conversely, chaotropes have a negative B-coefficient, are weakly hydrated and "salt-in" proteins. The order with which anions precipitate proteins is as follows:

$$HPO_4^{2-} > SO_4^{2-} > F^- > Cl^- > Br^- > I^- > SCN^-$$

F^- and Cl^- represent the split between kosmotropes and chaotropes, respectively. Although cations can also be ranked according to the Hofmeister series, the effects are often dominated by anions, which are more strongly hydrated and have a greater effect on polarizable molecules. Ions may also specifically interact with charged or polar groups of a peptide, the strength of which is often reflected in the affinity of ions for an ion-exchange resin, the so-called electroselectivity series (36-38). For monovalent ions, the electroselectivity series scales inversely with the Hofmeister series.

Here we show that increasing the ionic strength of a solution of IAPP monomers significantly increases the rate at which IAPP forms fibrils. The effects were examined at pH 5.5, where IAPP will has a net charge of +4, and at pH 8.0, where the net charge is close to +2, the exact value depending on the pKa's of His-18 and the N-terminus. We chose pH 5.5 because it is comparable to the inner granule pH of β-cells and pH 8.0 because the rate of amyloid formation is less sensitive to small pH changes at this value than it is at pH 7.4. The effects include more than simple Debye-Hückel screening since significant variations are observed between different anions at constant ionic strength. At lower ionic strengths at pH 8.0 the ability

of an anion to induce fibril formation is dependent on its order in the electroselectivity series, suggesting that ion binding plays a role. As the ionic strength is raised at pH 8.0, the dependence of the electroselectivity series disappears, possibly due to competing effects from the Hofmeister effect together with screening effects. At high ionic strength the variation is much smaller than at low ionic strengths and the Hofmeister effect appears to account for the observed inter-anion variation. In contrast, at pH 5.5 the effect of different anions scales with the electroselectivity series at all ionic strengths.

5.2 Materials and Methods

5.2.1 Peptide Synthesis and Purification

IAPP was synthesized on a 0.25 mmol scale using a CEM Liberty Microwave Peptide Synthesizer utilizing 9-fluorenylmethoxycarbonyl (Fmoc) chemistry. All solvents used were ACS grade. The microwave method and the use of Fmoc-protected pseudoproline dipeptide derivatives have been described previously (39, 40). Fmoc amino acids and pseudoproline dipeptide derivatives were purchased from Novabiochem. All other reagents were purchased from Sigma and Fisher Scientific. Use of a 5-(4'-Fmoc-aminomehtyl-3', 5-dimethoxyphenol) valeric acid (PAL-PEG) resin (Novabiochem) afforded an amidated C-terminus. Residues A8-T9 and L27-S28 were attached to the growing peptide chain as pseudoproline dipeptide derivatives and double coupled. The following residues were also double coupled: N3 through C7, R11, L16, V17, I26, T30 and V32. The peptide was cleaved from the resin through the use of standard trifluoroacetic acid (TFA) methods; ethanedithiol, thioanisole and anisole were used as scavengers. The disulfide bond was formed via incubation in DMSO (41, 42). IAPP was purified via reverse-phase high performance liquid chromatography (RP-HPLC) using a Vydac

C18 preparative column. A two buffer system was utilized in which buffer A consisted of 0.045% HCl in H_2O (v/v) and buffer B of 80% acetonitrile and 0.045% HCl in H_2O (v/v). TFA was avoided since small amounts of TFA can influence aggregation rates. The purity of the peptide was checked by HPLC using a Vydac C18 analytical column and the identity was confirmed by matrix-assisted laser desorption ionization time-of-flight mass spectrometry (MALDI-TOF MS); observed 3903.9 Da, expected 3903.4. Da.

5.2.2 Fluorescence Assays

All fluorescence assays were performed on a Beckman Coulter DTX 880 Multimode Detector plate reader. Thioflavin-T fluorescence was measured utilizing a 430 nm excitation filter (Beckman Coulter) with a 35 nm bandwidth and a 485 nm emission filter with a 20 nm bandwidth. The assays were performed in a Corning 96-well Non-Binding Surface black plate with a lid and a clear, flat bottom in bottom plate-reading mode. IAPP was prepared by dissolving the peptide in 100% hexafluoroisopropanol (HFIP) to a concentration of 1.58 mM and filtering through a 0.45 μm GHP Acrodisc filter once the peptide was fully dissolved. This solution was lyophilized to remove the HFIP. The lyophilized IAPP was dissolved in 10 mM Tris, pH 8.0 buffer to a stock concentration of 1.58 mM and immediately diluted to a concentration of 32 μM in each salt solution. For the pH 8.0 experiments, 1 M ionic strength salt solutions of Na_2HPO_4, Na_2SO_4, NaSCN, NaI, NaBr, NaCl, NaF, KCl and LiCl were prepared in 10 mM Tris-HCl, pH 8.0. Phosphate is approximately 86% HPO_4^{2-} at this pH. The 1 M salt solutions were diluted to 20, 100, 200, 400, 600 and 800 mM ionic strength solutions using 10 mM Tris buffer and the addition of peptide. The solutions also contained 32 μM thioflavin-T. For the pH 5.5 experiments, salt solutions were prepared as for the pH 8.0 experiments, but in

the presence of 10 mM MES buffer, pH 5.5. Phosphate is approximately 98% $H_2PO_4^-$ at this pH. The pH was checked after all samples were prepared. Reactions were incubated at 25°C in the plate reader with no agitation. Data points were recorded every 300 s for the first 8 hours and every 900 s thereafter. Data were fit to the expression:

$$r(t) = (m_1 + t + r_1)\alpha + (m_2 + t + r_2)(1 - \alpha) \quad (1)$$

where $\alpha = (1 + e^{((t_{50}-t)/\tau)})^{-1}$. Equation-1 describes a sigmoidal curve. The fit yields t_{50}, the time at which amyloid formation is 50% complete, as judged by the fluorescence response. The apparent maximum rate at $t = t_{50}$, or v_{max}, is calculated by converting the time constant of the transition, τ, to v_{max} by the equation

$$v_{max} = \frac{[IAPP]_{t=0}}{4\tau} \quad (2)$$

where $[IAPP]_{t=0}$ is the concentration of IAPP at the start of the reaction. The length of the lag phase, t_{lag}, was calculated by the equation $t_{lag} = t_{50} - 2\tau$.

5.2.3 Transmission Electron Microscopy (TEM)

TEM was performed at the University Microscopy Imaging Center at the State University of New York at Stony Brook. 15 µL samples from the end of the kinetic experiments were placed on a carbon-coated 300-mesh copper grid and negatively stained with saturated uranyl acetate.

5.3 Results

IAPP is a basic protein with single Lys, Arg and His residues and a positive charge from the N-terminus (Figure 5.1). There are no negatively charged groups on account of the amidated carboxyl C-terminus. Depending on the protonation state of the His residue, and N-terminus,

IAPP carries a +2, +3 or +4 charge at the physiological pH 7.4. In the solid-state NMR derived models from the Tycko group, IAPP forms in-register, parallel β-sheets with residues 8-17 and 28-37 comprising the two β-strand segments and residues 18-27 forming a loop or bend connecting the two strands (Figure 5.1). Two stacks of IAPP monomers pack together in a symmetric arrangement. The main chain hydrogen bonds are between adjacent monomers in a given stack. Arg-11 (Figure 5.1, blue) is the only charged residue located within a β-strand. In this model both Lys-1 (Red) and His-18 (Cyan) are located in more disorded regions, at the N-terminus and the start of the loop, respectively.

5.3.1 The rate of IAPP amyloid formation depends strongly on ionic strength.

We first examined salt-dependent effects at pH 8.0. The kinetics of amyloid formation by IAPP in the presence of various salts was followed by thioflavin-T fluorescence. Thioflavin-T is negligibly fluorescent in the absence of amyloid, but exhibits a significant increase in quantum yield upon binding to amyloid. The aggregation of IAPP can be described by a sigmoidal curve with a well-defined lag phase in which monomers and oligomers dominate the population, followed by a growth phase during which fibrils elongate. The ability of salts to induce the aggregation of IAPP was tested at 20, 100, 200, 400, 600 and 800 mM ionic strength. 10 mM Tris at pH 8.0 was present in all reactions and sodium was used as the counter-ion for all of the anions tested. pH 8.0 was chosen because minor variations in pH have only a small effect on amyloid kinetics at this pH, but have a significant effect at pH 7.4. Additional experiments were conducted with a set of chloride salts in order to probe the consequences of varying the cation.

The addition of salt increases the rate at which fibril formation occurs. Figure 5.2 displays the thioflavin-T kinetic curves for IAPP in the presence of increasing concentrations of NaCl, the weakest or most neutral chaotropic salt examined. Increasing the NaCl concentration leads to a reduction in both the lag phase and the value of t_{50}, the time required for the thioflavin-T signal change to reach half its maximum value. At 30 mM ionic strength (20 mM NaCl and 10 mM Tris-HCl) the t_{50} was 1343 minutes while it was only 128 minutes at 610 mM ionic strength (600 mM NaCl with 10 mM Tris-HCl). Further addition of salt eliminates the lag phase. At 800 mM added salt, fibril formation had already begun during the dead time of the experiment (data not shown) for nearly all of the anions and kinetic parameters could not be calculated.

5.3.2 The rate of amyloid formation depends on the choice of anion, but is less dependent on the choice of cation.

To probe the kinetics of amyloid formation by IAPP in the presence of different anions, thioflavin-T kinetic reactions were conducted in the presence of the monovalent salts SCN^-, I^-, Br^-, Cl^- and F^- and the divalent salts HPO_4^{2-} and SO_4^{2-}, at the ionic strengths listed above. Na^+ was the counter ion for all reactions. A plot of the log ($1/t_{50}$) versus the ionic strength (I) from 30 to 610 mM for the monovalent salts SCN^-, I^-, Br^-, Cl^- and F^- at pH 8.0 is shown in Figure 5.3a. The kinetics of amyloid formation are complex, involving multiple steps and likely parallel pathways. It is thus difficult, if not impossible, to extract microscopic rate constants from single thioflavin-T curves. We use $1/t_{50}$ as a proxy for the rate of amyloid formation and plotted its log since ionic strength effects on rates are usually plotted in this fashion. All of the salts decreased the t_{50} of fibril formation compared to buffer at all concentrations tested. As the ionic strength is increased the rate of amyloid formation increases for all salts, however, the trend does not follow

the form expected if the t_{50} or log ($1/t_{50}$) depends solely on electrostatic screening, the Hofmeister effect or direct anion binding. Electrostatic screening has been modeled using a Debye-Hückel limiting law $\sqrt{I}$ dependence expected for the activity coefficient of an ion, as well as using a relationship that predicts that the screening of charges should have a $e^{-\sqrt{I}}$ dependence on ionic strength. The plots of the log ($1/t_{50}$) versus either $\sqrt{I}$ or $e^{-\sqrt{I}}$ over the range of ionic strengths examined are both clearly non-linear (Figure 5.3b and 5.3c, respectively). In addition, different ions exert different effects at the same ionic strength. These observations show that ionic strength effects cannot be due to just Debye-Hückel screening.

Figure 5.4 displays the kinetic curves of all the salts at pH 8.0 at 30 mM total ionic strength. All of the salts decreased the lag phase and the t_{50} of fibril formation compared to buffer alone, but there is significant variation between the different anions. The order with which anions induce amyloid formation by IAPP under these conditions is as follows: SO_4^{2-} > HPO_4^{2-}> SCN^- > I^- > Br^- > Cl^- > F^-. The values of t_{50} ranged from 421 minutes in sulfate to 1,574 minutes in fluoride. The effect of varying the cation on the kinetics of amyloid formation was also probed at both 30 mM and 610 mM ionic strengths (Figure 5.5). Li^+, K^+ and Na^+ were tested with Cl^- used as the counter-ion. There is no major difference among the cations tested at both low and high ionic strength.

5.3.3 At pH 8.0, anionic selectivity is important at low ionic strength and Hofmeister effects are important at high ionic strength.

Comparing the rates of fibril formation in the presence of various salts reveals that the different anions influence the rate of amyloid formation by IAPP to varying extents. To distinguish if the effect of different anions on fibril formation by IAPP is dependent on

Hofmeister effects or direct anion binding, the rate of fibril formation ($1/t_{50}$) was plotted versus either the B-coefficient of each anion, a measure of the Hofmeister effect, or the electroselectivity series. At pH 8.0 at the lowest ionic strength, the rate of fibril formation scales inversely with the Hofmeister series for the monovalent salts, but follows the order of the electroselectivity series (Figure 5.6b and 5.6a, respectively). As the ionic strength is increased the correlation with the electroselectivity series disappears and no correlation is observed in the plot for 110, 210 and 410 mM ionic strengths (Figures 5.6c-h). At the highest ionic strength, 610 mM, the dependence on the identity of the anion is the opposite of that observed at 30 mM, although the variation caused by changing the anion is much smaller at high salt, varying by 8%, than at low salt. At 610 mM at pH 8.0, the $1/t_{50}$ scales with the B-coefficient of the Hofmeister series for all salts, with the exception of NaSCN (Figure 5.6j) and little correlation is observed with the electroselectivity series (Figure 5.6i). At intermediate salt concentrations no clear trends are observed. The lack of a clear correlation with the Hofmeister effect or the electroselectivity series at intermediate salt concentrations is likely due to competition between the different effects.

Salts can precipitate proteins into amorphous aggregates as well as into ordered fibrils, hence it is important to confirm that IAPP still forms amyloid under the conditions investigated. Consequently, we used TEM to examine the morphology of the material formed in the presence of each salt at low added salt (30 mM) and high added salt (610 mM). Amyloid fibrils were observed in all cases (Figure 5.7). There was no significant difference in the morphology at either concentration across the range of anions compared to fibrils formed in buffer alone.

5.3.4 At pH 5.5, anionic selectivity is important at both low and high ionic strength.

The rates of fibril formation were measured as above, but at pH 5.5. A significant dependence of the rate of amyloid formation on ionic strength is also observed at pH 5.5. Increasing the NaCl concentration leads to a reduction in both the t_{lag} and t_{50}, similar to the kinetics at pH 8.0 (Figure 5.8). At 30 mM ionic strength (20 mM NaCl, 10 mM MES) the t_{50} was 6,930 minutes and 685 minutes at 610 mM ionic strength (600 mM NaCl, 10 mM MES). The curves are broadly similar to those observed at pH 8.0, however, the rates are significantly slower as judged by comparison to the t_{50}'s at pH 8.0. A plot of the log ($1/t_{50}$) versus the ionic strength (I) from 30 to 610 mM for the monovalent salts SCN^-, I^-, Br^-, Cl^- and F^- at pH 5.5 is shown in Figure 5.9a. All of the salts decreased the t_{50} of fibril formation compared to buffer at all concentrations tested. The plots of the log($1/t_{50}$) versus ionic strength (I) (Figure 5.9a), $\sqrt{I}$ (Figure 5.9b) or $e^{-\sqrt{I}}$ (Figure 5.9c) from 30 to 610 mM at pH 5.5 for the monovalent salts are non-linear, similar to the plots at pH 8.0.

Similar to the kinetics observed at pH 8.0, there is significant variation among the salts tested and the t_{50} of each is decreased in comparison to buffer at the lowest ionic strength, 30 mM (Figure 5.10). The order with which anions induce amyloid formation by IAPP under these conditions is as follows: $SO_4^{2-} > SCN^- > I^- > Br^- > Cl^- > H_2PO_4^{2-} > F^-$. The values of the t_{50} range from 4,216 minutes for SO_4^{2-} to 8,412 minutes for F^- and follow the electroselectivity series. Note that phosphate is 98% monovalent at this pH and its order in the electroselectivity series shifts to a position between Cl^- and F^-. The behavior at pH 5.5 at high salt differs from high salt at pH 8.0. Unlike at pH 8.0, at high ionic strength the rate of fibril formation scales with the electroselectivity series, but not with the B-coefficient (Figure 5.11). The trend is the same at the intermediate ionic strengths as well.

5.4 Discussion

The analysis presented here reveals a complicated salt-dependence of amyloid formation by IAPP. The rate of amyloid formation is significantly accelerated with increasing ionic strength at both pH's, but the observed trends do not follow a simple relationship based only on Debeye screening. The t_{50} values vary by a factor of nearly four at low salt at pH 8.0, depending on the identity of the anion and by a factor of two at pH 5.5. At low salt anion binding appears to play a role at both pH's as judged by the dependence on anion identity and its correlation with the electroselectivity series. A different salt dependence is observed at pH 5.5 and pH 8.0 as the ionic strength is increased. The anion-dependent effects are much less pronounced at the highest salt concentrations at pH 8.0 and the value of t_{50} varies by less than 8% amongst all of the anions tested. The t_{50} no longer scales with the electroselectivity series at high ionic strength at pH 8.0. Anion binding will still occur at high salt concentrations, but the variation between the different ions will be less if saturating concentrations are reached for all ions. The anion is in 18,000-fold excess relative to IAPP at 600 mM ionic strength. In addition, Hofmeister effects will be more important at the higher salt concentrations, and these scale inversely with the electroselectivity series for the monovalent anions. The lack of a clear trend at the intermediate ionic strengths likely reflects competition among these effects. It is important to note that there is still significant variation in the rate with the identity of the anion at pH 8.0 at intermediate ionic strengths, varying by nearly 100%, and these effects should be taken into account when comparing studies conducted using different salts. In contrast to the behavior observed at pH 8.0, the effects of varying the anion scale with the electroselectivity series for all ionic strengths tested at pH 5.5. The polypeptide has a larger net positive charge at pH 5.5 than at pH 8.0 and this should enhance anion binding and thus account for a stronger dependence on the

electroselectivity series. The lack of a significant dependence on the cations tested is not surprising since IAPP contains no negatively charged groups and thus cation binding is not expected.

We used the value of t_{50} in our analysis, which includes contributions from both the lag phase and the growth phase. It is natural to inquire if anions exert different effects on the lag phase and the growth phase. The lag time, t_{lag}, and the apparent rate at t_{50}, which is believed to reflect the elongation rate, can be determined from the sigmoidal fits. We obtain similar results if we compare the effects of anions and ionic strengths on t_{50}, t_{lag}, or v_{max}. Plots of $1/t_{lag}$ and v_{max} versus ionic strength are included in Figure 5.12 at both pH 5.5 and 8.0. Plots of the two parameters versus the electroselectivity series and the B-coefficient for both pH 8.0 and 5.5 are shown in Figure 5.13 and Figure 5.14, respectively. The plots at all ionic strengths are very similar to those obtained from plotting $1/t_{50}$, indicating that the lag time and elongation rate are sensitive to the same factors that modulate the t_{50}. There is a strong relationship between the effects of different salts on the lag phase and growth phase of amyloid formation by IAPP. The variation of the elongation rate, v_{max}, and the inverse of the lag time are strongly correlated at pH 8.0 (Figure 5.15), with r^2=0.86 and an equally strong correlation (r^2=0.91) is observed at pH 5.5. A strong correlation is also observed if the pH 5.5 and pH 8.0 data are plotted together (r^2=0.80) (Figure 5.15c). Such a strong correlation implies that electrostatic effects, Hofmeister effects and anion binding influence both fibril elongation and the nucleation events in the lag phase. This is reasonable since nucleation involves association of charged IAPP monomers and thus has to overcome unfavorable electrostatic effects. The fibril growth phase involves binding of soluble cationic IAPP monomers to the cationic fibrils, and so must also involve unfavorable charge-charge interactions.

This work highlights the importance of screening the electrostatic repulsion that arises from the alignment of the positive charges in fibrils during amyloid formation by IAPP. At pH 8.0 specific anion binding is important at low ionic strengths, but at high salt concentrations at this pH it appears that the influence of ions on the properties of water via Hofmeister effects plays a role in driving amyloid formation. This contrasts with the influence of anions on the kinetics at pH 5.5, where IAPP carries a +4 charge, with two basic residues (Arg-11 and His18) in the β-sheet core of the fibril. At pH 5.5 anion binding drives fibril formation over the entire range of salt concentrations tested. The stronger dependence on anion binding at high salt at pH 5.5 likely reflects the higher net charge of the polypeptide.

5.5 Figures

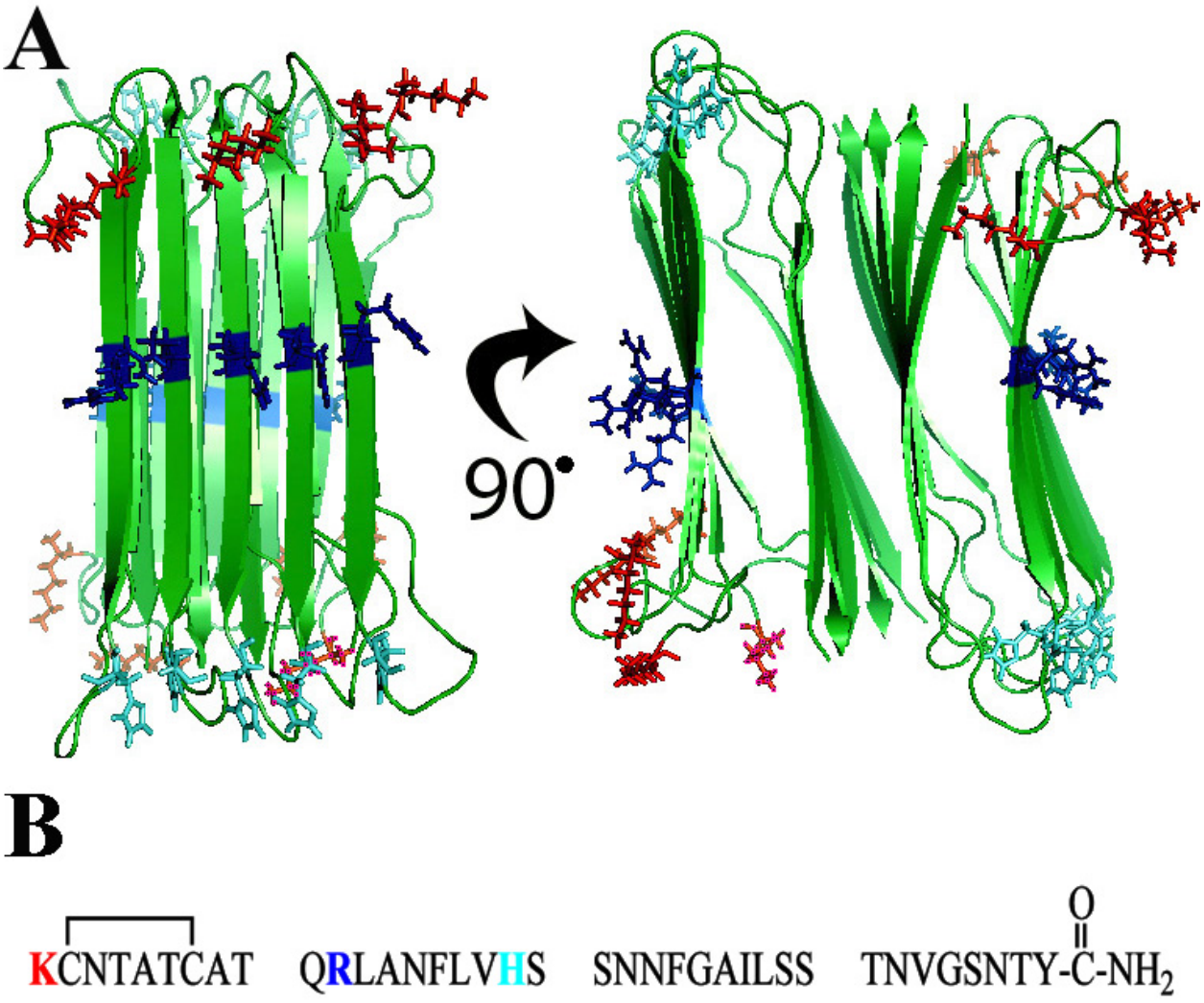

Figure 5.1: (A) Left: View of the IAPP amyloid fibril perpendicular to the axis of the fibril derived from the model of Tycko and colleagues. Right: Same structure rotated by 90°, view down the axis of the fibril. Red: Lys-1; Blue: Arg-11; Cyan: His-18. (B) Primary sequence of human IAPP. The polypeptide contains a disulfide bridge between residues 2 and 7 and has an amidated C-terminus. Lys-1, Arg-11 and His-18 are color coded as in panel A.

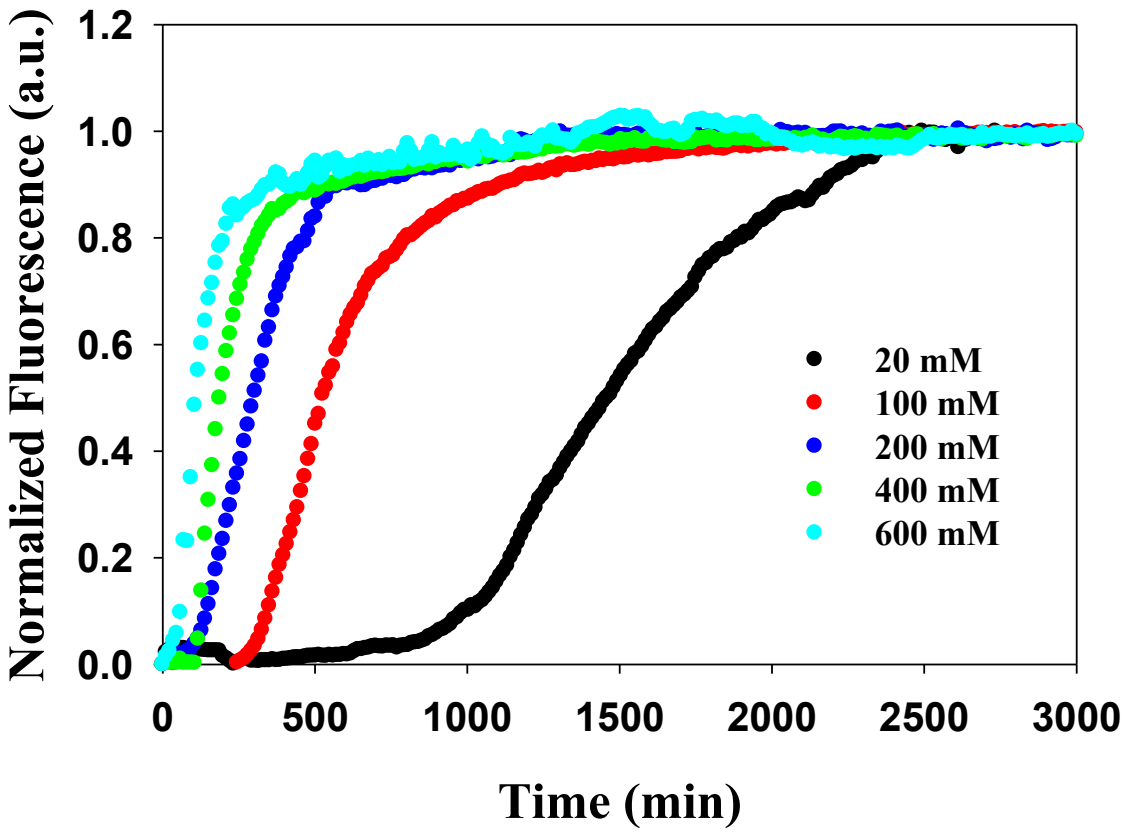

Figure 5.2: Dependence of the kinetics of amyloid formation on the ionic strength for various concentrations of NaCl at pH 8.0. Plots of thioflavin-T versus time are displayed. The concentration of added NaCl ranged from 20 to 600 mM. All experiments were conducted at 25 °C, pH 8.0 and all samples contained 10 mM Tris-HCl. The concentration of IAPP and thioflavin-T were both 32 μM.

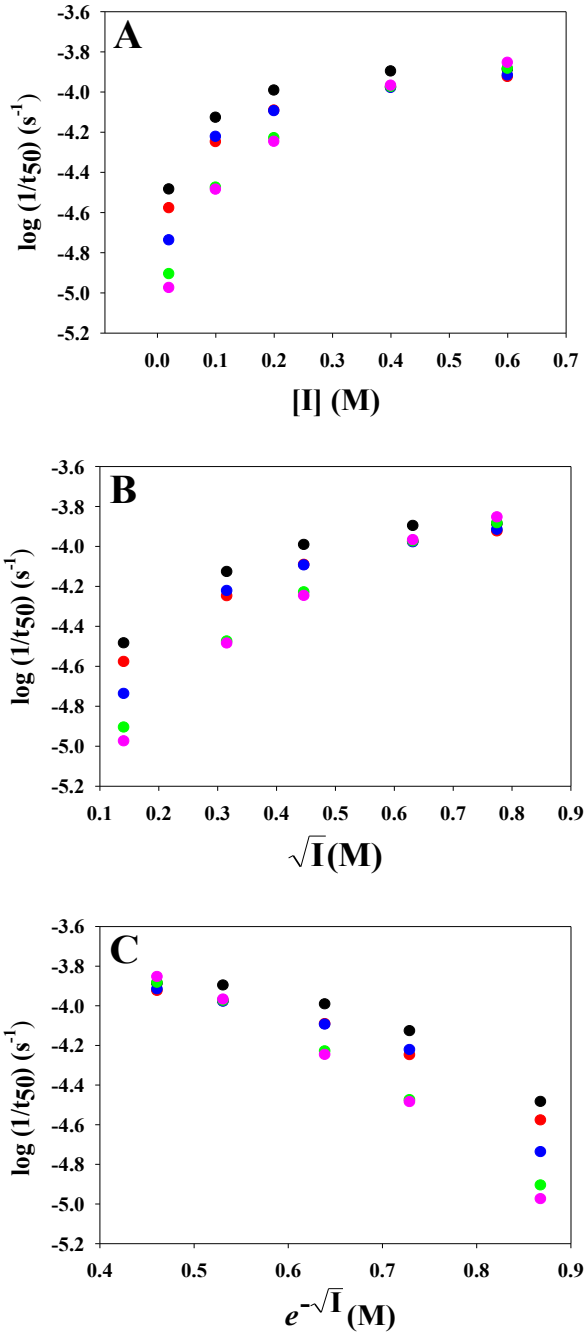

Figure 5.3: Analysis of the dependence of $\log(1/t_{50})$ on ionic strength, I, for the monovalent anions at pH 8.0. The observed values of $\log(1/t_{50})$ are plotted vs. (A) I; (B) $\sqrt{I}$; (C) $e^{-\sqrt{I}}$. Black, NaSCN; Red, NaI; Blue, NaBr; Green, NaCl; Pink, NaF.

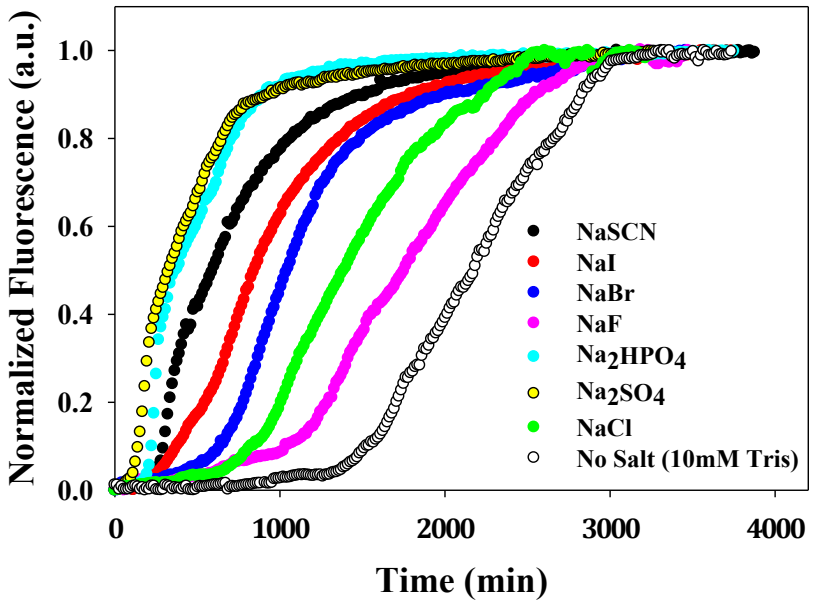

Figure 5.4: Dependence of the kinetics of amyloid formation on the anion identity at 20 mM added salt (30 mM ionic strength) at pH 8.0. Plots of thioflavin-T versus time are displayed. All experiments were conducted at 25 °C, pH 8.0 and all samples contained 10 mM Tris-HCl The concentration of IAPP and thioflavin-T were both 32 μM.

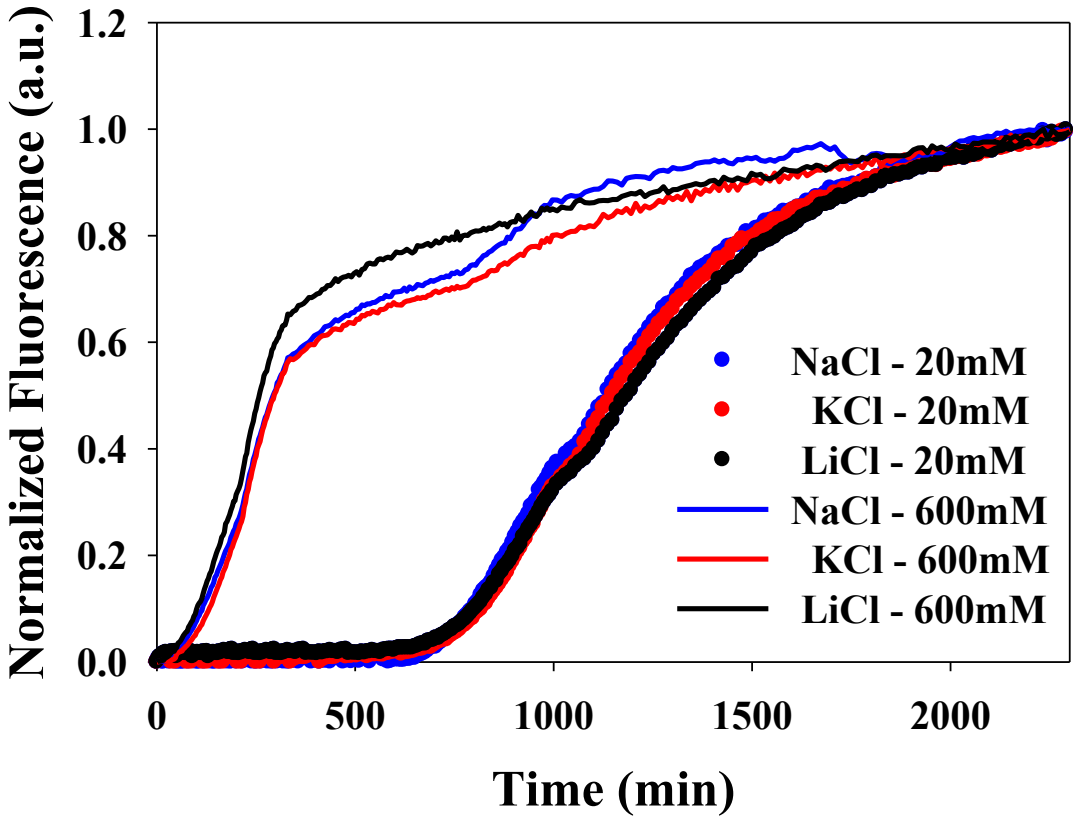

Figure 5.5: The identity of the cation has little effect on the kinetics of amyloid formation. Thioflavin-T curves are shown at 20 mM and 600 mM added salt for NaCl, KCl and LiCl. Experiment conducted at pH 8.0.

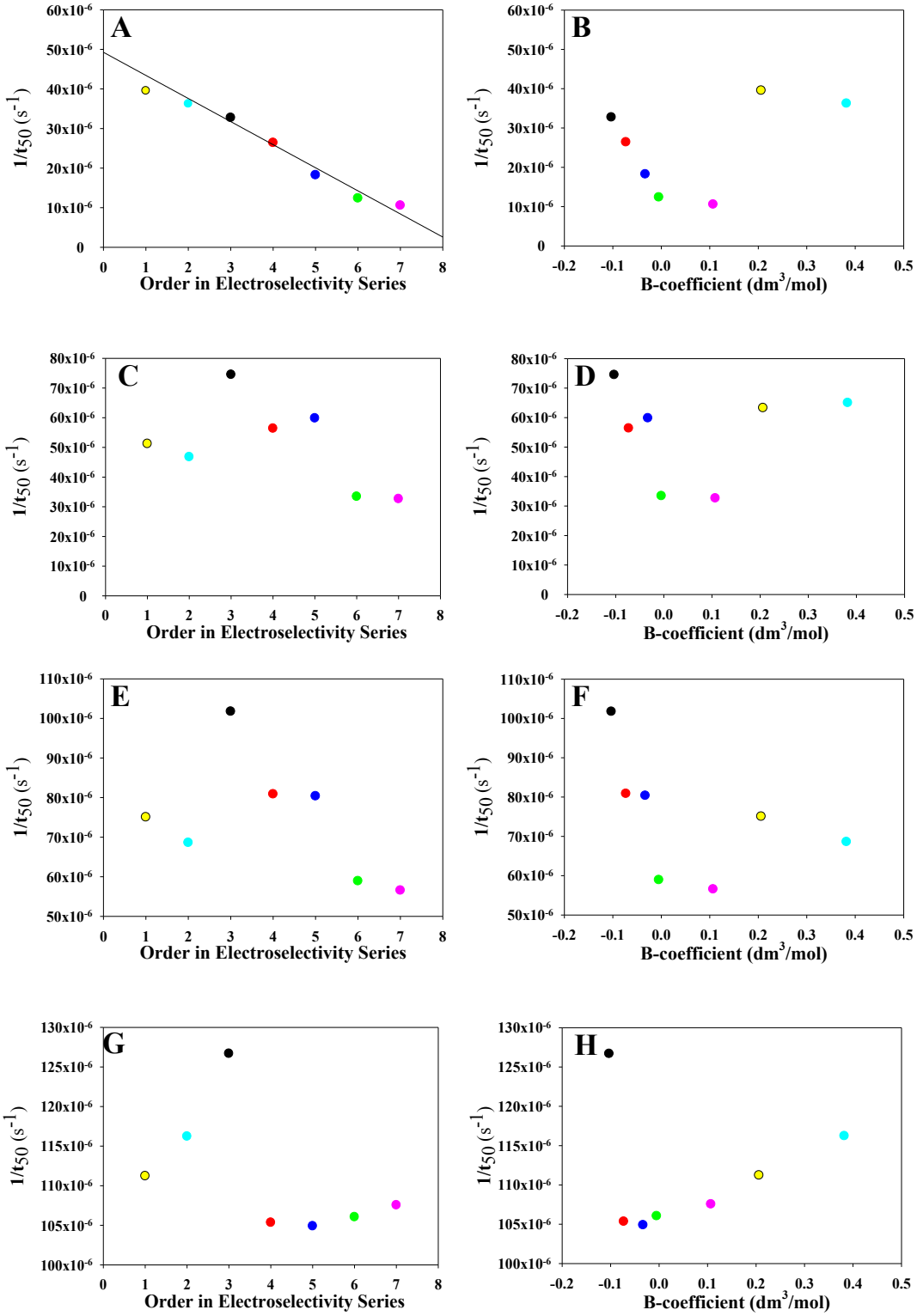
A
B
C
D
E
F
G
H
1/t50 (s-1)
Order in Electroselectivity Series
B-coefficient (dm3/mol)

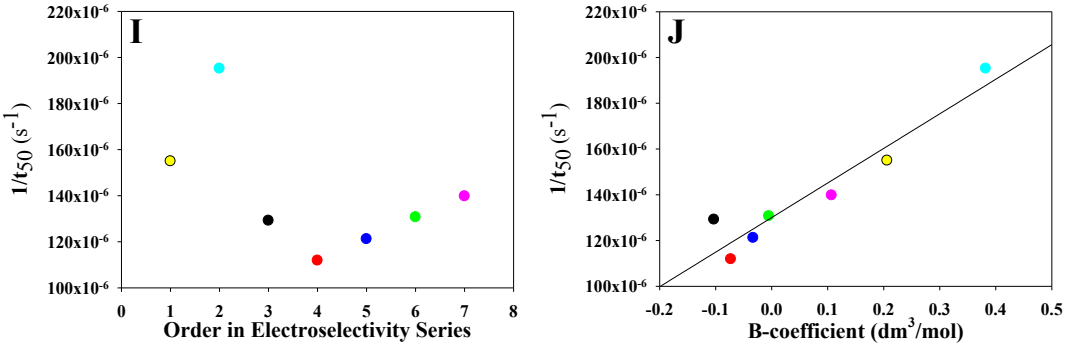

Figure 5.6: The rank order of the effects of different anions on the rate ($1/t_{50}$) of amyloid formation at pH 8.0 at 20 (A and B), 100 (C and D), 200 mM (E and F), 400 (G and H) and 600 mM (I and J) ionic strengths versus their order in the electroselectivity series (A, C, E, G and I) and the Hofmeister series (B, D, F, H and J). Note that the vertical axis scale is different for the different ionic strengths and the fits in A and F are to aid the eye only. At 20 mM ionic strength the order of the rate of amyloid formation for the anions scales with their order in the electroselectivity series (A), but not with the Jones-Dole B-coefficient, which is a measure of the Hofmeister series (B). At 100, 200 and 400 mM ionic strengths the trend disappears for both the electroselectivity series (C) and Hofmeister series (D), presumably from competing effects between the forces involved from each effect. At high ionic strength, 600 mM, the on amyloid formation scaled with the Hofmeister series (F), but not the electroselectivity series (E). Black, NaSCN; Red, NaI; Blue, NaBr; Green, NaCl; Pink, NaF; Yellow, Na_2SO_4; Cyan, Na_2HPO_4. All samples contained 10 mM Tris-HCl in addition to the added salt.

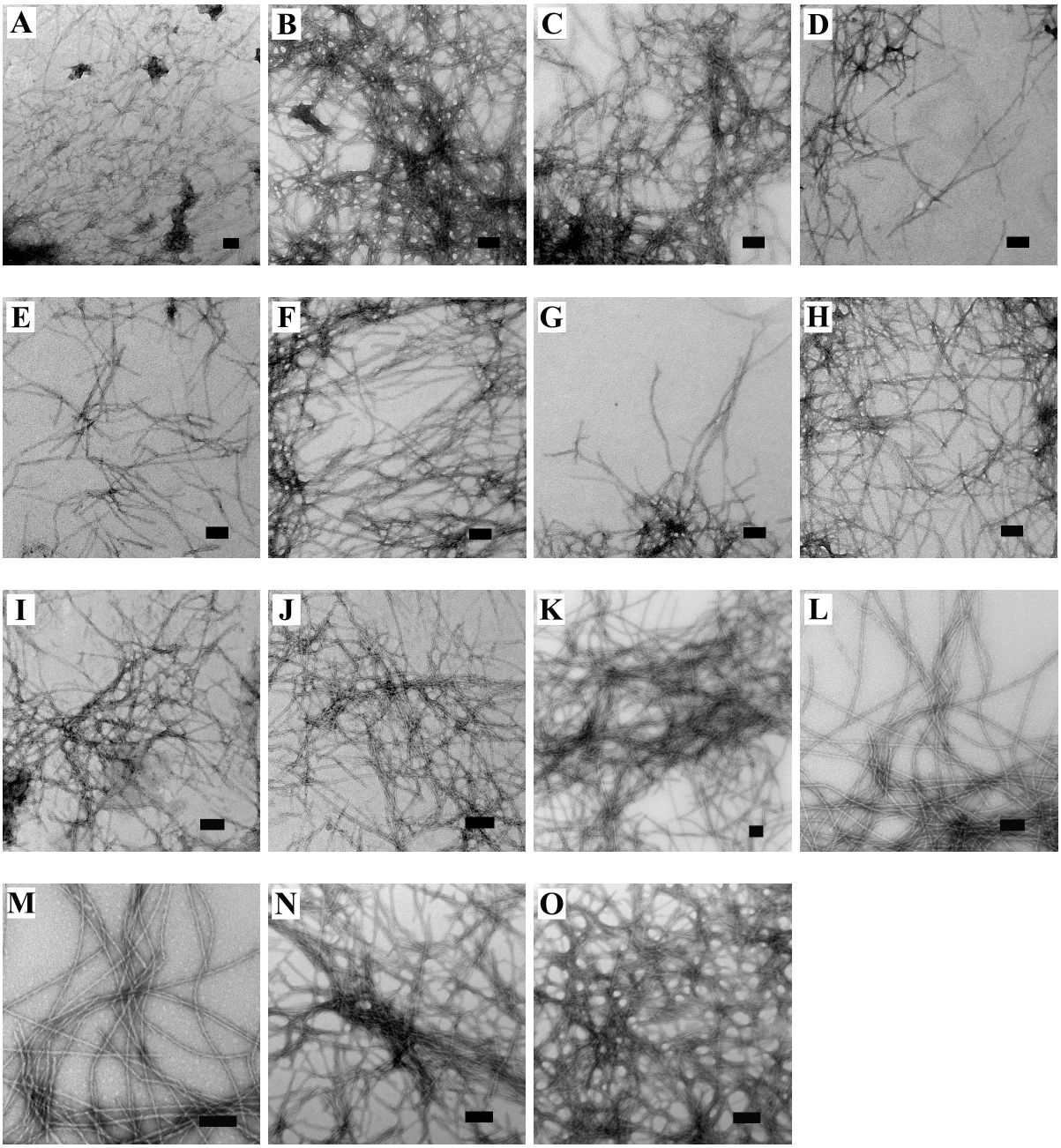

Figure 5.7: Salts induce amyloid formation, not amorphous precipitates. All samples were collected(22) at the end of the kinetic assays and contain 10 mM Tris-HCl, pH 8.0. (A) No added salt (B) 20 mM NaSCN, (C) 600 mM NaSCN, (D) 20 mM NaI, (E) 600 mM NaI, (F) 20 mM NaBr, (G) 600 mM NaBr, (H) 20 mM NaCl, (I) 600 mM NaCl, (J) 20 mM NaF, (K) 600 mM NaF, (L) 20 mM Na_2SO_4, (M) 600 mM Na_2SO_4, (N) 20 mM Na_2HPO_4, (O) 600 mM Na_2HPO_4. Scale bar is 100 nm.

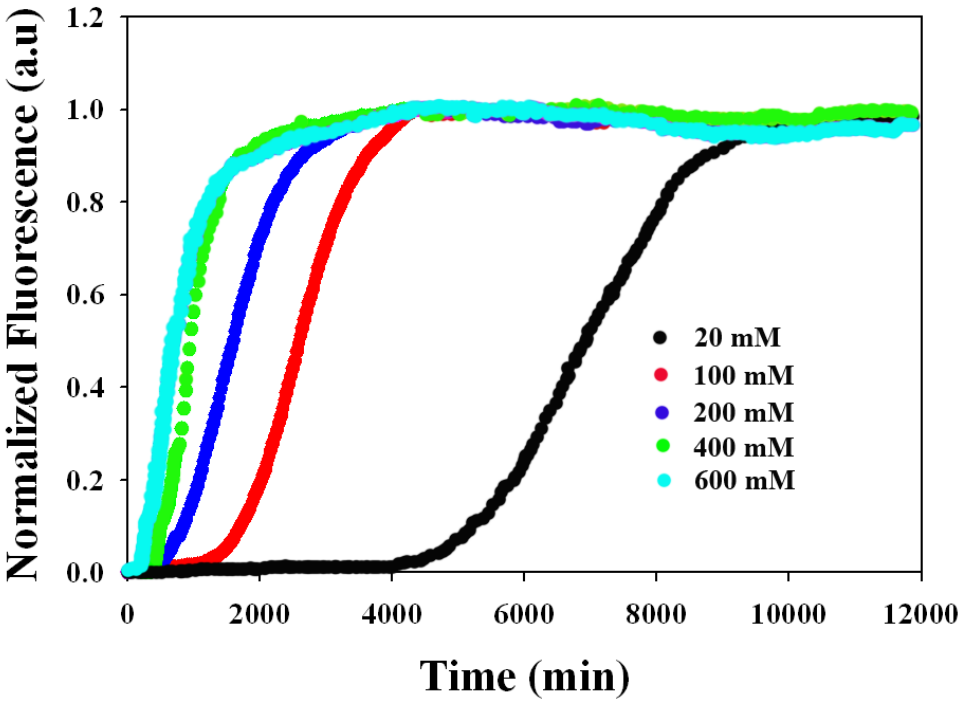

Figure 5.8: Dependence of the kinetics of amyloid formation at pH 5.5 on the ionic strength for various concentrations of NaCl. Plots of thioflavin-T fluorescence versus time are displayed. The concentration of added NaCl ranged from 20 to 600 mM. All experiments were conducted at 25 °C, pH 5.5 and all samples contained 10 mM MES. The concentration of IAPP and thioflavin-T were both 32 μM.

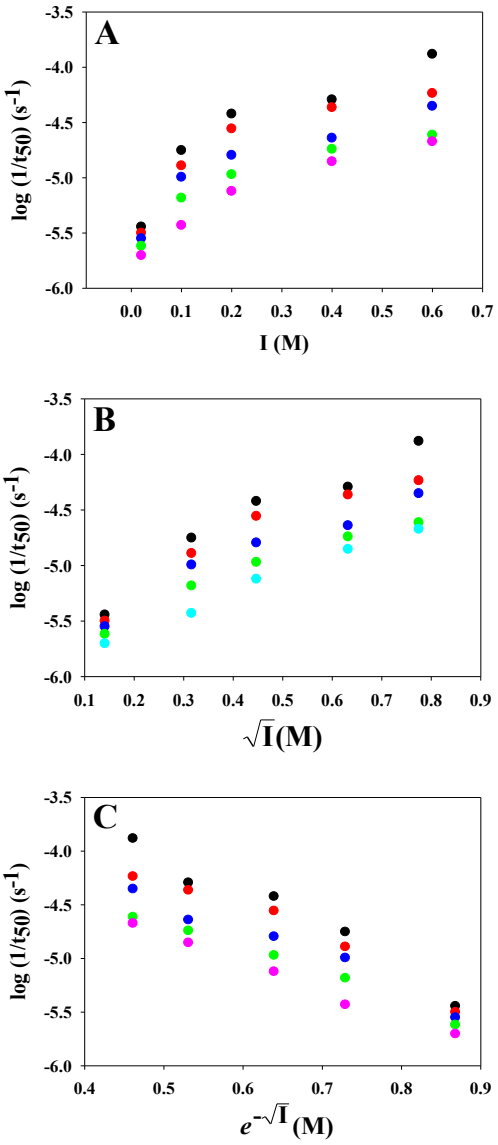

Figure 5.9: Analysis of the dependence of $\log(1/t_{50})$ on ionic strength, I, for the monovalent anions at pH 5.5. The observed values of $\log(1/t_{50})$ are plotted vs. (A) I; (B) $\sqrt{I}$; (C) $e^{-\sqrt{I}}$. Black, NaSCN; Red, NaI; Blue, NaBr; Green, NaCl; Pink, NaF.

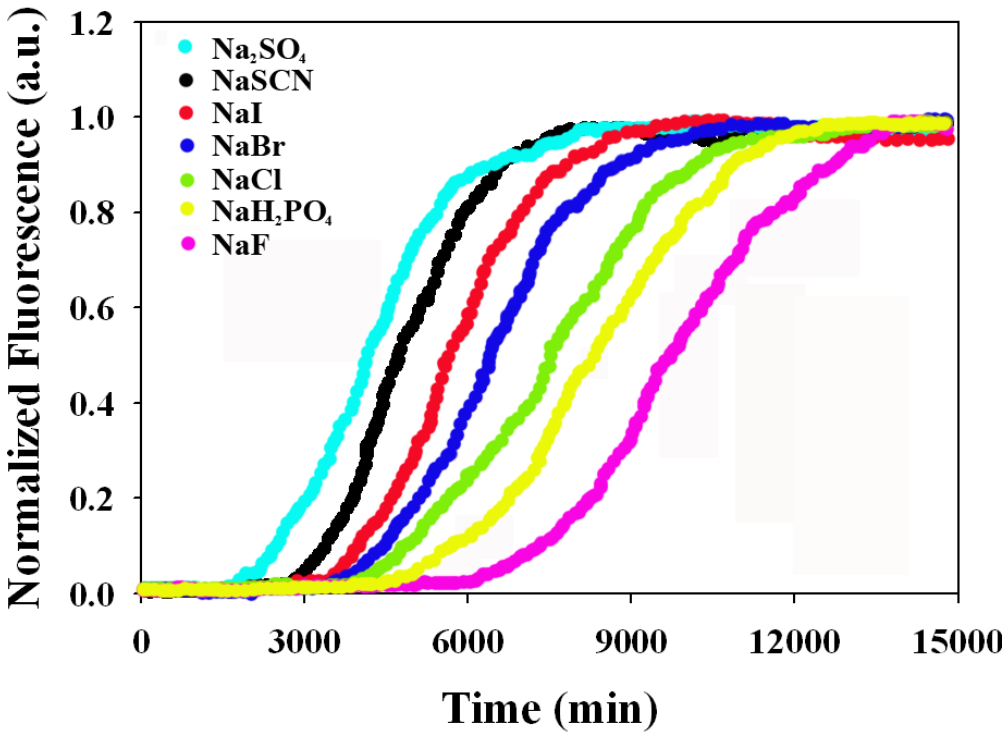

Figure 5.10: Dependence of the kinetics of amyloid formation on the anion identity at 20 mM added salt (30 mM ionic strength) at pH 5.5. Plots of thioflavin-T versus time are displayed. All experiments were conducted at 25 °C, pH 5.5 and all samples contained 10 mM MES. IAPP and thioflavin-T concentrations were both at 32 μM.

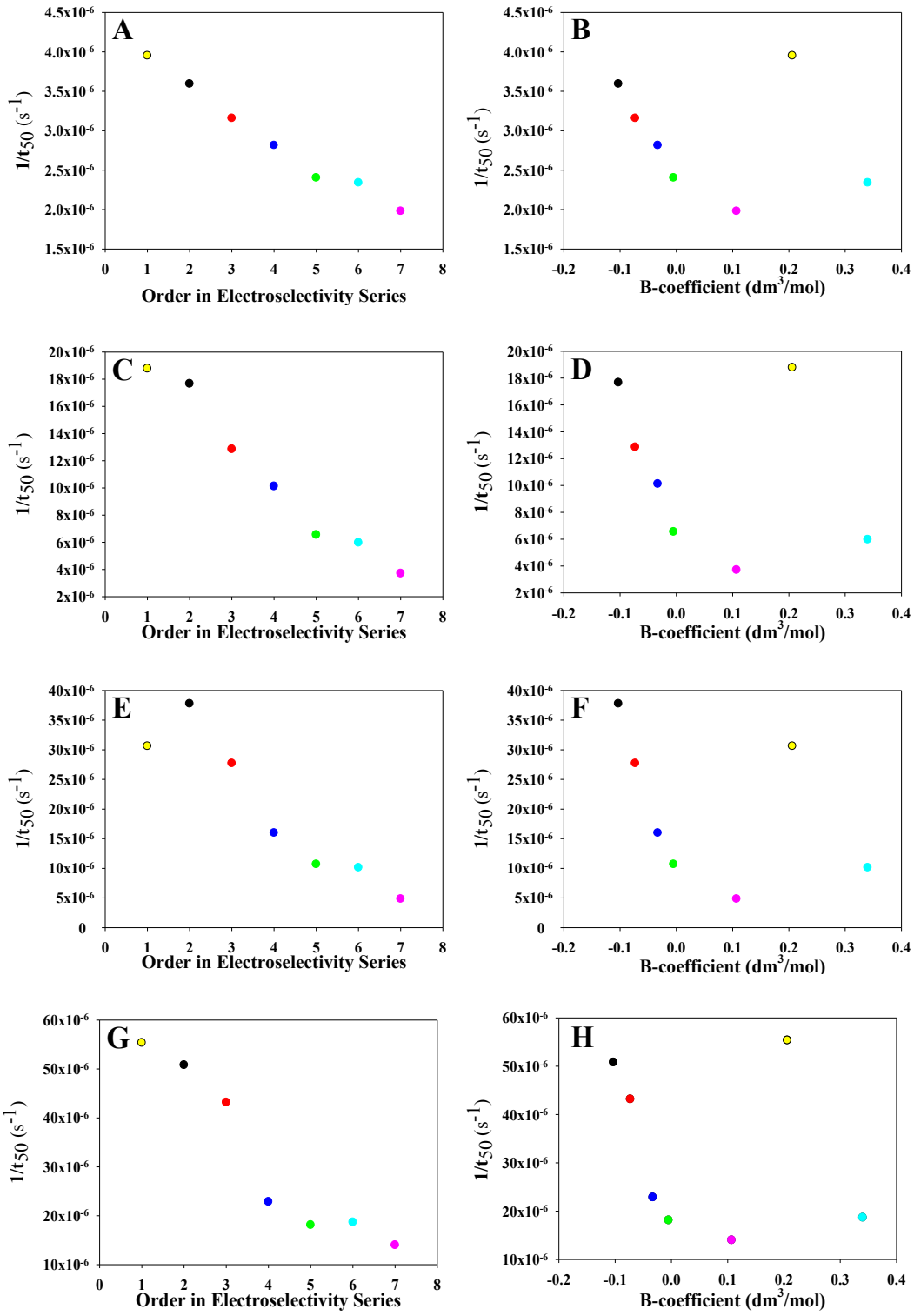
A
B
C
D
E
F
G
H
1/t50 (s-1)
Order in Electroselectivity Series
B-coefficient (dm3/mol)

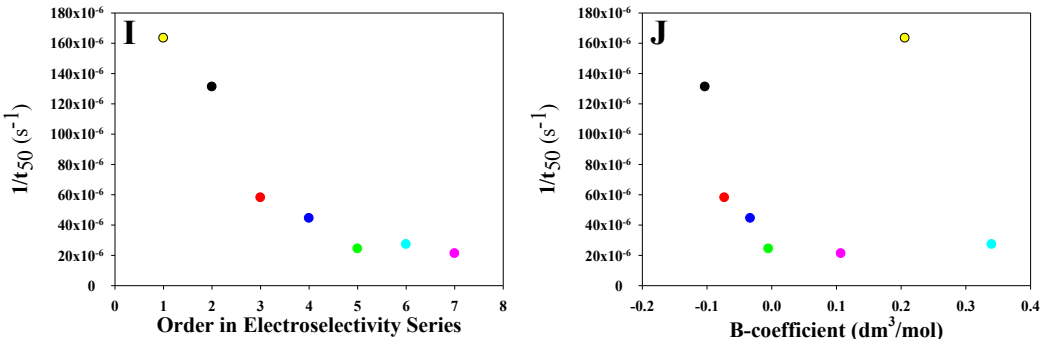

Figure 5.11: The rank order of the effects of different anions on the rate ($1/t_{50}$) of amyloid formation at pH 5.5 at 20 (A and B), 100 (C and D), 200 (E and F), 400 (G and H) and 600 mM (I and J) ionic strengths versus their order in the electroselectivity series (A, C, E, G and I) and the Hofmeister series (B, D, F, H and J). At 20 mM ionic strength the order of the rate of amyloid formation for the anions scales with their order in the electroselectivity series (A), but not with the Jones-Dole B-coefficient, which is a measure of the Hofmeister series (B). This trend is followed at every ionic strength tested at pH 5.5. Black, NaSCN; Red, NaI; Blue, NaBr; Green, NaCl; Pink, NaF; Yellow, Na_2SO_4; Cyan, Na_2HPO_4.

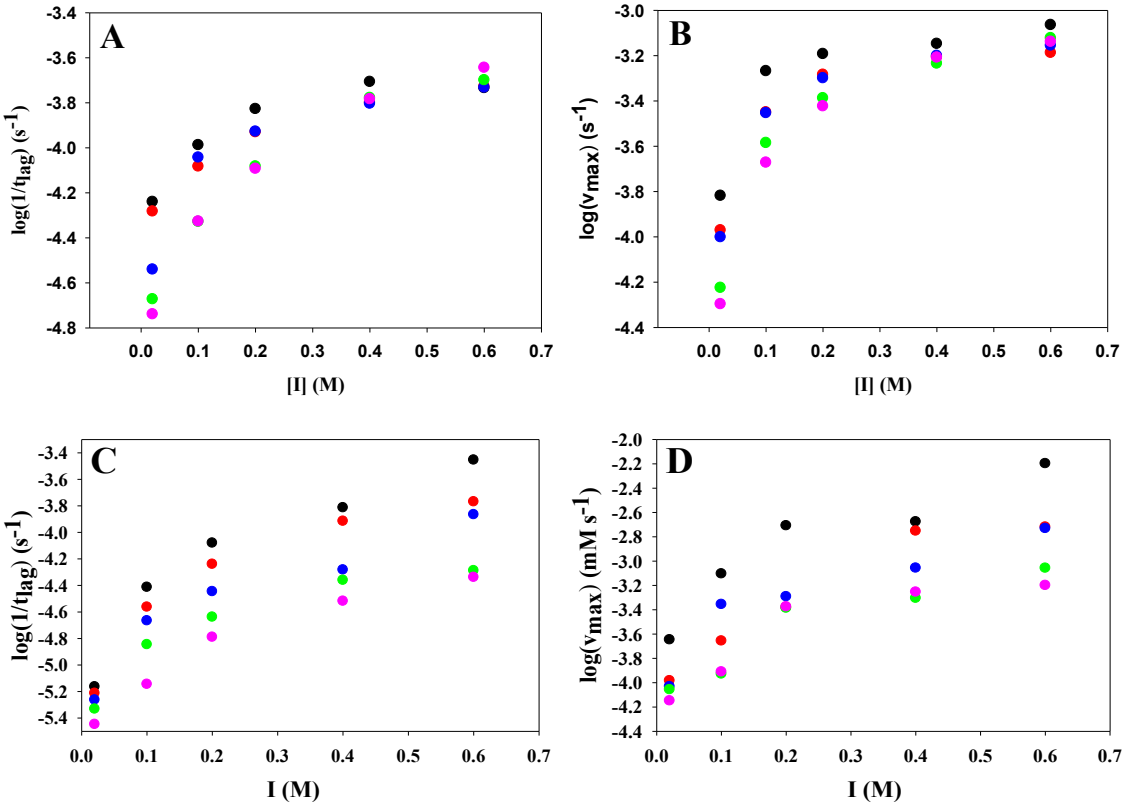

Figure 5.12: Plots of (A, C) $\log(1/t_{lag})$ and (B, D) $\log(v_{max})$ vs. ionic strength at (A, B) pH 8.0 and (C, D) pH 5.5 for the monovalent salts. NaSCN, black; NaI, red; NaBr, blue; NaCl, green; NaF, pink.

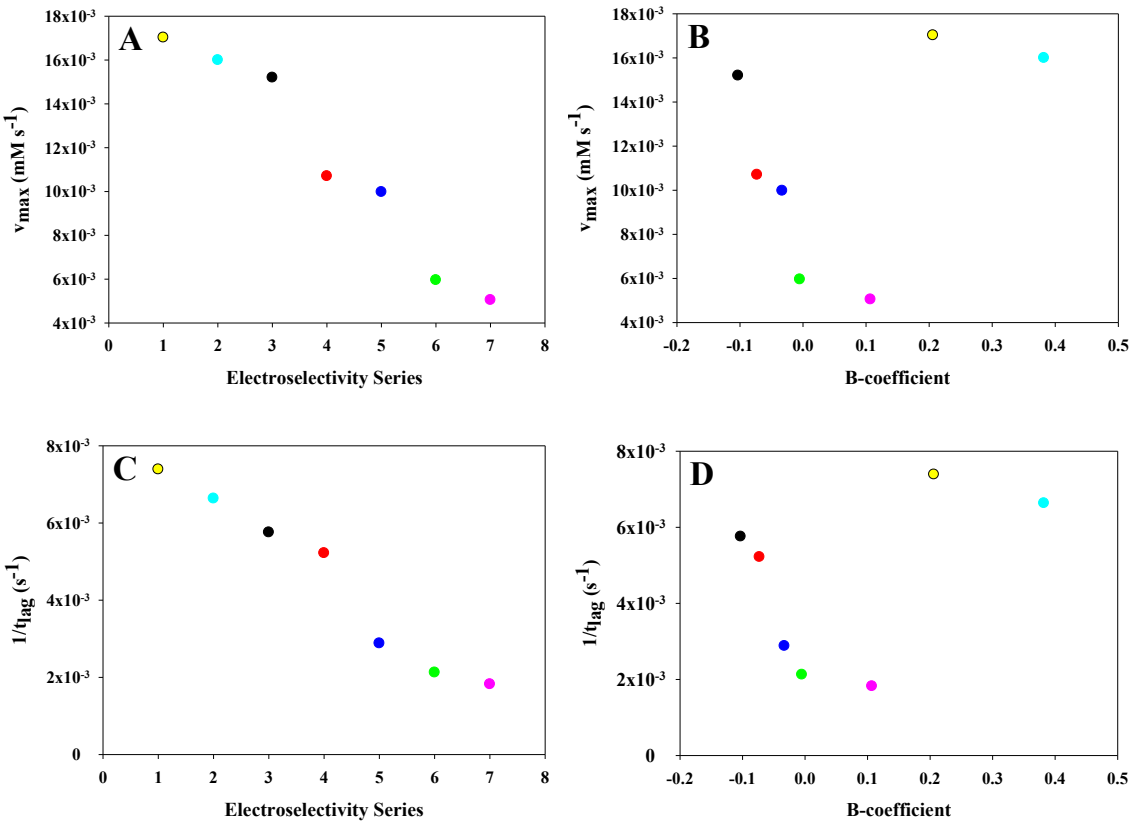

Figure 5.13: Dependence of $1/t_{lag}$ and the v_{max} on the anion identity at 20 mM added salt, pH 8.0. (A) v_{max} vs. the electroselectivity series (B) v_{max} vs the Jones-Dole B-coefficient (C) $1/t_{lag}$ vs. the electroselectivity series (D) $1/t_{lag}$ vs the Jones-Dole B-coefficient. Black, NaSCN; Red, NaI; Blue, NaBr; Green, NaCl; Pink, NaF; Yellow, Na_2SO_4; Cyan, Na_2HPO_4. All samples also contained 10 mM Tris-HCl, pH 8.0.

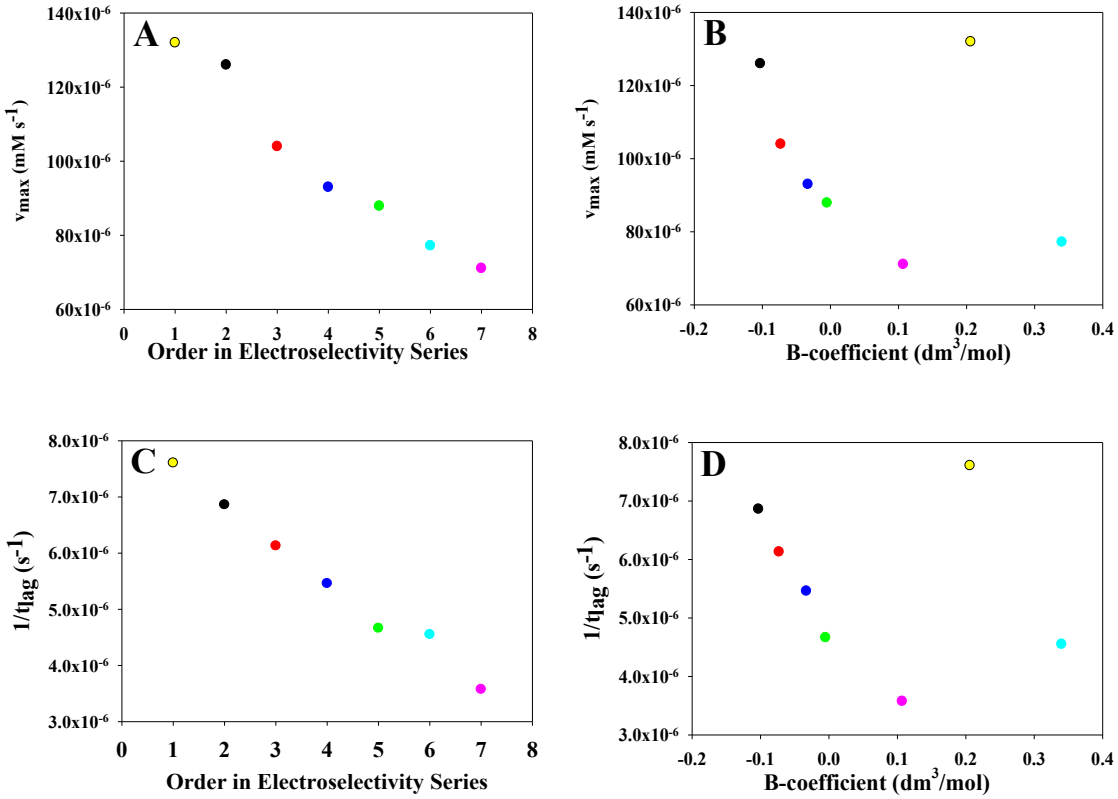

Figure 5.14: Dependence of $1/t_{lag}$ and the v_{max} on the anion identity at 20 mM added salt, pH 5.5. (A) v_{max} vs. the electroselectivity series (B) v_{max} vs the Jones-Dole B-coefficient (C) $1/t_{lag}$ vs. the electroselectivity series (D) $1/t_{lag}$ vs the Jones-Dole B-coefficient. Black, NaSCN; Red, NaI; Blue, NaBr; Green, NaCl; Pink, NaF; Yellow, Na_2SO_4; Cyan, Na_2HPO_4. All samples also contained 10 mM Tris-HCl, pH 5.5.

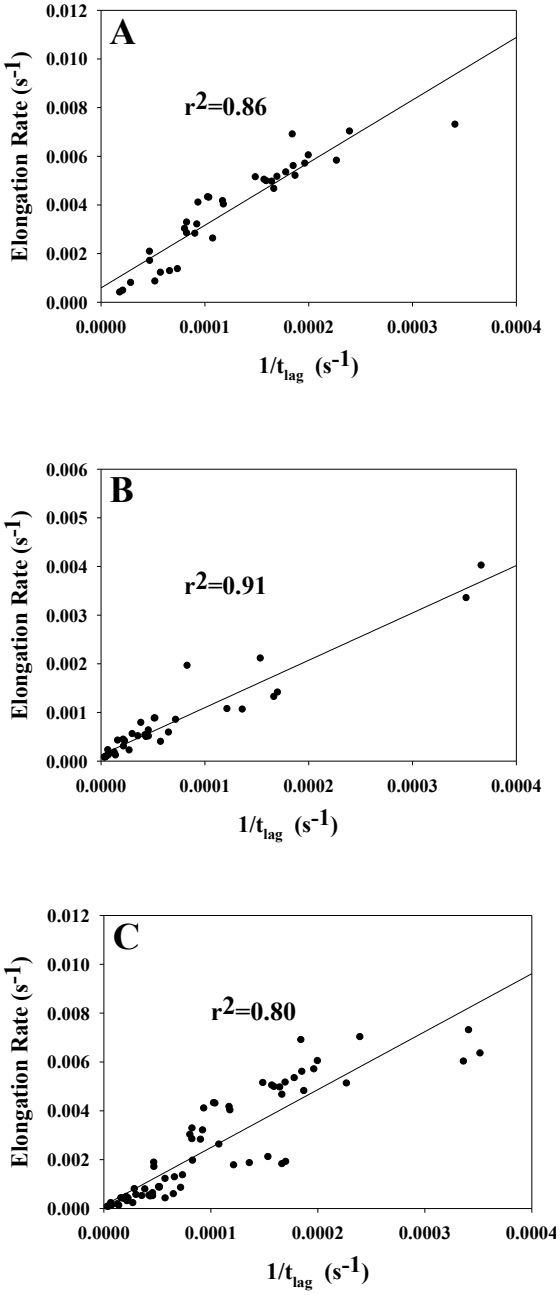

Figure 5.15: Correlation of the rate at t_{50}, v_{max}, with $1/t_{lag}$ for all anions at all ionic strengths at (A) pH 8.0 and (B) pH 5.5 (C) at both pH 5.5 and 8.0. The kinetic parameters are derived from the thioflavin-T kinetic assays fit with Equation-1. The data is fit to a straight line with an r^2 of 0.86, 0.91 and 0.80 for pH 8.0, pH 5.5 and pH 5.5 and 8.0 combined, respectively.

5.6 References

1. Abedini, A., Raleigh, D.P. (2006) Destabilization of human IAPP amyloid fibrils by proline mutations outside of the putative amyloidogenic domain: is there a critical amyloidogenic domain in human IAPP?, *J. Mol. Biol.* **355**, 274-281.

2. Maurer-Stroh, S., Debulpaep, M., Kuemmerer, N. Lopez, M., Martins, I., Reumers, J., et. al (2010) Exploring the sequence determinants of amyloid structure using position-specific scoring matrices, *Nat. Methods* **7**, 237-242.

3. Moriarty, D.F., Raleigh, D.P. (1999) Effects of sequential proline substitutions on amyloid formation by human amylin 20-29, *Biochemistry* **38**, 1811-1818.

4. Nerelius, C., Fitzen, M., Johansson, J. (2010) Amino acid sequence determinants and molecular chaperones in amyloid fibril formation, *Biochem. Biophys. Res. Comm.* **396**, 2-6.

5. Tjernberg, L., Hosia, W., Bark, N., Thyberg, J., Johansson, J. (2002) Charge attraction and beta propensity are necessary for amyloid fibril formation from tetrapeptides., *J. Biol. Chem.* **277**, 43243-43246.

6. Marshall, K.E., Morris, K.L., Charlton, D., O'Reilly, N., Lewis, L., Walden, H., Serpell, L.C. (2011) Hydrophobic, aromatic and electrostatic interactions play a central role in amyloid fibril formation and stability, *Biochemistry* **50**, 2061-2071.

7. Abrahamson, M., Grubb, A. (1994) Increased body-temperature accelerates aggregation of the Leu-68-Gln mutant cystatin-C, the amyloid-forming protein in hereditary cystatin-C amyloid angiopathy, *Proc. Natl. Acad. Soc. U.S.A.* **91**, 1416-1420.

8. Kusumoto, Y., Lomakin, A., Teplow, D.B., Benedek, G.B. (1998) Temperature dependence of amyloid beta-protein fibrillization, *Proc. Natl. Acad. Soc. U.S.A.* **95**, 12277-12282.

9. Su, Y., Chang, P.T. (2001) Acidic pH promotes the formation of toxic fibrils from beta-amyloid peptide, *Brain Res.* **893**, 287-291.

10. Zurdo, J., Guijarro, J.I., Jimenez, J.L. Saibil, H.R., Dobson, C.M. (2001) Dependence on solution conditions of aggregation and amyloid formation by an SH3 domain, *J. Mol. Biol.* **311**, 325-340.

11. Ferrao-Gonzales, A.D., Souto, S. O., Silva, J. L. & Foguel, D. (2000) The preaggregated state of an amyloidogenic protein: hydrostatic pressure converts native transthyretin into the amyloidogenic state, *Proc. Natl. Acad. Soc. U.S.A.* **97**, 6445-6450.

12. Harper, J.D., Lansbury, P.T. (1997) Models of amyloid seeding in Alzheimer's disease and scrapie: Mechanistic truths and physiological consequences of the time-dependent solubility of amyloid proteins, *Annu. Rev. Biochem.* **66**, 385-407.

13. Kamihira, M., Oshiro, Y., Tuzi, S., Nosaka, A.Y., Saito, H., Naito, A. (2003) Effect of electrostatic interactions on fibril formation of human calcitonin as studied by high resolution solid state 13C NMR, *J. Biol. Chem.* **278**, 2859-2865.

14. Yun, S., Urbanc, B., Cruz, L., Bitan, G., Teplow, D.B., Stanley, H.E. (2007) Role of electrostatic interactions in amlyoid β-protein (Aβ) oligomer formation: A discrete molecular dynamics study, *Biophys. J.* **92**, 4064-4077.

15. Abedini, A., Raleigh, D.P. (2005) The role of His-18 in amyloid formation by human islet amyloid polypeptide, *Biochemistry* **44**, 16284-16291.

16. Raman, B., Chatani, E., Kihara, M., Ban, T., Sakai, M., Hasegawa, K., Naiki, H., Rao, ChM, Goto, Y. (2005) Critical balance of electrostatic and hydrophobic interactions is required for beta 2-microglobulin amyloid fibril growth and stability, *Biochemistry* **44**, 1288-1299.

17. Jain, S., Udgaonkar, J.B. (2010) Salt-induced modulation of the pathway of amyloid fibril formation by the mouse prion protein, *Biochemistry* **49**, 7615-7624.

18. Klement, K., Wieligmann, K., Meinhardt, J., Hortschansky, P., Richter, W., Fändrich, M. (2007) Effect of different salt ions on the propensity of aggregation and on the structure of Alzheimer's abeta(1-40) amyloid fibrils, *J. Mol. Biol.* **373**, 1321-1333.

19. Westermark, P., Wernstedt, C., Wilander, E., Hayden, D.W., O'Brien, T.D., Johnson, K.H. (1987) Amyloid fibrils in human insulinoma and islets of Langerhans of the diabetic cat are derived from a neuropeptide-like protein also present in normal islet cells, *Proc. Natl. Acad. Soc. U.S.A.* **84**, 3881-3885.

20. Cooper, G.J., Willis, A.C., Clark, A., Turner, R.C., Sim, R.B., Reid, K.B.M. (1987) Purification and characterization of a peptide from amyloid-rich pancreases of type 2 diabetic patients, *Proc. Natl. Acad. Soc. U.S.A.* **84**, 8628-8632.

21. Potter, K.J., Abedini, A., Marek, P., Klimek, A.M., Butterworth, S., Driscoll, M., et. al (2010) Islet amyloid deposition limits the viability of human islet grafts but not porcine islet grafts, *Proc. Natl. Acad. Soc. U.S.A.* **107**, 4305-4310.

22. Williamson, J.A., Miranker, A.D. (2007) Direct detection of transient alpha-helical states in islet amyloid polypeptide, *Prot. Sci.* **16**, 110-117.

23. Abedini, A., Raleigh, D.P. (2009) A role for helical intermediates in amyloid formation by natively unfolded polypeptides?, *Phys. Biol.* **6**, 015005.

24. Charge, S.B.P., de Koning, E.J.P., Clark, A. (1995) Effect of pH and insulin on fibrillogenesis of islet amyloid polypeptide *in vitro*, *Biochemistry* **34**, 14588-14593.

25. Butler, P.C., Chou, J., Carter, W.B., Wang, Y.N., Bu, B.H., Chang, D., et. al (1990) Effects of meal ingestion on plasma IAPP concentration in NIDDM and nondiabetic humans, *Diabetes* **39**, 752-756.

26. Hanabusa, T., Kuba, K., Oki, C., Nakano, Y., Okai, K., Sanke, T., Nanjo, K. (1992) Islet amyloid polypeptide secretion from islet cells and its plasma concentration in patients with non-insulin-dependent diabetes mellitus, *Diabetes Res. Clin. Pratt.* **15**, 89-96.

27. Blundell, T.L., Dodson, G., Hodgkin, D.M., Mercola, D. (1972) Insulin: The structure in the crystal and its reflection in chemistry and biology, *Adv. Prot. Chem.* **26**, 279-402.

28. Smith, G.D., Pangborn, W.A., Blessing, R.H. (2003) The structure of T6 human insulin at 1.0 A resolution, *Acta. Crystallogr. D Biol. Crystallogr.* **59**, 474-482.

29. Westermark, P., Li, Z.-C., Westermark, G.T., Leckstrom, A., Steiner, D.F. (1996) Effects of beta cell granule components on human islet amyloid polypeptide fibril formation, *FEBS Lett.* **379**, 203-206.

30. Jaikaran, E.T., Nilsson, M.R., Clark, A. (2004) Pancreatic β-cell granule peptides form heteromolecular complexes which inhibit islet amyloid polypeptide fibril formation, *Biochem. J.* **377**, 709-716.

31. Knight, J.D., Williamson, J.A., Miranker, A.D. (2008) Interaction of membrane-bound islet amyloid polypeptide with soluble and crystalline insulin, *Prot. Sci.* **17**, 1-7.

32. Foster, M.C., Leapman, R.D., Li, M.X., Atwater, I. (1993) Elemental composition of secretory granules in pancreatic islets of Langerhans, *Biophys. J.* **64**, 525-532.

33. Baldwin, R.L. (1996) How Hofmeister ion interactions affect protein stability, *Biophys. J.* **71**, 2056-2063.

34. Hofmeister, F. (1888) Zur Lehre von der Wirkung der Salze, *Arch. Exp. Pathol. Pharmakol.* **24**, 247-260.

35. Collins, K.D., Washabaugh, M.W. (1985) The Hofmeister effect and the behavior of water at interfaces, *Q. Rev. Biophys.* **18**, 323-422.

36. Gjerde, D.T., Schmuchler, G., Fritz, J.S. (1980) Anion chromatography with low-conductivity eluents II, *J. Chromatogr.* **187**, 35-45.

37. Gregor, H.P., Belle, J., and Marcus, R. A. (1955) Studies on ion- exchange resins. XIII. Selectivity coefficients of quaternary base anion-exchange resins toward univalent anions, *J. Am. Chem. Soc.* **77**, 2713-2719.

38. Goto, Y., Calciano, L.J., Fink, A.L. (1990) Acid-induced folding of proteins, *Proc. Natl. Acad. Soc. U.S.A.* **87**, 573-577.

39. Marek, P., Woys, A.M., Sutton, K., Zanni, M.T., Raleigh, D.P. (2010) Efficient microwave-assisted synthesis of human islet amyloid polypeptide designed to facilitate the specific incorporation of labeled amino acids, *Org. Lett.* **12**, 4848-4851.

40. Abedini, A., Raleigh, D.P. (2005) Incorporation of pseudoproline derivtives allows the facile synthesis of human IAPP, a highly amyloidogenic and aggregation-prone polypeptide, *Org. Lett.* **7**, 693-696.

41. Abedini, A., Singh, G., Raleigh, D.P. (2006) Recovery and purification of highly aggregation-prone disulfide-containing peptides: Application to islet amyloid polypeptide, *Anal. Biochem.* **351**, 181-186.

42. Tam, J.P., Wu, C.R., Liu, W., Zhang, J.W. (1991) Disulfide bond formation in peptides by dimethyl sulfoxide. Scope and applications, *J. Am. Chem. Soc.* **113**, 6657-6662.

6. Full List of References

Abedini, A., Raleigh, D.P. (2005) The role of His-18 in amyloid formation by human islet amyloid polypeptide, *Biochemistry* **44**, 16284-16291.

Abedini, A., Raleigh, D.P. (2005) Incorporation of pseudoproline derivtives allows the facile synthesis of human IAPP, a highly amyloidogenic and aggregation-prone polypeptide, *Org. Lett.* **7**, 693-696.

Abedini, A., Raleigh, D.P. (2006) Destabilization of human IAPP amyloid fibrils by proline mutations outside of the putative amyloidogenic domain: is there a critical amyloidogenic domain in human IAPP, *J. Mol. Biol.* **355**, 274-281.

Abedini, A., Tracz, S. M., Cho, J. H., and Raleigh, D. P. (2006) Characterization of the heparin binding site In the N-Terminus of human pro-Islet amyloid polypeptide: Implications for amyloid formation, *Biochemistry* **45**, 9228-9237.

Abedini, A., Singh, G., Raleigh, D.P. (2006) Recovery and purification of highly aggregation-prone disulfide-containing peptides: Application to islet amyloid polypeptide, *Anal. Biochem.* **351**, 181-186.

Abedini, A., Raleigh, D.P. (2009) A role for helical intermediates in amyloid formation by natively unfolded polypeptides?, *Phys. Biol.* **6**, 015005.

Abedini, A., Raleigh, D.P. (2009) A critical assessment of the role of helical intermediates in amyloid formation by natively unfolded proteins and polypeptides, *Prot. Eng. Des. Sel.* **22**, 453-459.

Abrahamson, M., Grubb, A. (1994) Increased body-temperature accelerates aggregation of the Leu-68-Gln mutant cystatin-C, the amyloid-forming protein in hereditary cystatin-C amyloid angiopathy, *Proc. Natl. Acad. Soc. U.S.A.* **91**, 1416-1420.

Anguiano, M., Nowak, R.J., Lansbury, P.T.J. (2002) Protofibrillar islet amyloid polypeptide permeabilizes synthetic vesicles by a pore-like mechanism that may be relevant to type II diabetes, *Biochemistry* **41**, 11338-11343.

Apostolidou, M., Jayasinghe, S.A., Langen R. (2008) Structure of alpha-helical membrane-bound human islet amyloid polypeptide and its implications for membrane-mediated misfolding, *J. Biol. Chem.* **283**, 17205-17210.

Aprilakis, K.N., Taskent, H., Raleigh, D. P. (2007) Use of the novel fluorescent amino acid p-cyanophenylalanine offers a direct probe of hydrophobic core formation during the folding of the N-terminal domain of the ribosomal protein L9 and provides evidence for two-state folding, *Biochemistry* **46**, 12308-12313.

Azriel, R., Gazit, E. (2001) Analysis of the minimal amyloid-forming fragment of the islet amyloid polypeptide: An experimental support for the key role of the phenylalanine residue in amyloid formation, *J. Biol. Chem.* **276**, 34156-34161.

Balbach, J.J., Petkova, A.T., Oyler, N.A., Antzutkin, O.N., Gordon, D.J., Meredith, S.C., Tycko, R. (2002) Supramolecular structure in full-length Alzheimer's beta-amyloid fibrils: evidence for a parallel beta-sheet organization from solid-state nuclear magnetic resonance, *Biophys. J.* **83**, 1205-1216.

Baldwin, R.L. (1996) How Hofmeister ion interactions affect protein stability, *Biophys. J.* **71**, 2056-2063.

Basca, B., Horváti, K., Bõsze, S., Andreae, F., Kappe, C.O. (2008) Solid-phase synthesis of difficult peptide sequences at elevated temperatures: A critical comparison of microwave and conventional heating technologies, *J. Org. Chem.* **73**, 7532-7542.

Basca, B., Bõsze, S., Kappe, C.O. (2010) Direct solid-phase synthesis of the beta-amyloid (1−42) peptide using controlled microwave heating, *J. Org. Chem.* **75**, 2103-2106.

Bell, E.T. (1952) Hyalinization of the islets of Langerhans in diabetes mellitus, *Diabetes* **1**, 341-344.

Bell, E.T. (1959) Hyalinization of the islets of Langerhans in nondiabetic individuals, *Am. J. Pathol.* **35**, 801-805.

Bemporad, F., Taddei, N., Stefani, M., Chiti, F. (2006) Assessing the role of aromatic residues in the amyloid aggregation of human muscle acylphosphatase, *Prot. Sci.* **15**, 852-870.

Bemporad, F., Calloni, G., Campioni, S. Plakoutsi, G., Taddel, N., Chiti, F. (2006) Sequence and structural determinations of amyloid fibril formation, *Acc. Chem. Res.* **39**, 620-627.

Bendtzen, K., Mandrup-Poulson, T., Nerup, J., Nielsen, J.H., Dinarello, C.A., Svenson, M. (1986) Cytotoxicity of human pI 7 interleukin-1 for pancreatic islets of Langerhans, *Science* **232**, 1545-1547.

Berson, J.F., Theos, A.C., Harper, D.C., Tenza, D., Raposo, G., Marks, M.S. (2003) Proprotein convertase cleavage liberates a fibrillogenic fragment of a resident glycoprotein to initiate melanosome biogenesis, *J. Cell. Biol.* **16**, 521-533.

Biancalana, M., Makabe, K., Koide, A., Koide, S. (2009) Molecular mechanism of thioflavin-T binding to the surface of β-rich -peptide self-assemblies, *J. Mol. Biol.* **385**, 1052-1063.

Bieschke, J., Herbst, M., Wiglenda, T., Friedrich, R.P., Boeddrich, A., Schiele, F., et. al (2011) Small-molecule conversion of toxic oligomers to nontoxic β-sheet-rich amyloid fibrils, *Nat. Chem. Biol.* **8**, 93-101.

Bladen, H.A., Nylen, M.U., Glenner, G.G. (1966) The ultrastructure of human amyloid as revealed by the negative staining technique, *J. Ultra. Res.* **14**, 449-459.

Blazer, L.L., Neubig, R.R. (2009) Small molecule protein–protein interaction inhibitors as CNS therapeutic agents: Current progress and future hurdles, *Neuropsychopharmacology* **34**, 126-141.

Blundell, T.L., Dodson, G., Hodgkin, D.M., Mercola, D. (1972) Insulin: The structure in the crystal and its reflection in chemistry and biology, *Adv. Prot. Chem.* **26**, 279-402.

Brender J. R., H.K., Reid K. R., Kennedy R. T., Ramamoorthy A. (2008) A single mutation in the nonamyloidogenic region of islet amyloid polypeptide greatly reduces toxicity, *Biochemistry* **47**, 12680-12688.

Burley, S.K., Petsko, G.A. (1988) Weakly polar interactions in proteins, *Adv. Prot. Chem.* **39**, 125-189.

Butler, A.E., Janson, J., Bonner-Weir, S., Ritzel, R., Rizza, R.A., Butler, P.C. (2003) Beta-cell deficit and increased beta-cell apoptosis in humans with type 2 diabetes, *Diabetes* **52**, 102-110.

Butler, A.E., Jang, J., Gurlo, T., Carty, M.D., Soeller, W.C., Butler, P.C. (2004) Diabetes due to a progressive defect in beta-cell mass in rats transgenic for human islet amyloid polypeptide (HIP Rat): a new model for type 2 diabetes, *Diabetes* **53**, 1509-1516.

Butler, P.C., Chou, J., Carter, W.B., Wang, Y.N., Bu, B.H., Chang, D., et. al (1990) Effects of meal ingestion on plasma IAPP concentration in NIDDM and nondiabetic humans, *Diabetes* **39**, 752-756.

Cao, P., Tu, L.-H., Abedini, A., Levsh, O., Akter, R., Patsalo, V., Schmidt, A.M., Raleigh, D.P. (2012) Sensitivity of amyloid formation by human islet amyloid polypeptide to mutations at residue 20, *J. Mol. Biol.* **In Press**, DOI: 10.1016/j.jmb.2011.12.032.

Castillo, M.J., Scheen, A.J. LeFebvre, P.J. (1995) Amylin/islet amyloid polypeptide: Biochemistry, physiology and pathophysiology, *Diab. Metab.* **21**, 3-25.

Caughey, C., Lansbury, P. T. (2003) Protofibrils, pores, fibrils, and neurodegeneration: Separating the responsible protein aggregates from the innocent bystanders, *Annu. Rev. Neurosci.* **26**, 267-298.

Chang, E.S.-H., Liao, T.-Y., Lim, T.-S., Fann, W., Chen, R. P.-Y. (2009) A new amyloid-like β-aggregate with amyloid characteristics, except fibril morphology, *J. Mol. Biol.* **385**, 1257-1265.

Chapman, M.R., Robinson, L.S., Pinkner, J.S., Roth, R., Heuser, J., et al. (2002) Role of Escherichia coli curli operons in directing amyloid fiber formation, *Science* **295**, 851-855.

Charge, S.B.P., de Koning, E.J.P., Clark, A. (1995) Effect of pH and insulin on fibrillogenesis of islet amyloid polypeptide *in vitro*, *Biochemistry* **34**, 14588-14593.

Chiti, F., Stefani, M., Taddei, N., Ramponi, G., Dobson, C. M. (2003) Rationalization of the effects of mutations on peptide and protein aggregation, *Nature* **424**, 805-809.

Chiti, F., Dobson, C.M. (2006) Protein misfolding, functional amyloid and human disease, *Annu. Rev. Biochem.* **75**, 333-366.

Clark, A., Lewis, C. E., Willis, A. C., Cooper, G. J. S., Morris, J. F., Reid, K. B. M., Turner, R. C. (1987) Islet amyloid formed from diabetes-associated peptide may be pathogenic in type-2 diabetes, *Lancet* **2**, 231-234.

Clark, A., Wells, C.A., Buley, I.D., Cruickshank, J.K., Vanhegan, R.I., Matthews, D.R., et. al (1988) Islet amyloid, increased A-cells, reduced B-cells and exocrine fibrosis: quantitative changes in the pancreas in type 2 diabetes, *Diab. Res.* **9**, 151-159.

Cohen, A.S., Calkins, E. (1959) Electron microscopic observation on a fibrous component in amyloid of diverse origins, *Nature* **183**, 1202-1203.

Colletier, J.-P., Laganowsky, A., Landau, M., Zhao, M., Soriaga, A.B., Goldschmidt, L., et. al (2011) Molecular basis for amyloid-β polymorphism, *Proc. Natl. Acad. Soc. U.S.A.* **108**, 16938-16943.

Collins, K.D., Washabaugh, M.W. (1985) The Hofmeister effect and the behavior of water at interfaces, *Q. Rev. Biophys.* **18**, 323-422.

Cooper, G.J., Willis, A.C., Clark, A., Turner, R.C., Sim, R.B., Reid, K.B.M. (1987) Purification and characterization of a peptide from amyloid-rich pancreases of type 2 diabetic patients, *Proc. Natl. Acad. Soc. U.S.A.* **84**, 8628-8632.

Cooper, G.J.S. (1994) IAPP compared with calcitonin gene-related peptide: Structure, biology, and relevance to metabolic disease, *Endocrine Rev* **15**, 163-201.

Costes, S., Huang, C.J., Gurlo, T., Daval, M., Matveyenko, A.V., Rizza, R.A., Butler, A.E., Butler, P.C. (2011) Beta-cell dysfunctional ERAD/ubiquitin/proteasome system in type 2 diabetes mediated by IAPP-induced UCH-L1 deficiency, *Diabetes* **60**, 227-238.

D'Alessio, D.A., Verchere, C.B., Kahn, S.E., Hoagland, V., Baskin, D.G., Palmiter, R.D., Ensinck, J.W. (1994) Pancreatic expression and secretion of human islet amyloid polypeptide in a transgenic mouse, *Diabetes* **43**, 1457-1461.

Dalosto, S.D., Vanderkooi, J. M., Sharp, K. A. (2004) Vibrational stark effects on carbonyl, nitrile, and nitrosyl compounds including heme ligands, CO, CN, and NO, studied with density functional theory, *J. Phys. Chem. B* **108**, 6450-6457.

Davalli, A.M., Maffi, P., Socci, C., Sanvito, F., Freschi, M., Bertuzzi, F., et. al (2000) Insights from a successful case of intrahepatic islet transplantation into a type 1 diabetic patient, *J. Clin. Endocrinol. Metab.* **85**, 3847-3852.

de Koning, E.J.P., Bodkin, N.L., Hansen, B.C., Clark, A. (1993) Diabetes mellitus in Macaca mulatta monkeys is characterized by islet amyloidosis and reduction in beta-cell population, *Diabetologia* **36**, 378-384.

Dobson, C.M. (1999) Protein misfolding, evolution and disease, *Trends Biochem. Sci.* **24**, 329-332.

Dobson, C.M. (2003) Protein folding and misfolding, *Nature* **426**, 884-890.

Eizirik, D.L., Cardozo, A.K., Cnop, M. (2008) The role of endoplasmic reticulum stress in diabetes mellitus, *Endocrine Rev* **29**, 42-61.

Elayat, A.A., el-Naggar, M.M., Tahir, M. (1995) An immunocytochemical and morphometric study of the rat pancreatic islets, *J. Anatomy* **186**, 629-637.

Emamaullee, J.A., Merani, S., Toso, C., Kin, T., Al-Saif, F., Truong, W. (2009) Porcine marginal mass islet autografts resist metabolic failure over time and are enhanced by early treatment with liraglutide, *Endocrinology* **150**, 2145-2152.

Etcheberrigaray, R., Ito, E., Kim, C.S., Alkon, D.L. (1994) Soluble beta-amyloid induction of Alzheimer's phenotype for human fibroblast K+ channels, *Science* **264**, 276-279.

Ferandez-Escamilla, A.M., Rousseau, F., Schymkowitz, J., Serrano, L. (2004) Predication of sequence-dependent and mutational effects on the aggregation of peptide and proteins, *Nat. Biotechnol.* **22**, 1302-1306.

Ferrao-Gonzales, A.D., Souto, S. O., Silva, J. L. & Foguel, D. (2000) The preaggregated state of an amyloidogenic protein: hydrostatic pressure converts native transthyretin into the amyloidogenic state, *Proc. Natl. Acad. Soc. U.S.A.* **97**, 6445-6450.

Ferrier, G., Pierson, A., Jones, P., Bloom, S., Girgis, S., Legon, S. (1989) Expression of rat amylin (IAPP/DAP) gene, *J. Mol. Endocrinol.* **3**, R1-R4.

Fonseca, S.G., Burcin, M., Gromada, J., Urano, F. (2009) Endoplasmic reticulum stress in beta-cells and development of diabetes, *Curr. Opin. Pharmacol.* **9**, 763-770.

Foster, M.C., Leapman, R.D., Li, M.X., Atwater, I. (1993) Elemental composition of secretory granules in pancreatic islets of Langerhans, *Biophys. J.* **64**, 525-532.

Fox, N., Schrementi, J., Nishi, M., Ohagi, S., Chan, S.J., Heisserman, J.A., et. al (1993) Human islet amyloid polypeptide transgenic mice as a model of non-insulin-dependent diabetes mellitus (NIDDM), *FEBS Lett.* **323**, 40-44.

Friedman, R., Pellarin, R., Caflisch, A. (2009) Amyloid aggregation on lipid bilayers and its impact on membrane permeability, *J. Mol. Biol.* **387**, 407-415.

Garber, K. (2012) Amyloid disease drug approved, *Nat. Biotechnol.* **30**, 121.

Gazit, E. (2002) A possible role for pi-stacking in self-assembly of amyloid fibrils, *FASEB J.* **16**, 77-83.

Gazit, E. (2002) Mechanistic studies of the process of amyloid fibrils formation by the use of peptide fragments and analogues: Implications for the design of fibrillization inhibitors, *Curr. Med. Chem.* **9**, 1725-1735.

Getahun, Z., Huang, C. Y., Wang, T., Leon, B. D., DeGrado, W. F., Gai, F. (2003) Using nitrile-derivatized amino acids as infrared probes of local environment, *J. Am. Chem. Soc.* **125**, 405-411.

Gilead, S., Wolfenson, H., Gazit, E. (2006) Molecular mapping of the recognition interface between the islet amyloid polypeptide and insulin, *Angew. Chem. Int. Ed.* **45**, 6476-6480.

Gjerde, D.T., Schmuchler, G., Fritz, J.S. (1980) Anion chromatography with low-conductivity eluents II, *J. Chromatogr.* **187**, 35-45.

Glabe, C.G. (2006) Common mechanisms of amyloid oligomer pathogenesis in degenerative disease, *J. Neurobiol. Aging* **27**, 570-575.

Glabe, C.G. (2008) Structural classification of toxic amyloid oligomers, *J. Biol. Chem.* **283**, 29639-29643.

Glenner, G.G. (1980) Amyloid deposits and amyloidosis; the β-fibrilloses, *N. Engl. J. Med.* **302**, 1283-1292.

Goldsbury, C., Kistler, J., Aebi, U., Arvinte, T., Cooper, G.J.S. (1999) Watching amyloid fibrils grow by time-lapse atomic force microscopy, *J. Mol. Biol.* **285**, 33-39.

Goldsbury, C., Goldie, K., Pellaud, J., Seelig, J., Frey, P., Muller, S. A., Kistler, J., Cooper, G. J. S., Aebi, U. (2000) Amyloid fibril formation from full-length and fragments of amylin, *J. Struct. Biol.* **130**, 352-362.

Goldsbury, C.S., Cooper, G.J.S., Goldie, K.N., Muller, S.A., Saafi, E.L., Gruijters, W.T.M., Misur, M.P., Engel, A., Aebi, U., Kistler, J. (1997) Polymorphic fibrillar assembly of human amylin, *J. Struct. Biol.* **119**, 17-27.

Göpel, S.O., Kanno, T., Barg, S., Eliasson, L., Galvanovskis, J., Renström, E., Rorsman, P. (1999) Activation of Ca□-dependent K□ channels contributes to rhythmic firing of action potentials in mouse pancreatic beta cells, *J. Gen. Physiol* **114**, 759-770.

Goto, Y., Calciano, L.J., Fink, A.L. (1990) Acid-induced folding of proteins, *Proc. Natl. Acad. Soc. U.S.A.* **87**, 573-577.

Green, J.D., Goldsbury, C., Kistler, J., Cooper, G. J. S., Aebi, U. (2004) Human amylin oligomer growth and fibril elongation define two distinct phases in amyloid formation, *J. Biol. Chem.* **279**, 12206-12212.

Greenwald, J., and Riek, R. (2010) Biology of amyloid: structure, function, and regulation, *Structure* **18**, 1244-1260.

Gregor, H.P., Belle, J., and Marcus, R. A. (1955) Studies on ion- exchange resins. XIII. Selectivity coefficients of quaternary base anion-exchange resins toward univalent anions, *J. Am. Chem. Soc.* **77**, 2713-2719.

Groenning, M., Olsen, L., van de Weert, M., Flink, J. M., Frokjaer, S., Jørgensen, F. S. (2007) Study on the binding of thioflavin-T to β-sheet-rich and non-β-sheet cavities, *J. Struct. Biol.* **158**, 358-369.

Guardado-Mendoza, R., Davalli, A.M., Chavez, A.O., Hubbard, G.B., Dick, E.J., Majluf-Cruz, A., et. al (2009) Pancreatic islet amyloidosis, □cell apoptosis, and cell proliferation are determinants of islet remodeling in type-2 diabetic baboons., *Proc. Natl. Acad. Soc. U.S.A.* **106**, 13992-12997.

Guijarro, J.L., Sunde, M., Jones, J.A., Campbell, I.D., Dobson, C.M. (1998) Amyloid fibril formation by an SH3 domain, *Proc. Natl. Acad. Soc. U.S.A.* **95**, 4224-4228.

Hanabusa, T., Kuba, K., Oki, C., Nakano, Y., Okai, K., Sanke, T., Nanjo, K. (1992) Islet amyloid polypeptide secretion from islet cells and its plasma concentration in patients with non-insulin-dependent diabetes mellitus, *Diabetes Res. Clin. Pratt.* **15**, 89-96.

Harper, J.D., Lieber, C.M., Lansbury, P.T. (1997) Atomic force microscopic imaging of seeded fibril formation and fibril branching by the Alzheimer's disease amyloid-β protein, *Chem. Biol.* **4**, 951-959.

Harper, J.D., Lansbury, P.T. (1997) Models of amyloid seeding in Alzheimer's disease and scrapie: Mechanistic truths and physiological consequences of the time-dependent solubility of amyloid proteins, *Annu. Rev. Biochem.* **66**, 385-407.

Hazelwood, R.L. (1989). *The Endocrine Pancreas*, Prentice Hall, Englewood Cliffs, NJ.

Higham, C.E., Hull, R.L., Lawrie, L., Shennan, K.I., Morris, J.F., Birch, N.P., Docherty, K., Clark, A. (2000) Processing of synthetic pro-islet amyloid polypeptide (proIAPP)

"amylin" by recombinant prohormone convertase enzymes, PC2 and PC 3, in vitro, *Eur. J. Biochem.* **267**, 4998-5004.

Hofmeister, F. (1888) Zur Lehre von der Wirkung der Salze, *Arch. Exp. Pathol. Pharmakol.* **24**, 247-260.

Hou, X., Ling, Z., Quartier, E., Foriers, A., Schuit, F., Pipeleers, D., Van Schravendijk, C. (1999) Prolonged exposure of pancreatic beta cells to raised glucose concentrations results in increased cellular content of islet amyloid polypeptide precursors, *Diabetologia* **42**, 188-194.

Howard, C.F.J. (1978) Insular amyloidosis and diabetes mellitus in Macaca nigra, *Diabetes* **27**, 357-364.

Howard, C.F.J. (1986) Longitudinal studies on the development of diabetes in individual Macaca nigra, *Diabetologia* **29**, 301-306.

Huang, C.J., Lin, C.Y., Haataja, L., Gurlo, T., Butler, A.E., Butler, P.C. (2007) High expression rates of human islet amyloid polypeptide induce endoplasmic reticulum stress mediated beta-cell apoptosis, a characteristic of humans with type 2 but not type 1 diabetes, *Diabetes* **56**, 2016-2027.

Jack, E., Newsome, M., Stockley, P., Radford, S., Middleton, D. (2006) The organization of aromatic side groups in an amyloid fibril probed by solid-state 2H and 19F NMR spectroscopy, *J. Am. Chem. Soc.* **128**, 8098-8099.

Jaikaran, E., Clark, A. (2001) Islet amyloid and type 2 diabetes: From molecular misfolding to islet pathophysiology, *Biochim. Biophys. Acta.* **1537**, 179-203.

Jaikaran, E.T., Higham, C.E., Serpell, L.C., Zurdo, J., Gross, M., Clark, A., Fraser, P.E. (2001) Identification of a novel human islet amyloid polypeptide β-sheet domain and factors influencing fibrillogenesis, *J. Mol. Biol.* **308**, 515-525.

Jaikaran, E.T., Nilsson, M.R., Clark, A. (2004) Pancreatic β-cell granule peptides form heteromolecular complexes which inhibit islet amyloid polypeptide fibril formation, *Biochem. J.* **377**, 709-716.

Jain, S., Udgaonkar, J.B. (2010) Salt-induced modulation of the pathway of amyloid fibril formation by the mouse prion protein, *Biochemistry* **49**, 7615-7624.

Janson, J., Soeller, W.C., Roche, P.C., Nelson, R.T., Torchia, A.J., Kreutter, D.K., Butler, P.C. (1996) Spontaneous diabetes mellitus in transgenic mice expressing human islet amyloid polypeptide, *Proc. Natl. Acad. Soc. U.S.A.* **93**, 7283-7288.

Janson, J., Ashley, R.H., Harrison, D., McIntyre, S., Butler, P.C. (1999) The mechanism of islet amyloid polypeptide toxicity is membrane disruption by intermediate-sized toxic amyloid particles, *Diabetes* **48**, 491-498.

Jayasinghe, S.A., Langen, R. (2004) Identifying structural features of fibrillar islet amyloid polypeptide using site-directed spin labeling, *J. Biol. Chem.* **279**, 48420-48425.

Johnson, K.H., Stevens, J.B. (1973) Light and electron microscopic studies of islet amyloid in diabetic cats, *Diabetes* **22**, 81-90.

Johnson, K.H., O'Brien, T.D., Betsholtz, C., Westermark, P. (1989) Islet amyloid, islet-amyloid polypeptide, and diabetes mellitus, *N. Engl. J. Med.* **321**, 513-518.

Johnson, K.H., Wernstedt, C., O'Brien, T.D., Westermark, P. (1991) Amyloid in the pancreatic islets of the cougar (Felis concolor) is derived from islet amyloid polypeptide (IAPP), *Comp. Biochem. Physiol. B* **98**, 115-119.

Kahn, S.E., D'Alessio, D.A., Schwartz, M.W., Fujimoto, W.Y., Ensinck, J.W., Taborsky, G.J.J., Porte, D.J. (1990) Evidence of cosecretion of islet amyloid polypeptide and insulin by beta-cells, *Diabetes* **39**, 634-638.

Kahn, S.E., Andrikopoulos, S., Verchere, C.B. (1999) Islet amyloid: A long-recognized but underappreciated pathological feature of type 2 diabetes, *Diabetes* **48**, 241-253.

Kahn, S.E. (2000) The importance of the beta-cell in the pathogenesis of type 2 diabetes, *Am. J. Med.* **108**, 2s-8s.

Kajava, A.V., Aebi, U., Steven, A.C. (2005) The parallel superpleated beta structure as a model for amyloid fibrils of human amylin, *J. Mol. Biol.* **348**, 247-252.

Kajava, A.V., Steven, A.C. (2006) Beta-rolls, beta-helices, and other beta-solenoid proteins, *Adv. Prot. Chem.* **73**, 55-96.

Kamihira, M., Oshiro, Y., Tuzi, S., Nosaka, A.Y., Saito, H., Naito, A. (2003) Effect of electrostatic interactions on fibril formation of human calcitonin as studied by high resolution solid state 13C NMR, *J. Biol. Chem.* **278**, 2859-2865.

Kapurniotu, A. (2001) Amyloidogenicity and cytotoxicity of islet amyloid polypeptide, *Pept. Sci.* **60**, 438-459.

Kawahara, M., Kuroda, Y., Arispe, N., Rojas, E. (2000) Alzheimer's beta-amyloid, human islet amylin, and prion protein fragment evoke intracellular free calcium elevations by a common mechanism in a hypothalamic GnRH neuronal cell line., *J. Biol. Chem.* **275**, 14077-14083.

Kayed, R., Bernhagen, J., Greenfield, N., Sweimeh, K., Brunner, H., Voelter, W., Kapurniotu, A. (1999) Conformational transitions of islet amyloid polypeptide (IAPP) in amyloid formation in vitro, *J. Mol. Biol.* **287**, 781-796.

Kayed, R., Head, E., Thompson, J.L., McIntire, T.M., Cotman, C.W., Glabe, C.G. (2003) Common structure of soluble amyloid oligomers implies common mechanism of pathogenesis, *Science* **300**, 486-489.

Kayed, R., Glabe, C.G. (2006) Conformation-dependent anti-amyloid oligomer antibodies, *Methods Enzymol.* **413**, 326-344.

Kayed, R., Pensalfini, A., Margol, L., Sokolov, Y., Sarsoza, F., Head, E., Hall, J.E., Glabe, C. (2009) Annular protofibrils are a structurally and functionally distinct type of amyloid oligomer, *J. Biol. Chem.* **284**, 4230-4237.

Khemtemourian, L., Killian, J.A., Hoppener, J.W., Engel, M.F. (2008) Recent insights in islet amyloid polypeptide-induced membrane disruption and its role in beta-cell death in type 2 diabetes mellitus, *Exp. Diabetes Res.* **2008**, 421287.

Khurana, R., Coleman, C., Ionescu-Zanetti, C., Carter, S.A., Krishna, V., Grover, R.K., Roy, R., Singh, S. (2005) Mechanism of thioflavin T binding to amyloid fibrils., *J. Struct. Biol.* **151**, 229-238.

Kirkitadve, M.D., Condron, M.M., Teplow, D.B. (2001) Identification and characterization of key kinetic intermediates in amyloid beta-protein fibrillogenesis, *J. Mol. Biol.* **312**, 1103-1119.

Klement, K., Wieligmann, K., Meinhardt, J., Hortschansky, P., Richter, W., Fändrich, M. (2007) Effect of different salt ions on the propensity of aggregation and on the structure of Alzheimer's abeta(1-40) amyloid fibrils, *J. Mol. Biol.* **373**, 1321-1333.

Klöppel, G., Drenck, C.R. (1983) Immunzytochemische Morphometrie beim Typ-1- und Typ-2-Diabetes mellitus, *Deutsch. Med. Wschr.* **108**, 188-189.

Knight, J.D., Hebda, J. A., Miranker, A. D. (2006) Conserved and cooperative assembly of membrane-bound alpha-helical states of islet amyloid polypeptide, *Biochemistry* **45**, 9496-9508.

Knight, J.D., Williamson, J.A., Miranker, A.D. (2008) Interaction of membrane-bound islet amyloid polypeptide with soluble and crystalline insulin, *Prot. Sci.* **17**, 1-7.

Knowles, T.P.J., Waudby, C.A., Devlin, G.L., Cohen, S.I.A., Sperling, Aguzzi, A., Vendruscolo, M., et. al (2009) An analytical solution to the kinetics of breakable filament assembly, *Science* **326**, 1533-1537.

Knowles, T.P.J., White, D.A., Abate, A.R., Agresti, J.J., Cohen, S.I.A., Sperling, R.A., De Genst, E.J., et. al (2011) Observation of spatial propagation of amyloid assembly from single nuclei, *Proc. Natl. Acad. Soc. U.S.A.* **108**, 14746-17751.

Konarkowska, B., Aitken, J. F., Kistler, J., Zhang, S., Cooper, G.J. (2006) The aggregation potential of human amylin determines its cytotoxicity towards islet beta-cells, *FEBS J.* **273**, 3614-3624.

Koo, B.W., Hebda, J. A., Miranker, A. D. (2008) Amide inequivalence in the fibrillar assembly of islet amyloid polypeptide, *Prot. Eng. Des. Sel.* **21**, 147-154.

Korsgren, O., Sandler, S., Landström, A.S., Jansson, L., Andersson, A. (1988) Large-scale production of fetal porcine pancreatic isletlike cell clusters. An experimental tool for studies of islet cell differentiation and xenotransplantation, *Transplantation* **45**, 509-514.

Krampert, M., Bernhagen, J., Schmucker, J., Horn, A., Schmauder, A., Brunner, H., et. al (2000) Amyloidogenicity of recombinant human pro-islet amyloid polypeptide (ProIAPP), *Chem. Biol.* **7**, 855-871.

Krebs, M.R.H., Bromley, E. H. C., Donald, A. M. (2005) The binding of thioflavin-T to amyloid fibrils: localisation and implications, *J. Struct. Biol.* **149**, 30-37.

Kudva, Y.C., Mueske, C., Butler, P.C., Eberhardt, N.L. (1998) A novel assay in vitro of human islet amyloid polypeptide amyloidogenesis and effects of insulin secretory vesicle peptides on amyloid formation, *Biochem. J.* **331**, 809-813.

Kusumoto, Y., Lomakin, A., Teplow, D.B., Benedek, G.B. (1998) Temperature dependence of amyloid beta-protein fibrillization, *Proc. Natl. Acad. Soc. U.S.A.* **95**, 12277-12282.

Lansbury, P.T. (1997) Structural, neurology: are seeds at the root of neuronal degeneration?, *Neuron* **19**, 1151-1154.

Lara, C., Adamcik, J., Jordens, S., Mezzenga, R. (2011) General self-assembly mechanism converting hydrolyzed globular proteins into giant multistranded amyloid ribbons, *Biomacromolecules* **12**, 1868-1875.

Larsen, C.M., Faulenbach, M., Vaag, A., Volund, A., Ehses, J.A., Seifert, B., et. al (2007) Interleukin-1-receptor antagonist in type 2 diabetes mellitus, *N. Engl. J. Med.* **356**, 1517-1526.

Larson, J.L., Miranker, A.D. (2004) The mechanism of insulin action on islet amyloid polypeptide fiber formation, *J. Mol. Biol.* **335**, 221-231.

Lashuel, H.A., LaBrenz, S.R., Woo, L., Serpell, L.C., Kelly, J.W. (2000) Protofilaments, filaments, ribbons, and fibrils from peptidomimetic self-assembly: Implications for amyloid fibril formation and materials science, *J. Am. Chem. Soc.* **122**, 5262-5277.

Lashuel, H.A., Hartley, D., Petre, B.M., Walz, T., Lansbury, P.T.J. (2002) Neurodegenerative disease: amyloid pores from pathogenic mutations, *Nature* **418**, 291.

Last, N.B., Rhoades, E., Miranker, A.D. (2011) Islet amyloid polypeptide demonstrates a persistent capacity to disrupt membrane integrity, *Proc. Natl. Acad. Soc. U.S.A.* **108**, 9460-9465.

Laybutt, D.R., Preston, A.M., Akerfeldt, M.C., Kench, J.G., Busch, A.K., Biankin, A.V., Biden, T.J. (2007) Endoplasmic reticulum stress contributes to beta cell apoptosis in type 2 diabetes, *Diabetologia* **50**, 752-763.

Leighton, B., Cooper, G.J.S. (1988) Pancreatic IAPP and calcitonin gene-related peptide cause resistance to insulin in skeletal-muscle *in vitro*, *Nature* **335**, 632-635.

Levine, H. (1995) Thioflavin-T interactions with amyloid β-sheet structures, *Amyloid* **2**, 1-6.

Levine, H. (1999) Quantification of beta-sheet amyloid fibril structures with thioflavin T, *Methods Enzymol.* **309**, 274-284.

Lin, H., Bhatia, R., Lal, R. (2001) Amyloid ß protein forms ion channels: implications for Alzheimer's disease pathophysiology, *FASEB* **15**, 2433-2444.

Lorenzo, A., Razzaboni, B., Weir, G.C., Yankner, B.A. (1994) Pancreatic islet cell toxicity of amylin associated with type-2 diabetes mellitus, *Nature* **368**, 756-760.

Lorenzo, A., Yankner, B.A. (1996) Amyloid fibril toxicity in Alzheimer's disease and diabetes, *Ann. NY Acad. Sci.* **777**, 89-95.

Luca, S., Yau, W.-M., Leapman, R., Tycko, R. (2007) Peptide conformation and supramolecular organization in amylin fibrils: constraints from solid-state NMR *Biochemistry* **46**, 13505-13522.

Ludwig, G., Heitner, H. (1967) Zur Häufigkeit der Inselamyloidose des Pankreas beim Diabetes mellitus, *Zschr Inn Med* **22**, 814-818.

Magzoub, M., Miranker, A.D. (2012) Concentration-dependent transitions govern the subcellular localization of islet amyloid polypeptide, *FASEB* **26**, 1228-1238.

Maji, S.K., Perrin, M.H., Sawaya, M.R., Jessberger, S., Vadodaria, K., Rissman, R.A., et. al (2009) Functional amyloids as natural storage of peptide hormones in pituitary secretory granules, *Science* **325**, 328-332.

Makin, S.O., Serpell, L.C. (2004) Structural characterization of islet amyloid polypeptide fibrils, *J. Mol. Biol.* **335**, 1279-1288.

Maloy, A.L., Longnecker, D.S., Greenberg, E.R. (1981) The relation of islet amyloid to the clinical type of diabetes, *Hum. Pathol.* **12**, 917-922.

Marek, P., Abedini, A., Song, B., Kanungo, M., Johnson, M.E. Gupta, R., et. al (2007) Aromatic interactions are not required for amyloid fibril formation by islet amyloid polypeptide but do influence the rate of fibril formation and fibril morphology, *Biochemistry* **46**, 3255-3261.

Marek, P., Gupta, R., Raleigh, D.P. (2008) The fluorescent amino acid *p*-cyanophenylalanine provides an intrinsic probe of amyloid formation, *ChemBioChem* **9**, 1372-1374.

Marek, P., Mukherjee, S., Zanni, M.T., Raleigh, D.P. (2010) Residue-specific, real-time characterization of lag-phase species and fibril growth during amyloid formation: a combined fluorescence and IR study of p-cyanophenylalanine analogs of islet amyloid polypeptide, *J. Mol. Biol.* **400**, 878-888.

Marek, P., Woys, A.M., Sutton, K., Zanni, M.T., Raleigh, D.P. (2010) Efficient microwave-assisted synthesis of human islet amyloid polypeptide designed to facilitate the specific incorporation of labeled amino acids, *Org. Lett.* **12**, 4848-4851.

Margittai, M., Langen, R. (2008) Fibrils with parallel in-register structure constitute a major class of amyloid fibrils: molecular insights fromelectronparamagnetic resonance spectroscopy, *Q. Rev. Biophys.* **41**, 265-297.

Marina, K.D., Bitan, G., Teplow, D. B. (2002) Paradigm shifts in Alzheimer's disease and other neurodegenerative disorders: The emerging role of oligomeric assemblies, *Neurosci. Res.* **69**, 567-577.

Marshall, K.E., Morris, K.L., Charlton, D., O'Reilly, N., Lewis, L., Walden, H., Serpell, L.C. (2011) Hydrophobic, aromatic and electrostatic interactions play a central role in amyloid fibril formation and stability, *Biochemistry* **50**, 2061-2071.

Martínez-Álvarez, R.M., Volkoff, H., Munoz Cueto, J.A., Delgado, M.J. (2008) Molecular characterization of calcitonin gene-related peptide (CGRP) related peptides (CGRP, amylin, adrenomedullin and adrenomedullin-2/intermedin) in goldfish (Carassius auratus):cloning and distribution, *Peptides* **29**, 1534-1543.

Marzban, L., Soukhatcheva, G., Verchere, C.B. (2005) Role of carboxypeptidase E in processing of pro-islet amyloid polypeptide in β-cells, *Endocrinology* **146**, 1808-1817.

Marzban, L., Tomas, A., Becker, T.C., Rosenberg, L., Oberholzer, J., Fraser, P.E., Halban, P.A., & Verchere, C.B. (2008) Small interfering RNA-mediated suppression of proislet amyloid polypeptide expression inhibits islet amyloid formation and enhances survival of human islets in culture, *Diabetes* **57**, 3047-3055.

Masters, S.L., Dunne, A., Subramanian, S.L., Hull, R.L., Tannahil,l G.M., Sharp, F.A., et. al (2010) Activation of the NLRP3 inflammasome by islet amyloid polypeptide provides a mechanism for enhanced IL-1 in type 2 diabetes, *Nat. Immunol.* **11**, 897-904.

Masuda, M., Hasegawa, M., Nonaka, T., Oikawa, T., Yonetani, M., Yamaguchi, Y., et. al (2009) Inhibition of alpha-synuclein fibril assembly by small molecules: analysis using epitope-specific antibodies, *FEBS Lett.* **583**, 787-791.

Matveyenko, A.V., Butler, P.C. (2006) Islet amyloid polypeptide (IAPP) transgenic rodents as models for type 2 diabetes, *ILAR J.* **47**, 225-233.

Matveyenko, A.V., Butler, P.C. (2006) Beta-cell deficit due to increased apoptosis in the human islet amyloid polypeptide transgenic (HIP) rat recapitulates the metabolic defects present in type 2 diabetes, *Diabetes* **55**, 2106-2114.

Maurer-Stroh, S., Debulpaep, M., Kuemmerer, N. Lopez, M., Martins, I., Reumers, J., et. al (2010) Exploring the sequence determinants of amyloid structure using position-specific scoring matrices, *Nat. Methods* **7**, 237-242.

Meng, F., Abedini, A., Song, B., Raleigh, D.P. (2007) Amyloid formation by pro-islet amyloid polypeptide processing intermediates: examination of the role of protein heparan sulfate interactions and implications for islet amyloid formation in type 2 diabetes, *Biochemistry* **46**, 12091-12099.

Meng, F., Marek, P., Potter, K., Verchere, B., Raleigh, D. P. (2008) Rifampicin does not prevent amyloid fibril formation by human islet amyloid polypeptide but does inhibit fibril thioflavin-T interactions: implications for mechanistic studies of β-cell death, *Biochemistry* **47**, 6016-6024.

Merlini, G., Westermark, P. (2004) The systemic amyloidosis: clearer understanding of the molecular mechanisms offer hope for more effective therapies, *J. Intern. Med.* **255**, 159-178.

Milgram, S., Kho, S., Martin, G., Mains, R., Eipper, B. (1997) Localization of integral membrane peptidylglycine alpha- amidating monooxygenase in neuroendocrine cells, *J. Cell. Sci.* **110**, 695-706.

Mirzabekov, T.A., Lin, M., Kagan, B.L. (1996) Pore formation by the cytotoxic islet amyloid peptide amylin, *J. Biol. Chem.* **271**, 1988-1992.

Mishra, R., Bullic, B., Sellin, D., Jha, S., Waldman, H., Winter, R. (2008) Small-molecule inhibitors of islet amyloid polypeptide fibril formation, *Angew. Chem. Int. Ed.* **47**, 4679-4682.

Miyazato, M., Nakazato, M., Shiomi, K., Aburaya, J., Kangawa, K., Matsuo, H., Matsukura, S. (1992) Molecular forms of islet amyloid polypeptide (IAPP/amylin) in four mammals, *Diab. Res. Clin. Pract.* **7**, 31-36.

Mizushima, N., Yamamoto, A., Matsui, M., Yoshimori, T., Ohsumi, Y. (2004) In vivo analysis of autophagy in response to nutrient starvation using transgenic mice expressing a fluorescent autophagosome marker, *Mol. Biol. Cell* **15**, 1101-1111.

Moriarty, D.F., Raleigh, D.P. (1999) Effects of sequential proline substitutions on amyloid formation by human amylin 20-29, *Biochemistry* **38**, 1811-1818.

Mulder, H., Leckstrom, A., Uddman, R. Ekbald, E., Westermark, P., Sundler, F. (1995) Islet amyloid polypeptide (amylin) is expressed in sensory neurons, *Neurosci.* **15**, 7625-7632.

Mulder, H., Ahren, B., Sundler, F. (1996) Islet amyloid polypeptide and insulin gene expression are regulated in parallel by glucose in vivo in rats, *Am. J. Physiol.* **271**, E1008-E1014.

Mulder, H., Ekelund, M., Ekbald, E., Sundler, F. (1997) Islet amyloid polypeptide in the gut and pancrease: Localization, ontogeny and gut motility effects, *Peptides* **18**, 771-783.

Muthusamy, K.A., F.; Arvidsson, P.T.; Govender, P.; Kruger, H.G.; Maguire, G.E.M.; Govender, T. J. (2010) Microwave assisted SPPS of amylin and its toxicity of the pure product to RIN-5F cells, *Pept. Sci.* **94**, 323-330.

Nanga, R.P.R., Brender, J.R., Xu, J., Hartman, K., Subramanian, V., Ramamoorthy, A. (2009) Three-dimensional structure and orientation of rat islet amyloid polypeptide protein in a membrane environment by solution NMR spectroscopy, *J. Am. Chem. Soc.* **131**, 8252-8261.

Necula, M., Kayed, R., Milton, S., Glabe, C.G. (2007) Small molecule inhibitors of aggregation indicate that amyloid beta oligomerization and fibrillization pathways are independent and distinct, *J. Biol. Chem.* **282**, 10311-10324.

Nelson, R., Sawaya, M.R., Balbirnie, M., Madsen, A., Riekel, C., Grothe, R., Eisenberg, D. (2005) Structure of the cross-β spine of amyloid-like fibrils, *Nature* **435**, 773-778.

Nerelius, C., Fitzen, M., Johansson, J. (2010) Amino acid sequence determinants and molecular chaperones in amyloid fibril formation, *Biochem. Biophys. Res. Comm.* **396**, 2-6.

Nilsberth, C., Westlind-Danielsson, A., Eckman, C. B., Condron, M. M., Axelman, K., Forsell, C., Stenh, C., Luthman, J., Teplow, D. B., Younkin, S. G., Naslund, J., Lannefelt, L. (2001) The 'Arctic' APP mutation (E693G) causes Alzheimer's disease by enhanced A-beta protofibril formation, *Nat. Neurosci.* **4**, 887-893.

Nilsson, M., Raleigh, D. P. (1999) Analysis of amylin cleavage products provides new insights into the amyloidogenic region of human amylin, *J. Mol. Biol.* **294**, 1375-1385.

Nilsson, M.R., Driscoll, M. D., Raleigh, D. P. (2002) Low levels of asparagine deamidation have a dramatic effect on aggregation: Implications for the study of amyloid formation, *Prot. Sci.* **11**, 342-349.

Nishi, M., Chan, S.J., Nagamatsu, S., Bell, G.I., Steiner, D.F. (1989) Conservation of the sequence of islet amyloid polypeptide in five mammals is consistent with its putative role as an islet hormone, *Proc. Natl. Acad. Soc. U.S.A.* **86**, 5738-5742.

O'Nuallain, B., Williams, A.D., Westermark, P., Wetzel, R. (2004) Seeding specificity in amyloid growth induced by heterologous fibrils, *J. Biol. Chem.* **279**, 17490-17499.

O'Brien, T.D., Butler, A.E., Roche, P.C., Johnson, K.H., Butler, P.C. (1994) Islet amyloid polypeptide in human insulinomas. Evidence for intracellular amyloidogenesis, *Diabetes* **43**, 329-336.

Olzscha, H., Schermann, S.M., Woerner, A.C., Pinkert, S., Hecht, M.H., Tartaglia, G.G., et. al (2011) Amyloid-like aggregates sequester numerous metastable proteins with essential cellular functions, *Cell* **144**, 67-78.

Padrick, S.B., Miranker, A.D. (2001) Islet amyloid polypeptide: identification of long-range contacts and local order on the fibrillogenesis pathway, *J. Mol. Biol.* **308**, 783-794.

Padrick, S.B., Miranker, A.D. (2002) Islet amyloid: phase partitioning and secondary nucleation are central to the mechanism of fibrillogenesis, *Biochemistry* **41**, 4694-4703.

Palasek, S.A., Cox, Z.J., Collins, J.M. (2007) Limiting racemization and aspartimide formation in microwave-enhanced Fmoc solid phase peptide synthesis, *J. Pept. Sci.* **15**, 143-148.

Park, K., and Verchere, C. B. (2001) Identification of a heparin binding domain in the N-terminal cleavage site of pro-islet amyloid polypeptide. Implications for islet amyloid formation, *J. Biol. Chem.* **276**, 16611-16616.

Paulsson, J.F., Westermark, G.T. (2005) Aberrant processing of human proislet amyloid polypeptide results in increased amyloid production, *Diabetes* **54**, 2117-2125.

Paulsson, J.F., Andersson, A., Westermark, P., Westermark, G.T. (2006) Intracellular amyloid-like deposits contain unprocessed pro islet amyloid polypeptide (proIAPP) in beta-cells of transgenic mice overexpressing human IAPP and transplanted human islets, *Diabetologia* **49**, 1237-1246.

Pepys, M.B. (2006) Amyloidosis, *Annu. Rev. Med.* **57**, 233-241.

Petkova, A.T., Leapman, R. D., Guo, Z., Yau, W.-M., Mattson, M. P., Tycko, R. (2005) Self-propagating, molecular-level polymorphism in Alzheimer's beta-amyloid fibrils, *Science* **307**, 262-265.

Porat, Y., Kolusheva, S., Jelinek, R., Gazit, E. (2003) The human islet amyloid polypeptide formstransient membrane-active prefibrillar assemblies, *Biochemistry* **42**, 10971-10977.

Porat, Y., Mazor, Y., Efrat, S., Gazit, E. (2004) Inhibition of islet amyloid polypeptide fibril formation: A potential role for heteroaromatic interactions, *Biochemistry* **43**, 14454-14462.

Porat, Y., Abramowitz, A., Gazit, E (2006) Inhibition of amyloid fibril formation by polyphenols: Structural similarity and aromatic interactions as a common inhibition mechanism, *Chem. Biol. Drug Des.* **67**, 27-37.

Porte, D., Kahn, S.E. (1989) Hyperproinsulinemia and amyloid in NIDDM: Clues to etiology of islet β-cell dysfunction?, *Diabetes* **38**, 1333-1336.

Potter, K.J., Abedini, A., Marek, P., Klimek, A.M., Butterworth, S., Driscoll, M., et. al (2010) Islet amyloid deposition limits the viability of human islet grafts but not porcine islet grafts, *Proc. Natl. Acad. Soc. U.S.A.* **107**, 4305-4310.

Puchtler, H., Sweat, F., Levine, M. (1962) On the binding of Congo red by amyloid, *J. Histochem. Cytochem.* **10**, 355-364.

Qiang, W.Q.W., Yau, W.M., Tycko, R. (2011) Structural evolution of Iowa mutant beta-amyloid fibrils from polymorphic to homogeneous states under repeated seeded growth, *J. Am. Chem. Soc.* **133**, 4018-4029.

Quist, A., Doudevski, I., Lin, H., Azimova, R., Ng, D., Frangione, B., Kagan, B., Ghiso, J., Lal, R. (2005) Amyloid ion channels: a common structural link for protein-misfolding disease, *Proc. Natl. Acad. Soc. U.S.A.* **102**, 10427-10432.

Raman, B., Chatani, E., Kihara, M., Ban, T., Sakai, M., Hasegawa, K., Naiki, H., Rao, ChM, Goto, Y. (2005) Critical balance of electrostatic and hydrophobic interactions is required for beta 2-microglobulin amyloid fibril growth and stability, *Biochemistry* **44**, 1288-1299.

Reddy, G., Straub, J.E., Thirumalai, D. (2009) Dynamics of locking of peptides onto growing amyloid fibrils, *Proc. Natl. Acad. Soc. U.S.A.* **106**, 11948-11953.

Rodríguez-Rodríguez, C., Rimola, A., Rodríguez-Santiago, L., Ugliengo, P., Álvarez-Larena, A., Gutiérrez-de-Terán, H., et al. (2010) Crystal structure of thioflavin-T and its binding to amyloid fibrils: insights at the molecular level, *Chem. Commun.* **46**, 1156-1158.

Rogers, J.M., Lippert, L. G., Gai, F. (2010) Non-natural amino acid fluorophores for one- and two-step fluorescence resonance energy transfer applications, *Anal. Biochem.* **399**, 182-189.

Ryan, E.A., Paty, B.W., Senior, P.A., Bigam, D., Alfadhli, E., Kneteman, N.M., et. al (2005) Five-year follow up after clinical islet transplantation, *Diabetes* **54**, 2060-2069.

Saito, K., Yaginuma, N., Takahashi, T. (1979) Differential volumetry of A, B and D cells in the pancreatic islets of diabetic and nondiabetic subjects, *Tohoku J. Exp. Med.* **129**, 273-283.

Sakagashira, S., Sanke, T., Hanabusa, T., Shimomura, H., Ohagi, S., Kumagaye, K.Y., et. al (1996) Missense mutation of amylin gene (S20G) in Japanese NIDDM patients, *Diabetes* **45**, 1279-1281.

Salminen, A., Kauppinen, A., Suuronen, T., Kaarniranta, K., Ojala, J. (2009) ER stress in Alzheimer's disease: a novel neuronal trigger for inflammation and Alzheimer's pathology, *J. Neuroinflamm.* **6**, 41-54.

Sanke, T., Bell, G.I. Sample, C., Rubenstein, A.H., Steiner, D.F. (1988) An islet amyloid peptide is derived from an 89-amino acid precursor by proteolytic processing, *J. Biol. Chem.* **263**, 17243-17246.

Sanke, T., Hanabusa, T., Nakano, Y., Oki, C., Okai, K., Fujimoto, W.Y., et. al (1991) Plasma islet amyloid polypeptide (IAPP) levels and their responses to oral glucose in type-2 (non-insulin-dependent) diabetic patients, *Diabetologia* **34**, 129-132.

Sawaya, M.R., Sambashivan, S., Nelson, R., Ivanova, I.I., Sievers, S.A., Apostol, M.I., et. al (2007) Atomic structures of amyloid cross-β spines reveal varied steric zippers, *Nature* **447**, 453-457.

Schultz, K.C., Supekova, L., Ryu, Y., Xie, J., Perera, R., Schultz, P. G. (2006) A genetically encoded infrared probe, *J. Am. Chem. Soc.* **128**, 13984-13985.

Sedman, V.L., Allen, S., Chan, W.C., Davies, M.C., Roberts, C.J., Tendler, S.J.B. (2005) Atomic force microscopy of human amylin (20-29) fibrils, *Prot. Pept. Lett.* **12**, 79-83.

Seino, S. (2001) S20G mutation of the amylin gene is associated with Type II diabetes in Japanese, *Diabetologia* **44**, 906-909.

Selkoe, D.J. (2004) Cell biology of protein misfolding: The examples of Alzheimer's and Parkinson's diseases, *Nat. Cell Biol.* **6**, 1054-1061.

Serrano, A.L., Troxler, T., Tucker, M. J., Gai, F. (2010) Photophysics of a fluorescent non-natural amino acid: p-Cyanophenylalanine, *Chem. Phys. Lett.* **487**, 303-306.

Seyfried, M.S., Lauber, B.S., Luedtke, N.W. (2010) Multiple-turnover isotopic labeling of Fmoc- and Boc-protected amino acids with oxygen isotopes, *Org. Lett.* **12**, 104-106.

Shapiro, A.M.J., Lakey, J.R.T., Ryan, E.A., Korbutt, G.S., Toth, E.L., Warnock, G.L., et. al (2000) Islet transplantation in seven patients with type 1 diabetes mellitus using a glucocorticoid free immunosuppressive regiment, *N. Engl. J. Med.* **343**, 230-238.

Shim, S.-H., Gupta, R., Ling, Y. L., Strasfeld, D. B., Raleigh, D. P., Zanni, M. T. (2009) Two-dimensional IR spectroscopy and isotope labeling defines the pathway of amyloid formation with residue-specific resolution, *Proc. Natl. Acad. Soc. U.S.A.* **106**, 6614-6619.

Sipe, J.D., Cohen, A. S. (1994) Amyloidosis, *Crit. Rev. Clin. Lab Sci.* **31**, 325-354.

Sipe, J.D., Benson, M.D., Buxbaum, J.N., Ikeda, S.-I., Merlini, G., Saraiva, M.J.M., Westermark, P. (2010) Amyloid fibril protein nomenclature: 2010 recommendations from the nomenclature committee of the International Society of Amyloidosis, *Amyloid* **17**, 101-104.

Smith, G.D., Pangborn, W.A., Blessing, R.H. (2003) The structure of T6 human insulin at 1.0 A resolution, *Acta. Crystallogr. D Biol. Crystallogr.* **59**, 474-482.

Smith, P.E.S., Brender, J.R., Ramamoorthy, A. (2009) Smith PES, Brender JR, Ramamoorthy A. Induction of negative curvature as a mechanism of cell toxicity by amyloidogenic peptides: the case of islet amyloid polypeptide, *J. Am. Chem. Soc.* **131**, 4470-4478.

Soong, R., Brender, J. R., Macdonald, P. M., Ramamoorthy, A. (2009) Association of highly compact type II diabetes related islet amyloid polypeptide intermediate species at physiological temperature revealed by diffusion NMR spectroscopy, *J. Am. Chem. Soc.* **131**, 7079-7085.

Spanger, J., Kroke, A., Mohlig, M., Hoffman, K., Bergmann, M.M., Ristow, M., et. al (2003) Inflammatory cytokines and the risk to develop type 2 diabetes: results of the prospective population-based European Prospective Investigation into Cancer and Nutrition (EPIC)-Potsdam Study, *Diabetes* **52**, 812-817.

Strasfeld, D.B., Ling, Y.L., Gupta, R., Raleigh, D.P., Zanni, M.T. (2009) Strategies for extracting structural information from 2D IR spectroscopy of amyloid: application to islet amyloid polypeptide, *J. Phys. Chem. B* **113**, 15679-15691.

Stsiapura, V.I., Maskevich, A.A., Kuzmitsky, V.A., Uversky, V.N., Kuznetsova, U.M., Turoverov, K.K. (2008) Thioflavin-T as a molecular rotor: fluorescent properties of thioflavin T in solvents with different viscosities, *J. Phys. Chem. B* **112**, 15893-15902.

Su, Y., Chang, P.T. (2001) Acidic pH promotes the formation of toxic fibrils from beta-amyloid peptide, *Brain Res.* **893**, 287-291.

Sulatskaya, A.I., Maskevich, A.A., Kuznetsova, I.M., Uversky, V.N., Turoverov, K.K. (2010) Fluorescence quantum yield of thioflavin T in rigid isotropic solution and incorporated into the amyloid fibrils, *Plos One* **5**, e15385.

Suydam, I.T., Boxer, S. G. (2003) Vibrational stark effects calibrate the sensitivity of vibrational probes for electric fields in proteins, *Biochemistry* **42**, 12050-12055.

Swift, S.M., Clayton, H.A., London, N.J., James, R.F. (1998) The potential contribution of rejection to survival of transplanted human islets, *Cell Transplant* **7**, 599-606.

Tam, J.P., Wu, C.R., Liu, W., Zhang, J.W. (1991) Disulfide bond formation in peptides by dimethyl sulfoxide. Scope and applications, *J. Am. Chem. Soc.* **113**, 6657-6662.

Tang, J., Signarvic, R. S., DeGrado, W. F., Gai, F. (2007) Role of helix nucleation in the kinetics of binding of Mastoparan X to phospholipid bilayer, *Biochemistry* **46**, 13856-13863.

Tartaglia, G.G., Cavalli, A., Pellarin, R., Caflisch, A. (2004) The role of aromaticity, exposed surface and dipole moment in determing protein aggregation rates, *Prot. Sci.* **13**, 1939-1941.

Taskent-Sezgin, H., Chung, J., Patsalo, V., Miyake-Stoner, S. J., Miller, A. M., Brewer, S. H., Mehl, R. A., Green, D. F., Raleigh, D. P., Carrico, I. (2009) Interpretation of p-cyanophenylalanine fluorescence in proteins in terms of solvent exposure and contribution of side-chain quenchers: A combined fluorescence, IR and molecular dynamics study, *Biochemistry* **48**, 9040-9046.

Tenidis, K., Waldner, M., Bernhagen, J., Fischle, W., Bergmann, M., Weber, M., et. al (2000) Identification of a penta- and hexapeptide of islet amyloid polypeptide (IAPP) with amyloidogenic and cytotoxic properties, *J. Mol. Biol.* **295**, 1055-1071.

Thirumalai, D., Reddy, G., Straub, J.E. (2012) Role of water in protein aggregation and amyloid polymorphism, *Acc. Chem. Res.* **45**, 83-92.

Tjernberg, L., Hosia, W., Bark, N., Thyberg, J., Johansson, J. (2002) Charge attraction and beta propensity are necessary for amyloid fibril formation from tetrapeptides., *J. Biol. Chem.* **277**, 43243-43246.

Tomiyama, T., Kaneko, H., Kataoka, K.-I., Asano, S., Endo, N. (1997) Rifampicin inhibits the toxicity of pre-aggregated amyloid peptides by binding to peptide fibrils and preventing amyloid-cell interaction, *Biochem. J.* **322**, 859-865.

Tracz, S.M., Abedini, A., Driscoll, M., Raleigh, D.P. (2004) The role of aromatic interactions n amyloid formation by polypeptides: Analysis of peptides derived from human amylin, *Biochemistry* **43**, 15901-15908.

Tran, H., Mao, A., Pappu, R. (2008) Role of backbone-solvent interactions in determining conformational equilibria of intrinsically disordered polypeptides, *Proc. Natl. Acad. Soc. U.S.A.* **384**, 279-297.

Tucker, M.J., Getahun, Z., Nanda, V., DeGrado, W. F., Gai, F. (2004) A new method for determining the local environment and orientation of individual side chains of membrane-binding peptides, *J. Am. Chem. Soc.* **126**, 5078-5079.

Tucker, M.J., Oyola, R., Gai, F. (2005) Conformational distribution of a 14-residue peptide in solution: A fluorescence resonance energy transfer study, *J. Phys. Chem. B* **109**, 4788-4795.

Tucker, M.J., Oyola, R., Gai, F. (2006) A novel fluorescent probe for protein binding and folding studies: p-cyanophenylalanine, *Biopolymers* **83**, 571-576.

Tucker, M.J., Tang, J., Gai, F. (2006) Probing the kinetics of membrane-mediated helix folding, *J. Phys. Chem. B* **110**, 8105-8109.

Tycko, R. (2011) Solid state NMR studies of amyloid fibril structure, *Annu. Rev. Phys. Chem* **62**, 279-299.

Udayasankar, J., Kodama, K., Hull, R.L., Zraika, S., Aston-Mourney, K., Subramanian, S.L., Tong, J., Faulenbach, M.V., Vidal, J., Kahn, S.E. (2009) Amyloid formation results in recurrence of hyperglycaemia following transplantation of human IAPP transgenic mouse islets, *Diabetologia* **52**, 145-153.

Uversky, V.N., Fink, A.L. (2004) Conformational constraints for amyloid formation: The importance of being unfolded, *Biochim. Biophys. Acta.* **1698**, 131-153.

Vaiana, S.M., Best, R.B., Yau, W.M., Eaton, W.A., Hofrichter, J. (2009) Evidence for a partially structured state of the amylin monomer, *Biophys. J.* **97**, 2948-2957.

Ventura, S., Zurdo, J., Narayanan, S., Parreno, M., Mangues, R., Reif, B., et. al (2004) Short amino acid stretches can mediate amyloid formation in globular proteins: the Src homology 3 (SH3) case, *Proc. Natl. Acad. Soc. U.S.A.* **101**, 7258-7263.

Wasmer, C., Lange, A., Melckebeke, H.V., Siemer, A.B., Riek, R., Meier, B.H. (2008) Amyloid fibrils of HET-s(218-289) prionform a β-solenoid with a triangular hydrophobic core, *Science* **319**, 1523-1526.

Watt, B., Tenza, D., Lemmon, M.A., Kerje, S., Raposo, G., Andersson, L., Marks, M.S. (2011) Mutations in or near the transmembrane domain alter PMEL amyloid formation from functional to pathogenic, *Plos Genet.* **7**, e1002286.

Westermark, G.T., Westermark, P., Eizirik, D., Hellerström, C., Fox, N., Steiner, D.F., Andersson, A. (1999) Differences in amyloid deposition in islets of transgenic mice expressing human islet amyloid polypeptide versus human islets implanted into nude mice, *Metabolism* **48**, 448-454.

Westermark, G.T., Falkmer, S., Steiner, D.F., Chan, S.J., Engström, U., Westermark, P. (2002) Islet amyloid polypeptide is expressed in the pancreatic islet parenchyma of the teleostean fish, Myoxocephalus (Cottus) scorpius, *Comp. Biochem. Physiol. B* **133**, 119-125.

Westermark, G.T., Westermark, P., Berne, C., Korsgren, O. (2008) Widespread amyloid deposition in transplanted human pancreatic islets, *N. Engl. J. Med.* **359**, 977-979.

Westermark, P. (1972) Quantitative studies of amyloid in the islets of Langerhans, *Upsala J. Med. Sci.* **77**, 91-94.

Westermark, P., Wernstedt, C., Wilander, E., Hayden, D.W., O'Brien, T.D., Johnson, K.H. (1987) Amyloid fibrils in human insulinoma and islets of Langerhans of the diabetic cat are derived from a neuropeptide-like protein also present in normal islet cells, *Proc. Natl. Acad. Soc. U.S.A.* **84**, 3881-3885.

Westermark, P., Engström, U., Johnson, K.H., Westermark, G.T., Betsholtz, C. (1990) Islet amyloid polypeptide: Pinpointing amino acid residues linked to amyloid fibril formation, *Proc. Natl. Acad. Soc. U.S.A.* **87**, 5036-5040.

Westermark, P., Johnson, K.H., O'Brien, T.D., Betsholtz, C. (1992) Islet amyloid polypeptide: a novel controversy in diabetes research, *Diabetologia* **35**, 297-303.

Westermark, P. (1995). *Islet amyloid polypeptide and amyloid in the islets of Langerhans*. Diabetes: Clinical Science in Practice (Leslie, R. D. G., Robbins, D., Ed.), Cambridge Univ. Press, Cambridge, UK.

Westermark, P., Eizirik, D. L., Pipeleers, D. G., Hellerström, C., Andersson, A (1995) Rapid deposition of amyloid in human islets transplanted into nude mice, *Diabetologia* **38**, 543-549.

Westermark, P., Li, Z.-C., Westermark, G.T., Leckstrom, A., Steiner, D.F. (1996) Effects of beta cell granule components on human islet amyloid polypeptide fibril formation, *FEBS Lett.* **379**, 203-206.

Westermark, P., Andersson, A., Westermark, G.T. (2005) Is aggregated IAPP a cause of beta-cell failure in transplanted human pancreatic islets?, *Curr. Diab. Rep.* **5**, 184-188.

Westermark, P., Andersson, A., Westermark, G.T. (2011) Islet amyloid polypeptide, islet amyloid, and diabetes mellitus, *Physiol. Rev.* **91**, 795-826.

Whitty, A., Kumaravel, G. (2006) Between a rock and a hard place?, *Nat. Chem. Biol.* **2**, 112-118.

Williamson, J.A., Miranker, A.D. (2007) Direct detection of transient alpha-helical states in islet amyloid polypeptide, *Prot. Sci.* **16**, 110-117.

Williamson, J.A., Loria, J. P., Miranker, A. D. (2009) Helix stabilization precedes aqueous and bilayer-catalyzed fiber formation in islet amyloid polypeptide, *J. Mol. Biol.* **393**, 386-396.

Wiltzius, J.J.W., Sievers, S. A., Sawaya, M. R., Eisenberg, D. (2009) Atomic structures of IAPP (amylin) fusions suggest a mechanism for fibrillation and the role of insulin in the process, *Prot. Sci.* **18**, 1521-1530.

Winklhofer, K.F., Tatzelt, J., Haass, C. (2008) The two faces of protein misfolding: gain- and loss-of-function in neurodegenerative diseases, *EMBO* **27**, 336-349.

Wöhr, T., Wahl, F., Nefzi, A., Rohwedder, B., Sato, T., Sun, X., Mutter, M. (1996) Pseudo-prolines as a solubilizing, structure-disrupting protection technique in peptide synthesis, *J. Am. Chem. Soc.* **118**, 9218-9227.

Xue, W.-F., Homans, S.W., Radford, S.E. (2008) Systematic analysis of nucleation-dependent polymerization reveals new insights into the mechanism of amyloid self-assembly, *Proc. Natl. Acad. Soc. U.S.A.* **105**, 8926-8931.

Yagui, K., Kanatsuka, A., Makino, H. (1994) Construction of transgenic mouse system expressing human islet amyloid polypeptide, *Nippon. Rinsho.* **52**, 2746-2750.

Yankner, B.A., Dawes, L.R., Fisher, S., Villa-Komaroff, L., Oster-Granite, M.L., Neve, R.L. (1989) Neurotoxicity of a fragment of the amyloid precursor associated with Alzheimer's disease, *Science* **245**, 417-420.

Yankner, B.A., Duffy, L.K., Kirschner, D.A. (1990) Neurotrophic and neurotoxic effects of amyloid protein: reversal by tachykinin neuropeptides, *Science* **250**, 279-282.

Yonemoto, I.T., Kroon, G.J., Dyson, H.J., Balch, W.E., Kelly, J.W. (2008) Amylin proprotein processing generates progressively more amyloidogenic peptides that initially sample the helical state, *Biochemistry* **47**, 9900-9910.

Yoon, S., Welsh, W. J. (2004) Detecting hidden sequence propensity for amyloid fibril formation, *Prot. Sci.* **13**, 2149-2160.

Yoshiike, Y., Minai, R., Matsuo, Y., Chen, Y.R., Kimura, T., Takashima, A. (2008) Amyloid oligomer conformation in a group of natively folded proteins, *PloS One* **3**, e3235.

Yun, S., Urbanc, B., Cruz, L., Bitan, G., Teplow, D.B., Stanley, H.E. (2007) Role of electrostatic interactions in amlyoid β-protein (Aβ) oligomer formation: A discrete molecular dynamics study, *Biophys. J.* **92**, 4064-4077.

Zanuy, D., Porat, Y., Gazit, E., Nussinov, R. (2004) Peptide sequence and amyloid formation: Molecular simulations and experimental study of a human islet amyloid polypeptide fragment and its analogs, *Structure* **12**, 439-455.

Zhang, S., Liu, J., MacGibbon, G., Dragunow, M., Cooper, G.J. (2002) Increased expression and activation of c-Jun contributes to human amylin-induced apoptosis in pancreatic islet beta-cells, *J. Mol. Biol.* **324**, 271-285.

Zhang, S., Liu, J., Dragunow, M., Cooper, G.J. (2003) Fibrillogenic amylin evokes islet beta-cell apoptosis through linked activation of a caspase cascade and JNK1, *J. Biol. Chem.* **278**, 52810-52819.

Zhang, S., Liu, H., Liu, J., Tse, C.A., Dragunow, M., Cooper, G.J. (2006) Activation of activating transcription factor 2 by p38 MAP kinase during apoptosis induced by human amylin in cultured pancreatic beta-cells, *FEBS J.* **273**, 3779-3791.

Zhang, S., Liu, H., Yu, H., Cooper, G.J. (2008) Fas-associated death receptor signaling evoked by human amylin in islet beta-cells, *Diabetes* **57**, 348-356.

Zhao, H.L., Lai, F.M., Tong, P.C., Zhong, D.R., Yang, D., Tomlinson, B., Chan, J.C. (2003) Prevalence and clinicopathological characteristics of islet amyloid in Chinese patients with type 2 diabetes, *Diabetes* **52**, 2759-2766.

Zheng, X., Ren, W., Zhang, S., Liu, J., Li, S., Li, J., et. al (2010) Serum levels of proamylin and amylin in normal subjects and patients with impaired glucose regulation and type 2 diabetes mellitus, *Acta. Diabetol.* **47**, 265-270.

Zraika, S., Hull, R.L., Verchere, C.B., Clark, A., Potter, K.J., Fraser, P.E., Raleigh, D.P., Kahn, S.E. (2010) Toxic oligomers and islet beta cell death: guilty by association or convicted by circumstantial evidence?, *Diabetologia* **53**, 1046-1056.

Zurdo, J., Guijarro, J.I., Jimenez, J.L. Saibil, H.R., Dobson, C.M. (2001) Dependence on solution conditions of aggregation and amyloid formation by an SH3 domain, *J. Mol. Biol.* **311**, 325-340.